Technical University of Denmark

DTU

Catalytic synthesis of long-chained alcohols from syngas

Christensen, Jakob Munkholt; Jensen, Anker Degn; Jensen, Peter Arendt

Publication date:
2011

Document Version
Publisher's PDF, also known as Version of record

Link back to DTU Orbit

DTU Library
Technical Information Center of Denmark

Catalytic synthesis of long-chained alcohols from syngas

January 13th 2011

PhD-Thesis

Jakob Munkholt Christensen

Supervisors:
Professor Anker Degn Jensen
Associate Professor Peter Arendt Jensen

CHEC Research Centre
Department of Chemical and Biochemical Engineering
Technical University of Denmark

I Abstract

Ut desint vires, tamen est laudanda voluntas - Although the strength is lacking,
the will should be commended
- Ovid

This work has been an investigation of the catalytic conversion of syngas into mixed
alcohols with Mo-based catalysts. The primary focus has been on the use of alkali
promoted cobalt-molybdenum sulfide as a catalyst for the alcohol synthesis. The alcohol
synthesis is a possibility for the production of gasoline additives/replacements from
biomass via a gasification process.

It is observed that the sulfide catalyst is able to operate both with and without a sulfur
source in the syngas feed, but the presence of a sulfur source like H_2S can exert a
significant influence on the catalytic properties. The presence of 103 ppmv or more of
H_2S in the syngas feed stabilizes a large fraction of higher alcohols in the product. With
57 ppmv or less of H_2S in the feed the production of higher alcohols is however gradually
declining, while the methanol production increases.

The present investigations could suggest that these changes in the product distribution,
which occur in sulfur-free or sulfur-poor syngas, are related to changes in the state of
cobalt, which is added to the catalyst to promote chain-growth. The distribution of
methanol and higher alcohols in the product after 25 hours on stream is largely
independent of the cobalt content in the catalyst, although the fraction of higher alcohols
initially benefits significantly from an increased presence of cobalt. In catalysts that have
operated in sulfur free syngas, cobalt is incorporated into larger, coagulated structures,
and signs of crystalline Co_9S_8, which is considered to be inactive, can be observed in the
spent catalyst. It is hypothesized that the loss of sulfur from the catalyst in the reducing
atmosphere is driving the conversion of cobalt from its active form (possibly a mixed
cobalt-molybdenum sulfide) into larger, more sulfur-deficient structures and into Co_9S_8.
It must however be added that X-ray absorption spectroscopy investigations have not
provided direct evidence for a Co-Mo coordination in neither the fresh nor the spent
sulfide catalysts.

That the catalyst requires the presence of a sulfur source in the feed to stabilize a large
fraction of higher alcohols in the product introduces a dilemma, because the presence of a
sulfur sauce like H_2S in the gas can lead to an undesirable incorporation of sulfur species
into the alcohol product. It is observed that the sulfur content in the condensed alcohol
product increases linearly with the H_2S level in the syngas feed from 1250 ppmw S with
46 ppmv H_2S to 1905 ppmw S with 460 ppmv H_2S. Without H_2S in the feed sulfur
species are also incorporated into the condensed reaction product, but in this case the
products sulfur content decreases over time. The primary sulfur species in the alcohol
product are the thiols corresponding to the formed alcohols. With the increasingly
stringent regulations for sulfur in motor fuels this incorporation of sulfur into the alcohol
product is an important issue for the use of the alcohol product as a fuel
additive/substitute.

It has been discovered that alcohol coupling reactions, which appear to occur via aldol
condensation pathways, contribute to the chain-growth over the sulfide catalyst. Such

coupling reactions via aldol condensation pathways can explain the observed presence of branched alcohols (e.g. iso-butanol) in the product. This discovery arose from the observation that ethanol co-fed along with the syngas especially causes an increased production of 1-butanol.

Various investigations have been carried out to clarify the effect of the feed composition on the catalytic properties of the sulfide catalyst. In a sulfur free syngas it is observed that the production of higher alcohols is optimal with an equimolar mixture of CO and H_2 in the feed, while the methanol production benefits from an increasing hydrogen content in the feed. It has often been argued that the sulfides ability to operate in a sulfur containing atmosphere may enable the user to employ a less thorough and therefore less costly syngas cleaning. To evaluate, to which extent a removal of other components in the raw syngas is necessary, the influence of NH_3 and H_2O in the feed has also been investigated. Ammonia (741 ppmv) in the feed is observed to cause a general and largely reversible deactivation of the catalyst. Operation with elevated water levels in the syngas feed (4.7-13.4 mol%) is observed to cause a deactivation of the catalyst, and it is especially the chain-growth, which is affected. A permanent, general deactivation is observed once the water is removed from the feed – a deactivation which could be caused by an accelerated sintering in the presence of water.

Since the use of the sulfide catalyst encompasses the risk of sulfur being incorporated into the alcohol product, carbide catalysts have been investigated as a possible non-sulfided alternative. Various catalysts based upon the bulk carbides Mo_2C, WC and NbC have been synthesized and evaluated with respect to the catalytic behavior in high-pressure CO hydrogenation. NbC is largely inactive, and K_2CO_3/WC produces mainly methanol and methane with a low activity, while K_2CO_3/Mo_2C produces a mixture of methanol and higher alcohols, but also significant amounts of hydrocarbons.

The role of the choice of alkali cation in Mo_2C promoted by an alkali salt has also been evaluated at a promoter level of Alkali/Mo = 0.164±0.001 mol/mol. At 275 °C-300 °C the behavior of catalysts promoted by Cs_2CO_3 and K_2CO_3 is qualitatively similar, although K provides a markedly better activity (31 % at 300 °C, 100 bar, 5000 h^{-1}) and a better selectivity at identical conditions. At 275 °C an $Li(CH_3COO)$ promoted catalyst is very active and produces only hydrocarbons. If the effect of the different alkali promoters is compared at the same general activity level, corresponding to the Li-containing catalyst being operated at a lower temperature, the Li-promoted catalyst is however only slightly inferior to the K-promoted catalyst in terms of the alcohol selectivity.

Finally different multiply promoted Mo_2C catalysts have been evaluated in terms of the CO hydrogenation properties. Addition of Re (1 wt%) or Mn (1 or 5 wt%) to the K_2CO_3/Mo_2C system results in a slight reduction in the catalytic activity. The addition of Cu (0.84 wt%) was on the other hand observed to improve the activity (by 33 % at 275 °C, 100 bar, 5000 h^{-1}) and improve the selectivity of the K_2CO_3/Mo_2C system without altering the distribution of the alcohol product. Mo_2C modified with La (5 wt%) and V (3 wt%) produces mainly hydrocarbons.

II Dansk Resume (Summary in Danish)

Ak, lykkens dør går ikke indad, så man ved at storme løs på den kan trykke den op, men den går ud efter, og man har derfor intet at gøre
- Søren A. Kierkegaard

Dette arbejde er en undersøgelse af den katalytiske omdannelse af syntesegas til højere alkoholer over Mo-baserede katalysatorer. Det primære fokus er på brugen af alkalimodificerede sulfider af kobolt-molybdæn. Alkoholsyntesen udgør en mulighed for at fremstille benzinadditiver eller benzinerstatninger fra biomasse via en forgasningsproces.

Undersøgelserne viser, at sulfidkatalysatorerne er i stand til at fungere både med og uden svovlkilder i syntesegassen, men tilstedeværelsen af en svovlkilde som H_2S kan øve en væsentlig indflydelse på de katalytiske egenskaber. Tilstedeværelsen af 103 ppmv eller mere H_2S i fødestrømmen stabiliserer en stor fraktion af højere alkoholer i alkoholproduktet. Med 57 ppmv eller mindre H_2S i fødestrømmen daler produktionen af højere alkoholer imidlertid gradvist, mens methanolproduktionen stiger.

De nærværende undersøgelser antyder at disse ændringer i produktfordelingen, som fremkommer i en svovlfri eller svovlfattig syntesegas, er relateret til ændringer i kobolts tilstand. Kobolt tilsættes til katalysatoren for at øge kædevæksten. Fordelingen af methanol og højere alkoholer er efter 25 timer i en svovlfri syntesegas overordnet set uafhængig af katalysatorens koboltindhold, om end fraktionen af højere alkoholer indledningsvis drager en stor fordel af et øget koboltindhold. I katalysatorer, som har opereret i svovlfri syntesegas, er kobolt inkorporeret i større, koagulerede strukturer, og der er tegn på eksistensen af krystallinsk Co_9S_8, som anses for at være en fase uden katalytisk effekt. Det er foreslået, at katalysatorens tab af svovl i den reducerende syntesegas er den faktor, der driver ændringen af kobolt fra dets aktive form (muligvis et kobolt-molybdæn blandingssulfid) til større, mere svovlfattige strukturer og til den mere svovlfattige Co_9S_8-fase. Det må dog tilføjes at målinger med røntgenabsorptions-spektroskopi ikke har ført til en klar identifikation af Co-Mo bindinger i hverken friske eller brugte sulfidkatalysatorer.

At katalysatoren behøver en svovlkilde i gassen for at stabilisere produktfordelingen introducerer et dilemma, fordi tilstedeværelsen af en svovlkilde som H_2S i gassen kan føre til en højest uønsket indlemmelse af svovl i alkoholproduktet. Det observeres, at svovlindholdet i det kondenserede alkoholprodukt stiger lineært med H_2S-indholdet i fødestrømmen – fra 1250 ppmw S ved 46 ppmv H_2S til 1905 ppmw S ved 460 ppmv H_2S. Uden H_2S i fødestrømmen sker der også en inkorporering af svovl i alkoholproduktet, men i dette tilfælde falder produktets svovlindhold efterhånden som tiden går. De dominerende svovlspecier i alkoholproduktet er thiolerne svarende til de producerede alkoholer. De stadigt strengere lovkrav mht. det tilladte svovlindhold i bilbrændstoffer betyder, at denne inkorporering af svovl i alkoholproduktet er en meget væsentlig problemstilling mht. brugen af alkoholproduktet som brændstof eller benzinadditiv.

Det observeres at koblingen af alkoholer, via en reaktionsvej lig en aldolkondensation, bidrager til kædevæksten over sulfidkatalysatoren. Sådanne koblingsreaktioner ad en aldolkondensations-rute kan forklare tilstedeværelsen af forgrenede alkoholer (f.eks. iso-

butanol) i alkoholproduktet. Denne opdagelse kommer fra den observation at ethanol samfødet med syntesegassen især omdannes til 1-butanol.

Forskellige undersøgelser er udført med det formål at afklare hvilken effekt fødestrømmens sammensætning har på de katalytiske egenskaber. I en svovlfri syntesegas viser det sig, at produktionen af højere alkoholer er optimal med en ækvimolær blanding af CO og H_2 i føden, mens produktionen af methanol drager fordel af et øget brintindhold i fødestrømmen. Det er ofte blevet pointeret, at sulfidets evne til at fungere i en svovlholdig atmosfære kan tillade, at brugeren anvender en mindre omfattende og derfor billigere rensning af syntesegassen. For at undersøge i hvilken grad fjernelsen af andre komponenter i den rå syntesegas er nødvendig, er indflydelsen af NH_3 og H_2O i fødestrømmen også undersøgt. Ammoniak (741 ppmv) i føden giver en stort set generel og i høj grad reversibel forgiftning af katalysatoren. Drift med et forøget vandindhold i fødestrømmen (4.7-13.4 mol%) mindsker katalysatorens aktivitet, og det er især kædevæksten, som påvirkes. Et permanent, generelt aktivitetstab kan observeres, når vandet fjernes fra fødestrømmen – et aktivitetstab som kunne skyldes en forøget sintring under tilstedeværelse af vand.

Siden brugen af en sulfidkatalysator medfører en risiko for at indlejre svovl i alkoholproduktet er karbid-katalysatorer blevet undersøgt som et svovlfrit alternativ. Forskellige katalysatorer baseret på de ikke-bårne karbider Mo_2C, WC og NbC er blevet fremstillet og evalueret mht. de katalytiske egenskaber i højtryks CO-hydrogenering. NbC er uden nævneværdig aktivitet, og K_2CO_3/WC producerer primært methanol og methan med lav aktivitet, mens K_2CO_3/Mo_2C producerer en blanding af methanol og højere alkoholer, men også betydelige mængder af kulbrinter.

Den rolle, som valget af akali-kation spiller for Mo_2C modificeret med et alkalisalt er blevet undersøgt ved et Alkali/Mo forhold på 0.164 ±0.001 mol/mol. Ved 275 °C-300 °C er opførslen af katalysatorer med Cs_2CO_3 og K_2CO_3 kvalitativt ens, om end kalium giver en bedre aktivitet (31 % ved 300 °C, 100 bar, 5000 h^{-1}) og en bedre selektivitet ved identiske betingelser. Ved 275 °C er en katalysator modificeret med $Li(CH_3COO)$ meget aktiv og producerer kun kulbrinter. Hvis katalysatorerne med de forskellige alkalisalte sammenlignes ved det samme aktivitetsniveau, svarende til at den lithiumholdige katalysator benyttes ved en lavere temperatur, er den Li-modificerede katalysator dog kun lidt ringere end den kaliumholdige katalysator mht. alkoholselektiviteten

Endelig er CO-hydrogeneringsegenskaberne afprøvet for forskellige Mo_2C-katalysatorer med mere end et modificerende additiv. Tilsætning af Re (1 wt%) eller Mn (1 eller 5 wt%) til det grundliggende K_2CO_3/Mo_2C-system fører dog kun til en svag forringelse af de katalytiske egenskaber. Tilføjelsen af Cu (0.84 wt%) fører på den anden side til en forbedret aktivitet (med 33 % at 275 °C, 100 bar, 5000 h^{-1}) og forbedrer selektiviteten for K_2CO_3/Mo_2C-systemet uden at ændre fordelingen af akoholproduktet. Mo_2C modificeret med La (5 wt%) og V (3 wt%) producerer primært kulbrinter.

5

III Preface

Quod scripsi, scripsi – I wrote, what I wrote
- Pontius Pilate

If we meet someone, who ows us thanks, we are bound to remember it. How often do we not meet someone, to whom we owe thanks, and forget it?
- Johann Wolfgang von Goethe

IV Table of Contents

Look not at the vase, but at its contents
- From the Talmud

9

V Symbols

We are what we believe we are
- C. S. Lewis

A,a,B,b	In chapter 3 the component specific parameters in the equation of state
A_i	In chapter 5 the pre-exponential factor in the rate equation for component i
A_{wall}	In appendix B the area of the reactor wall
a_i, b_i, c_i	In chapter 5 the reaction orders of component i in H_2 (a), CO (b) and H_2S (c)
C_A	Concentration of the key reactant A in appendix D
C_{Mears}	Magnitude of the Mears expression: $C_{Mears} = \dfrac{-r'_{obs} \cdot \rho_b \cdot d_p \cdot n_A}{2 \cdot k_c \cdot C_{Ab}}$
C_{WP}	Magnitude of the Weisz-Prater expression: $C_{WP} = \dfrac{-r'_{obs} \cdot \rho_c \cdot \left(\frac{d_p}{2}\right)^2}{D_e \cdot C_{As}}$
$\tilde{C}_P$	Constant pressure heat capacity on a molar basis
$\frac{C_{2+}}{C_1}$	Weight ratio of higher alcohols to methanol
$D_{\alpha\beta}$	Diffusion coefficient for diffusion of component α in the surrounding gas β
D_e	Effective diffusion coefficient
D_K	Knudsen diffusion coefficient.
d_p	Particle diameter
$E_{a,i}$	Activation energy for the production of component i
F_i	Molar flow rate of component i
f_i	Fugacity of component i
G	Gibbs free energy
H	Enthalpy
K_j	Equilibrium constant for reaction j. For the methanol synthesis where non-ideality is of some significance the symbol K_f is used to emphasize the basis on fugacities.
K_{NH_3}	Ammonia adsorption equilibrium constant
k_c	Mass transfer coefficient
k'_{ij}	Binary interaction parameter for the i,j-pair. In this work $k'_{ij} = 0$ in all cases
k_j	Rate constant for reaction j
K_φ	Parameter collecting all the fugacity coefficients in equilibrium expressions, where non-ideality plays a role
L	Length of catalyst bed
M	Molar mass
m	Mass
$N_{X,i}$	Number of atoms of element X in component i in appendix C
n_A	Reaction order with respect to the key reactant A in appendix D
n_i	In chapter 6 the number of carbon atoms in product i
P	Pressure
P^{sat}	Vapor pressure
p_j	Partial pressure of component j
pK_a	Negative logarithm of the acid strength constant: $pKa = -\log_{10}(K_a)$

Q	Heat effect
q	Heat flux
R_i	Production rate of component i
R	Gas constant
Re	Reynolds number: $\mathrm{Re} = \frac{v_0 d_p \rho}{\mu}$
r_j	Reaction rate of reaction j per unit volume
r_j'	Reaction rate of reaction j per mass of catalyst
S_{Alc}	Alcohol selectivity
T	Temperature
T	Time
v_0	Linear gas velocity
V_0	Volumetric flow rate
V	Volume
V_m	Molar volume
w	Weight fraction
X_{CO}	CO conversion
X*	Component X adsorbed on a catalytic surface
x_i	Liquid phase molar fraction of component i
Y_i	Yield of product i
y_i	Gas phase molar fraction of component i
Z	Compressibility factor
z_i	In appendix C the molar fraction of component i in the feed mixture
*	Free site on a catalytic surface

Greek symbols

β	The liquid fraction in appendix C
$\frac{\varepsilon}{\kappa}$	Characteristic energy in the Lennard-Jones potential
θ	The fractional loss of activity in chapter 7, which may be equal to the fractional coverage of ammonia on the surface.
κ	Boltzmann constant
λ_i	Thermal conductivity of component/material i
μ_i	Viscosity of component i
v_i	Kinematic viscosity of component i $v = \frac{\mu}{\rho}$
ρ	Density
σ	Collision diameter in the Lennard-Jones potential
τ	Residence time
$\tilde{\tau}$	Tortuosity
φ_i	Fugacity coefficient for component i
ϕ	The Thiele modulus in appendix D
$\phi_{\alpha\beta}$	Interaction parameter describing the interaction of component α with component β
ψ	Porosity of the catalyst pellet

Ω_μ, Ω_D Non-rigidity parameter in the determination of viscosity, density
ω Acentric factor

Subscripts

α   Regarded component in a multi component mixture
β   A component with which component α can interact in a multi component mixture
b   Property of the bulk gas phase
C   Critical property
n   Carbon number
i   Component *i*
j   Component *j* in chapter 3, reactant *j* in chapter 5 and reaction *j* in appendices A and B
R   Reduced property (e.g. $T_R = \frac{T}{T_C}$)
r   Radial position
s   Property at the catalytic surface

VI Abbreviations

Make everything as simple as possible, but not any simpler
- Albert Einstein

α/β-position	Position in the oxygenate relative to the substituent: R-$^{\gamma}$C-$^{\beta}$C-$^{\alpha}$C-OH
ASF	Anderson Schultz Flory (product distribution)
AED	Atomic Emission Detector
BFM	Bubble flow meter
C_n-products	Products with n carbon atoms
CSTR	Continuously stirred tank reactor
DFT	Density functional theory
DME	Dimethyl ether
EDX	Energy dispersive X-ray analysis
EoS	Equation of state
EXAFS	Extended X-ray absorption fine structure
FID	Flame ionisation detector
FT	Fischer Tropsch (process)
GC	Gas Chromatograph
GHSV	Gas hourly space velocity i.e. volume of gas at 1 atm and 298.15 K per volume of catalytic bed per hour
HA	Higher Alcohols
HDS	Hydrodesulfurization
HE	Heating element
ICP-OES	Inductively Coupled Plasma – Optical Emission Spectroscopy
IGL	Ideal gas law
ISS	Ion scattering spectroscopy
KCoMo-X	Descriptor for the different potassium promoted cobalt-molybdenum sulfide catalyst samples. The samples all have an individual identifier (X).
LHV	Lower heating value
L-MFC	Mass flow controller for liquids
MF(P)C	Mass flow (pressure) controller
MS	Mass spectroscopy
NL	Normal litre i.e. the volume of 1 L at 273.15 K and 1 atm
OWV	One-way valve
P	In illustrations of the experimental setup P denotes a manometer
PR	Peng-Robinson (equation of state)
SIMS	Secondary ion mass spectroscopy
SRK	Soave-Redlich-Kwong (equation of state)
STL	Standard litre i.e. at 298.15 K and 1 atm
STM	Scanning tunnelling microscopy
STP	Standard temperature and pressure i.e. 298.15 K and 1 atm
STY	Space time yield i.e. mass of product per mass of catalyst and per time
TCD	Thermal conductivity detector

TEM	Transmission electron microscopy
TOS	Time on stream
TPR/C	Temperature programmed reduction/carburization
Type I/II	Supported sulfide particles with/without links to the support
Vir	Virial equation
XANES	X-ray absorption near edge structure
XAS	X-ray absorption spectroscopy
XPS	X-ray photoelectron spectroscopy
XRD	X-ray diffraction

VII Incorporated publications

James Norrington: And I half expected it to be made of wood. You are without doubt the worst pirate I've ever heard of.
Jack Sparrow: But you have heard of me.
- From the movie: Pirates of the Caribbean: The Curse of the Black Pearl

Publications in journals with peer review (2)

Christensen, J. M., Mortensen, P. M., Trane, R., Jensen, P. A., Jensen, A. D., *Effects of H_2S and process conditions in the synthesis of mixed alcohols from syngas over alkali promoted cobalt-molybdenum sulfide*, App. Catal. A 366 (2009) 29-43.

Christensen, J. M., Jensen, P. A., Schiødt, N. C., Jensen, A. D., *Coupling of Alcohols over Alkali-Promoted Cobalt-Molybdenum Sulfide*, ChemCatChem, 2 (2010) 523-526.

Participation in international conferences (3)

Poster presentation "*Catalytic conversion of syngas to mixed long chain alcohols, What is the effect of feed sulfur upon the alcohol synthesis over Alkali/Co/MoS$_2$ catalysts*" at the 14th International Congress on Catalysis in Seoul, Republic of Korea, 2008.

Oral presentation "*Effect of process conditions in the synthesis of higher alcohols from syngas over a K$_2$CO$_3$/Co/MoS$_2$/C catalyst*" at the 21st North American Catalysis Society Meeting in San Francisco, USA, 2009.

Oral presentation "*Catalytic conversion of syngas into mixed long-chain alcohols over cobalt-molybdenum sulfide*" at the 14th Nordic Symposium on Catalysis, Helsingør, Denmark, 2010.

Manuscripts submitted to peer reviewed journals (2)

Christensen, J. M., Jensen, P. A., Jensen, A. D., *Effects of feed composition and feed impurities in the catalytic conversion of syngas to higher alcohols over alkali-promoted cobalt-molybdenum sulfide*, Ind. Eng. Chem. Res., Submitted.

Christensen, J. M., Duchstein, L., Wagner, J. B, Jensen, P. A., Temel, B., Jensen, A. D., *Catalytic conversion of syngas into higher alcohols over carbide catalysts*, App. Catal. A, submitted.

Manuscripts in preparation (1)

Christensen, J. M., Beier, M. J., Duchstein, L., Boubnov, A., Wagner, J. B, Jensen, P. A., Grunwaldt, J.-D., Jensen, A. D., *Changes in a potassium promoted cobalt-molybdenum sulfide catalyst during the conversion of syngas into higher alcohols*, To be submitted to Journal of Catalysis.

Publications in journals without peer review aimed at a general audience (2)

Christensen, J. M, Jensen, P. A., Jensen, A.D., *Efficiency and CO_2-displacement for the synthesis of transportation fuels from biomass I. The possible options* (In Danish), Dansk kemi, nr. 10, 2008.

Christensen, J. M, Jensen, P. A., Jensen, A.D., *Efficiency and CO_2-displacement for the synthesis of transportation fuels from biomass II. Comparison of the syntesis options* (In Danish), Dansk kemi, nr. 11, 2008.

1 Introduction

Pleasure – it is beer. Discomfort – it is an expedition.
- Mesopotamian proverb ca. 2000 B.C.

The development of a way to synthesize bio-ethanol (beer) predates written history. Due to the potential advantage of an efficient, synthetic route to ethanol and/or other higher alcohols there has however over the last century been a continued exploration for a solution to this seemingly difficult task. This work continues this search with an exploration of the catalytic conversion of syngas into mixed higher alcohols over molybdenum based catalysts.

With the growing focus on the potential risks associated with the human emissions of CO_2 a tremendous challenge in the 21st century is the development of efficient chemical processes to produce fuels and chemicals from environmentally benign feedstocks – for example biomass. With respect to large scale biomass utilization in fuel/chemical production it is especially the use of so-called lignocellulosic biomass that offers significant environmental advantages [1-6]. A processing route that has the advantage of being able to utilize essentially all sources of biomass is a gasification process [7, 8]. By reaction with steam at high temperature and pressure the biomass can be converted into so-called synthesis gas or syngas [7, 8]. The gasification process can in principle use any kind of carbon source, and the biomass could be supplemented by coal or carbon containing waste fractions - for example to even out seasonal variations in biomass availability. After an appropriate cleaning the syngas can then be converted into fuel chemicals, and an interesting class of fuel chemicals is alcohols. By virtue of their high octane numbers alcohols are interesting as gasoline additives or replacements [9-11]. If the alcohols initially are used as gasoline additives the smaller alcohols (particularly methanol) do however have the problem that they can cause an undesirable phase separation in alcohol-gasoline mixtures. This occurs, if the temperature is too low, or the water content of the mixture is too high [10]. The addition of higher alcohols to mixtures of methanol-gasoline or ethanol-gasoline improves the miscibility of such mixtures [10], as the higher alcohols act as co-solvents, and stabilize the blends [10]. A mixture of methanol, ethanol and higher alcohols can be formed directly from syngas over various catalytic systems.

The topic of this PhD-thesis is direct catalytic conversion of syngas into such a mixture of alcohols over molybdenum based catalysts. The focus is upon catalyst based on molybdenum sulfide, and to a smaller extent catalysts based upon molybdenum carbide. This work has included preparation, characterization and testing of Mo-based catalysts. The focus of this work is experimental investigations of catalysts in a high pressure flow reactor setup. The studies of MoS_2-based catalysts include investigations of the incorporation of sulfur into the liquid reaction product, of the stability of the catalyst, of the reaction mechanism and the reaction kinetics as well as investigations of the influence of the process conditions. The MoS_2-based catalysts are interesting for several reasons. These catalysts are more tolerant towards sulfur species in the syngas [12-16], and that may enable the user to employ a less thorough and therefore less costly removal of sulfur from the syngas [17]. Furthermore alkali promoted cobalt-molybdenum sulfide

has previously been shown to yield a good alcohol selectivity – even at a high CO conversion [13, 18, 19]. Range Fuels, the company behind a newly constructed higher alcohols plant in the US, has also aquired numerous patents focusing on the sulfide catalysts [20-28]. Carbide catalysts have been investigated as a potential alternative to the sulfides, because the present investigations uncovered certain negative traits of the sulfide catalysts.

A short description should be given of the form chosen for this thesis. The thesis is predominantly a compilation of the papers and manuscripts presented in section VII, but it has been attempted to organize the material as a coherent report. Below it has been summarized, how the various chapters in this thesis are constructed from the papers and manuscripts presented in section VII:

Chapter 2 "The catalytic conversion of syngas into higher alcohols" provides a background for the higher alcohol synthesis. A part of the "Introduction" sections from the papers and manuscripts presented in section VII has been incorporated into this chapter. The focus is on the properties of Mo-based catalysts, and the treatment of peripheral topics like gasification is kept relatively brief.

Chapter 3 "Thermodynamic considerations" gives a brief introduction to the thermodynamic calculations performed in this work and discusses the issue of non-ideality in the gas phase at high pressure. This section is an expansion of the descriptions from the papers and manuscripts presented in section VII.

Chapter 4 "Experimental work" is collected from the experimental descriptions in the papers and manuscripts presented in section VII. A few additional comments and figures have been added in chapter 4 to further clarify the text.

Chapter 5 is the "Results and Discussion" section from the paper "*Effects of H$_2$S and process conditions in the synthesis of mixed alcohols from syngas over alkali promoted cobalt-molybdenum sulfide*" published in Applied catalysis A (2009).

Chapter 6 is the main body of the paper "*Coupling of Alcohols over Alkali-Promoted Cobalt-Molybdenum Sulfide*" published in ChemCatChem (2010).

Chapter 7 is the "Results and Discussion" section from the manuscript "*Effects of feed composition and feed impurities in the catalytic conversion of syngas to higher alcohols over alkali-promoted cobalt-molybdenum sulfide*", which has been submitted to Industrial and Engineering Chemistry Research.

Chapter 8 is the current state of the "Results and Discussion" section from the manuscript "*Changes in a potassium promoted cobalt-molybdenum sulfide catalyst during the conversion of syngas into higher alcohols*", which is currently being prepared, and which is intended for submission to Journal of Catalysis. For the final submission the material will be augmented with the XAS results from a beamtime at ANKA, Karlsruhe in December 2010 and with a further treatment of the XAS spectroscopy at the Mo-edge. Time does not permit the inclusion of this material in the present thesis.

Chapter 9 is the "Results and Discussion" section from the manuscript "*Catalytic conversion of syngas into higher alcohols over carbide catalysts*", which has been submitted to Applied Catalysis A.

For chapters 5-9 an abstract (typically from the original manuscript) has been included in the chapter to provide the reader with an accessible overview over the contents of that

chapter. To avoid too many repetitions overlapping segments from the papers and manuscripts have generally been omitted, but some overlaps may persist. In a few cases additional material has been added to the text to further clarify various points. If updated information has become available after the publication of the papers such information has also been included in the text.

2 The catalytic conversion of syngas into higher alcohols

Ethanol is the fuel for the future
- Henry Ford to the New York Times, 1925

The synthesis of ethanol from syngas is the future of catalysis
- John Armor at the 14th International Congress of Catalysis, 2008

The purpose of this work has been to study the catalytic conversion of syngas into a mixture of methanol and higher alcohols. The focus of this work has been on the alcohol synthesis as a possible way of utilizing biomass via a gasification process. This section will provide a background for the present investigations. A brief introduction is given to gasification and to the typical syngas composition. Its purpose is to set the stage for the present studies of how the syngas composition influences the catalytic properties. The properties of alcohol synthesis catalysts based upon molybdenum sulfide and molybdenum carbide are presented to introduce the present studies. Finally the fuel properties of the alcohol product are described to pave the way for the present studies of the properties of the condensed alcohol product.

The present background for the higher alcohol synthesis will mainly be limited to the work with molybdenum based catalysts, which are the topic of this work. A significant number of general reviews are available for this process. Several thorough reviews of the higher alcohol synthesis have been published over the years [29-35], and some are quite recent [33, 36]. Furthermore Wender [11] and Mills [37] have published thorough reviews of the various syngas conversion options including the synthesis of higher alcohols. For a description of other higher alcohol synthesis catalysts the reader is referred to these works.

2.1 Gasification

Gasification is the formation of syngas from carbonaceous materials like coal and biomass by reaction with a gasifying agent like H_2O, H_2 or CO_2 [7, 8, 38]. The main gasification reactions are endothermic, and the heat required to sustain the gasification is typically supplied by combustion of part of the carbonaceous material (so-called autothermic gasification) [38]. In the known processes converting solid, carbonaceous feedstocks into fuel chemicals the production and conditioning of the syngas does in fact constitute the dominant part of the plant cost. For the production of synthetic diesel fuel from coal in the Fischer Tropsch process Dry [39] reports that the systems generating of the syngas entering the reactor compose 70 % of the plant investment cost. For methanol produced from coal as much as 80-85 % of the plant investment cost is reportedly related to syngas generation [40, 41], while the figure is estimated to be around 78 % for a plant producing synthetic gasoline from coal via methanol [42]. An understanding of gasification and syngas conditioning is therefore very important for the production of fuel chemicals from solid feedstocks along this pathway. Since the gasification is only a peripheral part of the present work this section will however only provide a very general

overview of the gasfication process with the focus on the syngas composition, which is the most important aspect with respect to the present catalytic studies.

Table 2.1 and table 2.2 summarize respectively the dominant heterogeneous and homogeneous reactions taking place in the gasifier.

Table 2.1 Major heterogeneous reactions taking place in the gasifier [7, 8, 38, 43].

Reaction	ΔH°_{298K} [44] $\left[\frac{kJ}{mol}\right]$	Relative rate [43] [T = 800 K, $P_{reactant}$ = 0.1 atm]	
$C + CO_2 \rightleftharpoons 2CO$	172.5	1	R1
$C + H_2O \rightleftharpoons H_2 + CO$	131.3	3	R2
$C + 2H_2 \rightleftharpoons CH_4$	-74.6	$3 \cdot 10^{-3}$	R3
$C + \frac{1}{2}O_2 \rightleftharpoons CO$	-110.5	10^5	R4
$C + O_2 \rightleftharpoons CO_2$	-393.5	10^5	R5

Table 2.2 Major homogeneous reactions taking place in the gasifier [7, 8, 38, 45]

Reaction	ΔH°_{298K} [44] $\left[\frac{kJ}{mol}\right]$	
$CO + \frac{1}{2}O_2 \rightleftharpoons CO_2$	-283.0	R6
$H_2 + \frac{1}{2}O_2 \rightleftharpoons H_2O$	-241.8	R7
$CO + H_2O \rightleftharpoons H_2 + CO_2$	-41.2	R8
$CO + 3H_2 \rightleftharpoons CH_4 + H_2O$	-205.9	R9
$\frac{1}{2}CH_4 + O_2 \rightleftharpoons \frac{1}{2}CO_2 + H_2O$	-401.3	R10

For the reactions in table 2.1 the carbonaceous material is simply represented as "C". In addition to the reactions in table 2.1 and table 2.2 thermal gas phase cracking of tar (larger hydrocarbons) and small hydrocarbons will also occur in the reactor [7, 8]. These cracking reactions will to some extent be facilitated by the gasification agent [7, 8]. With respect to reactors there are three important categories, namely entrained flow gasifiers, fluidized bed gasifiers and moving bed gasifiers. Typical operating parameters and characteristic traits of the 3 gasifier types are provided in table 2.3 and table 2.4.

Table 2.3 Comparison of typical operating conditions for the 3 types of gasifiers when used for coal gasification [7, 8, 38, 46].

Type	P [bar]	$T_{reactor}$ [K]	T_{exit} [K]	O_2 addition [kg/kg coal]	Particle diameter [mm]	Ash condition
Entrained flow	20-40	1600-2200	1300	0.9	< 0.1	Slagging
Fluidised bed	10-30	1250-1400	1150	0.7	0.5-6	Dry/agglomerating
Moving bed*	25-30	1250-1350	700	0.5	20-50	Dry/slagging

*Counter current operation

Table 2.4 Comparison of the performance characteristics of the 3 types of gasifiers when used for coal gasification [38].

Design	Type	Feed form	Carbon efficiency [%]	Cold gas efficiency [%]
Texaco	Entrained flow	Slurry	97	74
Shell	Entrained flow	Dry	99	81
HTW	Fluidised bed	Dry	96	85
Slagging Lurgi	Moving bed	Dry	99.9	88

The term "cold gas efficiency" in table 2.4 refers to a combustion at standard conditions, where liquid water is formed, and the cold gas efficiency is thus the higher heating value of the syngas relative to the higher heating value of the feed. Moving bed gasifiers have a high efficiency, but a clear disadvantage for this type of gasifier is that the temperature decreases along the bed. This means that a significant amount of tar, which is released from the carbonaceous material, is carried along with the gas without being fully decomposed due to a relatively low temperature in the exit region of the gasifier [7, 8].

Table 2.5 summarizes several reported syngas compositions for various gasification processes.

Table 2.5 Reported wet syngas compositions for various gasification processes.

Gasifier Design	Lurgi	Texaco	Shell	Shell [a]	IGT
Type	Moving bed	Entrained flow	Entrained flow	Entrained flow	Fluidized bed
Fuel	Coal	Coal	Coal	Biomass	Biomass
Oxidant	O_2	O_2	O_2	O_2	O_2
Gasification agent	H_2O	H_2O	H_2O	H_2O	H_2O
Exit temperature [°C]	540 [b]	1315 [b]	1427	1085	982
Pressure [bar]				24.3	34
H_2O [vol%]	50	17	2.01	18.4	31.8
H_2 [vol%]	21	29.6	26.8	30.7	20.8
CO [vol%]	8	41	63.1	39.0	15.0
CO_2 [vol%]	15	10	1.5	11.8	23.9
CH_4 [vol%]	4.2	0.3	0.0	0.1	8.2
C_{2+} [vol%] [c]	0.5	0	0	0	0.3
H_2S + COS [vol%]	0.7	1.1	1.4		
NH_3 [vol%]	0.4	0.2			
N_2 [vol%]	0.2	0.8	4.08		0.4
H_2/CO [mol/mol]	2.78	0.72	0.49	0.79	1.39
Reference	[47]	[47]	[48]	[49]	[50]

[a] This syngas composition is calculated through an assumption of chemical equilibrium.
[b] These temperatures are reported as operating temperatures.
[c] The fraction of C_{2+} species in the syngas.

Table 2.5 illustrates that the gasifier type and the feedstock have a significant impact upon the syngas composition. It is therefore only possible to provide a general approximation of the typical H_2/CO ratio in the raw syngas. Biomass gasification generally results in a molar H_2/CO ratio in the order of 1 [49, 50], while coal gasification

often results in a lower H_2/CO ratio [31]. As seen for the Lurgi moving bed gasifier in table 2.5 there are however exceptions to these guidelines. Given the wide variation in the H_2/CO ratios for the gasification processes illustrated in table 2.5 it would be important to establish how the H_2/CO ratio influences the activity of the catalyst. It will of course be possible to regulate the H_2/CO ratio in the syngas fed to the synthesis reactor by means of the water-gas shift reaction. A class of water-gas shift catalysts, which are sometimes denoted raw gas shift catalysts, are in fact also based upon molybdenum sulfides (perhaps promoted with Co or Ni) similar to the presently studied sulfided alcohol synthesis catalysts [51-53].

The data in table 2.5 illustrate that coal gasification can yield a syngas with significant levels of sulfur containing compounds. For biomass gasification the sulfur content in the syngas is typically markedly lower than for coal gasification. For gasification of wood and straw the total content of sulfur species of the synthesis gas is typically below 200 ppmv, although some crops can yield slightly higher sulfur contents [7, 54, 55]. Hydrogen sulfide is the dominant sulfur species in the syngas. For high temperature gasification processes all the sulfur is present as H_2S or COS, and here 93-96 % of the sulfur is under typical conditions present as H_2S [7]. For a raw syngas derived from coal gasification in a Lurgi moving bed gasifier Supp [56] also report that 95 mol% of the sulfur is present in the form of H_2S. Hydrogen sulfide is therefore also used as the representative sulfur compound in the present investigations. Chapter 5 contains an investigation of how the feed sulfur level influences the properties of the sulfided catalyst.

The ammonia content in the raw syngas from the gasifier will depend upon the feedstock, the process conditions, and the type of gasifier employed in the gasification process. It is therefore only possible to provide some general levels for the nitrogen compounds in the syngas. Coal gasification typically results in a syngas with 10^3-10^4 ppmv of NH_3 and a few hundred ppmv of HCN [47, 57]. Wood gasification generally results in lower nitrogen levels in the syngas – often 100-1000 ppmv NH_3 and 10-100 ppmv HCN [57, 58]. Some nitrogen rich crops (e.g. alfalfa) can however yield higher ammonia contents in the syngas – even values in the 1-2 vol% range [54, 55]. It would be interesting to determine, how these levels of NH_3 could influence the activity of the sulfide catalyst. Concerning the HCN content in the gas MoS_2 based water-gas shift catalysts can reportedly [7] catalyze the hydrogenation of HCN into ammonia, and this can presumably also occur over the very similar sulfided alcohol synthesis catalysts.

Table 2.5 also illustrates that the raw syngas from the gasifier contains considerable amounts of water and CO_2. Water and CO_2 are also formed as by-products in the alcohol synthesis reactions. The sulfided alcohol synthesis catalyst has a significant activity in the water-gas shift reaction [15], and water and CO_2 are therefore largely parallel products in the alcohol synthesis reactor. In this work the effect that the water content in the syngas feed has upon the catalytic properties is evaluated, and the observed effect of water is compared to previous investigations of the role of CO_2 in the syngas.

An argument, which has also often been made in favor of the sulfided alcohol synthesis catalyst, is that the sulfide in comparison to other potential catalysts is more tolerant towards sulfur species in the syngas [12-16]. It has been suggested that this sulfur tolerance may enable the user to employ a less thorough and therefore less costly removal of sulfur from the syngas [17]. It could therefore be important to establish how the

27

catalyst is affected by the other components in the raw syngas in order to determine to what extent a cleaning/conditioning of the syngas can be avoided. Chapter 7 in this work is such an investigations of, how the composition of the feed stream (H_2/CO ratio, NH_3 level, H_2O level) influences the properties of the sulfided alcohol synthesis catalyst.

2.2 Higher alcohol synthesis

The search for an efficient catalytic process for converting syngas into higher alcohols has been ongoing for most of a century. As early as 1916 BASF patented a process for producing hydrocarbons and various higher oxygenates from syngas over an oxide of cobalt or osmium at high temperature (300-400 °C) and pressure (~100 atm) [59-61]. These patents seem to be part of the first investigations of the higher alcohol synthesis. In the early 1920's Fischer and Tropsch [62] developed a process for producing higher alcohols from syngas using an alkali promoted iron catalyst operated at temperatures of 400-450 °C and at pressures in excess of 100 bar. The synthesis of primarily iso-butanol with alkali modified methanol synthesis catalysts was also developed during the 1910's and 1920's [63]. Higher alcohol synthesis plants were operated in the US and in Germany from 1927 to 1945, but these plants were decommissioned in the wake of the Second World War due to increasing petroleum availability and due to an increasing demand for more pure alcohol products [30, 31]. In the 1980's Enichem, Snamprogetti and Haldor Topsøe A/S operated a 15000 tons per year plant producing higher alcohols, but this plant has subsequently been closed down [11]. Currently no commercial scale plants are using the synthesis, but the current focus on fuel ethanol appears to be creating an increased interest for the process. In fact the first commercial scale plant in the US that will produce alcohol from cellulosic feedstocks is expected to be based upon this technology. The company Range Fuels in 2010 finished the first stage of a commercial plant for production of biofuels from gasification of waste wood. At the time of writing in the winter of 2010 the plant is however only producing methanol [64]. The patents issued to Range Fuels mainly appear to focus on sulfided sytems (Alkali/Co(or Ni)/MoS_2(or WS_2)) similar to the the ones studied in the present text [20-28]. The present studies could thus also have a relevance for an actual application of the process.

The most important reactions occurring over the alcohol synthesis catalysts are the methanol synthesis (R11) and the higher alcohol synthesis (R12):

$$CO + 2H_2 \rightleftharpoons CH_3OH \tag{R11}$$

$$nCO + 2nH_2 \rightleftharpoons C_nH_{2n+1}OH + (n-1)H_2O, \; n \geq 2 \tag{R12}$$
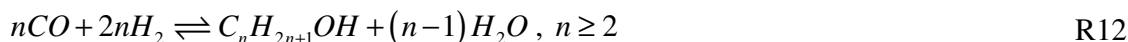
On most alcohol synthesis catalysts the water-gas shift reaction (R13) occurs as well:

$$CO + H_2O \rightleftharpoons H_2 + CO_2 \tag{R13}$$

The dominant by-product in the higher alcohol synthesis is typically short-chained hydrocarbons (R14):

$$nCO + (2n+1)H_2 \rightleftharpoons C_nH_{2n+2} + nH_2O \qquad \text{R14}$$

Oxygenated by-products include esters (R15) and aldehydes (R16) as well as ethers formed in the dehydration of the alcohols (R17):

$$(n+1)CO + 2nH_2 \rightleftharpoons C_{n-1}H_{2n-1}COOCH_3 + (n-1)H_2O \qquad \text{R15}$$
$$(n+1)CO + (2n+1)H_2 \rightleftharpoons C_nH_{2n+1}CHO + nH_2O \qquad \text{R16}$$
$$2C_nH_{2n+1}OH \rightleftharpoons C_nH_{2n+1}OC_nH_{2n+1} + H_2O \qquad \text{R17}$$
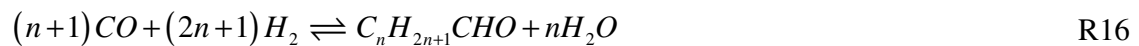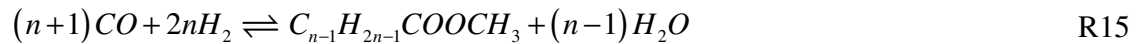
With thermodynamic data from Barin [65] it is found that the equilibrium constant for the water-gas shift reaction in the relevant temperature range varies from $K_{WGS} = 73$ at 250 °C to $K_{WGS} = 22$ at 350 °C, and many of the alcohol synthesis processes employ relatively CO rich feeds (see table 2.6 below), so most of the product water is shifted to CO_2. When full shift of product water is assumed, the stoichiometric feed for the production of ethanol corresponds to an H_2/CO ratio of 1:1 mol/mol. For the formations of propanol, butanol and pentanol the stoichiometric feed ratios are respectively 0.8, 0.71 and 0.67 under the assumption of full water-gas shift.

The catalysts and process for the higher alcohol synthesis can be divided into at least 6 subgroups [30, 31, 34]:

1) Alkali doped high-pressure MeOH synthesis catalysts: Alkali/ZnO/Cr_2O_3 [30, 66-68].
2) Alkali doped low-pressure MeOH synthesis catalysts: Alkali/Cu/ZnO [9, 69-71].
3) Modified Fischer Tropsch catalysts: Alkali/Cu/Co/M_2O_3 (M = Cr/Al) [35, 72, 73].
4) Sulfided molybdenum or cobalt-molybdenum catalysts [13, 74, 75].
5) Promoted rhodium based catalysts [76-78].
6) Mixed-metal catalysts (primarily focusing on Co) [79-85].

The distribution of the alcohol product depends upon the catalyst. Rhodium based systems have achieved fairly high selectivites to ethanol - even at reasonably high conversion levels [78, 86-88]. Modified methanol synthesis catalysts have a slow $C_1 \rightarrow C_2$ chain growth step to form ethanol, but ethanol is in relatively rapid aldol condensation reactions with methanol converted into first 1-propanol and then iso-butanol [9, 31]. This leads to a product that contains large amounts of methanol and iso-butanol. For modified Fischer Tropsch catalysts and Alkali/MoS_2 catalysts the product follows the so-called Anderson Schulz Flory (ASF) [89-91] distribution [72, 75], but for the sulfide system the product can be displaced towards the higher alcohols by addition of group VIII metals or by addition of H_2S to the syngas feed [31]. Table 2.6 summarizes reported operating conditions for various higher alcohol synthesis processes.

Table 2.6 illustrates that the higher alcohol synthesis typically takes place at 250-325 °C, 50-200 bar, $H_2/CO = 1$ mol/mol and GHSV = 2000-10000 h^{-1}. In comparison the dedicated methanol synthesis operates at a lower temperature and pressure (225 °C - 275

29

°C, <100 bar) with a more hydrogen rich feed (often 80-90 vol% H_2), and typically also with a higher space velocity [92-97].

Table 2.6 Typical operating conditions for various higher alcohol synthesis processes reported in the literature [31].

Catalyst	T [°C]	P [bar]	H_2/CO [mol/mol]	Feed CO_2 [vol%]	GHSV[‡] [h^{-1}]	CO conv. [mol%]
K/ZnO/Cr[*]	350-425	90-200	2-3	0-3	3000-15000	14
K/Cu/Zn/Al	270-300	60-100	0.5-2	0-1	400-6000	20-60
K/Cu/Co/Al	260-340	60-200	1-2	2-4	3000-6000	12-15
Cs/Cu/ZnO	275-325	50-100	0.45-1	0	3000-7000	10-20
K/MoS$_2$ or K/Co/MoS$_2$	255-325	30-200	1	0	2000-10000	10-20

[‡] Gas at standard conditions i.e. T = 25 °C and P = 1 atm
[*] Typical contains minor amounts of Cu: $K_{0.23}Cu_{0.018}ZnCr_{0.33}$

The present studies have predominantly focused on MoS_2-based catalysts, and in the subsequent section this catalytic system is treated in greater detail.

2.3   Molybdenum sulfide catalysts

Sulfides of molybdenum, perhaps promoted with group VIII metals like cobalt or nickel, are useful for a wide variety of catalytic reactions. A very important use of these systems is as hydrotreating catalysts in the removal of undesired heteroatoms like nitrogen, oxygen and sulfur from various petroleum streams in oil refineries [98-102].

Researchers at Dow Chemicals [13, 103, 104] and Union Carbide [105-108] found that alkali promoted molybdenum is able to produce mixed alcohols from syngas at elevated pressure. The Alkali/Mo catalysts can be used in the metallic form [18, 109-114] as well as in the form of carbides [18, 114-122], oxides [18, 114, 123], phosphides [124-127] and sulfides [18, 114], with the sulfide reportedly being the preferred state of the catalyst [18, 114]. Presumably for this reason most work on molybdenum based catalysts seems to have focused on the sulfided state, and the sulfide is also the main focus in this work. The alkali promoted sulfides primarily produce linear n-alcohols. Short chained hydrocarbons and particularly methane constitute the primary by-products of the synthesis. The main oxygenated by-products of the synthesis are reported to be methyl and ethyl esters [13, 75]. Molybdenum may be replaced by tungsten or rhenium, but molybdenum is the preferred active material [104]. Inclusion of group VIII metals like Co, Ni and Fe in the catalyst formulation has been observed to shift the product distribution towards higher alcohols [18, 128-130].

2.3.1 Structure of the sulfide

Substantial work has been conducted to clarify the structure and properties of the commercially important MoS_2-based hydrotreating catalysts. EXAFS investigations show that in supported molybdenum sulfide catalysts the sulfide exists as an MoS_2-like phase on the support [131, 132], and similar results from investigations of supported K/MoS_2 indicate that is also the case for the alkali promoted catalyst [133, 134]. MoS_2 has layered structure with a sheet of Mo atoms between two sheets of sulfur atoms. The sulfide has a hexagonal structure with Mo atoms placed in the triagonal-prismatic holes in the plane between the sheets of sulfur. Figure 2.1 shows a top and side view of the MoS_2 structure. The $MoS_2(0001)$ basal plane is essentially inert [135, 136], and several studies with probe molecules like NO, CO and O_2 have revealed that the catalytic activity of MoS_2 is related to the edges of the sulfide [137, 138]. MoS_2 can be terminated by two low index planes, namely the the $Mo(10\overline{1}0)$ edge and the $S(\overline{1}010)$ edge [139, 140]. These edges are described as respectively the Mo edge and the S edge due to the element nominally exposed at the two edges. Energetically the exposure of the naked metal atoms is however unfavourable, and depending upon the conditions the Mo atoms at the $(10\overline{1}0)$ edge are typically covered by sulphur monomers or dimers [140-143]. The arrangement of sulfur at the edges at different levels of sulphur coverage is depicted in figure 2.1.
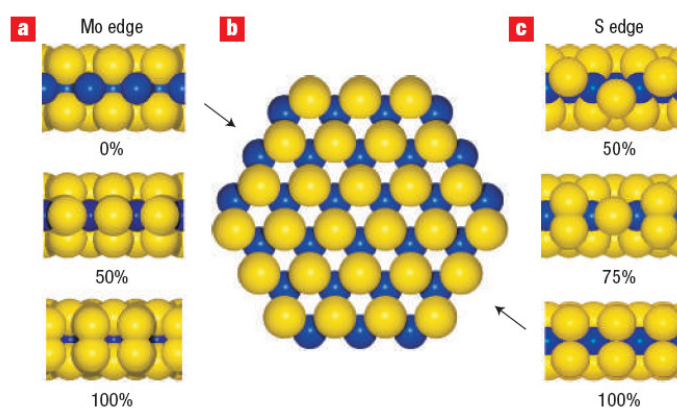
Figure 2.1 Ball model of a hexagonal MoS_2 nanocluster exposing both the $S(\overline{1}010)$ and $Mo(10\overline{1}0)$ edges along with depictions of the most stable edge structures. Blue atoms represent Mo, while yellow atoms represent S. a) Side view of the Mo edge of the cluster at 0, 50 and 100 % sulfur coverage; b) hexagonal slab of MoS_2; c) Side view of the S edge of the MoS_2 cluster at 50, 75 and 100 % sulfur coverage. This figure is reproduced from Lauritsen et al. [139].

The structure of the sulfide particle is dictated by the relative stability of the S and Mo edges, which again depends upon the prevailing atmosphere [140, 144]. If the sulfide particle is formed in a highly sulfiding atmosphere (H_2S/H_2 = 500 mol/mol) the dimer covered Mo edge is the most stable termination of the particle, and this causes the particle to attain a triangular shape, where only the Mo edge is exposed [140]. If synthesized in a more hydrogen rich atmosphere (H_2S/H_2 = 0.07 mol/mol) the adsorption of hydrogen at

the edges serves to stabilize the S edge relatively to the Mo edge, and for this reason the sulfide particle attains a more truncated hexagonal shape that exposes both edge types [140]. Experiments by Lauritsen et al. [140] indicated that the morphology of the nanoparticles on a gold support does not easily change with reaction conditions once the particles have been synthesized. The sulfidation conditions may therefore have a pronounced effect upon the catalytic properties.

In hydrotreating reactions it has, since the early proposals by Lipsch and Schuit [145] and Kolboe [146], been the theory that the catalytic activity predominantly was related to sulfur vacancies at the edges. The formation of such sulfur vacancies, generated by dosing of atomic hydrogen to the nanoclusters, has been depicted by STM [147]. Using infrared spectroscopy Travert et al. [148] observed that the intensity of bands related to CO adsorbed on MoS_2 decreased with increasing exposure of the catalyst to H_2S, while the band intensity increased with H_2 treatment. This result could suggest that the amount of CO adsorption sites is related to the number of vacancies, which would be increased by reducing treatment and decreased through blocking with sulfur derived from H_2S. Vacancy sites are however not the only source of catalytic activity for the sulfide. Recently STM investigations have revealed the presence of a bright brim parallel to the edges of the sulfide [139, 147, 149, 150]. This brim reflects a region of high electron density that is formed due to perturbation of the electronic structure near the edges of the sulfide [151]. A theoretical analysis of the electronic structure reveals the existence of one dimensional edge states that cross the Fermi level, and thereby are metallic in character. The presence of the brim was first discovered on model systems supported on gold, but also carbon supported MoS_2 shows this characteristic brim [152]. Recent investigations indicate that the metallic brim sites are very important for the activity of the sulfide [135, 150]. The hydrogenation activity of the MoS_2 slab is believed to be related to the brim along the top edge of the sulfide slab [151, 153]. The sulfide is able to dissociate H_2, and spectroscopic investigations have shown that hydrogen is present in the form of S-H groups on the surface [154, 155]. Recent DFT calculations and STM images indicate that hydrogen is adsorbed on both the Mo and S edges, where the H atoms are located as S-H species adjacent to the brim on outermost row of sulfur atoms on both edges [135, 140, 152, 156].

In connection with hydrotreating reactions it has been observed basic nitrogen compounds inhibit the activity of the sulfide catalyst [157], and it has been reported that it is especially the hydrogenation activity of the sulfide, which is inhibited by these basic nitrogen containing compounds [158]. It would be interesting to clarify, how basic nitrogen compounds influence the properties of the alcohol synthesis catalyst. It could be envisioned that a hampered hydrogenation activity could limit the hydrocarbon formation and thereby improve the alcohol selectivity. In section 7.4 it is investigated how a basic nitrogen compound, namely ammonia, influences the properties of the sulfided alcohol synthesis catalyst.

2.3.2 The alkali promoter

The preceding treatment has introduced some of the basic properties of the sulfide, but the sulfide alone does not constitute an alcohol synthesis catalyst. Without an alkali

promoter the sulfide produces essentially no alcohols in CO hydrogenation, regardless of the conversion level [31]. The addition of an alkali promoter to the sulfide causes a decrease in hydrotreating activity and a very significant decrease in the activity for both hydrogenation of ethene and methanation of CO [52]. Very importantly the addition of the alkali promoter shifts the product distribution in high pressure CO hydrogenation from hydrocarbons towards alcohols [159].

Several surface science studies have investigated the deposition of alkali metals on MoS_2. At low coverage deposition of an alkali metal on MoS_2 results in a disordered overlayer of strongly ionized adspecies. At higher coverage the alkali adspecies begin to form 2D islands and further alkali deposition yields 3D structures [160, 161]. For alkali adsorption on the $WS_2(0001)$ surface, which has the same structure as $MoS_2(0001)$, it is observed that the alkali addition causes the largest attenuation of the W signal in ion scattering spectroscopy [162], and this has been interpreted in the way that the alkali adatoms occupy the trifold hollow sites directly above the metal atoms [162]. DFT calculations suggest that this is also the preferred adsorption site on MoS_2 [163]. DFT calculations on a Mo_7S_{14} cluster have also indicated that the brim of the sulfide cluster may be the preferred adsorption site [164]. The reduced hydrogenation activity of the alkali promoted sulfide could very well be related to a position of the alkali adspecies at the brim of the sulfide. Jiang et al. [134] report that the adsorption capacities of both CO and H_2 (as well as O_2) decrease with increasing alkali content, but their experiments do not provide any information about effect upon the relative coverages.

Several researchers [162, 163, 165-167] have investigated the effect of alkali deposition on the basal (0001) plane of MoS_2 and WS_2. The alkali deposition causes the emergence of a weak density of states at the Fermi level, and the alkali promoted basal plane therefore also becomes weakly metallic in character. This means that the normally inert basal plane after alkali promotion has been observed to adsorb a range of electronegative adsorbates – including species like H_2O, alcohols and ketones that could play a role in the alcohol synthesis [163, 168, 169]. The alkali induced density of states at the Fermi level for Alkali/$MoS_2(0001)$ is observed to disappear upon adsorption of the various adsorbates, and charge may thus be transferred to the adsorbates [163]. It can thus not be excluded that the normally inert basal plane of the sulfide plays a role during the alcohol synthesis. If the reaction involves the entire surface, while the hydrogenation activity is confined to the brim of the particles, this could be related to the relatively good selectivity of the sulfide catalyst.

There are varius proposals regarding the reason for the promotional effect. Santiesteban et al. [75] described the effects of the alkali dopant as being twofold. One effect is in aiding the activation of CO, although the effect according to Santiesteban et al. [75] mainly leads to hydrogenation without breakage of the C-O bond. The other effect of the alkali dopant is according to Santiesteban et al. [75] as a suppressant of the hydrogenation ability of the catalyst through site blocking on the sulfide surface. This suggestion would be in line with the abovementioned preference of the alkali adspecies for the brim-sites associated with the hydrogenation activity. Anderson and Yu [170] have suggested that the role of the promoter is to interact with oxygen in various adjacent oxygenated intermediates and products. This provides a stabilization of the oxygenated species, which directs the synthesis towards alcohols rather than hydrocarbons. The interaction with the alkali adspecies may provide an energetic stabilization, and the alkali

adspecies could also physically block the access of hydrogen to the oxygenated species [170].

There are also some indications that the alkali species need to be present at the surface of the catalyst to promote alcohol formation [171]. Upon exposure of the sulfide to atmospheric air the sulfide is at least partially oxidized, and this causes the alkali atoms to segregate into the bulk of the sulfide. From this position the alkali species have been observed only to promote hydrocarbon chain growth and not alcohol formation [171-174]. What also appears to be certain is that the alkali promoter affects the CO adsorption upon the catalyst. For an unpromoted catalyst the adsorption of CO gives rise to characteristic IR bands in the 2000-2200 cm^{-1} range [52, 175-178], and these bands are believed to be related to CO adsorbed at the edges of the sulfide [179, 180]. These characteristic bands disappear almost entirely upon alkali promotion, but are replaced by a new series of bands in the 1350-1650 cm^{-1} range [52, 171, 178]. Some of these new bands have been assigned to formate species [52, 178], while Woo et al. [171] have observed bands at 1400 at 1650 cm^{-1}, which they assigned to "bicarbonate like" C-O-K and C-O-H species. Woo et al. [171] propose that the role of the alkali promoter is in the formation of a C-O-K species. The existence of such species could support the notion of the alkali adatoms stabilizing adjacent oxygenated intermediates, but it should be emphasized that C-C stretches in aromatic (1550-1630 cm^{-1}) and aliphatic (1400-1500 cm^{-1}) deposits on normal hydrotreating catalysts are observed at similar wavenumbers [176].

Generally it is reported that the heavier alkalis are preferable to Li or Na, but there are varying reports concerning the ranking among K, Rb and Cs. Kinkade [105, 107] reports the order of promotion to be:

Cs > Rb > K > Na > Li

Contrary to this ranking Iranmahboob et al. [181] found K to be a better promoter than Cs, and Woo et al. [182] found the order of promotion to be K > Rb > Cs. Potassium is also stated to be the preferable promoter in some patents [18, 183]. Koizumi et al. [184] on the other hand observed the order to change with the MoS$_2$ BET area, but with Rb and Cs generally being better promoters than K. The reason for this scattering of the results could well be that the effects of K, Rb and Cs are so similar that the differences might easily be countered by other uncontrolled factors. Given the similar effects of Rb, Cs, and K there may be litte little economic incentive to any other alkali metal than potassium.

The general effect of alkali addition is an increase in alcohol selectivity and productivity with a corresponding decrease in hydrocarbon selectivity and productivity. At higher dopant levels the alcohol selectivity begins to stagnate, and the alcohol productivity begins to decrease. There are varying reports concerning the optimal level of the alkali dopant, but the general consensus is that a high dopant level is required. Santiesteban et al. [75] studied a CsOOCH/MoS$_2$ catalyst at 295 °C, 83 bar and H$_2$/CO = 0.96 and found the optimal CsOOCH content to be around 20 wt%. At similar conditions, but with a lower temperature of 256 °C the optimum dopant level was found to be 8-10 wt% CsOOCH [31]. Youchang et al. [159] studied a K$_2$CO$_3$/MoS$_2$ catalyst at 250 °C, 69 bar and H$_2$/CO = 1. They found that the alcohol selectivity increases linearly with the K$_2$CO$_3$/MoS$_2$ weight ratio up to a ratio of around 0.2 (17 wt% K$_2$CO$_3$ in the formulation),

but the alcohol selectivity then stagnates and shows little change for K_2CO_3 contents above 30 wt%. Iranmahboob et al. [185] investigated a $K_2CO_3/Co/MoS_2/$clay catalyst at 140 bar and temperatures from 290 °C up to 320 °C and found the optimal K_2CO_3 content to be 12.5 wt% at a Mo/Co molar ratio of 2. It is generally observed that the optimal alkali content increases with increasing temperature, as the inherent tendency towards hydrocarbon formation increases [185-187].

The alkali promoter can be mixed with the active materials in the solid state using a mortar and pestle or alternatively the promoter can be added from an aqueous solution [75, 188]. At least when dry mixing is used the alkali promoter is initially very unevenly distributed across the surface, but during exposure to syngas the alkali species spread across the surface [171, 181]. To be a good alcohol promoter the alkali species must readily remove its counter-ion and spread itself evenly across the surface [173].

According to Lee et al. [173] a measure of this property to spread across the surface is the magnitude of the pK_a value of the conjugate acid to the basic counter ion to the alkali promoter (for KCl the low pK_a value of HCl for example implies that the salt is reluctant to spread across the surface, and KCl therefore does not constitute a good alkali promoter). Lee et al. [173] certainly found that the alcohol space time yield of an alkali promoted MoS_2 catalyst increases linearly with the pK_a-value of the conjugate acid to the basic counter ion.

It is generally reported that a freshly sulfided catalyst requires a period of 10-20 hours at reaction conditions to reach a stable activity [171, 173, 178, 188]. During this initial period the alcohol selectivity increases, while the CO conversion decreases. It is possible that this slow initial approach to steady state is associated with the spreading of the alkali promoter across the surface, since unpromoted sulfides do not show this slow initial approach to steady state. Catalysts promoted with alkali salts, which do not exhibit this uniform spreading (e.g. KCl, K_2SO_4) exhibit limited alteration in properties during this initial period [171, 173, 178, 182].

2.3.3   Promotion by group VIII metals

It is well established that addition of group VIII metals like Co and Ni improve the activity of MoS_2-based hydrotreating catalysts [98, 189-193]. In parallel to this addition of Co [13, 19, 129, 185, 194-196], Ni [13, 129, 197-199] and Fe [13, 129] to alkali promoted MoS_2-based catalysts also has a promotional effect upon the alcohol synthesis. The promotional effect is also observed, if MoS_2 is replaced with ReS_2 or WS_2 [129]. In the patent literature Co is generally reported to be the preferred promoter [128-130], and presumably for this reason most research seems to have focused on this element. As it will be discussed in greater detail subsequently the state of the group VIII metal promoter has not been fully clarified. In the present work a notation of the type $K_2CO_3/Co/MoS_2$ is adopted for promoted catalysts, but holds no assumptions regarding the state of the group VIII metal promoter. Table 2.7 provides a comparison between unpromoted K_2CO_3/MoS_2 and catalysts promoted with Co, Ni and Fe [129].

It has been observed that the addition of Co or Ni to the catalyst can improve both the activity and selectivity of the sulfide, and as it is illustrated in table 2.7 the group VIII

metals also cause a significant shift towards the higher alcohols [16, 19, 129, 194, 196]. Furthermore the alcohol selectivity of these doubly promoted (alkali and group VIII metal) catalysts is less influenced by temperature than the basic Alkali/MoS_2 system [13]. This means that the catalysts can be operated above 300 °C and still provide a high CO_2-free alcohol selectivity, and selectivities above 80 mol% has been observed [13]. It has also been reported that further promotion of a K/Ni/MoS_2 catalyst with Mn [16] or La [200] provides an additional improvement in catalyst performance. The role of the group VIII metal is as a promoter and not as an alcohol synthesis catalyst in its own right. Potassium promoted cobalt sulfide on a carbon support is reported to yield only C_1-C_4 alkanes with a low activity in CO hydrogenation [194].

Table 2.7 Comparison of K_2CO_3/MoS_2 to K_2CO_3/Me/MoS_2 (Me:Mo = 1:2 mol/mol) [129]. The experimental conditions are: P = 104.5 bar, H_2/CO = 1.01 ± 0.03 mol/mol, 50 ppm H_2S.

Catalyst	K_2CO_3/MoS_2	K_2CO_3/Co/MoS_2	K_2CO_3/Ni/MoS_2	K_2CO_3/Fe/MoS_2
T [°C]	265	305	300	321
GHSV [h^{-1}]	1200	1300	1330	1480
CO conv. [mol%]	33.1	39.0	33.1	27.1
CO conv. $\left[\frac{g_{CO}}{g_{cat}\cdot h}\right]$	0.19	0.23	0.26	0.27
CO_2 selec. [mol%]	31.3	33.5	32.9	36.9
CO_2-free carbon based selectivities [mol%]				
CH_4	20.2	12.6	18.0	7.4
C_{2+} hydrocarbons	4.3	5.7	2.7	16.4
Methanol	32.3	16.1	15.2	6.9
Ethanol	31.8	39.9	41.8	21.0
Propanols	7.7	14.9	11.5	17.9
Butanols	1.6	4.3	1.4	10.8
Pentanols	0.2	0.5	1.5	7.1

For hydrotreating catalysts numerous investigations have sought to elucidate the state and effect of the group VIII metal in the sulfided catalyst. Using various spectroscopic techniques Topsøe et al. [132, 201-204] discovered that the promoting effect of cobalt for hydrotreating catalysts is due to the formation of a mixed sulfide, which the authors termed the Co-Mo-S phase. It was found that in the Co-Mo-S phase the promoter exists in an MoS_2-like mixed sulfide. Here Co replaces Mo at the edge of the sulfide, and Co exists in the same plane as molybdenum, although not at perfect Mo edge sites [205]. This substitution takes place at the S edge of the mixed sulfide [141, 206-208]. Promotion of MoS_2 with Ni results in the formation a similar Ni-Mo-S phase, and promotion with Fe also seems to yield a Fe-Mo-S structure [138, 208-210]. Recently a Cu-Mo-S structure was also observed with STM [211], and there are also indications [212] that Cu can confer a promotional effect to the sulfide in the alcohol synthesis. Figure 2.2 shows an STM image of the Co-Mo-S structure along with a ball model that illustrates the location of the promoter atoms.
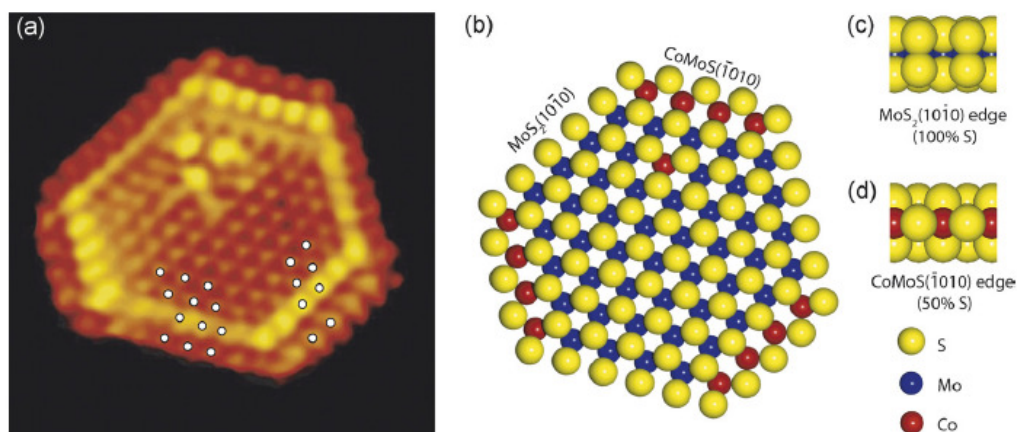
Figure 2.2 a) STM image of the Co-Mo-S structure. The bright cluster inside the basal plane is believed to arise from incorporation of a Co atom into the interior structure of the mixed sulfide. Notice also the bright brim along the edge of the particle. b) Ball model of the Co-Mo-S particle showing the location of the promoter atoms. c) Ball model illustrating the dimer covered Mo edge. d) Ball model illustrating a monomer covered S edge with the outer layer of Mo atoms replaced by Co. The figure is reproduced from Lauritsen et al. [208].

The incorporation of the group VIII promoter into the sulfide has a significant effect on both the structure and the properties of the catalyst. The presence of for example Co at the S edge serves to stabilize this edge compared to the Mo edge, and for this reason Co/MoS_2 has a more truncated hexagonal shape than pure MoS_2, when sulfided at similar conditions [207].

As described above alkali promoted cobalt sulfide is not an alcohol synthesis catalyst on its own. For the alcohol synthesis catalysts it is not well established, if the promotional effect of cobalt also is connected to the formation of a Co-Mo-S phase, although it has been suggested that this is the case [194, 213]. A comparison of EXAFS investigations could also suggest that the Co-S bond length in doubly promoted alcohol synthesis catalysts [195] is similar to the Co-S bond length in the Co-Mo-S phase [209, 214]. In EXAFS investigations Li et al. [194] reported a Co-Mo coordination in sulfided alcohol synthesis catalysts, but there seemed to be no clear relationship between the observed Co-Mo coordination numbers, and the catalytic properties. Furthermore Murchison et al. [13] observed that cobalt promoted catalysts, for which the XRD patterns showed clear signs of the isolated cobalt sulfide, Co_9S_8, were less efficient and behaved much like regular MoS_2 without the Co promoter. These observations generally point towards a Co-Mo-S phase as the active phase in the promoted catalyst, but there are also observations that make it difficult to rule out a contribution from isolated cobalt sulfide species. As described above an important role of the group VIII promoter is to promote the chain-growth and shift the product towards the desired higher alcohols. As it will be discussed in greater detail subsequently the chain-growth for the sulfide catalysts can occur by addition of CO to an alkyl group to form an acyl species that can be hydrogenated into the corresponding alcohol [75, 187]. Alternatively chain-growth can take place by alcohol coupling reactions, which seem to occur via an aldol condensation pathway [215]. Calafat and Laine [216, 217] studied the use of sulfide catalysts for the carbonylation of

methanol, a reaction that is closely related to the CO addition reactions occurring in the course of the regular alcohol synthesis. Calafat and Laine [216, 217] observed that the mixed cobalt-molybdenum sulfide was superior to either of the individual sulfides, but they also [216, 217] observed that cobalt sulfide had an appreciable activity for the addition of CO to methanol, while molybdenum sulfide was inactive. This could suggest that also isolated cobalt species, if they are present in the right form, could benefit the chain-growth over the sulfide catalyst. For the alcohol coupling reactions that constitutes the alternative chain-growth pathway it is difficult to find any information about the properties of cobalt sulfide, but supported cobalt has been reported [218] to exhibit an activity for this reaction. Overall it seems very likely that the promotional effect of group VIII metals like cobalt can be traced back to a Co-Mo-S type mixed sulfide. It is however possible that isolated cobalt sulfide species, save larger Co_9S_8 particles, can contribute to the chain-growth reactions.

In chapter 8 it is investigated, whether or not changes in the state of the cobalt chain-growth promoter can help to explain a gradually declining production of higher alcohols, when a cobalt-molybdenum sulfide catalyst is operated in sulfur free syngas.

There are various reports concerning the ideal amount of the group VIII metal promoter in the catalyst formulation. In the patents from Dow Chemicals [128-130] it is reported that the process can operate with a wide variety of Mo/Co ratios, but that a molar ratio of Mo/Co = 2 is preferred. A more recent patent [183] reports an optimum ratio in the 1.1-2 range. Iranmahboob et al. [185] have investigated a series of catalysts and these authors also report that catalysts prepared for a molar Mo/Co ratio of 2 exhibit the best performance. Li et al. [194] also observed the best performance for a molar ratio of 2. Some of these optimal Mo/Co ratios seem a bit low compared to the amount of Co that can be accommodated at the S-edge of the Co-Mo-S structure. As an example the Co-Mo-S particle illustrated in figure 2.2 has a ratio of Mo/Co ~ 4 mol/mol, but one must of course expect that not all added cobalt is incorporated into the mixed sulfide.

2.3.4 Role of the support

It is reported that the sulfide catalyst can be prepared from both oxide and sulfide precursors, but the sulfide precursors do reportedly yield better alcohol synthesis catalyst [13]. Despite this fact all the catalysts employed in the present investigations are prepared in the oxide form and then sulfided. One difference that has been observed between the use of sulfide and oxide precursors is that Brorson et al. [219] in a TEM study found that the sulfide precursors yield a more well-ordered structure of the prepared sulfide. It is certainly possible that a more well-ordered structure of the sulfide could lead to a more well-controlled CO hydrogenation and thereby a more selective catalyst.

In the patent literature [18, 103] it is stated that the unsupported sulfide is the preferred state of the catalyst, but that the active materials might be supported on suitable carriers like carbon, Al_2O_3, SiO_2 and MgO. In the patent literature it is reported that the support should be basic or should be rendered so by the addition of the basic alkali dopant, and it is generally reported that carbon is the preferred support material for the alcohol synthesis catalyst [18, 103]. For similar hydrotreating catalysts the support is usually alumina, because a large support surface area and a strong interaction with the sufide phase yields

highly dispersed sulfide particles [98]. It is however known that the use of a carbon-support can yield highly active hydrotreating catalysts [98, 220, 221].

For the alcohol synthesis Murchison et al. [13] compared a carbon supported sulfide to an alumina supported one and found the alcohol selectivity to be substantially higher with the carbon supported catalyst. It is interesting to notice that Murchison et al. [13] did not observe any dimethyl ether (DME) formation over either of the two supported catalyst. Bian et al. [14] have investigated different K/MoS_2 catalysts and found that the selectivity of the catalysts observes the following order:

Unsupported > SiO_2 support > Al_2O_3 support

The differences between the various supports have typically been explained in terms of the support acidity and thereby the activity of the support for alcohol dehydration. Acidic oxides can catalyze the dehydration of alcohols into ethers – for example the formation of DME from methanol [222, 223]. Acidic supports like alumina should thus not be suitable supports, while supports like carbon and silica, which are essentially neutral in this respect [224, 225], should be more suitable carriers for the active materials. However the acidity of the catalyst is to some extent suppressed, as the active materials are deposited on the support. As an example the deposition of the active components on alumina to a significant extent quells the inherent acidity of the support, since the active components primarily anchor to the strongest acid sites on the surface [226-228]. On the alumina supported catalyst the activity for ethanol decomposition is also significantly decreased at higher metal loadings [228]. The support acidity should therefore be less of a problem in the final, alkali promoted catalyst.

It is interesting to observe that the abovementioned comparison of carbon and Al_2O_3 by Murchison et al. [13] showed no indication of DME formation, which would have been expected, if alcohol dehydration on acidic support sites is the dominant reason for the lower selectivity of the alumina supported sulfide. Another contributing factor to the inferiority of the Al_2O_3-supported catalyst could be that alumina has a stronger interaction with the sulfide, which is detrimental to the alcohol synthesis activity of the sulfide. Candia et al. [229] observed that sulfidation of alumina supported Co-Mo catalysts at high temperature (>875 K) rather than at 675 K yielded more active hydrodesulfurization catalysts. The authors termed the sulfide formed at low sulfidation temperature *Type I* sulfide and the sulfide formed at higher temperature *Type II* sulfide. Candia et al. [229] hypothesized that the difference between these two sulfide structures was that the Type I variety had remaining Mo-O-Al linkages to the support, while the Type II sulfide did not. The presence of such linkages has since been indicated by experimental observations using a variety of experimental techniques [230-233]. DFT calculations by Hinnemann et al. [234] have indicated that the linkages are present at the outermost S edge of the sulfide slabs. Furthermore these DFT calculations have indicated that these oxygen linkages cause a drastic increase in the energy required to form sulfur vacancies in the vicinity of the linkages, and the hydrogen adsorption energy above or near the oxygen linkages is also significantly affected by the their presence [234]. This could imply that the hydrogenation activity of the sulfide is modified by the presence of the oxide linkages, something that is also indicated by studies of hydrotreating catalysts [235-238]. It has been reported that for Type II sulfides the individual slabs have a

39

tendency to stack on top of each other [205]. The tendency of the MoS_2 slabs to stack and form three dimensional structures is not necessarily an artifact of the Type II sulfide, but may simply originate from a larger surface mobility due to the weaker support interactions, since Type II sulfides can also be present in the form of single slabs on the support [239]. Apart from using high temperature sulfidation, which might result in undesired particle sintering, Type II sulfides can be obtained by using various additives or chelating agents in the preparation [232, 239-241] or by using supports that interact weakly with the sulfide. Examples of such weakly interacting supports could be carbon or silica [220, 221, 242].

It is interesting to notice that the preferable supports with respect to alcohol synthesis are in fact supports like silica and especially carbon that promote the formation of Type II sulfides. The modified hydrogenation ability of the Type I sulfide could have a detrimental effect upon the alcohol synthesis. The stacks of sulfide slabs found in Type II sulfides also have relatively fewer of the brim sites, to which the hydrogenation activity is believed to be confined. Such effects could contribute to the superiority of the supports favoring Type II structures.

Furthermore the patent literature states that the support, if present, preferably should compose 50-70 wt% of the formulation, which indicates that substantial loadings of active materials are required for the alcohol synthesis [18, 103]. For K/MoS_2 catalysts supported on both carbon [243] and alumina [228] the alcohol selectivity increases essentially monotonously with increasing metal loading, although the productivity per mass of active components will reach an optimal level.

There could be different reasons for the requirement of a large fraction of active materials in the formulation. As the fraction of active materials increases this will at least initially lead to more active sites and therefore to a greater activity, and that will enable operation at a lower temperature, where the selectivity is better. An increasing fraction of active materials will ultimately also lead to larger sulfide structures. Larger sulfide structures have relatively fewer brim sites compared to the sites on the basal plane and to the sites at edges of the stacked slabs. This should, as it is discussed above, lead to a relatively reduced hydrogenation activity that could favor the alcohol selectivity.

Based upon the preceding discussion the present work with MoS_2-based catalysts presented in chapters 5-8 has been conducted with carbon supported catalysts.

2.3.5 Catalyst stability

The discussion has hereto focused on the sulfide, and the catalytic properties have been discussed in terms of the properties of the sulfide. An element of uncertainty is however the long term stability of the sulfided state of the catalyst at alcohol synthesis conditions. Courty et al. [35] state that the catalyst requires 50-100 ppmv of H_2S in the syngas to retain the active sulfided state. However it seems that the sulfide catalyst is able to operate in the absence of sulfur sources in the feed. For $Alkali/MoS_2/C$ it has been observed [13] that the catalyst stabilizes in a sulfur free syngas, although it occurs after a protracted initiation period of approximately 100 h. Bian et al. [133] investigated a $K/MoS_2/Al_2O_3$ catalyst operated without H_2S in the feed and observed that it took 200 hours to reach a stabilized activity for the catalyst. Using XPS and total sulfur analysis

(combustion) they [133] found that the composition of the sulfide had changed from $MoS_{2.5}$ before the reaction to $MoS_{1.8}$ after 80 hours of reaction and to $MoS_{1.6}$ after 200 hours of reaction. EXAFS studies by Bian et al. [133] also showed that Mo-S coordination number as well as the Mo-Mo coordination number of the stable catalyst was significantly decreased compared to the freshly sulfided catalyst. It thus seems that the sulfide in a sulfur free syngas undergoes some alterations, before a stabilized catalyst is achieved. For sulfides promoted with group VIII metals there are conflicting reports concerning the stability of the catalyst. It has been reported [19, 128-130] that the cobalt promoted alcohol synthesis catalysts are unaffected by feed sulfur at levels up to around 100 ppmv, and that no benefit is achieved by having sulfur sources in the gas. While some authors [15] mention that the catalytic properties essentially are unaltered by extended exposure to sulfur-free syngas, other investigations have however indicated that operation with a sulfur free or sulfur poor syngas leads to a gradual decline in the fraction of higher alcohols in the product [186, 244]. In the present work the investigations in sections 5.2 and 8 seek to evaluate the stability of $K_2CO_3/Co/MoS_2/C$ catalysts in both H_2S-containing and H_2S-free syngas. Section 5.6 also contains a discussion of the changes that may occur to the sulfide in a sulfur free syngas.

As stated above the sulfide catalyst seems to undergo some changes during operation in a sulfur free syngas, although the stabilised form of the sulfide catalyst in a sulfur free syngas is matter of some uncertainty. Using thermodynamic data from Barin [65] and assuming ideality in gas and solid phases it can be determined that molybdenum carbide is the stable phase at typical alcohol synthesis conditions without H_2S in the gas. Assuming an ideal solid phase could however be a severe error for the nanoscale particles. Even for hydrotreating reactions it has however been suggested [245-247] that the stabilized from of the catalyst is a sulfide core with an outer shell of metal carbide, and the same situation could potentially be possible for the alcohol synthesis catalyst. As it will be discussed subsequently alkali promoted carbides of molybdenum have been shown to posses an activity for the alcohol synthesis, so the possibility of a carbide or surface carbide as the stabilised form of the catalyst cannot be excluded.

Concerning the long time stability of the catalyst Dow Chemicals conducted an extended life test for 9 months with an Alkali/MoS_2/C catalyst, and during that period the activity (19 mol% CO conv., 80 mol% CO_2-free alcohol selctivity) was maintained with a ~20 °C temperature increase (290-310 °C) [13, 74]. Unfortunately the detailed reaction conditions for this test are not available.

2.3.6 Reaction conditions

The alcohol synthesis is a kinetically controlled reaction that benefits from a high reactant pressure, a relatively low temperature and a relatively short residence time. Increasing conversion is as a rule linked to a decreasing alcohol selectivity [74], and the parameter space available for the reaction constitutes the region, where an acceptable alcohol selectivity can be achieve at a reasonable conversion. Generally 240-325 °C is reported as the relevant temperature range for the alcohols synthesis, with the doubly promoted catalysts exhibiting the best temperature stability in terms of alcohol selectivity [13, 18, 103]. For a fixed pressure increasing temperature shifts the selectivity towards

hydrocarbons, but within the relevant temperature range increasing temperature generally also favours chain growth [12]. The temperature, at which the alcohol selectivity will become unacceptably low, will thus depend upon the pressure.

In terms of the reaction pressure the trend is that increasing pressure shifts the selectivity towards alcohols, and high operating pressures are typically needed to obtain a good alcohol selectivity [159]. Operating pressures are generally reported to be in the 30-200 bar range, and the preferred pressure range for an industrial process is reportedly between 80 and 120 bar [18, 103, 183]. For an industrial application of the synthesis the operating pressure will represent a compromise between alcohol selectivity/productivity and compression duty, so economic constraints are likely to govern the actual reaction pressure.

For the kinetically controlled alcohol synthesis it is reported that the alcohol selectivity generally increases with increasing space velocity (decreasing residence time) [186], and also the productivity increases with increasing space velocity [13]. This tendency indicates that hydrocarbons are formed from alcohols as secondary products in the reaction. Alcohols are compared to hydrocarbons thermodynamically unfavorable products at the process conditions, and an increasing conversion will therefore generally lead to a decreasing alcohol selectivity [74]. The chain-growth will on the other hand suffer from an increasing space velocity. This is presumably related to the fact that re-adsorption and elongation of shorter alcohols is an important pathway in the formation of higher species [186]. The space velocity employed should generally be in the 100-24000 h^{-1} range [18, 103, 105, 107]. In the patent literature it is commonly suggested that the space velocity should be in the 2000-5000 h^{-1} range [18, 103], although the Union Carbide patents [105, 107] suggest the use of an even higher space velocity - preferably in excess of 12000 h^{-1}.

The parameter set employed in the present investigations is typically 325 °C, 100 bar, 2500-5000 h^{-1}.

With respect to the feed composition it is reported [18, 103] that the catalyst can operate with a wide range of H_2/CO ratios, but that a ratio in the range of 0.7-1.2 mol/mol is preferred. This range is in the vicinity of the stoichiometric feed for the formation of ethanol assuming a full shift of co-produced water. The H_2/CO ratios commonly encountered in syngas derived from gasification of coal and biomass (see table 2.5 on page 26) are thus relatively close to the optimal composition with respect to alcohol synthesis. In section 7.2 it is investigated, how the feed composition influences the catalytic activity.

The presence of CO_2 in the syngas feed is generally reported to have a detrimental effect upon the alcohol synthesis over MoS_2 based catalysts. In the patent literature [18, 103] it is recommended that the partial pressure of carbon dioxide is kept below 1 bar at the reactor entry. It is reported that the overall productivity of the catalyst decreases with increasing CO_2 concentration in the feed. The production of higher alcohols and hydrocarbons are more severely affected than the production of C_1 products i.e. CO_2 shifts the product distribution towards shorter chain length [15, 248]. An additional undesired effect arising from the presence of CO_2 in the feed stream is a reallocation of the water-gas shift equilibrium towards H_2O and CO. This lowers the removal of of produced water in the water-gas shift reaction and increases the water content of the

condensed reaction product. This is undesirable, when the alcohol product is intended for fuel use, since the water level in this case should be kept as low as possible.

Gang et al. [15] employed a $K_2CO_3/Co/MoS_2/C$ catalyst operated at the conditions P = 100 bar, GSHV = 6000 h^{-1}, H_2/CO = 2.33, 290-340 °C, and their results indicate that the water gas shift reaction, at least at temperatures above 300 °C, is close to equilibrium. Given that MoS_2-based catalysts are used as dedicated water-gas shift catalysts [51], it does not seem unreasonable that the water gas shift reaction is relatively rapid compared to the synthesis reactions and therefore is able to reach equilibrium.

In section 7.3 the influence of H_2O in the syngas is investigated and the reason for the effects of H_2O/CO_2 is discussed in greater detail. Due to the significant water-gas shift activity of the sulfide catalyst H_2O and CO_2 are largely parallel products in the synthesis reactor.

Although it was described in the previous section that the Alkali/MoS_2 based catalysts can operate both with and without sulfur sources in the syngas, it is observed that Alkali/MoS_2 catalysts are significantly affected by the presence of H_2S or other sulfur sources in the feed. It is generally reported that an increasing concentration of H_2S in the syngas feed causes an increasing shift the selectivity from alcohols towards hydrocarbons, but the presence of hydrogen sulfide also favors chain growth [15, 19, 249]. Murchison et al. [13] report that the effect of H_2S in the feed is much lower for unsupported Alkali/MoS_2 catalysts, than for carbon supported catalysts. The role of H_2S and other sulfur sources is most likely to replenish sulfur that is lost from the catalyst in the reducing syngas atmosphere. It is difficult to know, if bulk sulfides have a greater stability in a sulfur free atmosphere or just a longer period of stability, because the bulk of the material acts as a sulfur storage that counteracts a loss of sulfur in the reducing atmosphere. The reason for the effects of the feed sulfur level will be discussed in greater detail in sections 5.6 and 5.7, which contain a disscussion of the presently observed effects of the feed sulfur level.

In the previous section it was described that catalysts promoted with group VIII metals have been reported not to be influenced by feed sulfur up to a level of 100 ppmv [19, 128-130]. In section 5.2 of this work the effect of the H_2S level upon a $K_2CO_3/Co/MoS_2/C$ catalyst is investigated, and also for this catalyst it can be observed that the effect of H_2S is very different above and below 100 ppmv H_2S. As it will be discussed in section 5.6 and in chapter 9 there are marked, gradual changes in the catalytic properties, when a $K_2CO_3/Co/MoS_2/C$ catalyst is operated in sulfur poor (<100 ppmv) or sulfur free syngas, and these changes are most likely linked to a net loss of sulfur from the catalyst.

2.4 Molybdenum carbide based catalysts

MoS_2-based catalysts have been the clear focus of this work, and most of the reports of alkalized Mo-based catalysts in the literature have focused on sulfides, but as it will be described in greater detail subsequently, the sulfided catalysts have some problematic issues. These issues are related to the stability in a sulfur free syngas and related to incorporation of feed sulfur into the liquid alcohol product. For this reason the present

work has also evaluated the alkali promoted bulk carbides Mo_2C, WC and NbC as catalysts for the alcohol synthesis. Those investigations are presented in chapter 9.

Woo et al. [115] provided the first systematic investigations of alkali promoted molybdenum carbides as alcohol synthesis catalysts and established the systems ability to produce alcohols in high pressure CO hydrogenation. In recent years Xiang et al. [117-122] have conducted several investigations of alcohol synthesis over molybdenum carbides.

Very importantly the use of the carbide circumvents the risk of incorporating sulfur species into the alcohol product. Another interesting aspect is that the carbides can exhibit properties that resemble those of more noble metals. As it was touched upon in section 2.2, catalysts based upon the noble metal rhodium are interesting, because these catalytic systems have achieved fairly high selectivites to ethanol at even reasonably high conversion levels [78, 86-88]. With the high cost of rhodium it would however be attractive to develop cheaper catalysts that emulate the attractive qualities of rhodium, and here the carbides could be a possibility. A carburization has been observed to exert an ennobling effect upon early transition metals that makes the properties of the carbides similar to the more noble metals [250], and previous researchers have observed an activity for the alcohol synthesis with carbides of at least molybdenum and tungsten [115, 251].

2.4.1 Alcohol synthesis with K_2CO_3/Mo_2C

Woo et al. [115] observed that alkali promotion of bulk Mo_2C shifted the selectivity towards alcohols in CO hydrogenation. Figure 2.3 and figure 2.4 summarize reported selectivities to alcohols and hydrocarbons as well as reported CO conversion levels as functions of the K_2CO_3 content in K_2CO_3/Mo_2C.
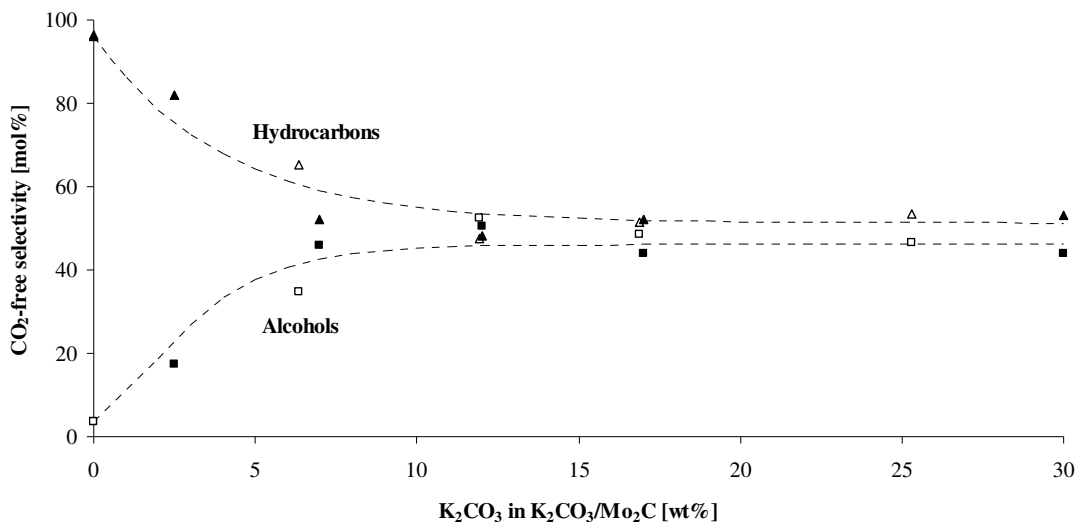
Figure 2.3 The selectivity to alcohols (■,□) and hydrocarbons (▲,△) as functions of the K_2CO_3 content in K_2CO_3/β-Mo_2C catalysts. Filled symbols are from Woo et al. [115], while open symbols are from Xiang et al. [121, 122]. Experimental Conditions are given in figure 2.4.
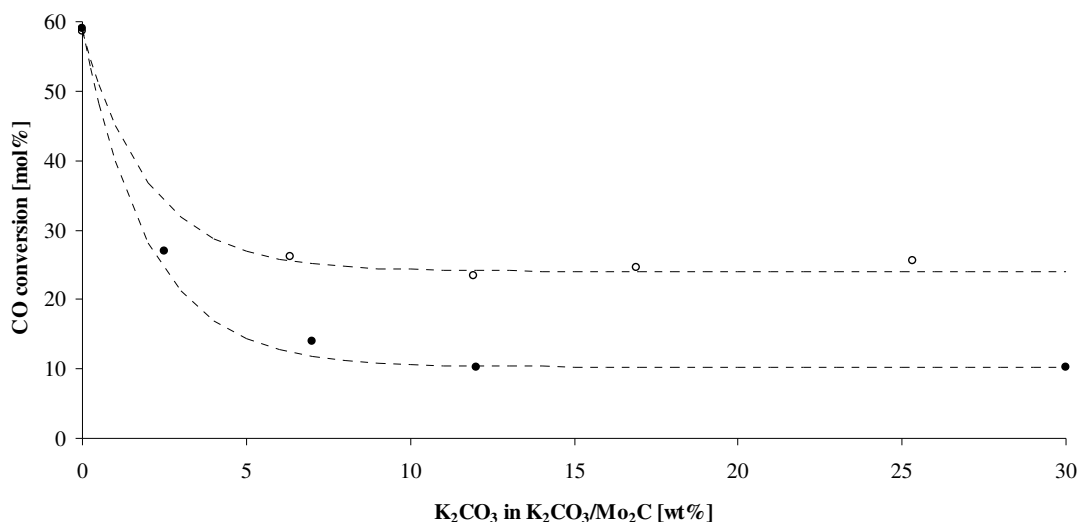
Figure 2.4 The CO conversion as a function of the K_2CO_3 content in $K_2CO_3/\beta\text{-}Mo_2C$ catalysts. Filled symbols are from Woo et al. [115], while open symbols are from Xiang et al. [121, 122]. Experimental conditions: Xiang et al. [121, 122]: 80 bar, 300 °C, 2000 h^{-1}. Woo et al. [115]: 80 bar, 300 °C, 3400 STL (kg cat.)$^{-1}$ h^{-1}.

The results in figure 2.3 and figure 2.4 illustrate that the catalytic activity of the carbide decreases with increasing alkali addition, while the alcohol selectivity of the carbide increases with increasing alkali addition. This development continues until 10-12 wt% K_2CO_3 in the K_2CO_3/Mo_2C catalyst, where the properties begin to stabilize. As it is seen for the sulfided catalyst an alkali promoter is thus essential for an alcohol selective Mo_2C-based catalyst.

Lee et al. [116] evaluated the promotion with different potassium salts and observed that the salts K_2CO_3, KOH and CH_3COOK result in an increased alcohol selectivity for the catalyst. On the other hand potassium in the form of K_2SO_4 and KCl does not seem to confer any alcohol selectivity to the catalyst.

As for the sulfide catalysts it has also been reported that addition of group VIII metals to the basic K_2CO_3/Mo_2C system can improve the alcohol productivity [117-120, 252, 253]. Those results are presented in section 9.4, as part of a comparison with the presently obtained results.

2.4.2 Preparation of carbide catalysts

An interesting aspect of the carbides is that unsupported carbides can be prepared with high surface areas [254, 255]. In combination with the high densities of the carbide materials (for example 9.18 g/cm^3 for Mo_2C) this should in principle allow for the preparation of catalysts with very high surface areas per reactor volume. For this reason the present investigations in chapter 9 have focused on the use of bulk carbides.

45

The preparation of bulk carbides is typically achieved through a temperature programmed reduction/carburization (TPR/C) – a method originally developed by Lee et al. [254]. In this process a precursor, typically the corresponding oxide, is heated in a flow of carburizing gas. The carburizing gas mixture generally contains a carbon source (most commonly methane) in hydrogen.

In the preparation of carbides an often used gas composition seems to be 20 mol% CH_4 in H_2 [122, 254, 256-258], and this is also the carburizing gas used in the present experiments. With this carburizing gas it should be possible to achieve a reasonably large surface area without covering the surface with free carbon. Generally the surface area of the carbide increases with an increasing methane content in the carburizing gas as illustrated in figure 2.5. However increasing methane levels also lead to increasing deposition of free carbon on the carbide surface, and this free carbon blocks the active surface [254]. To actually achieve the higher surface areas obtained with higher methane content in the carburizing gas it is necessary to clean the surface – for example by a subsequent H_2 treatment (a successful result has been obtained with 80 minutes in H_2 flow at 875 K) [254].
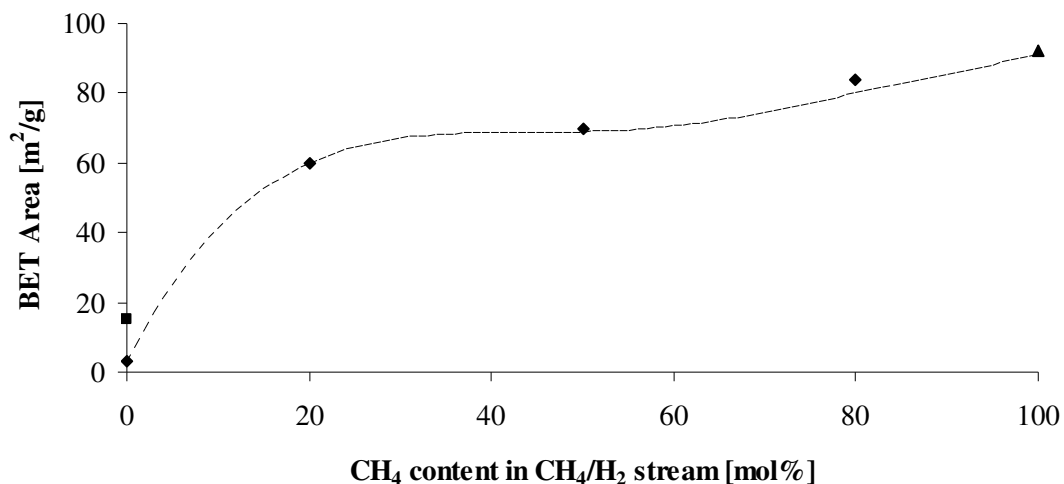
Figure 2.5 Surface areas of β-Mo_2C powders prepared by temperature programmed reaction/carburization (TPR/C) as a function of the methane content in the gas. All experiments are conducted with a heating rate of 30 K/h. TPR/C between 670 and 950 K (♦), TPR/C between 670 and 1020 K (▲), Isothermal reduction in H_2 at 770 K for 30 h (■). At higher methane levels the surface is cleaned of free carbon by H_2 treatment. The data are taken from Lee et al. [254].

The background for the risk of carbon deposition during the carburization is illustrated in figure 2.6, which for the case of Mo carburization shows the temperature regions, where Mo_2C formation and methane dissociation/graphite formation become thermo-dynamically favorable.
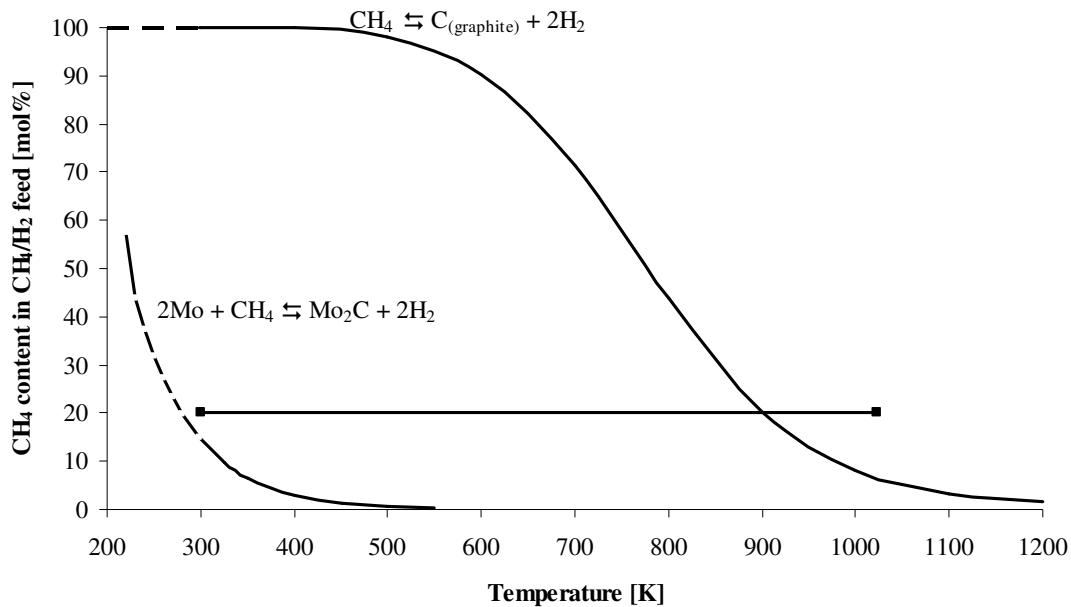
Figure 2.6 The temperature limits above which Mo carburization and carbon deposition become thermodynamically favorable in a CH_4/H_2 gas mixture at atmospheric pressure. The thermodynamical data are taken from Barin [65]. The black bar illustrates the temperature range traversed in the actul carburization run from the present experiments.

The black bar in figure 2.6 illustrates the gas composition and the temperature range employed in the present carburizations (see section 4.9.3 and chapter 9). Figure 2.6 illustrates that the carbide in a 20 mol% CH_4 in H_2 mixture is thermodynamically favorable already at room temperature, but to make the kinetics feasible it is necessary to heat the system and cross into the region, where carbon deposition becomes feasible. The thermodynamics of the Mo carburization in figure 2.6 deviates from the work of Lee et al. [254]. This is because of differences between the thermodynamic values given in the 1973 edition of "Thermodynamical properties of Inorganic Substances" [259] used by Lee et al. [254] and the values given in the 1995 edition of the text [65], which is used in the present work.

    Another parameter in the carburization is the gas flow rate. Generally the surface area of the resulting carbide is increased with increasing CH_4/H_2 flow rate during the carburization [257]. Higher surface areas are obtained with space velocities in the 10000-30000 h^{-1} range.

    The final parameter in the carburization is the temperature. The carburization process can be viewed as a kinetic competition between transport rates of O and C in the solid material and the rate of particle growth. For this reason the temperature should generally be kept as low as possible. An argument for the use of methane rather than a more reactive carbon source is that methane decomposition occurs at higher temperatures, where the diffusion of carbon into the solid is more rapid, wherefore the risk of carbon deposition should be smaller. The higher carburization temperatures required with methane can on the other hand lead to sintering, which also reduces the surface area.

Before the prepared carbide is exposed to the atmosphere the carbide powder is typically stabilized by room temperature exposure to dilute O_2 – often 0.5-1 % O_2 in N_2 (or another inert gas) [122, 258, 260]. It has been reported that both freshly prepared carbides and carbides that have operated in CO hydrogenation can contain considerable amounts of oxygen [117, 119, 260, 261]. The oxygen content might be an additional parameter, which can exert an influence upon the catalytic properties.

As illustrated in figure 2.3 the addition of an alkali promoter to molybdenum carbide is paramount in obtaining an alcohol selective catalyst. The alkali promoter is typically added after the carburization. It was observed by Kojima and Aika [262] that an alkali promoted oxide resited the carburization and only yielded metallic molybdenum. In the present work the alkali promoter is also added after the carburization. A possible reason for the poisoning effect of alkali species on the carburization is discussed in section 9.3. Although it certainly is possible to form bulk carbides with large specific surface areas (see for example figure 2.5) a major hindrance is the large amount of an alkali promoter, which is required to shift the selectivity towards alcohols (see figure 2.3 and figure 2.4). The addition of the alkali promoter causes a significant degree of pore blocking that lowers the available surface area to a relatively low level. This is illustrated in table 2.8, which shows reported volume and mass specific surface areas for Mo_2C promoted with various levels of K_2CO_3. For comparison reported values for K_2CO_3/MoS_2 are provided as well.

Table 2.8 Reported surface areas for various unsupported MoS_2 and Mo_2C catalysts.

Reference	Catalyst	K_2CO_3 content [wt%]	BET area [m^2/g]	Area per volume [a)] [m^2/mL]
Woo et al. [115]	K_2CO_3/Mo_2S	0	65	329
		17	45	228
Park et al. [258]	K_2CO_3/β-Mo_2C	0	38	349
		12	8	73
Xiang et al. [121]	K_2CO_3/β-Mo_2C	0	23.8	218
		6.4	5.6	51
		11.9	3.5	32
		16.9	2.0	18
		25.3	1.8	17

a) Calculated using the solid densities of Mo_2C and MoS_2 from the CRC Handbook of Chemistry and Physics [44].

The data in table 2.8 illustrate that the surface area of the catalyst with the alkali levels necessary to optimize the selectivity have dropped to < 10 m^2/g. Although bulk carbides with high surface areas can be obtained it is thus difficult to obtain large surface areas in the final, promoted alcohol synthesis catalysts.

2.4.3 Similarities between metal carbides and more noble metals

In was described in the beginning of section 2.4 that part of the reason for this works interest in carbides is their ability to emulate more noble metals, of which especially rhodium is interesting for the higher alcohol synthesis.

Levy and Boudart [263] as well as subsequent researchers have observed that WC to some extent exhibits similarities with the noble metal platinum in terms of both catalytic properties [263-265] and electronic structure [266-269]. It should however be emphasized that there also are cases, where the catalytic properties of WC differ from those of Pt [265, 270, 271]. Several researchers [250, 261, 272-274] have also pointed out that the CO hydrogenation properties of Mo_2C resemble those of ruthenium, although there are differences between Ru and Mo_2C – for example in terms of the activity for the simultaneously occurring water gas shift reaction [273, 274]. In terms of the electronic structure a comparison of the XPS valence band spectrum of Mo_2C [270] to that of ruthenium [275] also indicates that there are similarities in the bulk phase valence bands of the two materials.

There are several factors that may contribute to the observed ennobling effect. First of all the carburization of the early transition metals can result in structural changes. The carburization of the often *bcc* structured early transition metals commonly results in carbides with *fcc* or hexagonal (*hcp* or simple hexagonal) structures [250]. The carburization may thus create a structural resemblance to *hcp* or *fcc* structured d-metals further to the right in the periodic system [250].

One possibility that has been discussed as the origin of the ennobling effect of a carburization is related to the total valence electron count [276, 277]. It is certainly intriguing that the combination of W ([Xe] $4f^{14}5d^46s^2$) with carbon, which has four valence electrons, yields a material with properties somewhat like Pt ([Xe] $4f^{14}5d^96s^1$) four places to the right of tungsten in the periodic system. Similarly the Mo_2C structure combines two Mo ([Kr] $4d^56s^1$) atoms with a single carbon atom and obtains properties somewhat like Ru ([Kr] $4d^76s^1$) two places to the right of molybdenum in the periodic system. However based upon DFT calculations on Mo_2C Kitchin et al. [276] found that the ennobling effect does not appear to arise from a significantly increased number of d-electrons per surface metal atom. Previously Eberhart and Maclaren [277] have also spoken against the notion of an electron transfer from carbon to the metal d-band. Eberhart and Maclaren [277] have on the basis of their full potential electronic structure calculations reported that it is a strong hybridization between the carbon p-orbitals and the metal d-orbitals, which creates an electronic structure reminiscent of the more noble metals. It is the occupied part of the carbide valence band below the Fermi level, which may exhibit similarities with a more noble metal. In terms of the unoccupied states above the Fermi level there are for example significant differences between Pt and WC [268, 278]. For metal surfaces it has been reported that the entire valence band, including the empty d-states above the Fermi level, may influence the catalytic activity of the surface [279]. It therefore does not seem unreasonable that previous researchers have found both similarities and dissimilarities between the catalytic properties of carbides and noble metals.

The reason for trying out Mo_2C and WC has been that these materials already have shown some ability for alcohol formation, and the topic of this thesis is after all the

alcohol synthesis with Mo-based catalysts. The reason for evaluating the activity of NbC has largely been to test the abovementioned, discredited hypothesis of the total valence electron count as the reason for the similarities between carbides and more noble metals. If the catalytic properties of the carbide simply would be dictated by the valence electron count one could argue that the combination of Nb ([Kr] $4d^4s^1$) with carbon having 4 valence electrons would resemble rhodium ([Kr] $4d^8s^1$) four elements to the right of Nb in the periodic table. The electronic structure of NbC is however significantly different from that of rhodium, and the catalytic properties are, as it will be shown in section 9.4, also very different.

The electronic structure of NbC may be explained in terms of the abovementioned hybridization. Vojvodic and Ruberto [280] conducted a DFT study of NbC and other transition metal carbides in the NaCl structure. These authors [280] report that the electronic structure in a simplified picture can be understood on the basis of a two-level system comprised of the metal d-states and the carbon p-states. The interaction between the metal d-states and the carbon p-states gives rise to the formation of a set of bonding and anti-bonding states. The bonding states are located a few eV below the Fermi level, while the anti-bonding states are located above or around the Fermi level. For NbC this creates a filled part of the valence band with a pronounced density of states ~5 eV below the Fermi level (the bonding states arising from the hybridization) and a non-vanishing density of states at the Fermi level [280-282]. In terms of a similarity to more noble metals the filled part of the NbC valence band close to the Fermi level is most similar to band structure for the coinage metals (Cu, Ag, Au), which have their normal d-bands located a few eV below the Fermi level [283]. A comparison of XPS valence band spectra for NbC [281] and the coinage metals [284, 285] especially points to certain similarties between NbC and silver. As it will be discussed in section 9.7 the CO hydrogenation properties of NbC are much more reminiscent of silver than of rhodium, it would thus seem that it is not the total valence electron count that directs the properties of the carbide. It seems more likely that it is the detailed electronic structure created by the hybridization between the carbon p-orbitals and the metal d-orbitals, which, possibly in combination with the total valence electron count, creates the catalytic properties.

The anti-bonding states arising from the pd-hybridization, which are located around or above the Fermi level, may not necessarily have a counterpart for the more noble metals, and this should contribute to the abovementioned observation that the metal carbides can be different from more noble metals in terms of the empty states above the Fermi level. Compared to the carbides in a cubic structure (e.g. NbC) the density of states curve for a hexagonally structured carbide like WC also shows a separation into bonding and anti-bonding peaks, but for WC the bonding states stretch from the Fermi level to about 8 eV below the Fermi level [286]. This creates the abovementioned "Pt-like" structure of WC valence band below the Fermi level.

While this discussion has focused on the similarities between carbides and more noble metals in terms of the bulk electronic structure, it should be added that catalysis is a surface phenomenon, and in the surface the picture may however be somewhat more complex. The surface electronic structure may to some extent differ from the bulk electronic structure [286], and factors like the degree of carburization and the presence of oxygen impurities may influence the surface structure, since it is well established that

considerable amounts of oxygen may be present in the surface of carbide materials [251, 287].

2.5 Reaction mechanism

The descriptions in sections 2.3 and 2.4 have introduced the investigated alkali promoted Mo-based catalysts. This section will provide a description of the reaction mechanism for the synthesis of alcohols over MoS_2. The main purpose of this section is to provide a background for the mechanistic understanding that is obtain from the present work and presented in chapter 6. The last part of this section contains a brief discussion of the reaction mechanism over Mo_2C-based catalysts.

On Alkali/MoS_2 Santiesteban et al. [75] have proposed that methanol is formed from direct hydrogenation of CO, through aldehydic CH_xO intermediates. Recently several researchers have conducted theoretical investigations of CO hydrogenation [288-290] and water-gas shift [291] over MoS_2. Huang and Cho [288] and Shi et al. [290] studied CO hydrogenation at the edges of MoS_2 with different assumptions regarding the sulfur coverage of the edges. These authors [288, 290] agree that methane is the result of CO hydrogenation on the unmodified sulfide, and they both report pathways that pass through formaldehyde, but they come to different conclusions regarding the detailed reaction pathway. The catalytic properties of the sulfide could thus depend upon the sulfur coverage, and that could be part of the reason, why the H_2S level, as it is described in section 2.3.6, is observed to influence the catalytic properties of Alkali/MoS_2 catalysts. DFT calculations by Shi et al. [291] have suggested that formaldehyde also may be formed from CO_2 hydrogenation over MoS_2 via the following pathway:

$$CO_2 \xrightarrow{H} HCO_2 \xrightarrow{H} H_2CO_2 \rightarrow CH_2O + O \qquad \text{R18}$$

On the alkali promoted sulfide there is, as previously discussed, a greatly enhanced chance of C-O bond retention in the CO hydrogenation. It has previously been discussed how electropositive alkali species could stabilize electronegative oxygen containing intermediates, and it may be this stabilization that guides the hydrogenation to oxygenates rather than hydrocarbons. This may be the reason, why hydrogenation of CO (and perhaps CO_2) is more likely to lead to methanol over the alkali promoted catalyst.

Experiments with co-feeding of syngas and lower alcohols like methanol and ethanol by Murchison et al. [13, 292] and Santiesteban et al. [75] have shown that a readsorption and elongation of the smaller alcohols is contributing to the chain-growth over the sulfide catalysts.

The primary mechanistic understanding of the formation of higher species over MoS_2 based catalysts comes from isotopic labeling studies performed by Santiesteban et al. [75]. These authors [75] used injection of ^{13}C-labeled methanol into the syngas passed over K/Co/MoS_2 and Cs/MoS_2 catalysts to elucidate the general mechanism in the synthesis of higher alcohols.

With respect to first chain growth step, i.e. the $C_1 \rightarrow C_2$ step, the experiments with injection of ^{13}C-labeled methanol revealed that the formed ethanol molecule

predominantly is labeled in the β position relative to the hydroxy bearing carbon [75, 187]:

$$^{13}CH_3OH + {}^{CO}\!\!/\!_{H_2} \rightarrow {}^{13}CH_3CH_2OH \qquad \text{R19}$$

Santiesteban et al. [75] interpreted this result as a mechanism of CO insertion into a methyl precursor (CH$_3$*), derived from methanol, to form an acyl species (CH$_3$CO*):

$$^{13}CH_3* + CO* \rightleftharpoons {}^{13}CH_3CO* \qquad \text{R20}$$

This acyl species is then hydrogenated to ethanol. An argument for such a mechanism involving CH$_3$* is that the formed methane predominantly is ^{13}C-labeled, when ^{13}C-labeled methanol and CO/H$_2$ is passed over an Alkali/MoS$_2$ catalyst [75]. Herman [31] has proposed the following mechanism for ^{13}CH$_4$ formation from ^{13}CH$_3$OH:

$$H_{2(g)} + 2* \rightleftharpoons 2H* \qquad \text{R21}$$
$$^{13}CH_3OH_{(g)} + * \rightleftharpoons {}^{13}CH_3OH* \qquad \text{R22}$$
$$^{13}CH_3OH* + * \rightleftharpoons {}^{13}CH_3* + OH* \qquad \text{R23}$$
$$^{13}CH_3* + H* \rightleftharpoons {}^{13}CH_{4(g)} + 2* \qquad \text{R24}$$

An alternative to R23 could be the formation of an alkoxy species and severance of the C-O bond in this species:

$$^{13}CH_3OH* + * \rightleftharpoons {}^{13}CH_3O* + H* \qquad \text{R25}$$
$$^{13}CH_3O* + * \rightleftharpoons {}^{13}CH_3* + O* \qquad \text{R26}$$

A further indication of the involvement of alkyl groups in the chain-growth mechanism is that co-feeding of C$_n$ olefins with the syngas yields an increased productivity of C$_{n+1}$ alcohols [106, 108]. In this case the co-fed olefins may serve to increase the amount of alkyl groups on the surface.

Karolewski and Cavell [168] have used secondary ion mass spectroscopy (SIMS) to study the chemisorption of acetone, propanal and 2-propanol on Cs/MoS$_2$(0001). Karolewski and Cavell [168] also observed that exposure of Cs/MoS$_2$(0001) to 2-propanol yields both molecular adsorption of the alcohol as well as formation of a 2-propoxy species and dehydrogenation to a chemisorbed species identical to the one observed when the catalyst is exposed to acetone. This may suggest a route from the acyl species (to which acetone is similar) to the alcohol via an alkoxy species. In that case the CO insertion in R20 might be followed by a series of hydrogenation steps like the ones below:

$$^{13}CH_3CO* + H* \rightleftharpoons {}^{13}CH_3CHO* + * \qquad \text{R27}$$
$$^{13}CH_3CHO* + H* \rightleftharpoons {}^{13}CH_3CH_2O* + * \qquad \text{R28}$$

$$^{13}CH_3CH_2O*+H* \rightleftharpoons\ ^{13}CH_3CH_2OH*+* \hspace{3cm} \text{R29}$$
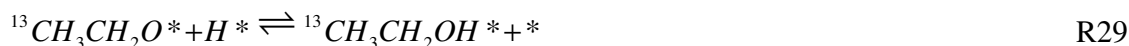
The experiments with co-feeding of $^{13}CH_3OH$ indicated that the $C_2 \rightarrow C_3$ step to some extent proceeds in the same way as the $C_1 \rightarrow C_2$ step, although there were som uncertainties [75, 187]. Over Cs/MoS_2 the formed 1-propanol was mainly labeled at the γ-carbon with respect to the hydroxy bearing carbon [75, 187]. In light of the previously described labeling of the formed ethanol the reaction can be written in the following way:

$$^{13}CH_3CH_2OH + {}^{CO}/_{H_2} \xrightarrow{\ Cs/MoS_2\ }\ ^{13}CH_3CH_2CH_2OH \hspace{2cm} \text{R30}$$

The location of the labeled carbon atom could suggest that 1-propanol is formed by a CO insertion mechanism similar to the ethanol forming reaction.

For the $C_2 \rightarrow C_3$ step Santiesteban et al. [75] did however observe a different behaviour with a cobalt containing catalyst. For a $K/Co/MoS_2$ catalyst it was observed that ^{13}C-labeled carbon in the formed 1-propanol molecule is found in equal amounts at the β and γ positions. Santiesteban et al. [75] evaluated the ^{13}C-labeling of the product by means of ^{13}C-NMR spectroscopy. Because the NMR spectrum showed no doublets, which would be the result of ^{13}C-^{13}C coupling, the authors [75] came to the conclusion that the labeled carbon atoms were not part of the same molecule ($^{13}CH_3^{13}CH_2CH_2OH$), but rather part of two equally abundant (~10×), singly labeled molecules ($^{13}CH_3CH_2CH_2OH$ and $CH_3^{13}CH_2CH_2OH$):

$$2\ ^{13}CH_3CH_2OH + {}^{CO}/_{H_2} \xrightarrow{\ K/Co/MoS_2\ }\ ^{13}CH_3CH_2CH_2OH + CH_3^{13}CH_2CH_2OH \hspace{1cm} \text{R31}$$

Santiesteban et al. [75] suggested that propanol, on $K/Co/MoS_2$ catalysts, is formed from CO insertion into a symmetric di-σ-bonded $*CH_2CH_2*$ species, and that mechanism could certainly explain the equivalence of the two labeled positions.

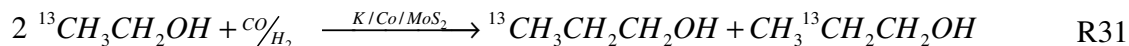As it will be described in greater detail in chapter 6 the present investigations show that another route to chain-growth for this system is a coupling of alcohols, and this coupling seems to progress according to a pathway resembling a classical aldol condensation. Such a coupling pathway could represent an alternative explanation for the observed labeling in 1-propanol. In the experiments of Santiesteban et al. [75] the two prevailing alcohols were $^{13}CH_3OH$ and $^{13}CH_3CH_2OH$. An aldol condensation type coupling between these two alcohols would in fact lead to doubly labeled 1-propanol ($^{13}CH_3^{13}CH_2CH_2OH$). Typically doublets are not observed in ^{13}C-NMR because of the low natural abundance of ^{13}C [293], and the question is, if the enrichment used by Santiesteban et al. [75] was sufficient to rule out the presence of doubly labeled 1-propanol from the observed absence of coupling.

In the case of the $C_3 \rightarrow C_4$ step Bian et al. [14] observed that iso-butanol and n-butanol are formed in similar amounts over a K/MoS_2 catalyst. As it will be described in chapter 6 the present experiments with a $K_2CO_3/Co/MoS_2/C$ catalyst also show that similar amounts of iso-butanol and n-butanol are formed over the cobalt promoted catalyst. Iso-butanol would be the result of an "aldol condensation"-type coupling between methanol and 1-propanol, while 1-butanol would be the result of a CO addition reaction (or a

coupling between two ethanol molecules). These observations could suggest that both coupling and CO addition pathways are available in the $C_3 \rightarrow C_4$ step. These observations may also suggest that both catalysts with and without cobalt have the alcohol coupling pathway available. The production of alcohols higher than C_4 is typically rather limited (see perhaps table 2.7).

In the Fischer Tropsch reaction the available evidence suggests that the chain-growth occurs by combination of alkyl species [294-300]. The labeling studies can in principle not exclude that the CO insertion is a termination step in a Fischer-Tropsch like chain growth that involves alkyl species i.e. a pathway of the following type:

$$CH_n* + CH_m* \rightarrow CH_nCH_m* \xrightarrow{CO} CH_nCH_mCO* \xrightarrow{H} \cdots \xrightarrow{H} CH_3CH_2CH_2OH* \qquad \text{R32}$$
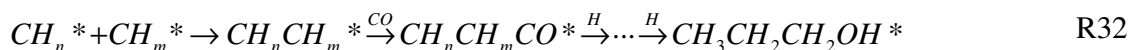
Theoretical studies have however indicated that alkyl group couplings are unfavorable over MoS_2 [170, 288].

It has already been mentioned that methyl and ethyl esters are the significant oxygenated by-products of the synthesis over molybdenum based catalysts. Santiesteban et al. [75] suggested a mechanism for the formation of methyl formate, which is based upon the fact that only the methyl group of produced methyl formate is ^{13}C-labeled, when the syngas contains ^{13}C-labeled methanol. With CsOH as the alkali species the suggested mechanism of methyl formate formation can be expressed as:

$$CsOH + {}^{13}CH_3OH \underset{-H_2O}{\overset{+H_2O}{\rightleftharpoons}} {}^{13}CH_3OCs \xrightarrow{CO} {}^{13}CH_3OCOCs \underset{-H_2O}{\overset{+H_2O}{\rightleftharpoons}} {}^{13}CH_3OCHO + CsOH \qquad \text{R33}$$

This mechanism does explain the position of the labeled carbon atom in the final methyl formate product. It should also be remembered that the SIMS experiments by Karolewski and Cavell [168] revealed the formation of alkoxy species upon alcohol adsorption on Cs/MoS_2.

Methyl acetate, formed when ^{13}C-labeled methanol is added to the syngas passed over the sulfided catalysts, shows labeling of both the terminal methyl groups. This suggests a mechanism, where a methanol derived acyl precursor (CH_3CO*) reacts with a methanol derived methoxy species (CH_3O*) [75]:

$$^{13}CH_3CO* + {}^{13}CH_3O* \rightleftharpoons {}^{13}CH_3COO^{13}CH_3 \qquad \text{R34}$$
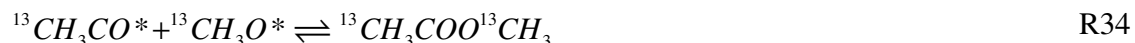
It seems reasonable to expect that ethyl esters such as ethyl acetate are formed through a similar mechanism with the metoxy species replaced by an ethoxy (CH_3CH_2O*) species.

In summary methanol is formed by CO_x hydrogenation over alkali promoted molybdenum sulfide. Experiments with isotopic labeling have previously indicated that an important route to chain growth over MoS_2-based catalysts is the addition of CO to a growing alkyl group (RCH_2) to form an acyl species (RCH_2CO). The formed acyl species can then be hydrogenated into the corresponding alcohol or to a new, now longer alkyl group. Hydrocarbons are believed to be formed from hydrogenation of the alkyl groups. These general mechanistic considerations above are collected in the reaction network depicted in figure 2.7. This figure is drawn on the basis of figures from Santiesteban et al.

[75] and from Smith et al. [301], and these authors do not consider the possibility of alcohol coupling reactions. In chapter 6 it will be shown that such reactions should be included in the reaction mechanism. The inclusion of coupling reactions via aldol condensation pathways could for example explain the presence of branched alcohols like iso-butanol in the alcohol product. In figure 2.7 the alcohol formation is shows as a reversible step due to the abovementioned results of experiments with alcohol co-feeding. The remaining steps are shown as irreversible steps.
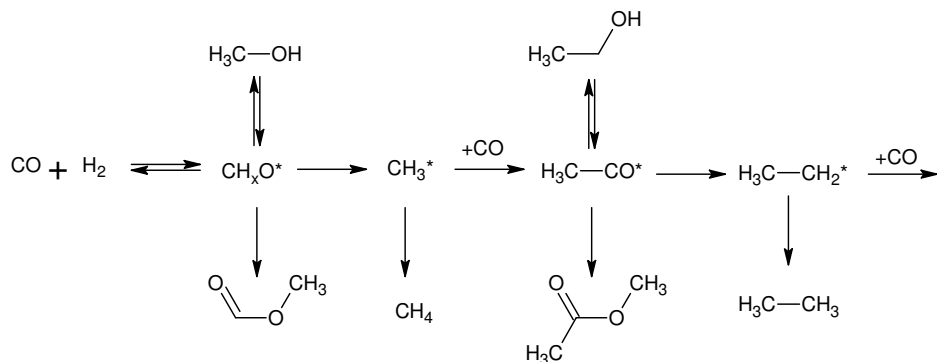
Figure 2.7 Reaction network for the synthesis of higher alcohols (up to C_2 species) over Alkali/MoS$_2$ and Alkali/Co/MoS$_2$ catalysts. This figure is drawn on the basis of figures from Santiesteban et al. [75] and from Smith et al. [301]. As in the text in general an asterisk denotes a species bound to the surface

On metallic Alkali/Mo catalysts mechanistic investigations with co-feeding of probe molecules have indicated that the reaction pathway is the same as for the sulfided system [302, 303]. Ko and Madix [304] studied methanol adsorption on metallic Mo(100) as well as on carburized and oxidized surfaces and observed dissociative adorption of methanol to yield methoxy groups on all these surfaces. These authors [304] also observed methanol production from formaldehyde TPD on clean and carburized Mo(100). This suggests that the alcohol formation also on the metallic/carburized systems occurs via aldehydes and alkoxides. Although no dedicated mechanistic studies are available it is likely that systems based upon molybdenum carbide should observe the same pathways as systems based upon MoS$_2$ or metallic Mo. In recent years Solymosi et al. [305-316] and Chen et al. [276, 317-319] have conducted a range of surface science studies on carburized molybdenum. An especially interesting finding in these studies has been that addition of potassium to a carburized Mo(100) surface facilitated the coupling of CH$_2$I$_2$ derived methylene groups into ethylene [309]. Contrary to the situation for the sulfide it is thus possible that "Fischer-Tropsch"-like alkyl combination reactions may play a role in the chain-growth over alkali promoted molybdenum carbide.

2.6 Industrial use of the higher alcohol synthesis

This section contains a brief description of a few selected alcohol synthesis projects and presents some key parameters in the practical application of the alcohol synthesis process with the clear focus on the use of sulfide catalysts.

In section 2.2 the history of the higher alcohol synthesis was briefly introduced, and a few selected larger plants and projects related to the synthesis were mentioned. Table 2.9 contains a summary of selected alcohol synthesis projects.

Table 2.9 Selected plants and development projects for the higher alcohol synthesis.

Company	Key catalyst elements	Scale	Operating period	Reference
Enichem Snamprogetti Haldor Topsøe	Alkali/ZnO/Cr$_2$O$_3$/Cu	15000 ton/year	1980's	[11, 35]
Dow Chemicals	Alkali/Co/MoS$_2$	Bench scale (28 L cat.)	1980's	[35]
Institut Francais du Pétrole (IFP) Idemitsu-Kosan	Co/Cu/Al$_2$O$_3$/Na/ZnO Co/Cu/Cr$_2$O$_3$/Alkali	7000 bbl/year	1984-1985	[35, 320]
Range Fuels	Several patents on Alkali/Co(or Ni)/MoS$_2$(or WS$_2$)	Currently 4 mio gallons of MeOH per year. Projected scale is 60 mio. gallons of mixed alcohols per year.	Currently operating	[64, 321]

Dow chemicals designed a process for the conversion of natural gas through the synthesis of higher alcohols over sulfided catalysts. The process has however never been implemented on an industrial scale. IFP and Idemitsu-Kosan also developed a process for the conversion of natural gas into higher alcohols by means of a cobalt-cupper catalyst and operated a mini-plant in Japan.

Anno 1988 calculations by Dow Chemicals indicated that a commercial process (presumably from natural gas) would require single pass conversions of at least 15-20 mol% with a CO_2-free alcohol selectivity above 80 mol% [13]. In a recent system study Phillips [322] investigated the conversion of biomass into mixed higher alcohols via gasification. Phillips [322] assumed alcohol synthesis with 90 mol% selectivity at 60 mol% CO conversion and found that with these operating characteristics the delivered, moist biomass could be converted into higher alcohols with an energy efficiency of 55 % on an LHV-basis.

Figure 2.8 shows a block diagram of the Dow Chemicals process for production of higher alcohols from natural gas. Figure 2.9 shows a block diagram for the IFP/Idemitsu-Kosan process for the production of higher alcohols from natural gas, while figure 2.10 provides a flow sheet for the synthesis and separation sections of that process.
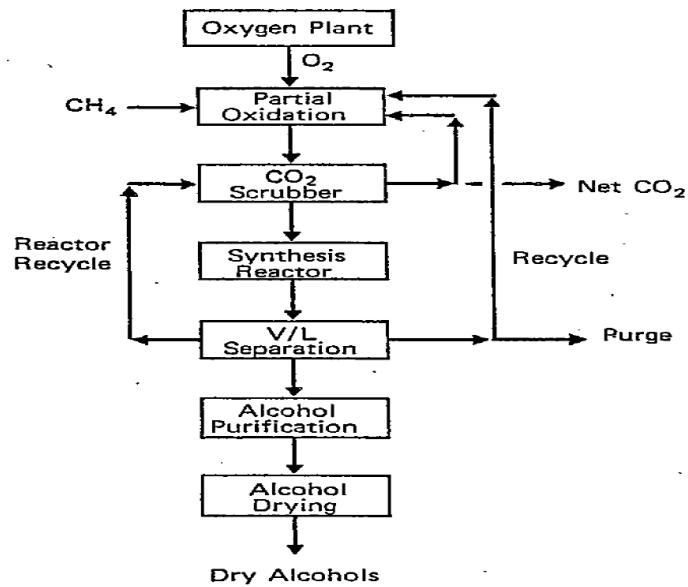
Figure 2.8 Block diagram for the Dow Chemicals alcohol synthesis process. This figure is from Quarderer [74].
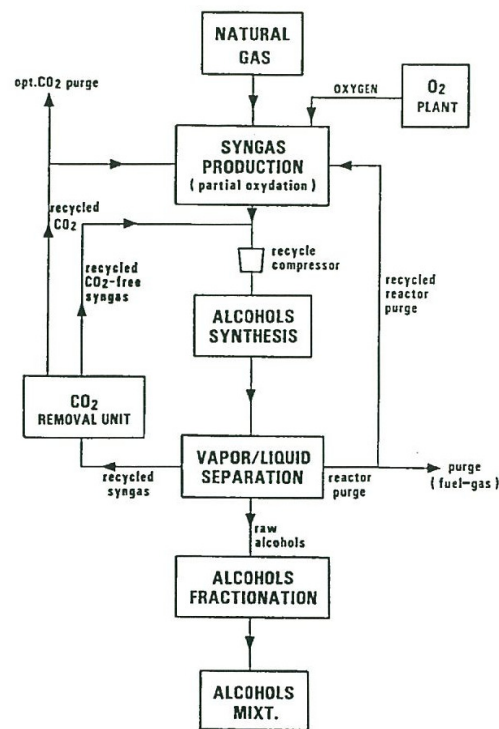
Figure 2.9 Block diagram for the IFP/Idemitsu-Kosan alcohol synthesis process from natural gas. This figure is from Courty et al. [35].
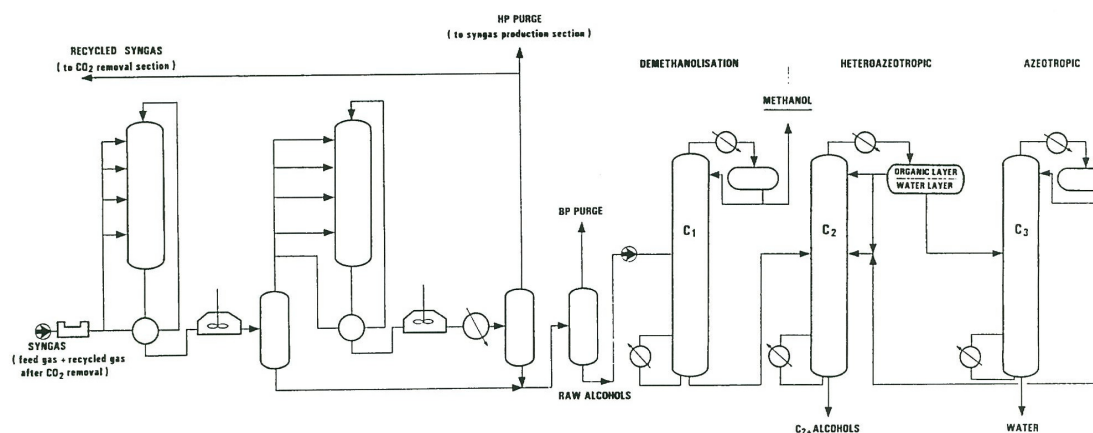
Figure 2.10 Flow sheet for the synthesis and separation sections in the IFP/Idemitsu-Kosan alcohol synthesis process. This figure is from Courty et al. [35].

Figure 2.8 and figure 2.9 illustrate that block diagrams for the two processes are very similar. The alcohol synthesis plant can be separated into three main stages, namely syngas generation, alcohol synthesis and alcohol fractionation and drying. If the product is intended for use as a gasoline additive, the water content of the alcohol product must, as it will be described in the following section, be very low.

Most investigations of the sulfided higher alcohol synthesis catalysts have been carried out in fixed bed reactors. Operation of the sulfided alcohol synthesis catalyst in a gas-solid fluidized bed has previously been shown to be less desirable than fixed bed operation with respect to the alcohol selectivity [104]. This is quite reasonable, since the fluidized bed is more like a continuously stirred tank reactor in its behavior, and in such a reactor the thermodynamically unfavorable alcohol product will, for a given conversion, experience a longer residence time than in a fixed bed reactor. Because an increasing temperature, as it is described in section 2.3.6, is observed to shift the selectivity from alcohols towards hydrocarbons, it will be important to avoid a significant temperature rise in the synthesis reactor due to the exothermic synthesis reactions. A suitable reactor type that can provide an approximately isothermal operation could be the Lurgi-type methanol synthesis reactor. In the Lurgi-type reactor the catalyst pellets are placed inside fixed tubes. The tubes are surrounded by boiling water and the heat of reaction is used to generate high pressure steam. The temperature inside the reactor is controlled via the steam pressure on outside of the tubes [323]. This setup ensures that the catalytic bed is essentially isothermal along the long axis of the tubes, while the maximal temperature gradient between the tube centreline and the boiling water in the methanol synthesis typically is in the scale of 10-12 °C [324].

As for the conventional methanol synthesis reaction [325-327], the use of a liquid slurry reactor has also been proposed for the employment of the sulfided alcohol catalysts [328]. In the so-called "Ecalene" process particles of K/MoS_2 or $K/Co/MoS_2$ in the 100 nm size range are suspended in an inert hydrocarbon oil (Ethylflo-164: a commercial poly-α-olefin oil). It is claimed that the process can produce a liquid product with up to 70 wt% ethanol. It is reportedly [328] by virtue of a superior heat management in the inert oil that the process is able to achieve 20-25 % conversion at 74 % selectivity and to

achieve a space time yield of around 0.5 g g_{cat}^{-1} h^{-1}. The sulfided state of the catalyst is in this process maintained by the addition of a sulfur source to the slurry - typically elemental sulfur [329, 330].

Figure 2.10 shows that the IFP/Idemitsu-Kosan process contains a separation of methanol and higher alcohols. The methanol, which in the present context is a less desirable product, could then be recirculated to the synthesis reactor. For the use of the mixed alcohols as gasoline additives a very important part of the separation section is a removal of water from the alcohol product. If water is present in the condensed product in a concentration of 2 wt% or less, the H_2O can be removed by absorption with a molecular sieve [18]. In this way the planned Dow Chemicals process removed water with a system of zeolite units [331]. Figure 2.10 shows that the IFP/Idemitsu-Kosan process employed an alternative approach, namely an azeotropic distillation with benzene as a water entrainer [35]. Both processes reportedly result in an alcohol product with ≤ 0.2 wt% water [35, 331].

For the sulfide catalysts several studies have investigated the possibility of improving the alcohol formation rate by co-feeding components of a lower value. It was described in section 2.5 that Murchison et al. [13, 292] and Santiesteban et al. [75] have experimented with co-feeding the smaller alcohols methanol and ethanol along with the syngas. The alcohols could come from recirculation of part of the alcohol product. Co-feeding methanol has little effect upon the product distribution, but results in an increased productivity i.e. the methanol in the feed is adsorbed and converted into higher products in the same chain growth scheme as is seen for alcohol formation from H_2 and CO. Similarly co-fed ethanol is incorporated into higher alcohols, while the methanol production is unaffected. The chain growth from co-fed ethanol is however reportedly [13, 292] not as efficient, as it is the case for co-fed methanol. As previously mentioned it has been found that the presence of C_n olefins in the synthesis gas greatly improves the formation rate of C_{n+1} alcohols (e.g. addition of CH_2CH_2 to the syngas feed yields an increased production of $CH_3CH_2CH_2OH$) [106, 108]. Recent patents report that co-feeding of ethers [332] or aldehydes [183] with the syngas is highly beneficial with respect to alcohol selectivity, productivity and stability. At the conditions P = 90 bar, T = 310 °C, $H_2/CO = 1$, 50 ppm H_2S Bolton and Gracey [183] have included 0.20 mol% acetaldehyde in the synthesis gas passed over a $K_2CO_3/Co/MoS_2$ catalyst. The introduction of acetaldehyde to the reactor results in a 42 % increase in ethanol productivity and an increase in the productivity of butanols of nearly 300 %. The reason for this larger boost of the butanol production could be the coupling reactions that will be discussed in chapter 6.

2.7   Fuel Properties of mixed alcohols

The focus of the present work is the use of the higher alcohol synthesis as a way to produce gasoline additives from biomass via a gasification. The interest in alcoholic fuels is as old as the car industry itself. The first units of the famous Ford Model T, which were produced, were configured to operate on ethanol [333], and although gasoline turned out to be cheaper and more convenient, the famous early proponents of ethanol as an

59

automotive fuel included Henry Ford, Charles F. Kettering, Alexander Graham Bell and Thomas Edison [334].

Methanol, the simplest alcohol, can today be produced from syngas in a highly efficient process [335-338], but mixtures of methanol and gasoline can experience certain miscibility problems that are prohibitive for the fuel use of pure methanol. These miscibility problems can to some extent be avoided by including higher alcohols in the blend, and that is an important part of the reason for the interest in the higher alcohol synthesis.

Table 2.10 contains a summary of various properties for various oil-derived and synthetic fuels.

Table 2.10 Comparison of natural gasoline and diesel with various synthetic fuels. For the non-pure components the values given represent typical values [9, 44, 339-345].

Fuel	Gasoline	Diesel	Methanol	Ethanol	Iso-butanol	Liquid DME	Fisher Tropsch diesel
Composition	$\sim C_8H_{15}$	$\sim C_{16}H_{34}$	CH_4O	C_2H_6O	$C_4H_{10}O$	C_2H_6O	$\sim C_{16}H_{34}$
Octane nr. $\left[\frac{RON+MON}{2}\right]$ a)	87	8-15	108	115	102	-	-
Cetane nr.	5-20	40-55	3-5	8	13	55-60	75
$P_{37.8°C}^{vap}$ [bar] b)	0.60	0.03	0.32	0.16	0.04	8.44	-
Blend $P_{37.8°C}^{vap}$ c) [bar]	-	-	2.14	1.24	0.34	-	-
LHV $\left[\frac{kJ}{g}\right]$	43.31	42.78	18.23	26.81	38.28	28.62	43.9
Density $\left[\frac{g}{cm^3}\right]$ d)	0.74	0.86	0.79	0.79	0.69	0.66	0.78
Energy density (LHV) $\left[\frac{kJ}{cm^3}\right]$	32.05	36.79	14.42	21.16	26.42	18.89	34.24
Normal boiling point [°C]	38-204	163-399	65	78	108	-25	210-338
Oxygen content [wt%]	0	0	49.93	34.73	21.6	34.73	0-1
Stoichiometric Air/fuel ratio [wt/wt]	14.51	14.87	6.43	8.94	11.12	8.94	14.87

a) This is the average of the reseach and motor octane numbers. The number on the refuelling station is the higher research octane number. b) The so-called Ried Vapor Pressure. c) Blend of the appropriate alcohol that contains 2.7 wt% oxygen. d) DME: P = 1 atm, T = -25 °C; Gasoline, diesel and FT diesel: P = 1 atm, T = 20 °C; Alcohols: P = 1 atm, T = 25 °C.

Table 2.10 shows the most attractive feature of alcohols used as motor fuels, namely the high octane numbers of the alcohols. An increased octane number enables a spark-ignition (gasoline) engine to run at a higher compression ratio, whereby the energy efficiency is increased. Alcohols also exhibit shorter burn times and require less air intake. These factors all serve to improve the fuel efficiency [339]. For this reason some high powered racing cars use methanol as a fuel [11, 340]. Table 2.10 also illustrates that

alcohols have low cetane numbers, which means that the alcohols are poorly suited for use in compressed ignition (diesel) engines. Synthetic fuels like DME or Fischer Tropsch diesel are much better suited as replacements for oil-derived diesel.

The alcohol octane numbers table 2.10 are representative values, but a great deal of scattering is seen in the reported octane numbers for alcohols [10]. Gautam and Martin [346] have investigated the octane enhancing capability for various mixed alcohol/gasoline blends, and their data indicates that the octane enhancing capability is linked to the oxygen content of the blend. There are however varying results with respect to the use of different alcohols. Gautam and Martin [346] experienced the best octane enhancements for blends that have a high methanol/ethanol ratio and relatively few higher alcohols, which suggests that methanol has a better octane enhancing capability than the higher alcohols.Yacoub et al. [347] have investigated binary alcohol/gasoline blends, and their results showed that for the same blend oxygen content, the addition of smaller alcohols (C_1-C_3) improves the octane number, while the addition of higher alcohols (C_4-C_5) decreases the octane number. Of the binary alcohol/gasoline mixtures studied by Yacoub et al. [347], ethanol was found to be the best alcohols tested with respect to octane enhancing capabilities. That is also the conclusion from the reports summarized in table 2.10. Overall it seems that methanol and ethanol provide a similar octane enhancing effect, while the higher alcohols (C_4 and higher species) provide less improvement or perhaps even a reduction in the blends octane number. The octane numbers shown in table 2.10 are averages of the so-called research and motor octane numbers, which are obtained in two different tests. Figure 2.11 shows the research and motor octane numbers as functions of the mixed alcohol content in the blend, when the mixed alcohol product from an Alkali/MoS_2 catalyst is added to gasoline.
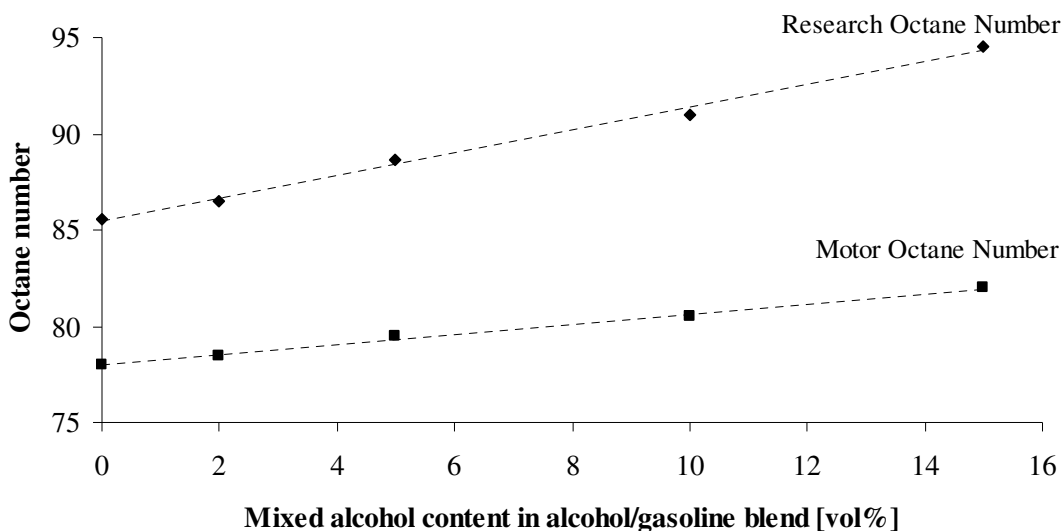
Figure 2.11 The research and motor octane numbers for the alcohol/gasoline blend, when the mixed alcohol product (presumably 50 % MeOH) from an Alkali/MoS_2 catalyst is added to gasoline. The data are from Quarderer [74].

Figure 2.11 illustrats that a significant enhancement of the octane number can be achieved by adding the mixed alcohol product from an Alkali/MoS$_2$ catalyst to gasoline.

There are however also challenges associated with the use of alcohols as motor fuels or fuel additives. Although alcohols are completely miscible with gasoline at normally encountered temperatures a significant problem is that small amounts of water are able to cause a phase separation into an upper gasoline rich phase and a lower alcohol/water phase [10]. The phase separation occurs, if the temperature is too low, or if the water content of the blend is too high. Figure 2.12 shows the water content that various alcohol/gasoline mixtures at 10 °C can tolerate before a phase separation occurs. Figure 2.13 shows for a variety of alcohol/gasoline mixtures the temperature, where the phase separation occurs, as a function of the water content.
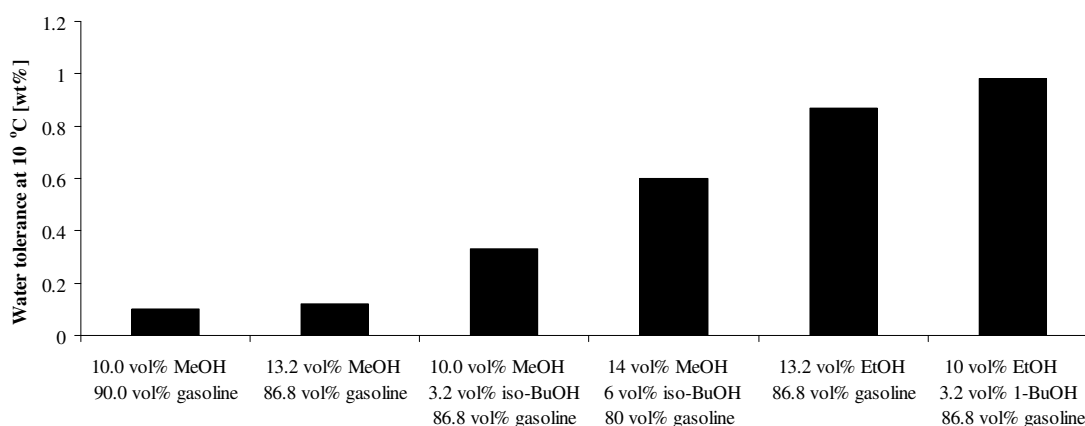
Figure 2.12 The water level that various alcohol/gasoline mixtures at 10 °C can tolerate before a phase separation occurs. The data are from Keller [10].
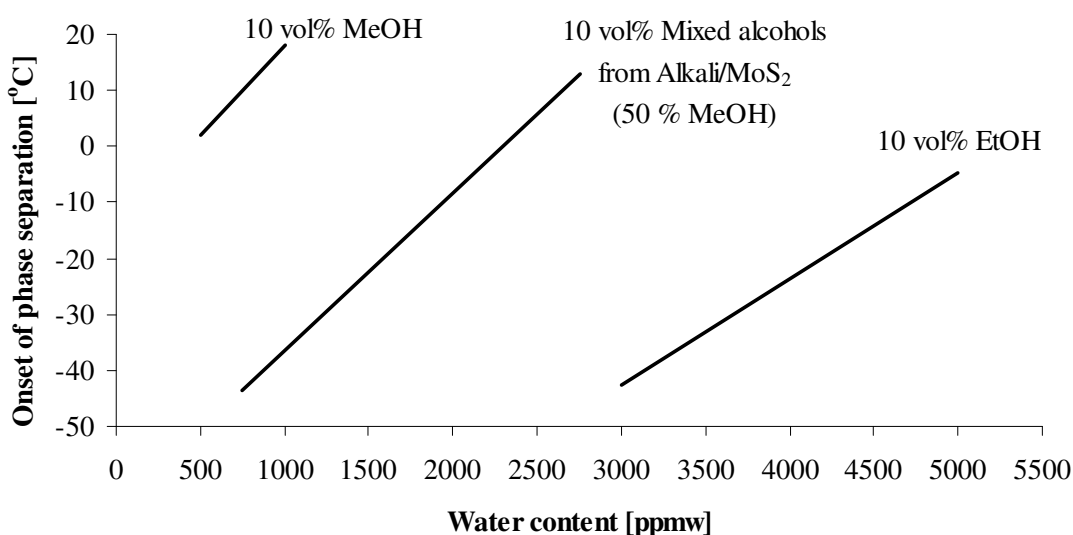
Figure 2.13 The temperature, where the phase separation begins to occur, as a function of the water content for different alcohol/gasoline blends. Data are from Quarderer [74].

There are several reasons, why a phase separation is a problem. The alcohol/water phase is reportedly much more prone to pick up dirt or sediments that potentially can stall the engine [10]. If the phase separation occurs in the storage tanks at the refueling station and results in an upper gasoline phase and a lower alcohol/water phase, then an uneven drainage of the two phases will eventually cause problems [10]. Most importantly the alcohol/water phase is highly corrosive. Dry methanol blends do not appear to be corrosive [10, 348, 349]. It has been repoted that virtually unmodified cars have operated without problems with 15% methanol in gasoline blends for several years [348, 349]. The presence of enough water to cause phase separation will however make the blend seriously corrosive to steel, aluminum, and zinc [10]. Methanol is also known to be highly corrosive to magnesium, lead and lead-tin alloys [10, 348, 349]. Lead-tin alloys are used for coating of steel fuel tanks and lines [10]. Some reports of methanol attacks on cupper and brass also exist [348, 349]. Some non-metallic components that may be present in fuel systems are less serviceable under methanol-rich conditions. Those materials include Viton, cork, leather and polyester bonded fiberglass, but few problems would be expected for those materials with low alcohol concentrations in the blend [10]. Polyurethane, which is used in some gasoline fuel systems, stands out in the sense that it deteriorates even more in methanol-poor blends than in methanol-rich blends [10]. There are fewer specific data for the corrosiveness of ethanol containing blends. Ethanol seems to be less corrosive than methanol, although not necessarily very much so [350]. It has for example been reported that damp blends of ethanol and methanol attack cupper in the same way [10]. Ethanol rich fuel blends ($\geq$30%) are also observed to be corrosive to steel and aluminum, and, as it is seen for methanol, the presence of water increases the corrosiveness of the blend [351]. It has been observed that the use of anodized aluminum provides an efficient corrosion protection - even at high ethanol concentrations ($\leq$85 wt%) [340, 351]. It should be added that making new cars fully compatible with ethanol/gasoline blends up to 85 % ethanol reportedly adds little to the vehicle cost – perhaps as little as 100 \$/car [352], but retrofitting existing cars to operation with fuels containing high alcohol fractions is very costly [353].

While alcohol rich gasoline blends may be corrosive in their own right, the above results indicate that blends with lower alcohol contents primarily cause corrosion problems, if a phase separation creates an isolated alcohol-rich phase. For this reason the introduction of alcohol fuels in the existing energy infrastructure, via lower alcohol content blends, may be easier with alcohols or alcohol-mixtures that are sufficiently resistant towards a phase separation. Figure 2.12 illustrates that the water tolerance of methanol/gasoline and ethanol/gasoline mixtures benefits from the inclusion of higher alcohols in the mixture. Since a mixture that contains higher alcohols has a greater water tolerance, it could be more easy to introduce a large scale fuel use of alcohols with a mixture of methanol, ethanol and higher alcohols than with pure methanol. For service station tanks in the US it has been reported that the water content varies widely, but that typical water contents are found in the 500-1000 ppm range [10, 348, 349]. The results in figure 2.13 indicate that this water level at common temperatures would be a problem for methanol/gasoline mixtures, but not for a mixed alcohols/gasoline mixture with 50 % higher alcohols. As discussed above the lower alcohols methanol and ethanol provide the best octane enhancement, so it may also be desirable to have some amount of these lower

alcohols in the mixture. A mixture of methanol, ethanol and higher alcohols could thus be a way to introduce a wide-scale fuel use of alcohols.

It might be added various alternative strategies have been explored in the search for a way to stabilize methanol rich fuel blends. Trials with a wide variety of surfactants were unsuccessful at any practicable concentrations [10]. Olson et al. [354] investigated a blend of gasoline with 10 % of an alcohol mixture similar to the one obtained with a modified methanol synthesis catalyst. These authors [354] observed that the conversion of the mixed alcohols to the corresponding acetate esters by esterification with acetic acid improved the water tolerance of the gasoline/oxygenate mixture. It was also observed [354] that the octane number was increased by the esterification of the alcohol mixture.

The risk of a phase separation is however not the only challenge associated with the use of alcohol/gasoline mixtures. Another problematic issue is that the addition of alcohols to gasoline increases the vapor pressure of the blend significantly. Both methanol and ethanol are known to form low-boiling azeotropes with certain C_5 species and with higher hydrocarbons in the mixture [10]. Figure 2.14 shows the increase in vapor pressure at 37.8 °C (the so-called Reid vapor pressure) as a function of the alcohol content, when various alcohol mixtures are added to gasoline.
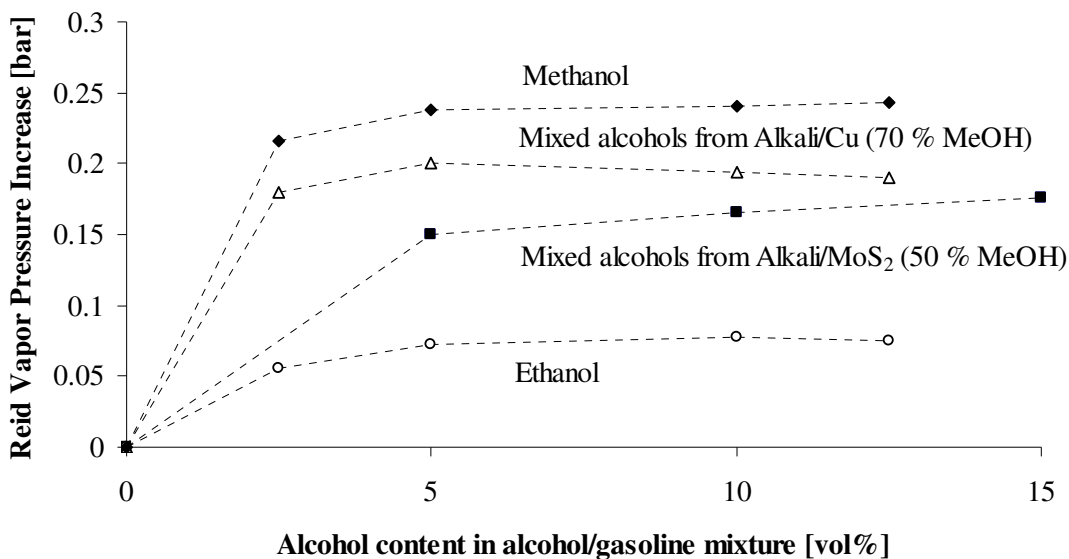
Figure 2.14 The so-called Reid vapor pressure (i.e. the vapor pressure at 100 °F or 37.8 °C) of the alcohol/gasoline blend, when various alcohol mixtures are added to gasoline. The data are from Quarderer [74] and Keller [10].

Figure 2.14 illustrates that the typical alcohol mixtures formed over Alkali/Cu modified methanol synthesis catalysts, and over Alkali/MoS$_2$ catalysts cause a smaller vapor pressure increase than methanol, but a larger vapor pressure increase than pure ethanol. The increased vapor pressure leads to increased evaporative emissions [346], and the increased volatility can cause problems with so-called "vapor lock", where the vehicles fuel supply is disrupted by the formation of gas pockets in the fuel delivery system [10, 348, 349]. It will most likely be necessary to remove the volatile butanes fraction of the

gasoline in order to compensate for the increased vapor pressure that follows from the alcohol addition [10, 348, 349, 354]. This of course raises the question of what should be done with the C_4 fraction that is removed from the gasoline [348].

Table 2.10 shows that another disadvantage of the alcohols is their lower energy densities compared to ordinary gasoline. For alcohol-poor blends this is a modest problem, but for alcohol-rich mixtures the use of the alcohols would lead to a significantly reduced mileage. For example a mixture of 90 % methanol and 10 % gasoline with the engine adjusted to take advantage of the the higher octane number of methanol may yield a 10-25 % improvement in energy efficiency over gasoline [10, 355], but even so the lower energy density of methanol means that the mileage is reduced by 55-65 % compared to gasoline [10, 350].

For modern cars with closed loop control systems, where the air intake is regulated to the stoichiometric value via a measurement of the oxygen content in the exhaust, and where the exhaust gas is catalytically rectified, it is reported that the presence of alcohols in the fuel has little or no influence upon the emission characteristics of the vehicle except during start-up [356].

An unresolved issue related to the use of the sulfided alcohol synthesis catalyst studied in this work has been the possible incorporation of sulfur species into the liquid alcohol product. Early research by the Dow Chemical Company showed that small amounts of low boiling, sulfur containing compounds are incorporated into the alcohol product [18, 74, 249]. To solve this problem the Dow process included a stabilizer column, which reportedly would be able to reduce the sulfur level in the alcohol product to 10 ppm with a modest vapor boil-up [74]. The environmental regulations concerning the sulfur level in automotive fuels are becoming increasingly strict. In the US the EPA Tier II regulations have since 2006 limited the average sulfur concentration in gasoline to 30 ppmw, while the limit on sulfur in highway diesel is 15 ppmw [357]. Within the EU an upper sulfur limit of 10 ppmw in gasoline and diesel should be completely phased in at the beginning of 2009 [358]. A substantial concentration of sulfur in the alcohol product would therefore be highly undesirable, if the product is to be used as an automotive fuel or a fuel additive. However despite the importance of such a potential incorporation of sulfur species into the reaction product, this subject has received very little attention in the open literature. It is therefore not entirely clear, to what extent sulfur is incorporated into the alcohol product, and which sulfur compounds that might be present in the condensed product. Section 5.5 in this work contains an investigation of the incorporation of sulfur into the liquid alcohol product.

3 Thermodynamic considerations

What we obtain too cheaply, we esteem too lightly
- Thomas Paine

The present work includes various thermodynamic calculations. At the high reaction pressure, which is typically in the range of 100 bar, the gas phase could exhibit significant departures from ideal gas behavior. Thermodynamic equilibrium may also limit or at least influence some of the reactions that are involved in the reaction network. This section will briefly introduce the methodology employed in the thermodynamic calculations conducted in this work.

The relationship between pressure, temperature and molar volume is contained within a so-called equation of state (EoS) with the simplest equation of state being the ideal gas law. Significant departures from ideal gas behavior could however occur as a result of molecular interactions at the high reaction pressure. A more accurate description of molecular interactions can be achieved through the use of a cubic equation of state. The equation of state, which is used in this work, when non-ideality is considered, is the Soave-Redlich-Kwong (SRK) equation, which is a 3-parameter, cubic equation of state. The reason for this choice is that the SRK equation has been shown to provide the best description of the methanol synthesis equilibrium, which also can also play a role in the synthesis of higher alcohols.

In the regular methanol synthesis the gas mixture differs considerably from ideality at the high reaction pressure [359]. Particularly the polar components H_2O and CH_3OH show fugacity coefficients differing substantially from 1. Chang et al. [360] have determined that it is desirable to use of an equation of state to describe the fugacity coefficients in of the components coexisting in the gas mixture rather than to use a pure component fugacity coefficient at corresponding conditions. Graaf et al. [361] have evaluated the description of non-idealities in the gas phase using the Redlich-Kwong (RK) EoS [362], the Soave-Redlich-Kwong (SRK) EoS [363], the Peng-Robinson (PR) EoS [364], the ideal gas law (IGL) and the virial equation (Vir). These authors find the accuracy in the description of the equilibrium to observe the following order:

SRK > IGL > PR > RK > Vir

The results of Graaf et al. [361] thus suggest that the SRK equation is the only equation of state that actually appears to offer an improvement over a simple ideality assumption. It should however be remembered that the SRK EoS is not well suited for hydrogen – a major component in the syngas. The Soave-Redlich-Kwong equation of state is given in equation (3.1):

$$P = \frac{RT}{V_m - b} - \frac{a}{V_m \left(V_m + b \right)} \qquad (3.1)$$

Here a and b are again component specific parameters that are described by the components critical temperature, T_C, critical pressure, P_C, acentric factor, ω, and reduced temperature, $T_R = \frac{T}{T_C}$.

$$a = 0.42747 \frac{R^2 T_C^{\,2}}{P_C} \left[1 + w \left(1 - \sqrt{T_R} \right) \right]^2 \tag{3.2}$$

$$b = 0.08664 \frac{R T_C}{P_C} \tag{3.3}$$

$$w = 0.480 + 1.574\omega - 0.176\omega^2 \tag{3.4}$$

The acentric factor, ω, is defined in the following way [365, 366]:

$$\omega = -\log_{10} \left(P^{sat} \left(T_R = 0.7 \right) \right) - 1 \tag{3.5}$$

Here $P^{sat}(T_R = 0.7)$ is the vapor pressure at a reduced temperature of 0.7.
Equation (3.1) can be rewritten to the following form:

$$Z^3 - Z^2 - Z\left(B^2 + B - A \right) - AB = 0 \tag{3.6}$$

Where the compressibility factor, Z, which is defined as:

$$Z = \frac{PV}{nRT} = \frac{PV_m}{RT} \tag{3.7}$$

Here n is the molar amount, R is the gas constant, V is the volume and V_m is the molar volume. The parameters A and B in equation (3.6) are defined in the following way:

$$A = \frac{aP}{R^2 T^2} \tag{3.8}$$

$$B = \frac{bP}{RT} \tag{3.9}$$

Equation (3.6) is the so-called characteristic equation for the SRK equation of state.
    For mixtures the following general mixing rules are used to determine the parameters in the equation of state:

$$b = \sum_i x_i b_i \tag{3.10}$$

$$a = \sum_i \sum_j x_i x_j a_{ij} \tag{3.11}$$

Here x_i is the molar fraction of component i. Additionally we have:

$$a_{ij} = \left(1 - k_{ij}^{'}\right)\sqrt{a_i a_j} \tag{3.12}$$

Here $k_{ij}^{'}$ is an empirical binary interaction parameter for the ij-pair. This interaction parameter can be used to adapt the model to experimental data. In this work all calculations are conducted with the assumption that all interaction parameters are $k_{ij}^{'} = 0$. This choice of the $k_{ij}^{'}$-values is mainly due to the lack of a complete interaction parameter set.

The components in the non-ideal gas phase are described in terms of their fugacity, f, instead of their partial pressure, p. Here f_i is the fugacity of component i, which can be expressed in terms of the total pressure, P, the molar fraction of component i, y_i, and the fugacity coefficient of component i, φ_i;

$$f_i = \varphi_i y_i P \tag{3.13}$$

With the SRK EoS and the mixing rules in equations (3.10) and (3.11) the final expression for the fugacity coefficient of component i in the mixture becomes:

$$\ln\left(\varphi_i\right) = -\ln\left(Z - B\right) - \frac{A}{B}\ln\left(1 + \frac{B}{Z}\right)\left(\frac{2\sum_j a_{ij} x_j}{a} - \frac{b_i}{b}\right) + \frac{b_i}{b}\left(Z - 1\right) \tag{3.14}$$

For a known gas composition the fugacity coefficients can be determined with equation (3.14). In this calculation the H_2O content in the gas is estimated through an assumption of equilibrium for the water gas shift reaction, but this assumption is not found to have a large impact on the calculated set of fugacity coefficients. In practice the calculation is carried out by means of the Visual Basic module Thermo.bas under Microsoft Excel. This module has been written by docent at the Department of Chemical Engineering at DTU, Michael L. Michelsen and distributed as part of the teaching material for the course "Technical Thermodynamics" at the Department of Chemical and Biochemical Engineeing. The critical properties and acentric factors used in the calculations are presented in table 3.1.

Generally the evaluations of the compressibility factor and the individual fugacity coefficients reval that the gas phase is relatively close to ideality at the presently employed conditions. For the present experiments the compressibility factor and the individual fugacity coefficients are generally within 5 % of unity. Table 3.2 shows an example of the gas composition and the calculated fugacity coefficients for a CO hydrogenation experiment.

Table 3.1 The critical properties and acentric factors used in this work.

Component	T_C [K]	P_C [bar]	ω	Ref.
N_2	126.21	33.9	0.038	[44, 367]
H_2	32.97	12.93	-0.22	[44, 368]
CO	132.91	34.99	0.049	[44, 368]
CO_2	304.14	73.75	0.225	[44, 368]
CH_4	190.56	45.99	0.012	[44, 367]
C_2H_4	282.34	50.41	0.085	[44, 368]
C_2H_6	305.32	48.72	0.098	[44, 368]
C_3H_8	369.83	42.48	0.152	[44, 368, 369]
H_2O	647.14	220.6	0.344	[44, 369, 370]
H_2S	373.2	89.4	0.1	[44, 369]
MeOH	512.5	80.84	0.572	[44, 370]
EtOH	514.0	61.37	0.635	[44, 370]
1-PrOH	536.8	51.69	0.625	[44, 370]
1-BuOH	563.0	44.14	0.59	[44, 370]
Iso-BuOH	547.8	42.95	0.589	[44, 371]

Table 3.2 An example of the calculated fugacity coefficients in an experiment with a $K_2CO_3/Co/MoS_2/C$ catalyst.

Reaction conditions

T [°C]	325.6
T [K]	598.7
P [bar]	100

Feed stream				Product stream			
Component	y_i	φ_i	$y_i\varphi_i$	Component	y_i	φ_i	$y_i\varphi_i$
N_2				N_2			
H_2	0.490	1.034	0.507	H_2	0.449	1.036	0.465
CO	0.510	1.048	0.535	CO	0.471	1.048	0.494
CO_2				CO_2	$3.64\cdot10^{-2}$	1.020	$3.72\cdot10^{-2}$
CH_4				CH_4	$1.22\cdot10^{-2}$	1.034	$1.26\cdot10^{-2}$
C_2H_4				C_2H_4	$3.46\cdot10^{-4}$	1.032	$3.57\cdot10^{-4}$
C_2H_6				C_2H_6	$9.53\cdot10^{-2}$	1.033	$9.84\cdot10^{-4}$
C_3H_8				C_3H_8	$4.99\cdot10^{-2}$	1.042	$5.21\cdot10^{-4}$
H_2O				H_2O [a]	$1.25\cdot10^{-3}$	0.959	$1.20\cdot10^{-3}$
H_2S				H_2S			
MeOH				MeOH	$2.22\cdot10^{-2}$	0.996	$2.21\cdot10^{-2}$
EtOH				EtOH	$5.50\cdot10^{-3}$	1.010	$5.56\cdot10^{-3}$
1-PrOH				1-PrOH	$2.59\cdot10^{-3}$	1.018	$2.64\cdot10^{-3}$
1-BuOH				1-BuOH	$3.31\cdot10^{-4}$	1.027	$3.40\cdot10^{-4}$
Iso-BuOH				Iso-BuOH	$8.88\cdot10^{-4}$	1.033	$9.17\cdot10^{-4}$
EtAc				EtAc	$6.49\cdot10^{-5}$	1.045	$6.78\cdot10^{-5}$
		Z	1.042			Z	1.044

[a] The water content in the product is estimated through an assumption of equilibrium for the water gas shift reaction.

Table 3.2 illustrates how the compressibility factor and fugacity coefficients are relatively close to unity, and the values seen in table 3.2 are quite representative. It is especially the relatively high reaction temperatures required by the sulfide catalyst that help to ensure a proximity to ideal gas behavior. Due to the relatively ideal gas phase the kinetic model in chapter 5.3 employs partial pressures and not fugacities, although as the accumulated effects on the products involved in the kinetic expressions may lead to moderately increased deviations from the ideal case.

In some cases the equilibrium for the methanol synthesis reaction (R11) is evaluated, and in such cases the accumulated effects in products of multiple fugacities can in fact lead to more pronounced deviations from ideality. For this reason non-ideality effects are included in the equilibrium calculations. If the standard state is chosen to be an ideal gas at 1 bar the fugacity based equilibrium constant for a reaction like the methanol synthesis (R11) can be expressed in the following way [371]:

$$\frac{f_{MeOH}}{f_{H_2}^2 f_{CO}} = \exp\left(-\frac{\Delta G_{R1,T}^{\circ}}{RT}\right) = K_f \Leftrightarrow \frac{f_{MeOH}}{K_f f_{H_2}^2 f_{CO}} = 1 \tag{3.15}$$

The fugacity coefficients are calculated on the basis of the measured effluent gas composition and the known temperature and pressure. When the partial pressure of methanol has not reached its equilibrium value one will have $\frac{f_{MeOH}}{K_f f_{H_2}^2 f_{CO}} < 1$, and the quantity $\frac{f_{MeOH}}{K_f f_{H_2}^2 f_{CO}}$ can thus be used to provide a measure of the degree of equilibration for the methanol synthesis in a given experiment. Equation (3.15) can also be expressed as:

$$K_f = \frac{f_{MeOH}}{f_{H_2}^2 f_{CO}} = \frac{\varphi_{MeOH}}{\varphi_{H_2}^2 \varphi_{CO}} \frac{y_{MeOH}}{y_{H_2}^2 y_{CO}} \frac{1}{P^2} = K_\varphi \frac{y_{MeOH}}{y_{H_2}^2 y_{CO}} \frac{1}{P^2} \tag{3.16}$$

Where the fugacity coefficients are collected in the parameter K_φ:

$$K_\varphi = \frac{\varphi_{MeOH}}{\varphi_{H_2}^2 \varphi_{CO}} \tag{3.17}$$

4 Experimental work

Do what you can, with what you have, where you are
- Theodore Roosevelt

The present work has predominantly focused on experimental investigations. This section provides a general description of the experimental work, the experimental setup, the catalysts used in the investigations and the studies performed in the characterization of these catalysts.

4.1 Experimental setup

As stated in the introduction the main focus of this work has been experimental investigations of high pressure CO hydrogenation. These investigations have been performed in a high pressure flow reactor setup, which is illustrated in the diagram in figure 4.1.
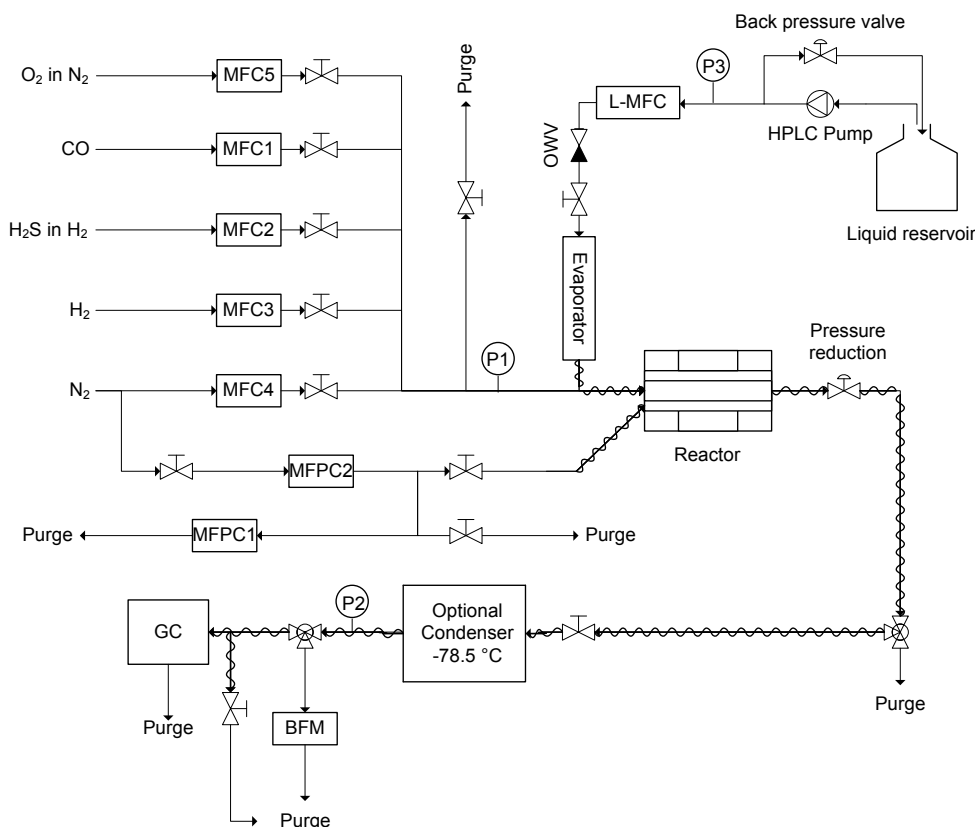

Figure 4.1 Simplified diagram illustrating the experimental setup. BFM: Bubble Flow Meter; GC: Gas Chromatograph; L-MFC: Mass Flow Controller for liquids; MF(P)C: Mass Flow (Pressure) Controller; OWV: One-Way Valve; P: Manometer. Heat traced tubing is indicated by sinusoidal curves.

The experimental setup has previously been used for investigations of homogeneous gas phase chemistry, and in this connection additional descriptions of the setup have been provided [372-377]. A setup manual is also available from the CHEC research group at the Department of Chemical and Biochemical Engineering, DTU [378]. The setup has been modified to accommodate the specific needs of the present investigation of the higher alcohol synthesis. The modifications of the setup include the addition of a system for condensation of the liquid product, the addition of a system for feeding normally liquid compounds to the reactor, the addition of several safety features, the addition of new feed gas lines and rebuilding of part of the tubing.

The core of the setup is the quartz reactor tube located inside a stainless steel pressure shell. As the interior of the quartz tube is pressurized, nitrogen is dosed to the pressure shell to ensure that no pressure gradient exists across the quartz tube wall. After the reactor the pressure is reduced, and the gas enters the downstream section. In the downstream section it is possible to condense the liquid reaction product, to analyze the gas composition with a GC-FID/TCD detection system and to measure the gas flow rate by means of a soap film bubble flow meter. The gas flow rates and the pressure regulation system are controlled from the computer program LABVIEW on a PC connected to the setup.

4.2 Upstream section: Gas feeding system

The feed gases are supplied to the reactor from pressurized cylinders via Brooks 5850S mass flow controllers, and the feed gasses are mixed before entering the reactor. In a few of the presented experiments the gas line used to supply N_2 to the inside of the reactor was instead used to supply NH_3 in H_2 to the reactor. Table 4.1 summarizes the gasses used in the present experimental work.

Table 4.1 Gasses used in the present experiments.

Gas	Purity	Supplier
CO	$\geq 99.97\,\%$	AGA A/S
H_2	$\geq 99.999\,\%$	AGA A/S
N_2	$\geq 99.97\,\%$	AGA A/S
2.00 mol% H_2S in H_2	Composition $\pm 2\,\%$	AGA A/S
9.998 mol% H_2S in H_2	Composition $\pm 1\,\%$	Strandmøllen A/S
5729 ppmv NH_3 in H_2	Composition $\pm 2\,\%$	AGA A/S
6115 ppmv NH_3 in H_2	Composition $\pm 2\,\%$	AGA A/S
0.6 mol% O_2 in N_2	Composition $\pm 2\,\%$	AGA A/S

The initial results presented in chapters 5 and 6 showed that there is a tendency for the catalyst to become relatively hot, when it is first exposed to syngas. In the subsequent experiments the syngas feed was therefore for the first hour diluted (1:1) with nitrogen, and the nitrogen was then gradually phased out.

The feed stream used in a given catalytic test was always pre-calibrated at the reaction pressure with an empty reactor tube, and flow (BFM) and composition (GC) measurements were used to adjust the feed to the desired composition.

The gas O_2/N_2 gas mixture in table 4.1 has only been used for passivation of the catalyst samples before these are removed from the reactor.

4.3   Upstream section: Liquid feeding system

Part of the experimental work includes dosage of the normally liquid compounds ethanol and water to the reactor at high pressure. This controlled liquid dosage is achieved using a liquid feeding system, which has been added to the high pressure reactor as a part of this PhD-project. The system is designed by the author and has been built by the workshop at the Department of Chemical Engineering.

An HPLC pump (Knauer K-120, 0-10 mL/min), which draws the liquid from a feed reservoir, pressurizes the liquid. The pressure in the feeding section is controlled by a back pressure valve (Tescom 26-1764-24-154) that directs part of the liquid flow back into the feed reservoir. The liquid flow to the reactor is controlled by a Brooks Flomega 5881 mass flow controller (0-15 g H_2O/h). The controlled liquid flow is evaporated in a custom made evaporator. In the evaporator the liquid/vapor flows through a 4.45 m steel tube (⅛"), which is coiled around a hollow cupper rod (outer diameter 20 mm). The heating for the evaporation is supplied by a heating cartridge (500 W) that fits exactly into the hollow cupper rod. After the evaporator the vaporized component is mixed with the incoming gaseous feed. The tubing between the evaporator and the reactor entrance is wrapped in heat tracing cables to avoid a condensation of liquids. The temperatures of the evaporator and of the heat tracing cables are regulated by Eurotherm controllers and monitored by Type-K thermo elements. The water co-fed with syngas in chapter 7 is ultra-pure, distilled water (resistivity: 18.2 M$\Omega\cdot$cm) that has been prepared using an Elgastat Maxima Analytical water purification system. The ethanol added to the syngas feed in chapter 6 is from Merck ($\geq$ 99.9 %).

Prior to use the liquid feeding system is tested in an experiment without reaction, where ethanol is evaporated into a 1 NL/min stream of N_2, and the ethanol concentration in the reactor effluent is measured using the GC downstream from the reactor. Figure 4.2 shows the measured ethanol concentration as a function of time during the test experiment.
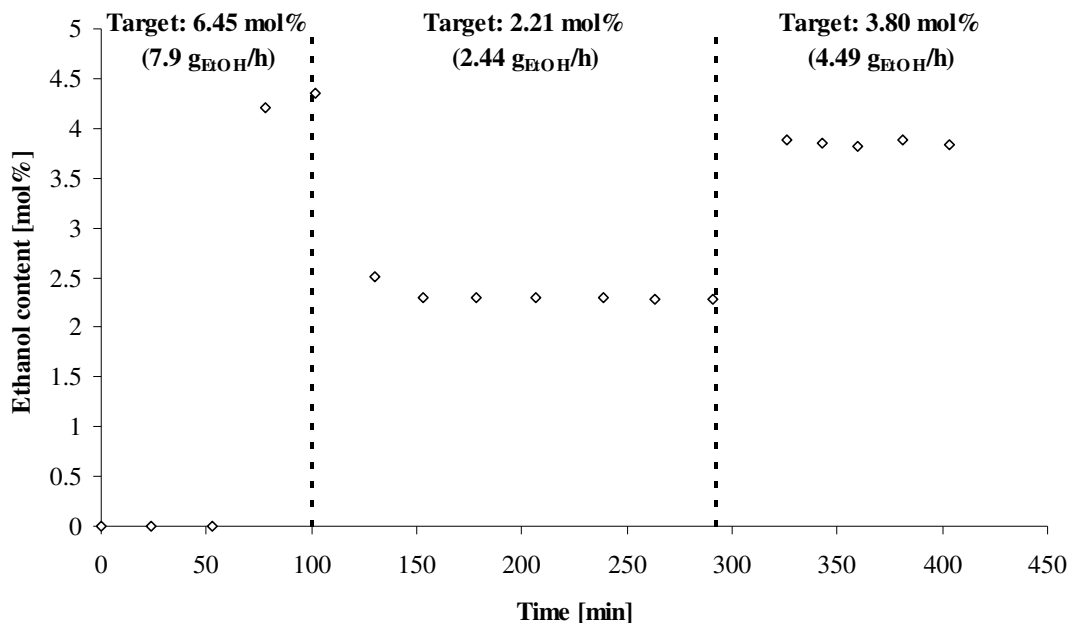
Figure 4.2 Measured ethanol concentration in the outlet stream coming from the reactor, when ethanol is evaporated into a flow of N_2. Experimental conditions: N_2 flow 1 NL/min, $T_{reactor}$ = 325 °C, $T_{evaporator}$ = 260 °C, 100 bar.

Figure 4.2 shows that there is a considerable delay from the start of the liquid feeding until liquid is actually detected in the effluent stream. This is because the length of the tubing in the liquid feeding section is considerable compared to the liquid volumes transported. However it can be seen from figure 4.2 that the system is able to dose liquid at high pressure with very limited fluctuations. In the present case the steady state concentrations are maintained within 0.5 % of the average value.

The test experiment reported in figure 4.2 has the weakness that the GC measurements are only conducted every 20th minute, and there could in principle be fluctuations on a shorter time scale. For this reason an additional test experiment is conducted. In this experiment methanol (Sigma-Aldrich ≥99.9 %) fed to the system is homogeneously oxidized at 625 °C and 100 bar under fuel rich conditions (O_2 is 20 % of the stoichiometric amount). Nitrogen is used to dilute the reacting gasses. The effluent concentrations of the combustion products CO and CO_2 are monitored using a conventional Fisher-Rosemount MLT1 $CO/CO_2/O_2$, infrared gas analyzer located immediately after the pressure reduction (in order to avoid unnecessary mixing in the tubing). The conventional gas analyzer has the advantage that it is able to transmit an online signal, and the analyzer can therefore be used to verify the absence of feeding fluctuations on a shorter time scale. Figure 4.3 shows the CO and CO_2 measurements from the gas analyzer as functions of time during the verification experiment.
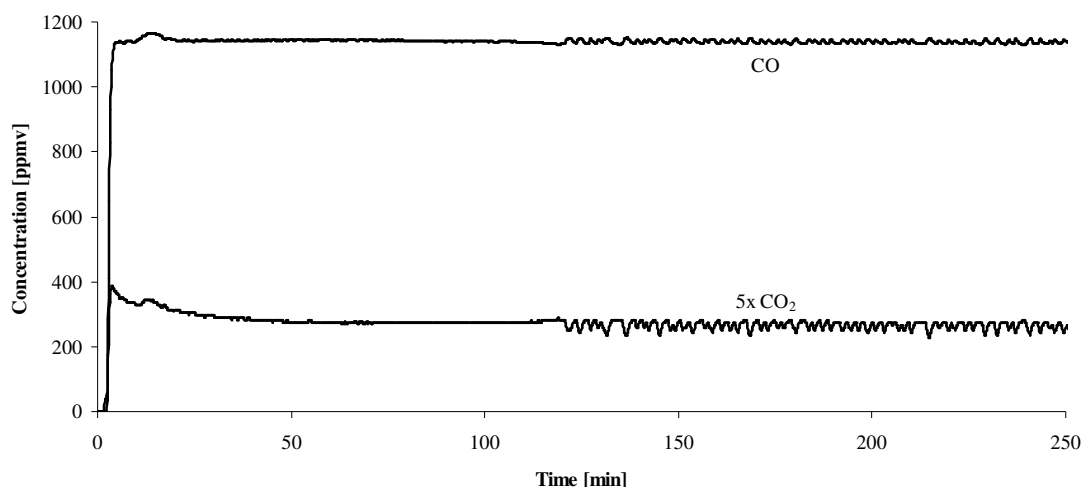
Figure 4.3 The content of CO and CO_2 in the reactor effluent stream during oxidation of CH_3OH at fuel rich conditions. The experimental conditions are 100 bar, 625 °C, 3070 ppmv CH_3OH and 921 ppmv O_2 in N_2.

Figure 4.3 generally corroborates the conclusion from figure 4.2 namely that the liquid dosage, when monitored through the methanol oxidation products, seems remarkably stable – even at a short time scale. After 120 minutes of the experiment in figure 4.3 a vibrating solid feeder in a neighbouring experimental setup is however initiated, and the vibrations from this feeder actually translates into oscillations in the liquid feeding. There are thus factors that can introduce instabilities in the liquid feeding system, but overall the liquid feeding system is deemed operational.

4.4   Reactor, oven and pressure shell setup

The reactor consists of a quartz tube (i.d. 8 mm; o.d. 10 mm; length 1545 mm), which contains the bed of catalyst particles (up to 25 cm in length). The quartz tube is placed inside a TP347 stainless steel pressure shell. As the interior of the quartz tube is pressurized, nitrogen is dosed to the pressure shell to ensure that no pressure gradient exists across the quartz tube wall. The shell side pressure is regulated by two Brooks 5866 mass flow pressure controllers. When the pressure inside the quartz tube has reached its set point there is no nitrogen flow into or out of the pressure shell. Figure 4.4 shows a diagram of the pressure shell.

The ensemble of reactor tube and pressure shell is placed inside an Entech tube oven that provides the relevant reaction temperature. Figure 4.5 shows a diagram of the oven and the pressure shell.
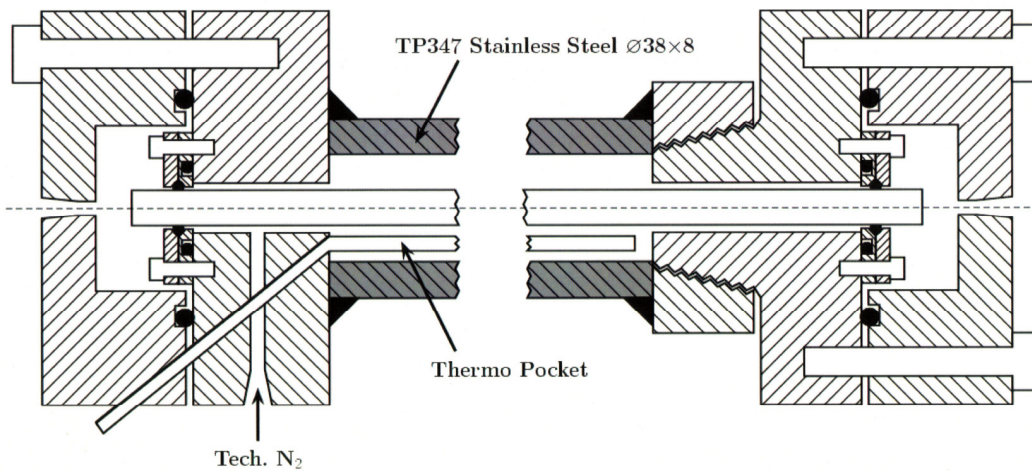
Figure 4.4 Diagram illustrating the principles of the steel flanges, the sealing of the reactor and the pressure control system. White hatched parts represent AISI 316 stainless steel flanges. Grey hatched parts indicate the TP 347 stainless steel pressure shell. Black circles indicate Viton O-rings. Black triangles represent welded connections. Each flange is fixed by four bolts, with the position of the bolts illustrated by white silhouettes. The quartz reactor is also represented by a white silhouette.
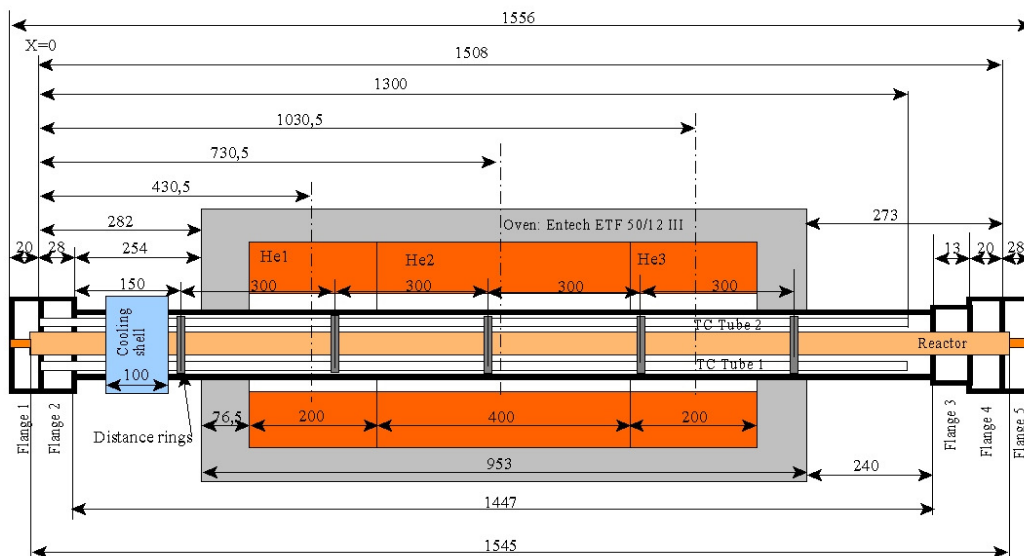
Figure 4.5 Diagram showing the dimensions of the pressure shell setup. All measurements are in mm. The cooling shell shown in the diagram was disconnected in the experiments with feeding of liquids.

The reactor temperature is monitored by type K (± 2.2 K or 0.75 %) thermoelements positioned inside two steel thermo pockets placed in the void between the quartz tube and

the pressure shell. The bed of catalyst is contained within the isothermal zone (± 1.5 K) in the oven. Figure 4.6 shows a series of representative temperature profiles.
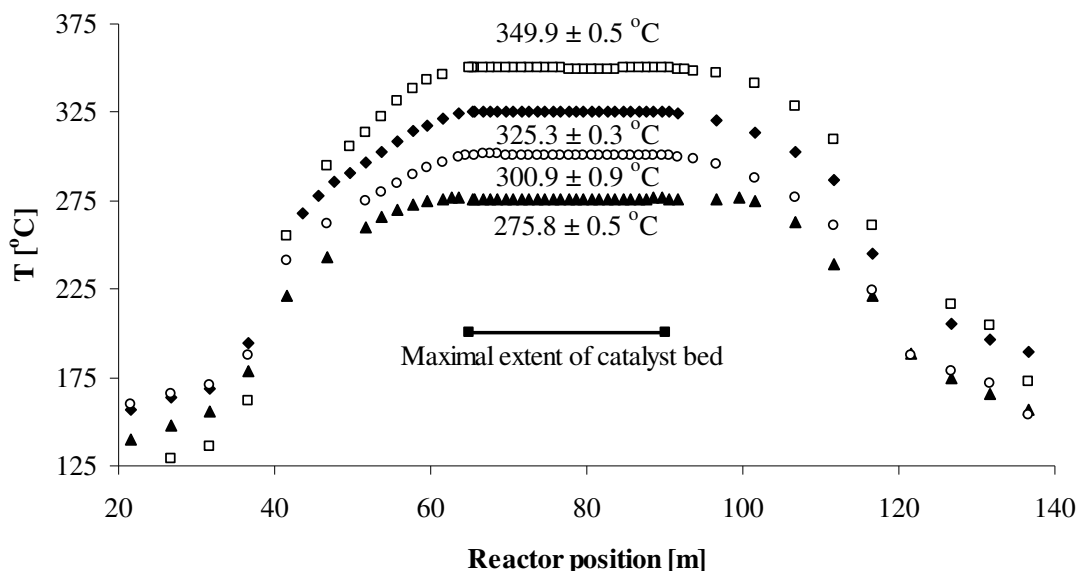
Figure 4.6 Representative temperature profiles measured in the thermo pocket (see figure 4.4). The process temperature is noted above each profile along with the temperature variation along the catalyst bed. The temperatures in the ends of the reactor are determined by the temperature of the heat tracing tapes.

An element of uncertainty in the measurements is introduced by the fact that the temperature is monitored in the thermo pocket in the shell and not within the catalyst bed itself. Due to the strong exothermicity of the studied reactions the adiabatic temperature rise is potentially very large - in some cases several hundred degrees (see appendix A for a calculation of the adiabatic temperature rise), but the flow rates are quite small, and the effect that needs to be removed in order to eliminate the temperature rise entirely is also very small. A bigger issue is that the thermo pocket in some locations is separated from the quartz tube by a stationary layer of nitrogen. Appendix B contains a relatively simple calculation of the possible difference between the measured temperature and the real temperature, if conduction through the stationary nitrogen layer in the shell is the only mechanism of heat transfer. The calculation in appendix B reveals that there could be a significant disparity between the temperature in the bed and the temperature measured in the thermo pocket. In the most relevant range of CO conversions from 3-15 mol% the temperature may, depending upon the conversion and the product distribution differ by 4-15 °C. This is definitely a quite significant uncertainty. There are however some redeeming factors that should help to reduce the uncertainty on the temperature. The primary factor is that the thermo pocket is not completely straight, as it is depicted in figure 4.4 and figure 4.5. Instead the thermo pocket has some wriggles, and the pocket is in places brushing up against the quartz tube. This should ensure a greatly improved heat transfer compared to a stationary layer of nitrogen, and therefore a lower temperature difference. If a temperature gradient does evolve across the stagnant nitrogen layer in the

pressure shell this would also introduce motion in the gas, which again would help to improve heat transfer. Finally radiation, which is not considered in the simple calculation in appendix B, could also contribute to the heat transfer and lower the uncertainty on the measured temperature.

The uncertainty regarding the difference between the bed temperature and the measured temperature should thus be of a limited magnitude, but it is nevertheless a factor that must be considered, when the results from the present setup are regarded.

4.5 Downstream section: Product collection and analysis

Downstream from the reactor the pressure is relieved by means of a pneumatically operated Flowserve Kämmer pressure reduction valve, and the reactor effluent is directed to the characterization section. As the effluent stream from the reactor potentially can contain condensable components heat tracing of the tubing is employed throughout the downstream section. To estimate the necessary temperature for the heat tracing tapes the dew point of the reactor effluent has been calculated. The estimate is based upon a product composition provided by Shaeiwitz et al. [379], and the product composition is estimated to be independent of conversion. As it will be shown subsequently this is however not entirely true, but the assumption provides an estimate of the "worst case scenario", since it is the gaseous products that are favored by an increasing conversion. The dew point temperature is determined though an iterative procedure. At each temperature the phase composition is determined through a modified version [380] of the Rachford-Rice [381] algorithm. A detailed description of the calculation procedure is provided in appendix C. Figure 4.7 shows the calculated dew points before and after the pressure reduction as functions of the CO conversion.
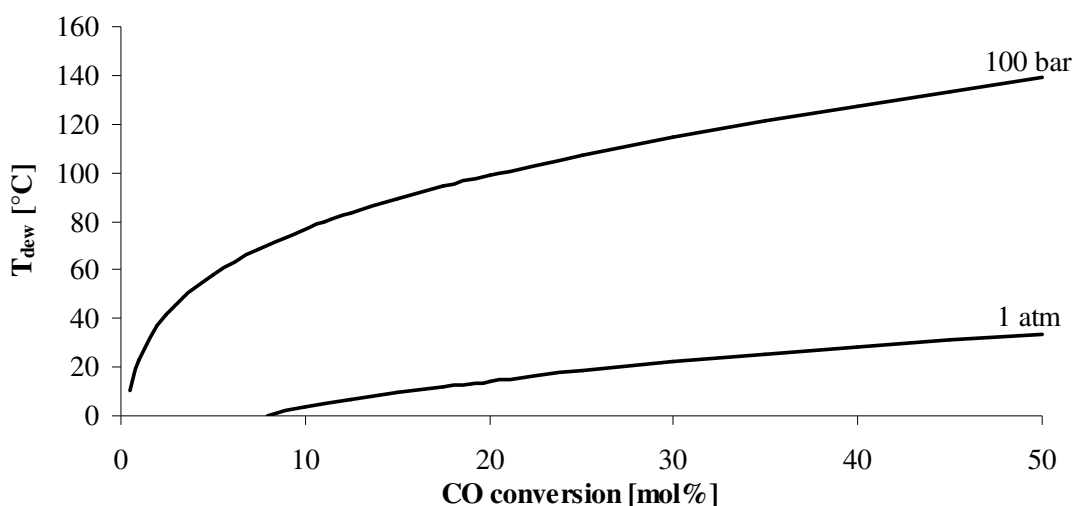

Figure 4.7 Calculated dew points for the reactor effluent at 100 bar and 1 atm as functions of the CO conversion to the product distribution provided by Shaeiwitz et al. [379].

Figure 4.7 shows that relatively high heat tracing temperatures are necessary to avoid a condensation before the pressure reduction. Typically the target temperature for the heat tracing is 125-135 °C, which with the relevant conversion levels should be sufficient even for the high pressure part of the downstream section. The product distribution from Shaeiwitz et al. [379], which is employed in the calculation of the dew points in figure 4.7, is actually slightly optimistic, and the product streams obtained with the presently employed catalysts generally do require slightly lower tracing temperatures, than it is indicated in figure 4.7.

After the pressure reduction the reaction product is analyzed. Generally the system is operated without condensation of the liquid reaction product, and in that case the analysis of the reactor effluent relies on a GC analysis, but in some cases the alcohol product is condensed and collected. This is done at atmospheric pressure and dry ice temperature (-78.5 °C). In such cases a custom made U-tube condenser is attached to the system (see the location in figure 4.1). The sulfur content in the condensed liquid samples has been determined in a process, where the sample is first decomposed by microwave heating to 230 ºC in a mixture of HNO_3 and H_2O_2. The mixture is then diluted with H_2O, and finally the sulfur content in the diluted sample is determined using Inductively Coupled Plasma – Optical Emission Spectroscopy (ICP-OES). To determine the speciation of the sulfur present in the alcohol product, the liquid product has been subjected to a qualitative sulfur analysis by means of GC-AED. The analysis of the liquid product has been conducted by Haldor Topsøe A/S.

In the downstream section the reactor effluent can be directed to the GC or to the manually operated, soap film, bubble flow meter. The bubble flow meter operates at ambient temperature and near atmospheric pressure (0.975 bar). The near-ambient pressure in the flow meter is achieved by having a long (~5 m) gas line from the flow meter into the purge system (see perhaps figure 4.1). The temperature and pressure in the flow meter have been determined by attachment of a manometer and a thermo element to the flow meter, but for safety reason these units are normally not attached to the system.

The use of the bubble flow meter was chosen, because the flow meter with the available equipment was estimated to have a better accuracy than the use of an internal standard like N_2. A single situation, where there is a contribution to the uncertainty from the use of the bubble flow meter, occurs when noteworthy fractions of condensable components are present in the rector effluent. The capture of such components in the bubble flow meter will lead to a corresponding error in the measurement of the flow. In the present experiments the total fraction of alcohols in the effluent stream never reaches more than at most a few percent, so even if all condensable components are captured in the bubble flow meter, the uncertainty on the flow is still of a limited magnitude.

4.6   GC: Analysis of the gaseous products

The reactor effluent is characterized using a GC-FID/TCD detection system (6890N from Agilent Technologies), which uses helium as the carrier gas. Alcohols, esters and H_2S are separated using a DB1 column. Hydrocarbons, CO, H_2, CO_2 and N_2 are separated using a dual column system, where a Porapak N column is followed by a 13× Molsieve column. The properties of the GC columns are summarized in table 4.2.

Table 4.2 The stationary phases in the GC.

Column	Length [m]	Stationary phase material
DB1	50	100 % Dimethyl polysiloxane
Porapak N	3.05 (10 ft)	Bonded divinylbenzene/ethylene glycol dimethacrylate
13× Molsieve	1.22 (4 ft)	5 Å molecular sieve zeolite

The two classes of gas phase constituents (alcohols and hydrocarbons/simple gasses) are quantified in two separate analysis runs, and both these two runs employ both the TCD and the FID detector. Helium is used as the carrier gas in the gas chromatograph. The rationale for using helium as the carrier gas is related to the strength of the TCD signal. The use of either N_2 or Ar as the carrier gas would make it difficult to measure small concentrations of CH_4, CO and CO_2, since these gasses all have thermal conductivities similar to N_2 and Ar. On the other hand the use of helium as the carrier gas means that the detection limit for hydrogen is positioned somewhat higher, than what is the case for the other components detected by the TCD. Since hydrogen is a reactant typically composing around 50 vol% of the feed gas, and since the conversions typically are modest, the higher detection limit for hydrogen is however not considered a problem in the present work. It must however be said that the hydrogen signal is rather weak, which could result in a larger uncertainty in the quantification of the hydrogen content in the gas.

To account for the appearance of uncharacterized reaction products the number of calibrated compounds was gradually increased throughout the present experimental campaign. For this reason not all the compounds listed in table 4.3 are quantified in all experiments. The compounds above the dotted line in table 4.3 are those that have been quantified in all experiments including those presented in chapter 5. The compounds below the dotted lines were added for the experiments presented in chapters 6-9.

Table 4.3 Compounds characterized in the GC-analysis.

Alcohols	Hydrocarbons	Feed gases	Sulfur compounds	Oxygenates
Methanol	Methane	CO	H_2S	DME
Ethanol	Ethane	H_2	SO_2	Ethyl acetate
1-Propanol	Ethene	N_2		Butyl acetate
1-Butanol	Propane	CO_2		Ethyl butyrate
Iso-Butanol				
2-Butanol				
Ethylene glycol				

The identification and quantification of peaks in the GC spectra rely on prior calibration against gas mixtures with known compositions.

For normally gaseous compounds the GC peak areas are related to molar fractions by calibration against certified gas mixtures (± 2 % from AGA A/S).

For normally liquid compounds the calibration is made against gas mixtures prepared by injecting a known quantity of the liquid component (≥99.9 % from Sigma-Aldrich) into a known volume of nitrogen (≥99.7 % from AGA A/S) in a Tedlar bag and allowing

the liquid to evaporate. The gas filled bag is given approximately 24 h for the gaseous components to mix, and the gas mixture is then analyzed with the GC. It must be expected that the calibration for liquid components holds a greater uncertainty than the calibration for gaseous compounds.

For normally gaseous components the calibration curves rely on 2-3 calibration points, while the calibration curves for normally liquid components typically rely on 4-5 calibration points. The calibration points are generally chosen to be representative of the typical experimental concentrations. For all compounds except hydrogen the molar fraction of the component is linearly related to the GC peak area. In the case of hydrogen the calibration curve the peak area is a cubic function of the molar fraction of hydrogen in the gas mixture.

Before the GC inlet there is an outlet into the purge, which can be regulated with a needle valve. By adjustment of the needle valve the GC inlet pressure is always adjusted to atmospheric pressure, which is also the inlet pressure used in the calibrations. This is done to avoid an influence of a varying inlet pressure on the GC measurements.

4.7 Characterization of the reaction

A single data point consists of a flow measurement and two GC analyses of respectively alcohols and hydrocarbons/simple gasses. In several cases the catalytic properties are monitored as functions of the time on stream, but the GC requires a considerable amount of time (two sample injections over a period of 18 min) to perform a full characterization of the product stream. In such investigations the convention is that the GC analysis of alcohols and oxygenates is initiated first, and while this analysis is running the flow is measured. Once the first GC analysis is finished the second one (hydrocarbons/simple gasses) is initiated. The location in time of the whole set of measurements that constitutes a data point is considered to be the mid-point between the two GC injections.

The measured volumetric flow rate and the measured concentration of component i can be used to determine the molar flow rate of component i, which is denoted F_i. The reported CO conversion (X_{CO}) is calculated from the molar flow rates of CO into and out of the reactor:

$$X_{CO} = \frac{F_{CO}^{in} - F_{CO}^{out}}{F_{CO}^{in}} \qquad (4.1)$$

The alcohol selectivity (S_{Alc}) presented in this paper is the carbon based, CO_2-free selectivity, which is calculated on the basis of the characterized C_1-C_4 alcohols (see table 4.3):

$$S_{Alc} = \frac{\sum_{n=1}^{4} n F_{Alc,n}^{out}}{F_{CO}^{in} - F_{CO}^{out} - F_{CO_2}^{out}} \qquad (4.2)$$

Here n is the carbon number in the alcohol. It should be noted that this expression is somewhat susceptible to experimental uncertainty, when the conversion is low. A departure from this (4.2) evaluation of the selectivity on the basis of the CO converted is the investigations of carbide catalysts in chapter 9. The carbide catalysts seem produce a significant amount of an uncharacterized product, which could be carbonaceous deposits on the catalyst (the mass of the catalyst sample increases significantly during use). To focus on the synthesis products the selectivities reported in chapter 9 are therefore the carbon based selectivites based upon the characterized products and upon the consumed CO as in equation (4.2).

Another evaluation parameter, which is used in the subsequent text, is the weight ratio between the production of higher alcohols and the production of methanol:

$$\frac{C_{2+}}{C_1} = \frac{\sum_{n=2}^{4} M_{Alc,n} \cdot F_{Alc,n}^{out}}{M_{MeOH} \cdot F_{MeOH}^{out}} \tag{4.3}$$

Here $M_{Alc,n}$ denotes the molar mass of the alcohol with n carbon atoms.

An additional characterization parameter is the space time yield (STY) of alcohols, which is the production rate of alcohols per mass of catalyst:

$$STY_{Alc} = \frac{\sum_{n=1}^{4} M_n F_{Alc,n}^{out}}{m_{cat}} \tag{4.4}$$

It should be emphasized that when a space time yield (STY) is reported in the subsequent text, the STY is the mass of alcohol produced per hour and per mass of catalyst. Here the mass of catalyst is referring to the total mass of the active materials and the carbon carrier.

In the kinetic investigations in section 5.3 the parameter space employed is T = 275-350 °C, P = 100 bar, $\frac{P_{H_2}}{P_{CO}} \in [0.5;5]$, GHSV $\cong$ 5000 h^{-1} (based on total bed volume and referring to 298.15 K and 1 atm). The kinetic studies have been performed with 260 ppmv of H_2S in the syngas feed to avoid the gradual changes in product distribution, which, as it will be discussed in section 5.2, are observed for long periods of time in the absence of co-fed H_2S. The measurements in the kinetic investigations are performed after at least 15 hours on stream and constitute an average over two hours with stable measurements. The partial pressures of CO and H_2 are varied at a constant total pressure and a constant GHSV by replacing part of the flow of one reactant with a flow of nitrogen. The partial pressure of H_2S is also varied as part of the kinetic investigations. As the H_2S concentration is very low, the H_2S pressure is varied by replacing a very small part of the H_2 flow with an H_2S flow, whereby the GHSV is kept constant. As the H_2S concentration in the feed is very low, the H_2 concentration in the feed is approximately constant (within 0.4 %) even though the H_2S concentration in the feed is changed by a factor of 6. The absence of both internal and external mass transfer limitations in the

performed experiments has been verified by evaluating the observed reaction rates against the Mears [382] and Weiss-Prater [383, 384] criteria. Diffusion coefficients and viscosities used in these calculations have been estimated using the Chapman-Enskog kinetic theory [385]. A detailed description of these calculations can be found in appendix D.

4.8 Reproducibility

Another issue that should be discussed is the reproducibility of measurements. Figure 4.8 shows the average production rates of methanol and higher alcohols after 25-30 h on stream for a $K_2CO_3/Co/MoS_2/C$ catalyst in 5 different experimental runs.
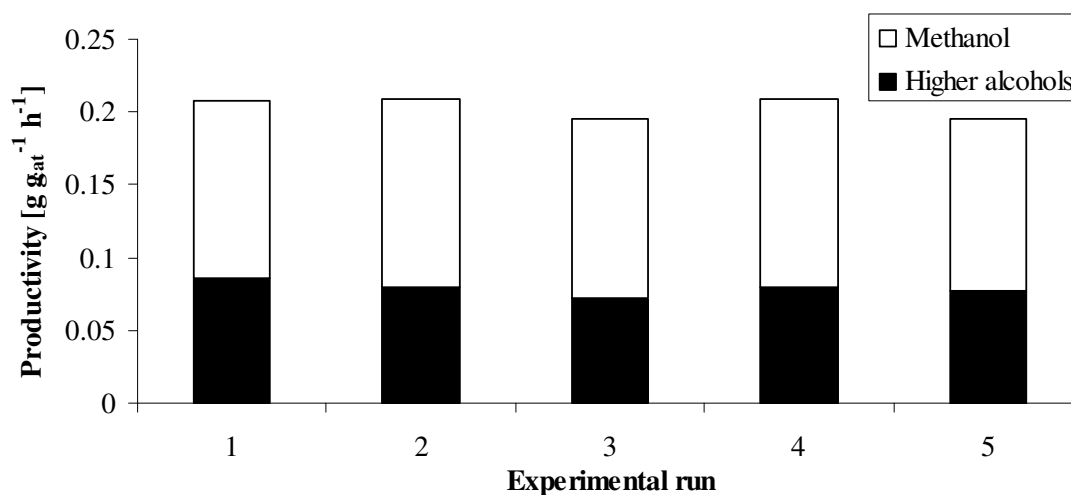
Figure 4.8 Production rates of methanol and higher alcohols for 5 experimental runs with a potassium promoted cobalt-molybdenum sulfide catalyst. The experimental conditions are 100 bar, 326 ± 1 °C, 5420 ± 125 h^{-1}, +25 h on stream. The catalyst used is KCoMo-3 in table 4.4.

Figure 4.8 illustrates that the reproducibility in the experimental runs is relatively good. The total alcohol production can vary up to 3.6 %, while the production of higher alcohols may exhibit larger variations – up to 6.6 %. As it will be discussed in detail in chapters 5 and 8 the catalytic properties of the cobalt-molybdenum sulfide catalyst undergo marked alterations during the first ~25 h on stream. That the activity despite the marked, initial changes in catalytic properties, is so relatively reproducible after 25-30 h is taken as evidence for a rather good reproducibility in the present experiments.

The subtle variations that are seen between the experimental runs in figure 4.8 may especially be related to the differences in the temperature history for the samples (it will be discussed in section 5.2 how the initial temperature can be difficult to control). Factors like minor inhomogenities in the catalyst sample, differences in the temperature profile and differences in the gas flow through the bed could however also contribute to the variations seen in figure 4.8.

4.9 Catalysts

4.9.1 K$_2$CO$_3$/Co/MoS$_2$/C catalysts

A total of 4 different samples were used in the studies of carbon supported, potassium promoted cobalt-molybdenum sulfide. The support material for all these catalysts is Daihope carbon and the particle size is $d_{p,\ avg}$ = 1.2 ± 0.3 mm. Table 4.4 summarizes selected physical properties for these four catalyst samples.

Table 4.4 Selected physical properties of the catalyst samples used in the experiments.

Catalyst	Metal Content [wt%]			Co/Mo [mol/mol]	BET area [m^2/g]	Pore volume [mL/g]	Bulk density [g/mL]
	Mo	Co	K				
KCoMo-1	4.23	2.30	9.3	0.89	543	1.15	1.15
KCoMo-2	5.33	2.01	14.2	0.61	490	0.99	0.99
KCoMo-3	13.60	2.71	9.0	0.32	526	1.23	1.23
KCoMo-4 [a]	13.60	1.39	9.0	0.17	402		

[a] The composition of this catalyst is a nominal composition based upon the weighed amount of the various precursors. For the other samples analyzed compositions are given.

The samples KCoMo-1, KCoMo-2 and KCoMo-3 in table 4.4 were provided by Haldor Topsøe A/S. These catalysts have been prepared in the oxide form, but the details of the preparation have not been disclosed. The exact preparation method for these catalysts has not been disclosed. To evaluate the role of the Co content in the catalyst an additional catalyst (KCoMo-4) was prepared. The catalyst KCoMo-4 was prepared to have the same contents of Mo and K as KCoMo-3, but to have a lower Co content. This catalyst KCoMo-4 was prepared by sequential incipient wetness impregnation of Daihope carbon with aqueous solutions of $(NH_4)_6Mo_7O_{24}$ · $4H_2O$ (Sigma-Aldrich, ≥ 99 %), $Co(CH_3COO)_2$ · $4H_2O$ (Sigma-Aldrich, ≥ 98.0 %) and K_2CO_3 (Sigma-Aldrich, ≥ 99 %). In certain cases gentle heating over a water bath was necessary to dissolve the precursors. The order of impregnation was Mo, Co and finally K. Between each impregnation the catalyst was dried in flowing air at 100 °C for at least 3 h. The catalyst was finally calcined in flowing N$_2$ for 2 h at 450 °C.

Prior to use the catalysts have all been sulfided in a flow of 2 mol% H$_2$S in H$_2$. In the sulfidation procedure the reactor was purged with nitrogen, and the temperature was increased to 100 °C. The catalyst was then at atmospheric pressure exposed to an 80 NmL/min (with NmL relating to 273.15 K and 1 atm) flow of 2 mol% H$_2$S in H$_2$, and the temperature was increased at a rate of 3 °C/min to the reaction temperature of 325 °C. The sulfidation was maintained at the final temperature for approximately 15 h. At that point no further sulfur uptake was observed.

The catalyst KCoMo-1 has been used for the experiments presented in sections 5.2 and 5.5. The catalyst KCoMo-2 has been used for the experiments presented in section 5.3, and the catalyst KCoMo-4 has been used for part of the experiments presented in section 8. The catalyst KCoMo-3 has been used for all the other investigations of the sulfide catalysts. In section 2.3.3 it was described how optimal, molar Co:Mo ratio reportedly is 1:2, and from table 4.4 it can be seen that the catalyst KCoMo-3, which has

been used in most of the investigations, has a lower cobalt content than it is dictated by the optimal ratio. The catalyst KCoMo-2, which has been used for the kinetic investigations in section 5.3, is closest to the optimal ratio.

4.9.2 Sample handling for the experiments in chapter 8

Chapter 8 contains a description of various spectroscopic investigations conducted on fresh and spent sulfide catalyst samples. Below is a brief description of the sample treatment.

A catalyst of the type KCoMo-3 was sulfided according to the procedure described above. The catalyst was then used for CO hydrogenation for 42 hours. The experiments were conducted with a 25 cm long bed of catalyst. After the CO hydrogenation samples were taken out from the outermost 2 cm of respectively the front and rear ends of the catalyst bed. The term "front end" refers to the end of the bed, where the syngas enters the bed. These samples of the spent catalyst have then been compared to a freshly sulfided catalyst by the various analysis techniques described below. Before the fresh and spent sulfide samples were removed from the reactor, they were all first passivated in a flow of 0.6 mol% O_2 in N_2 for at least 3 hours. This was done in an attempt to protect the catalyst from excessive oxidation by the ambient air. The samples were generally stored for approximately 1 week before the spectroscopic investigations and 2-3 weeks before the microscopy investigations. As it will be discussed in more detail in section 8.3 the sulfide may be susceptible to oxidation by air at room temperature.

4.9.3 Carbide based catalysts

The objective of the catalyst preparation was to synthesize the bulk carbides Mo_2C, WC and NbC. The bulk carbides employed in the present investigations have been synthesized by temperature programmed reduction/carburization of oxide precursors in a flow of 20 vol% CH_4 in H_2 (Air Liquide). This preparation method was developed by Lee et al. [254]. The presently employed carburization conditions were inspired by reported procedures for the preparation of Mo_2C [254, 386, 387], WC [388, 389] and NbC [390-394]. In this work the starting point has been MoO_3 (Sigma-Aldrich, $\geq$99.5%), WO_3 (Haldor Topsøe A/S, from decomposition of ammonium paratungstate at 550 °C), and Nb_2O_5 (Heraeus $\geq$99.9%), and the exact conditions employed in the carburizations were the result of a series of trial runs, wherein the durations and temperatures necessary for the carburization reactions were established. First the oxide precursor was pressed, crushed and sieved to a size range of 600-1400 µm. In each carburization run a quartz sample holder was filled with 12-13 g of the granulated, oxide precursor, and the sample holder was placed in a quartz tube (i.d. 30 mm) inside a Carbolite tube furnace. The depth of the layer of oxide granulates in the sample holder was approximately 3 mm. In this arrangement the carburizing gas passed by the sample rather than though a packed bed of sample. After purging of the system with N_2 the oxide was subjected to a 40 NmL/min (with NmL relating to 273.15 K and 1 atm) flow of 20 vol % CH_4 in H_2, and the temperature programmed carburization was initiated. Lee et al. [254] reported that no

significant reaction occurred in the carburization of MoO_3 below 280 °C, and in the present work the temperature was always increased to 280 °C at a relatively high heating rate. The temperature was then ramped up to a final temperature (T_{final}) and maintained at the final temperature for a given holding time (t_{hold}). The operating parameters for the carburization procedures are summarized in table 4.5.

Table 4.5 Operating parameters for the carburization procedures.

Carbide	$\Delta T_{ramp, <280\ °C}$ [°C/min]	$\Delta T_{ramp, >280\ °C}$ [°C/min]	T_{final} [°C]	t_{hold} [h]
Mo_2C	5	0.5	750	5
WC	5	2.5	850	7
NbC	10	10	1000	13

After the holding time at the final temperature the sample was allowed to cool down in the prevailing flow of 20 vol% CH_4/H_2, until the temperature fell below 280 °C. At that point the flow of carburizing gas was replaced with a flow of N_2, which was maintained until room temperature was reached. Before the prepared carbide was removed from the furnace, the carbide sample was exposed to a flow of 1 vol% O_2 in N_2 for at least 2 hours in order to passivate the sample. The success of a given carburization experiment was evaluated on the basis of the X-ray diffraction spectrum of the carburized material and on the basis of the weight change of the oxide samples. For the final carburization conditions presented in table 4.5 the sample weights after the carburizing treatments were in all cases within 1 % of the predictions for the formation of Mo_2C, NbC and WC respectively.

Most of the carbide catalysts investigated in this work were modified by one or more additives. After the carburization the pore volume of the carbide was determined though the water uptake of a small part of the carbide sample. The carbide was then impregnated to incipient wetness with an aqueous solution of the precursor for the relevant additive. The reported catalyst compositions are nominal compositions based upon the weighed amounts of the employed precursors. Table 4.6 summarizes the precursors used in the impregnations.

Table 4.6 Precursors used in the preparation of promoted carbides.

Additive	Precursor	Purity	Supplier
K	K_2CO_3	≥99%	Ridel de Haën
Cs	Cs_2CO_3	≥99%	Fluka
Li	$Li(CH_3COO)\cdot 2H_2O$	≥98%	Sigma-Aldrich
Mn	$Mn(CH_3COO)_2\cdot 4H_2O$	≥99%	Sigma-Aldrich
Cu	$Cu(CH_3COO)_2$	≥99%	Fluka
La	$La(CH_3COO)_3\cdot xH_2O$	≥99.9%	Sigma-Aldrich
V	NH_4VO_3	≥99%	Fluka
Re	NH_4ReO_4	≥99%	Sigma-Aldrich

The vanadium containing solution used in the impregnation was prepared by heating a stirred slurry of NH_4VO_3 and oxalic acid ($C_2O_4H_2/NH_4VO_3 = 2/1$ mol/mol) in water to 80 °C over a water bath, until a clear, blue solution was obtained. The use of nitrate salts was generally avoided in the impregnations, after it was observed that the use of iron(III)

nitrate in the impregnation of Mo_2C resulted in the evolution of brown gas – possibly NO_x species formed in the decomposition of the nitrate salt. The nitrate decomposition might be associated with some degree of oxidation of the carbide material. No attempt was made to calcine or utilize the nitrate impregnated material. It is possible that a more extensive passivation would render the carbide more resistant towards the nitrate, but this was not investigated. It should be mentioned that other researchers have succeeded in impregnating carbides with nitrate salts. Griboval-Constant et al. [388, 395] impregnated Mo_2C and WC with an aqueous solution of cobalt nitrate and do not report any problems of this kind.

After the impregnation the wetted carbide was allowed to age for 2 hours. Following the aging period the wetted carbide was dried for 2 h in flowing N_2 at 100 °C and then calcined for 2 h at 450 °C in flowing N_2. If more than one additive was employed this was achieved by sequential impregnation steps with intermediate drying. To avoid the formation of volatile rhenium oxide species a Rhenium containing catalyst was not calcined. Table 4.7 summarizes the compositions of all the prepared catalysts

Table 4.7 Nominal compositions of the catalysts used in the present work.

Sample	Nominal Composition
$K_2CO_3/Mo_2C^{a)}$	10.00 wt% K_2CO_3, 90.00 wt% Mo_2C
$K_2CO_3/WC^{\,a)}$	5.50 wt% K_2CO_3, 94.50 wt% WC
NbC	Unpromoted NbC
$Cs_2CO_3/Mo_2C^{\,a)}$	20.68 wt% Cs_2CO_3, 79.32 wt% Mo_2C
$Li(CH_3COO)/Mo_2C^{\,a)}$	9.59 wt% $Li(CH_3COO)$, 90.41 wt% Mo_2C
$K_2CO_3/Re(1)/Mo_2C$	10.00 wt% K_2CO_3, 1.00 wt% Re, 89.00 wt% Mo_2C
$K_2CO_3/Mn(1)/Mo_2C$	10.00 wt% K_2CO_3, 1.00 wt% Mn, 89.00 wt% Mo_2C
$K_2CO_3/Mn(5)/Mo_2C$	10.00 wt% K_2CO_3, 5.01 wt% Mn, 84.99 wt% Mo_2C
$Cu(0.84)/K_2CO_3/Mo_2C$	0.84 wt% Cu, 9.91 wt% K_2CO_3, 89.25 wt% Mo_2C
$La(CH_3COO)_3/V/Mo_2C$	5.00 wt% La, 3.00 wt% V, 92.00 wt% Mo_2C

[a)] Prepared for an Alkali/Me (Me =Mo/W) ratio of 0.164±0.001 mol/mol.

The convention for the notation in this work is that the additives are written from right to left in the order of their impregnation. In the material $Cu/K_2CO_3/Mo_2C$ the potassium carbonate is for example added before cupper. Because the nature of the employed alkali salt has been observed to have a considerable influence upon the catalytic properties of Mo_2C in the alcohol synthesis [116], the full structure of the employed alkali salt is always written. The content of the alkali promoter is expressed in terms of the weight fraction of the alkali salt to retain consistency with previous work [115].

Prior to the CO hydrogenation experiments the carbide catalysts were subjected to a reducing treatment. The system was purged with nitrogen, and the temperature was increased to 100 °C in a 72 NmL/min flow of N_2. The catalyst was then subjected to a 82 NmL/min flow of 12 vol% H_2 in N_2, and the temperature was increased at a rate of 3 °C/min to a final temperature of 350 °C. The final temperature was maintained for 2 hours, and the catalyst was then cooled to the reaction temperature in a flow of N_2. There were two exceptions to this treatment. The Re containing catalyst was heated to 450 °C instead of 350 °C. This choice was based upon previous TPR investigations for Re containing catalysts [396]. The Cu containing catalyst was heated to 275 °C instead of 350 °C in an attempt to avoid a too severe sintering of the Cu particles. The purpose of

the reducing treatment was to remove at least part of the passivating oxide layer prior to the catalytic reaction. It is possible that further catalyst reduction occurs during the high pressure CO hydrogenation.

4.10 Catalyst characterization

4.10.1 XAS investigations

X-ray absorption spectroscopy (XAS) was performed at the X1 beamline at the Hamburger Synchrotronstrahlungslabor (HASYLAB) at the Deutsche Elektronen-Synchrotron (DESY, Hamburg). Additional XAS measurements were also conducted at the XAS beamline at the Ångströmquelle Karlsruhe (ANKA) at the Karlsruhe Institute of Technology (KIT) [397]. The XAS spectra were obtained in transmission mode. The measurements were conducted with 20-25 mg of catalyst sample (crushed down to 50-200 μm) in a pellet cell with gas streaming on both sides of the cell [398]. Approximately 10-15 mg of BN was also added in order to fill the cell. It is discussed in chapter 8 how air exposure may cause a partial oxidation of the sulfide. In an attempt to obtain a system that more closely resembles the working state of the catalyst XAS measurements were carried out with an in-situ treatment in a reducing gas. For the in-situ reduction experiments the catalyst sample was subjected to a 30 NmL/min flow of 5 mol% H_2 in He or 2.4 mol% CO + 2.4 mol% H_2 in He. The cell was then, by means of an external oven, heated at a rate of 5 °C/min to a final temperature of 325 °C, which was maintained for 1 h. XANES spectra were acquired around the Co K-edge during the heating of the catalyst to monitor the reduction behavior. The cell was then cooled down, while the gas flow was maintained, and the full EXAFS spectrum was obtained at room temperature. XAS spectra were recorded in step-scanning mode around the Co K-edge with an Si(111) double crystal monochromator and around the Mo K-edge with an Si(311) double crystal monochromator. The monochromator was detuned to 70 % intensity in order to diminish the presence of higher harmonics. Cobalt or molybdenum foils were used for energy calibration. The XAS data were processed using the WinXAS 3.1 software [399]. EXAFS spectra were processed by energy calibration, background subtraction, deglitching when necessary, and finally normalization. The EXAFS spectra were then Fourier-transformed after k^3-weigthing. EXAFS data fitting was performed in R-space for the first metal-metal and metal-oxide/sulfide shell. The fitting was made with dampening factors obtained from the model compounds Co_9S_8 and MoS_2. Theoretical scattering amplitudes and phase shifts were calculated with the FEFF 7.0 code [400, 401].

A few investigations of the iron content in fresh and spent sulfide catalysts were conducted to determine, if iron deposition from the decomposition of carbonyls was influencing the catalytic properties. These measurements were carried out at ANKA, KIT in the fluorescence mode with a 5-element solid state detector.

4.10.2 TEM investigations

Transmission electron microscopy data were acquired using an FEI Titan 80–300 aberration corrected microscope operated at 300 kV and an FEI Tecnai T200ST microscope operated at 200 kV. Both microscopes are equipped with Oxford Instruments INCA EDX spectrometers for elemental analysis.

The catalyst samples were dispersed in dry form on the TEM grids, which were Cu-grids coated with a holey carbon film. In some experiments the catalyst sample was in-situ subjected to a reducing treatment in 1.5 mbar H_2 at 325 °C. In such cases Cu-grids without the carbon film were used.

4.10.3 X-ray diffraction studies

X-ray diffraction (XRD) was measured with a PANalytical X'Pert PRO diffractometer with a Cu-Kα X-ray source operated at 45 kV and 40 mA equipped with a Ni filter and a slit. Diffractograms were recorded between $2\theta = 10°$ and $2\theta = 80°$ with a step width of 0.00164°. For the carbide catalysts described in chapter 9 the total scan time was 45 min. For the supported sulfide catalysts presented in chapter 8 the total scan time was 7 h.

An estimate of the average particle diameter ($d_{p,XRD}$) was also obtained from the diffraction peak broadening by means of the Sherrer equation [402]:

$$d_{p,XRD}\left[nm\right] = \frac{0.9\lambda\left[nm\right]}{\beta_{\frac{1}{2}}\left[rad.\right]\cos\left(\theta\right)} \tag{4.5}$$

Here λ is the X-ray wavelength, θ is the Bragg angle, and $\beta_{\frac{1}{2}}$ is the full width at half maximum of the diffraction peak corrected for Kα–doublet separation and instrumental broadening.

4.10.4 BET and porosimetry measurements

The pore structure of the catalyst is characterized by means of mercury porosimetry using a Micromeritics Autopore II 9220 porosimeter.

For the carbide catalysts presented in chapter 9 the specific surface area was determined by nitrogen adsorption at liquid nitrogen temperature by means of a QuantaChrome Autosorb iQ$_2$ gas sorption analyzer. The specific surface area (S_g) was determined through a 7-point, linear BET plot in the range of $p/p_0 = 0.05–0.3$. Prior to the BET measurement the sample was dried/degassed under vacuum at 250 °C for 4 h. The average particle size ($d_{p,BET}$) was estimated on the basis of the specific surface area (S_g) assuming spherical particles and utilizing carbide densities (ρ) from the CRC Handbook of Chemistry and Physics [44]:

$$d_{p,BET} = \frac{6}{\rho S_g} \qquad\qquad (4.6)$$

The surface areas of the sulfide catalysts presented in table 4.4 was instead measured with a Micromeritics ASAP 2000 surface area analyzer.

5 Effects of H$_2$S and process conditions in the synthesis of higher alcohols from syngas

There are two great tragedies in life: one is not getting what you want, the other one is getting it
- George Bernard Shaw

5.1 Abstract

The present work is an investigation of how the process conditions influence the synthesis of mixed alcohols from syngas over a K$_2$CO$_3$/Co/MoS$_2$/C catalyst. The emphasis in the investigations is upon the effects of H$_2$S in the syngas feed. However the effects of the temperature and of the partial pressures of H$_2$ and CO are also investigated. With or without H$_2$S in the feed the pre-sulfided catalyst requires an initiation period to reach a stabilized behavior, but the duration of this period depends upon the H$_2$S level. Operation with a feed containing more than 103 ppmv H$_2$S leads to a fairly rapid stabilization of the product distribution and ensures that higher alcohols are the dominant reaction products. With less than 57 ppmv H$_2$S in the feed the stabilization of the product distribution is much slower, and methanol is the dominant product. An investigation of the reaction kinetics indicates a high CO coverage and a low hydrogen coverage. Hydrogen sulfide in the syngas feed generally promotes chain growth for both alcohols and hydrocarbons, but lowers the alcohol selectivity by enhancing the hydrocarbon formation. The highest alcohol productivity reached in these investigations was 0.276 g (g cat.)$^{-1}$ h^{-1}, and this was achieved at 350 °C, 100 bar, GHSV = 5244 h^{-1}, Feed: 49.9 vol% H$_2$, 50.1 vol% CO. Finally it is found that sulfur fed to the reactor as H$_2$S is incorporated into the condensed alcohol product, and the incorporation of sulfur species into the product continues for some time after H$_2$S has been removed from the feed. When the catalyst is operated with an S-free syngas feed, the amount of sulfur in the condensed liquid product decreases over time, but after 35 hours of operation with an S-free syngas the alcohol product still contains 340 ppmw of sulfur. Thiols appear to be the dominant sulfur compounds in the product.

5.2 Stability

The first part of this investigation concerns the stability of the catalyst in the syngas atmosphere and the influence of co-fed H$_2$S upon the stability. This investigation is conducted using the catalyst KCoMo-1. Figure 5.1 shows the CO conversion and the CO$_2$-free alcohol selectivity as functions of time on stream in an H$_2$S-free syngas. In parallel figure 5.2 shows the CO conversion and the alcohol selectivity as functions of time on stream with a syngas feed that contains 218 ppmv H$_2$S.

From figure 5.1 and figure 5.2 it can be seen that irrespective of the feed sulfur level, the catalyst requires an initiation period to reach a stabilized behavior, but the duration of this period depends upon the H$_2$S level. With 218 ppmv H$_2$S in the syngas feed the selectivity stabilizes within the first 10 hours on stream, but in the absence of H$_2$S the catalyst requires 30-35 hours on stream to before the selectivity stabilizes.

Figure 5.1 The CO conversion and the CO_2-free alcohol selectivity as functions of time on stream in sulfur free syngas. The experimental conditions are T = 327 °C, P = 100 bar, GHSV = 5247 h^{-1}, Feed: 50.1 vol% H_2, 49.9 vol% CO. The catalyst is KCoMo-1.
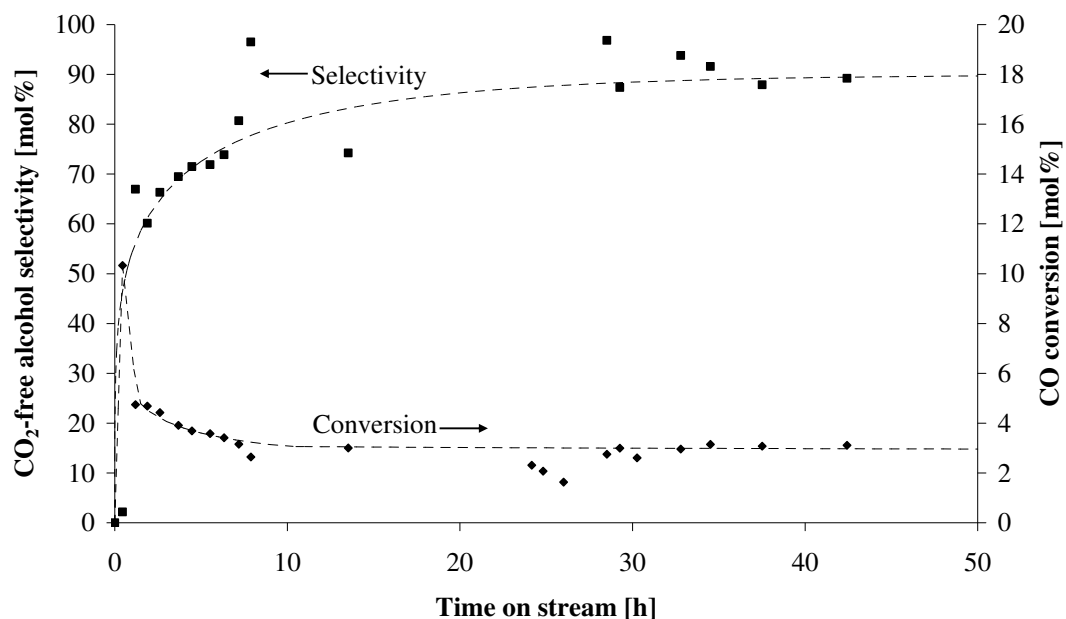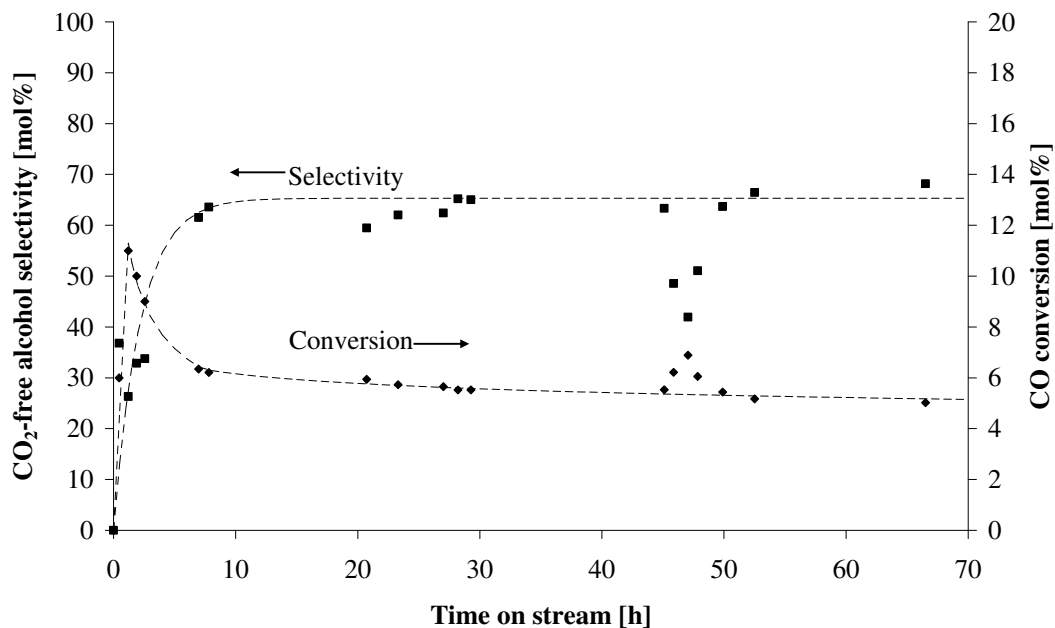

Figure 5.2 The CO conversion and the CO_2-free alcohol selectivity as functions of time on stream in an H_2S containg syngas. The experimental conditions are T = 326 °C, P = 100 bar, GHSV = 5418 h^{-1}, Feed: 50.3 vol% H_2, 49.7 vol% CO, 218 ppmv H_2S. The catalyst is KCoMo-1.

During the first hours on stream the alcohol selectivity gradually increases, while the CO conversion gradually decreases. There are presumably several factors that contribute to the behavior seen in figure 5.1 and figure 5.2. The temperature in the catalytic bed rises significantly (15-20 °C), when the catalyst is first exposed to syngas, and this is to some extent contributing to the initial peak in conversion. However the gradual changes in conversion and selectivity prevail even after the temperature has reverted to the set point (after approximately 1 hour on stream). A factor that might contribute to the gradual developments in selectivity and activity is a gradual spreading of the alkali promoter across the catalytic surface. An enhanced alcohol selectivity at the cost of a decreased CO conversion is the reported effect of the alkali promoter [173], and this is the behavior that develops during the first hours on stream. Iranmahboob et al. [181] investigated Alkali/Co/MoS$_2$/Clay catalysts by means of X-ray photoelectron spectroscopy (XPS) before and after exposure to syngas, and these authors report a surface enrichment of the alkali promoter after exposure to syngas. Woo et al. [171] investigated MoS$_2$ promoted with different potassium salts and mapped out the coverage of the alkali promoter before and after reaction using Auger electron spectroscopy (AES). These authors [171] found that prior to the exposure to syngas, the potassium promoter was poorly distributed. After exposure to syngas potassium in the form of some salts like K$_2$CO$_3$ and KOH had spread across the catalyst surface. K$_2$CO$_3$ and KOH were also the salts that were found to promote alcohol formation, and when these salts were used as promoters the alcohol selectivity gradually increased with time on stream [171]. This behavior is also seen with the present K$_2$CO$_3$ promoted catalyst. Some salts like KCl and K$_2$SO$_4$ do reportedly not promote alcohol formation, and potassium present in the form of these salts do not show this spreading across the surface [171, 173]. Furthermore catalysts promoted with KCl or K$_2$SO$_4$ do not undergo these marked changes in conversion and alcohol selectivity with time on stream that are observed with salts that promote alcohol formation (e.g. K$_2$CO$_3$) [171, 173]. The salts, which promote alcohol formation, are thus the salts that lead to a spreading of potassium across the catalyst surface and the salts that lead to marked, gradual changes in conversion and selectivity with time on stream. On this basis one might hypothesize that the changes in conversion and selectivity at least in part is due to the spreading of the alkali promoter. It should be mentioned that all of these studies [171, 173, 181] used catalysts prepared from sulfide precursors, while oxide precursors have been used in the present work. The importance of this difference is unknown, since it is not clear, to what extent the abovementioned redistribution of the alkali promoter occurs during the sulfidation of the catalyst.

An additional factor that might play a role in the observed developments in catalytic properties is a gradual loss of sulfur. As it will be shown subsequently, the catalyst appears to be loosing sulfur, and this decrease in sulfur content could also affect the catalytic properties. A question here is whether this loss of sulfur is accompanied by a complete or partial phase change. The possible developments in the structure of the active phase are discussed in more detail in section 5.6 on page 114.

A final parameter, which may contribute to the developments observed in figure 5.1 and figure 5.2, is that very active hydrocarbon forming sites gradually might be blocked by carbonaceous deposits. This could also lead to a gradual reduction in hydrocarbon formation with time on stream. The development in catalyst carbon content is also discussed in section 5.6 on page 114 .

It seems quite certain that the initial development in catalytic activity with time on stream is due to changes in the structure of the catalyst and not just due to the surface reactions approaching steady state. In the present experiments it is observed that, if at steady state the syngas flow is replaced by a nitrogen flow for several hours, and the syngas then is reintroduced, the catalyst returns to steady state within approximately an hour. Judging from this observation the stabilization of the surface reactions appears to be relatively fast in comparison to the developments observed in figure 5.1 and figure 5.2.

A comparison of figure 5.1 and figure 5.2 shows that the presence of H_2S in the feed to some extent shifts the selectivity from alcohols to hydrocarbons. Without co-fed H_2S the alcohol selectivity is 90 mol%, while addition of 218 ppmv H_2S to the syngas feed lowers the selectivity to 65 mol%. The production of alcohols is only moderately affected by the presence of H_2S, and the selectivity change in the presence of H_2S therefore mainly reflects an increased production of hydrocarbons. The stabilized CO conversion does rise from 3 mol% without co-fed H_2S to 5 mol%, when 218 ppmv H_2S is added to the syngas feed. This effect of H_2S is not without precedence. Previous studies of dedicated hydrocarbon synthesis over sulfide catalysts have shown that H_2S exerts a positive influence on the hydrocarbon production [403, 404]. In the present investigations methane is the dominant hydrocarbon produced, and CH_4 typically constitutes more than 70 wt% of the characterized C_1-C_3 hydrocarbons.

The alcohol selectivity of 90 mol% in the absence of H_2S is a fairly good result. However one should remember the limited CO conversion. In a recent system study Phillips [322] assumed alcohol synthesis with 90 mol% selectivity at 60 mol% CO conversion and found that with these operating characteristics the delivered, moist biomass could be converted into higher alcohols with an energy efficiency of 55 %. Unfortunately an increase in conversion is connected to a decrease in selectivity [74], and the catalysts used in these investigations still have some way to go before achieving the operating characteristics assumed by Phillips [322]. Indeed one of the main challenges with regard to the alcohols synthesis is to raise the alcohol selectivity of the available catalysts.

The effects of co-fed H_2S are however not entirely negative. An important positive effect of co-fed H_2S is that it promotes chain growth and stabilizes a high ratio of longer alcohols relative to methanol in the alcohol product. This is illustrated in figure 5.3, which shows the weight ratio between higher alcohols and methanol in the alcohol product as a function of time on stream with different H_2S levels in the feed. Figure 5.3 shows that with H_2S levels at or above 103 ppmv the alcohol distribution stabilizes relatively fast, but with H_2S concentrations at or below 57 ppmv the weight fraction of higher alcohols decreases over time.
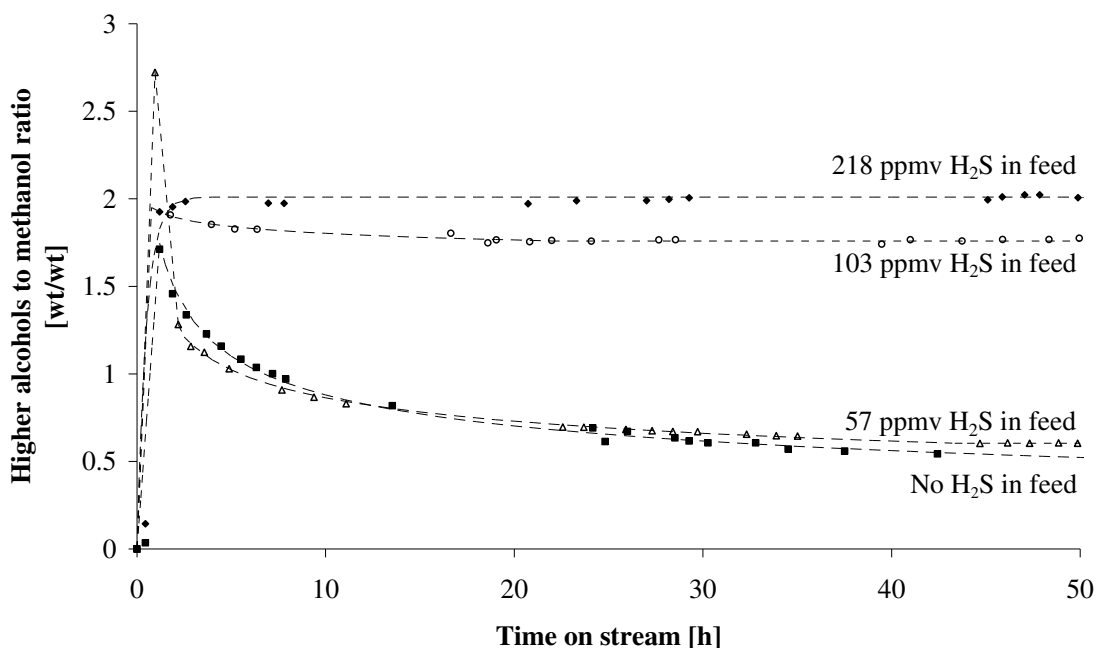
Figure 5.3 The weight ratio of higher alcohols relative to methanol in the reaction product as a function of time on stream at different H_2S levels. T = 326±1 °C, P = 100 bar, GHSV = 5300±200 h^{-1}, Feed: 50±1 vol% H_2, 50±1 vol% CO. The catalyst is KCoMo-1.

The decrease in the fraction of higher alcohols with time on stream in a sulfur free syngas is the result of an initial decrease in the production of the higher alcohols and a gradually increasing production of methanol. This is illustrated in figure 5.4, which shows the space time yields of the four characterized alcohols as functions of the time on stream in a sulfur free syngas. Figure 5.4 shows that the space time yields of the higher alcohols initially decline, but after 13 hours at reaction conditions the production of higher alcohols has essentially stabilized. Figure 5.4 also shows the interesting behavior of the methanol production. The methanol STY seems to have stabilized after 13 hours on stream, but then the methanol production starts to increase, and this increase continues, until the methanol STY after 30-35 hours on stream once again appears to be stabilizing. Figure 5.1 shows that this second stabilization of the methanol production coincides with the approximate stabilization of the alcohol selectivity, which also seems to reach a steady state after around 30 hours on stream. It cannot be excluded that the observed behavior of the methanol production is due to changes in the active phase of the catalyst that start to take effect after around 13 hours on stream. Operation with 57 ppmv H_2S in the feed results in a behavior that is similar to the one described for sulfur free operation, and it might be added that the H_2S conversion in this case is in the range of 90-100 %. As previously mentioned it is very difficult to discern the signal from the noise level, when the sulfur concentration falls below 15-20 ppmv.

Figure 5.5 shows the space time yields of the individual alcohols as functions of time on stream with 218 ppmv H_2S in the syngas feed. A comparison of figure 5.4 and figure 5.5 clearly shows that the space time yields of C_{2+} alcohols are significantly higher with

218 ppmv of hydrogen sulfide in the feed. Additionally the data presented in figure 5.5 indicate a slight, gradual deactivation of the catalyst in the presence of H$_2$S, but after around 15-20 hours on stream the tendency does become relatively weak. This trend is also observed with 103 ppmv H$_2$S in the feed.
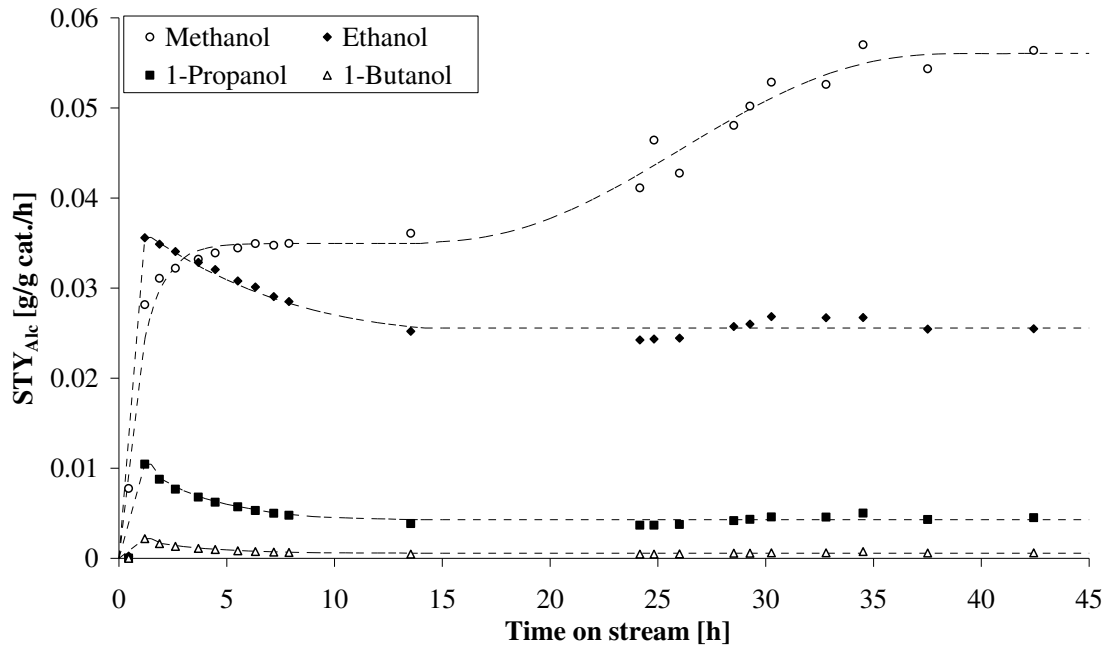
Figure 5.4 Space time yields of the four characterized alcohols as functions of the time on stream in a sulfur free syngas. After approximately 13 hours the space time yields of the higher alcohols have essentially stabilized. The production of methanol does however show a gradual increase. The experimental conditions are described in connection with figure 5.1.
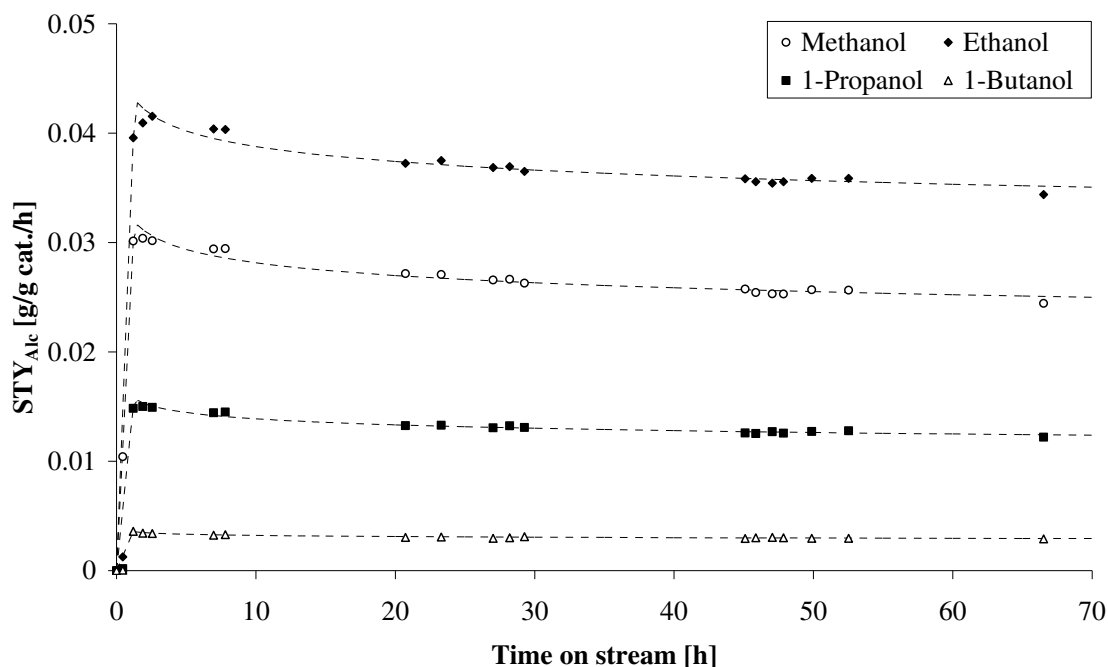
Figure 5.5 Space time yields of the four characterized alcohols as functions of the time on stream in a syngas containing 218 ppmv H_2S. After approximately 20 hours the space time yields of the alcohols have essentially stabilized although a slight deactivating tendency might be seen. The experimental conditions are described in connection with figure 5.2.

In general the presented results show that the presence of hydrogen sulfide shifts the selectivity towards hydrocarbons, but H_2S also promotes chain growth. It has previously been reported that the cobalt promoted alcohol synthesis catalysts are unaffected by sulfur at levels up to around 100 ppmv [13, 15, 18, 19, 186], and this is fairly consistent with our observations. Figure 5.3 shows that the development in product distribution with time on stream can be divided into two distinct types of behavior depending upon the sulfur concentration. Our results show that with the presently used conditions the catalyst is only weakly affected by H_2S concentrations in the range of 0-57 ppmv, but in the region between 57 and 103 ppmv H_2S there is a remarkable shift in the influence of hydrogen sulfide (see figure 5.3). At levels above 103 ppmv H_2S serves to stabilize a significantly increased production of higher alcohols, whereas methanol is the dominant product at lower sulfur levels. The difference between 57 and 103 ppmv H_2S might be, whether or not the H_2S level is sufficient to sustain the sulfide phase. The issue of a possible change in the active phase is discussed in more detail in 5.6 on page 114.

It is difficult to estimate the exact sulfur level, which is required to stabilize the catalyst. At experimental conditions of figure 5.2 with 218 ppmv H_2S in the feed the conversion of H_2S fluctuates around 31($\pm$7) mol%. This would correspond to full H_2S conversion, if the H_2S level had been 69 ppmv, so this might be a reasonable estimate of the required sulfur level at the present conditions. As the products of the sulfur conversion are not determined this estimate should of course be regarded with some caution, but 69 ppmv is between the observed limits of 57 and 103 ppmv.

In the treatment above the alcohol selectivity is expressed on a CO_2-free basis, while the reported CO conversion levels include CO that is converted into CO_2. One could argue that this presentation of conversion and selectivity is somewhat misleading, but it is the presentation typically used, as the alcohol synthesis catalysts generally have a high water gas shift activity, which makes CO_2 an inevitable reaction product. This is also the case for MoS_2 based systems. Previous investigations [15] with $K/MoS_2/C$ catalysts have indicated that the water gas shift reaction is close to equilibrium at typical alcohol synthesis conditions. With an equilibrium constant for the water-gas shift reaction (R13) of $K_{WGS} = 39$ at 300 ºC the water gas shift equilibrium strongly favors CO_2 over H_2O [13], and in fact CO_2 constitutes a significant part of the CO consumed in the reaction. In the experiment presented in figure 5.1 and figure 5.4 the CO conversion stabilizes at 3 mol%, but the overall carbon based selectivity to CO_2 is 35 mol%. In the experiment presented in figure 5.2 and figure 5.5 figures 4 and 7 with 218 ppmv H_2S in the syngas the CO conversion stabilizes at around 5 mol%, but in this case the overall CO_2 selectivity is 40 mol%. The higher CO_2 selectivity in the experiment with H_2S in the syngas is both due to a larger hydrocarbon formation and a larger formation of higher alcohols (pure hydrocarbon formation with full shift of product water would yield 50 mol% CO_2 selectivity on a carbon basis). The downside of the large CO_2-selectivity is of course that the shift reaction consumes carbon monoxide that could otherwise have been used in alcohol formation. The positive aspect of the large CO_2-formation is that the water content of the alcohol product is reduced, which is an aid in a water removal stage downstream of the synthesis reactor.

In essentially all the performed experiments the CO_2 formation is observed to be slightly higher than what would be expected from a full shift of the water formed in the synthesis reactions. This could be related to experimental uncertainty, but it could also be due to CO_2 formed in connection with carbon deposition on or carburization of the sulfide catalyst. As previously mentioned these issues will be treated in greater detail subsequently.

5.3 Kinetic studies

The second part of this investigation deals with the reaction kinetics. The objective of the present analysis is to formulate a series of empirical rate expressions (5.1) that describe the production of the characterized alcohols and hydrocarbons. In doing so we assume that the production of alcohols and hydrocarbons can be described as parallel reactions, despite the presumably successive nature of the chain growth (which is illustrated in figure 2.7) and the potential conversion of already formed alcohols. The kinetic investigations are performed using the catalyst KCoMo-2 (see table 4.4).

$$R_i = A_i \exp\left(-\frac{E_{a,i}^{app}}{RT}\right) p_{H_2}^{a_i} p_{CO}^{b_i} p_{H_2S}^{c_i} \tag{5.1}$$

In equation (5.1) R_i is the production rate of component i, p_j denotes the partial pressure of reactant j, while a_i, b_i and c_i are the apparent reaction orders in H_2, CO and H_2S

respectively. A_i denotes a pre-exponential factor, and $E_{a,i}^{app}$ is the apparent activation energy. In the present work the reaction order in H_2S is only investigated for H_2S concentrations at or above 260 ppmv. Equation (5.1) will of course be invalid for $p_{H_2S} = 0$, but judging from the results in the preceding section the validity of the model will already become questionable for H_2S concentrations below 100 ppmv, where we have observed a marked shift in the effect of H_2S.

The model parameters are determined through systematic variations in temperature and partial pressures. Although the partial pressures of the reactants change through the reactor they never differ by more than 12 % from the average reactant pressures. For this reason the reactor is assumed to behave as a differential reactor with a constant reactant pressure corresponding to the average between the inlet and the outlet. Although the reaction occurs at elevated pressure, the model uses partial pressures and not fugacities. This is justified through an evaluation of the compressibility factor and of the individual fugacity coefficients by means of the Soave-Redlich-Kwong (SRK) equation of state [362, 363] (see chapter 3 on page 66). The determination shows that the compressibility factor and all the individual fugacity coefficients are within 5 % of unity in all the performed experiments, and on this basis the gas phase is regarded as being approximately ideal. The calculation of the compressibility factor is based upon a random mixing approximation with all binary interaction parameters assumed to be 0 [371]. The SRK equation of state is used, since it has previously been shown to provide the best description of the methanol synthesis, which occurs at similar conditions [361]. In this calculation the H_2O content in the gas is estimated through an assumption of equilibrium for the water gas shift reaction.

As stated above the catalyst was operated with 260 ppmv H_2S in the feed, and no noticeable changes in catalyst behavior were observed during the kinetic investigations, but the reader should remember that a very weak gradual deactivation was observed for the similar catalyst KCoMo-1 (see figure 5.5), when it was operated with similar concentrations of H_2S in the feed.

The first parameter investigated is the temperature, and figure 5.6 shows an Arrhenius plot for the formation rates of alcohols over the catalyst KCoMo-2. The apparent activation energies for alcohol formation are derived from this plot.
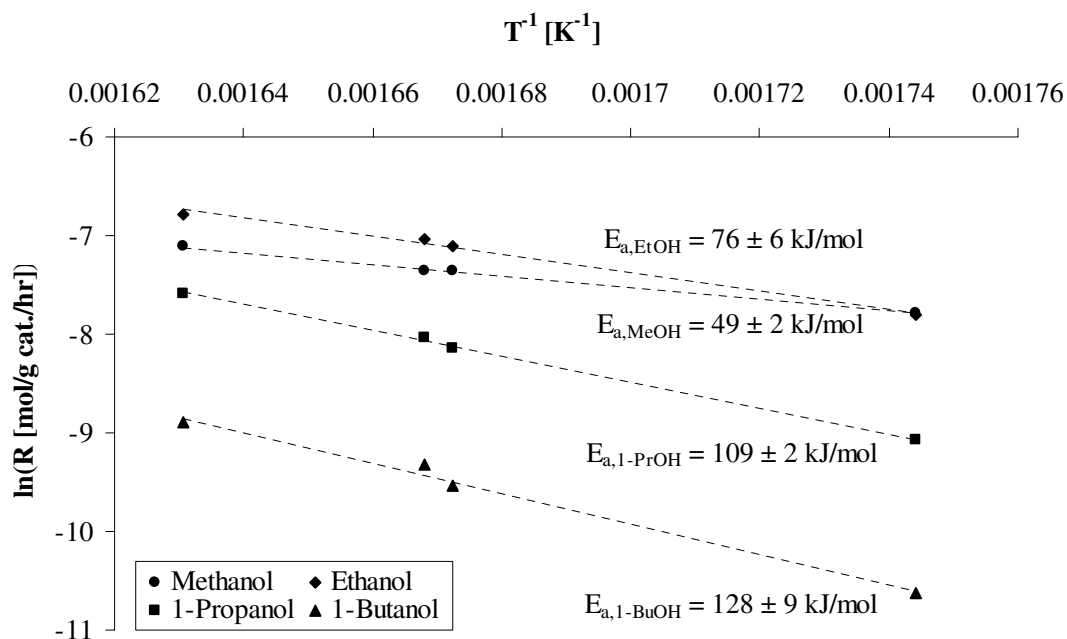
Figure 5.6 Arrhenius plot for the formation of alcohols over the catalyst KCoMo-2. The apparent activation energies for the four characterized alcohols are noted next to the appropriate curves. The experimental conditions are P = 100 bar, GHSV = 5106 h^{-1}, Feed: 50.2 vol% H_2, 49.8 vol% CO, 260 ppmv H_2S. T = 300-350 °C.

Also the influence of the partial pressures of H_2, CO and H_2S has been investigated. Figure 5.7-figure 5.9 show doubly logarithmic depictions of the alcohol production rates against the partial pressures of H_2, CO and H_2S respectively. The reaction orders are inferred from the slopes in these figures.
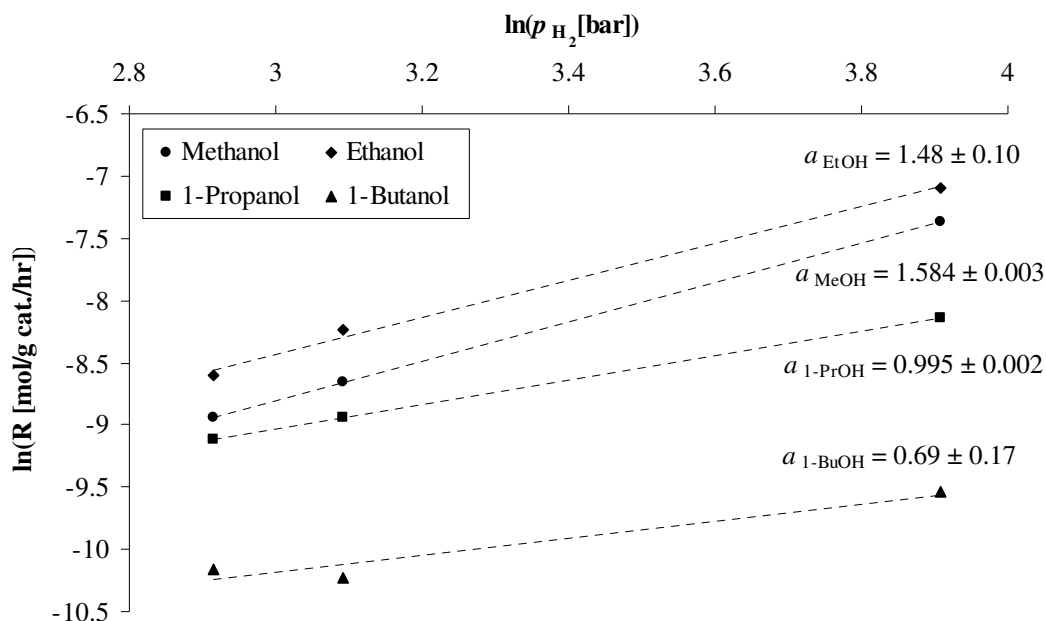
Figure 5.7 The logarithm of the alcohol formation rates against the logarithm of the partial pressure of H_2. The reaction orders in H_2 for the characterized alcohols are noted next to the appropriate curves. The experimental conditions are T = 325 ºC, P = 100 bar, GHSV = 5106 h⁻¹, Feed: 50±1 vol% CO, 260 ppmv H_2S, 18-50 vol% H_2. The catalyst is KCoMo-2.
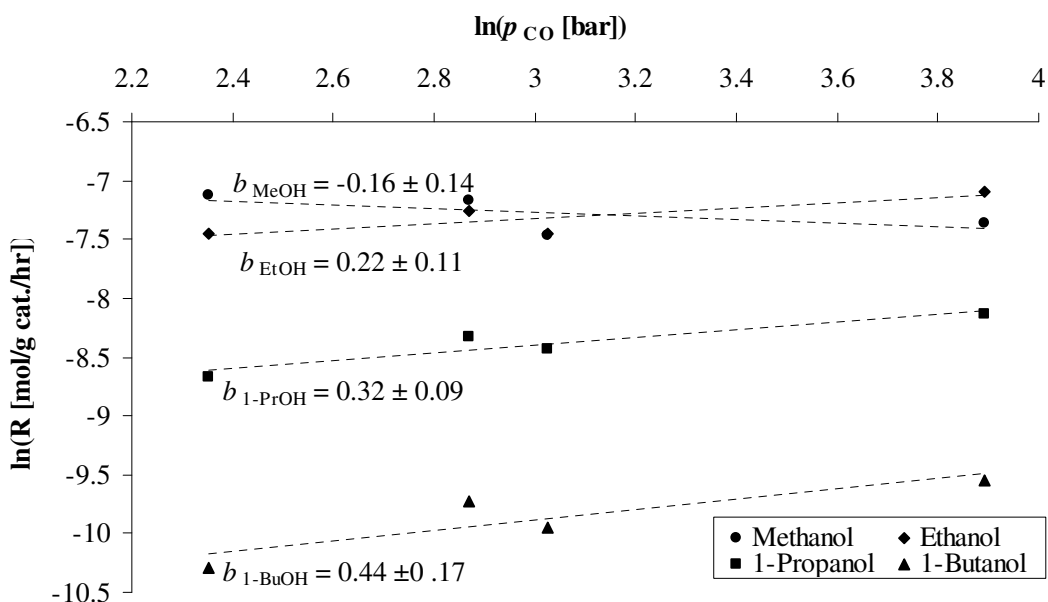
Figure 5.8 The logarithm of the alcohol formation rates against the logarithm of the partial pressure of CO. The reaction orders in CO for the characterized alcohols are noted next to the appropriate curves. The experimental conditions are T = 325 ºC, P = 100 bar, GHSV = 5106 h⁻¹, Feed: 50.2 vol% H_2, 260 ppmv H_2S, 11-50 vol% CO. The catalyst is KCoMo-2.
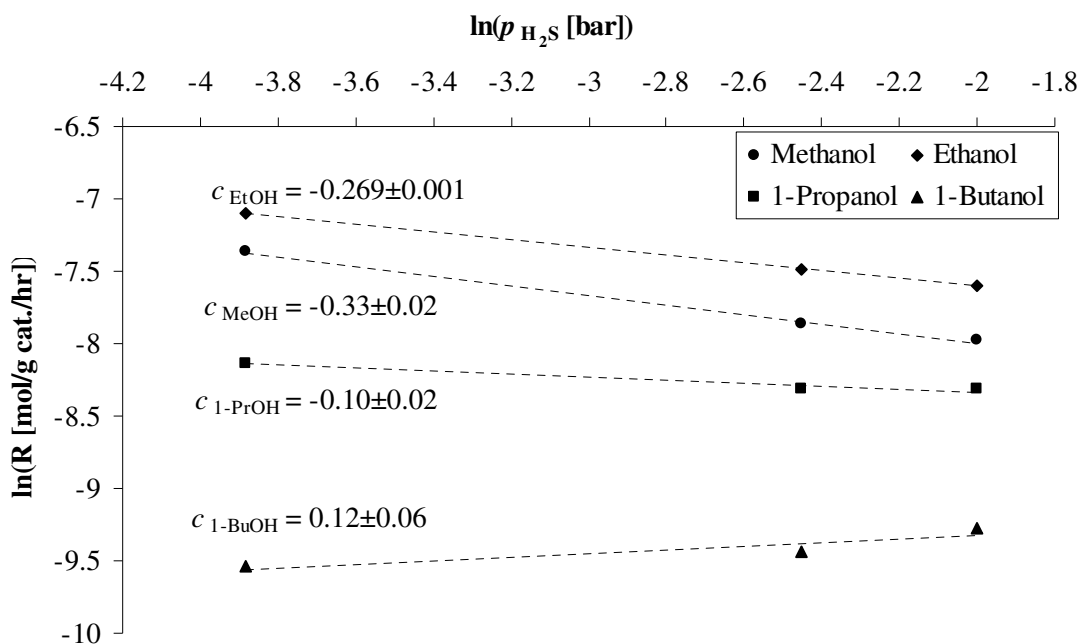
Figure 5.9 The logarithm of the alcohol formation rates against the logarithm of the partial pressure of H_2S. The reaction orders in H_2S for the characterized alcohols are noted next to the appropriate curves. The experimental conditions are T = 325 ºC, P = 100 bar, GHSV = 5106 h^{-1}, Feed: 50.2 vol % H_2, 49.8 vol% CO, 260-1600 ppmv H_2S. The catalyst is KCoMo-2.

Table 5.1 summarizes the kinetic parameters for the formation of the individual alcohols over the catalyst. The kinetic parameters for the reactions forming hydrocarbons have been obtained in the same way as the parameters for alcohol formation. Table 5.2 summarizes these kinetic parameters for the formation of the characterized hydrocarbons over the catalyst. To extend the usefulness of the experimental model all reaction orders have been provided with at least two decimals, and more when this is warranted by the statistical significance.

Table 5.1 Kinetic parameters for the synthesis of alcohols over the $K_2CO_3/Co/MoS_2/C$ catalyst. The parameters relate to equation (5.1).

Component (i)	$A_i \left[\frac{mol}{s \cdot g \cdot bar^{a_i+b_i+c_i}} \right]$	$E_{a,i}^{app} \left[\frac{kJ}{mol} \right]$	Reaction orders		
			H_2 (a_i)	CO (b_i)	H_2S (c_i)
Methanol	$3.58 \cdot 10^{-6}$	49 ± 2	1.584 ± 0.003	-0.16 ± 0.14	-0.33 ± 0.02
Ethanol	$4.55 \cdot 10^{-4}$	76 ± 6	1.48 ± 0.10	0.22 ± 0.11	-0.269 ± 0.001
1-Propanol	1.08	109 ± 2	0.995 ± 0.002	0.32 ± 0.09	-0.10 ± 0.02
1-Butanol	58.78	128 ± 9	0.69 ± 0.17	0.44 ± 0.17	0.12 ± 0.06

Table 5.2 Kinetic parameters for the synthesis of hydrocarbons over the $K_2CO_3/Co/MoS_2/C$ catalyst. The parameters relate to equation (5.1).

Component (i)	$A_i \left[\frac{mol}{s \cdot g \cdot bar^{a_i+b_i+c_i}} \right]$	$E_{a,i}^{app} \left[\frac{kJ}{mol} \right]$	Reaction orders		
			H_2 (a_i)	CO (b_i)	H_2S (c_i)
Methane	469.55	118 ± 8	1.31 ± 0.43	-0.65 ± 0.11	0.05 ± 0.04
Ethane	$5.57 \cdot 10^5$	144 ± 7	0.36 ± 0.04	-0.15 ± 0.10	0.37 ± 0.06
Ethene	$1.21 \cdot 10^5$	143 ± 2	0.04 ± 0.10	-0.02 ± 0.06	0.33 ± 0.05
Propane	$8.86 \cdot 10^5$	155 ± 6	-0.07 ± 0.05	0.10 ± 0.06	0.50 ± 0.05

Table 5.1 and table 5.2 reveal that the reaction orders in H_2 generally are quite high, while the CO reaction orders on the other hand are fairly low. This indicates a relatively large surface coverage of CO and a low hydrogen coverage at the reaction conditions. The reaction orders for alcohols are generally larger than the ones for hydrocarbons, and this agrees well with previous investigations, which show that increasing pressure enhances the selectivity to alcohols [159]. For both alcohols and hydrocarbons the reaction orders in hydrogen are observed to decrease with increasing chain length, while the CO reaction orders follow the opposite tendency. These tendencies might be explained in terms of the reaction mechanism. Figure 2.7 on page 55 shows the presumed reaction mechanism, where adsorbed CO is inserted into an adsorbed alkyl group to form an acyl species. The formed acyl species can then be hydrogenated to the corresponding alcohol or all the way to a new alkyl group. Alternatively the alkyl species can be hydrogenated to the corresponding hydrocarbon. When moving upwards in chain length the risk of chain termination, which increases with increasing hydrogenation activity, becomes progressively more important. This can explain the generally positive albeit decreasing reaction order in hydrogen with increasing chain length, since the higher species are more affected by an increased chance of termination. Correspondingly the increasing need for additional CO insertion steps is responsible for the increase in CO reaction order with increasing chain length.

The H_2S reaction orders in table 5.1 and table 5.2 show that hydrogen sulfide enhances hydrocarbon formation and generally promotes chain growth. In section 5.2 it is described that the formation of higher alcohols is significantly increased, when going from low levels of H_2S (0-57 ppmv) to higher H_2S levels (103-218 ppmv). The data in table 5.1 do however show that both ethanol and propanol have small, negative reaction orders in H_2S. This must be ascribed to the fact that the kinetic investigations summarized in table 5.1 have been performed with relatively high (≥ 260 ppmv) concentrations of H_2S, where the influence of hydrogen sulfide apparently differs from the effect at low H_2S levels.

It should be noticed that hydrocarbons generally show higher activation energies than alcohols, which implies that increasing temperature favors hydrocarbon formation. It is also worth noticing that in the investigated temperature range the activation energies increase with increasing chain length. This is an uncommon behavior for such chain growth reactions, where increasing temperature typically favors methane formation [299, 403]. An important reason for this beneficial effect of the temperature upon the chain growth is presumably that, as the catalyst becomes more active at higher temperature, there is an increased chance of conversion of already formed alcohols into higher species. It was mentioned in section 2.3.6 that this can occur. It is presumably the high CO surface

coverage in the investigated temperature range, which ensures that the dominant effect of increasing temperature is an increase in the rate of the CO insertion step that yields chain growth (R35).

$$RCH_2*+CO* \rightleftharpoons RCH_2CO*+* \hspace{4cm} R35$$

It is interesting to compare the kinetic parameters obtained in the present investigation to values reported in the literature, however such investigations of alcohol formation are rather scarce, and the comparison is limited to the activation energies for the three simplest alcohols, which are shown in table 5.3. The results in table 5.3 show that there is a general agreement concerning the increase in activation energy with increasing chain length, however the reported activation energies show a great deal of scattering. With respect to kinetics the most well studied syngas reaction over sulfide catalysts appears to be methane formation, and table 5.4 summarizes a series of kinetic parameters reported for this reaction over various MoS_2-based catalysts.

Table 5.3 Reported apparent activation energies (in kJ/mol) for alcohol formation over sulfide catalysts.

Reference	Present work	Gunturu et al. [17]	Santiesteban et al. [75]	Surisetty et al. [405]
Catalyst	K/Co/MoS$_2$/C	K/Co/MoS$_2$/C	Cs/MoS$_2$	K/Co/Rh/MoS$_2$/MWCNT [a]
Conditions	100 bar H$_2$/CO = 1.01 260 ppmv H$_2$S	40-70 bar No H$_2$S	82.7 bar H$_2$/CO = 0.96 No H$_2$S	55.2-96.5 bar H$_2$/CO = 0.5-2.0 No H$_2$S
Methanol	49	-	68	35
Ethanol	76	38.3	94.9	57
1-Propanol	109	97.9	98.5	94 [b]

[a] This sulfide catalyst, which is promoted by both Rh and Co, is supported by multiwalled cabon nanotubes.
[b] This is a lumped value for alcohols higher than ethanol.

Perhaps the most striking feature of the kinetic data summarized in table 5.3 and table 5.4 is the absence of any significant agreement between the various kinetic studies. However the reaction kinetics are affected by the composition and structure of the active phase as well as by the catalyst support and the reaction conditions. Furthermore the very nature of the active phase could as discussed in the preceding section depend upon the process conditions. For this reason it is perhaps not unexpected that the reported kinetic parameters show a great deal of scattering. When looking at methane formation, the data in table 5.4 generally indicate that the CO coverage is increased (the CO reaction order decreases) by increasing pressure and by alkali promotion. It also appears that the conditions, which lower the reaction order in CO, simultaneously results in an increased activation energy and a decreasing H$_2$S reaction order for methane formation.

Table 5.4 Reported kinetic parameters for methane formation over molybdenum sulfide catalysts. The parameters relate to equation (5.1).

Catalyst	Selected conditions	E_{a,CH_4}^{app} $\left[\frac{kJ}{mol}\right]$	Reaction orders			Reference
			H$_2$ (a)	CO (b)	H$_2$S (c)	
K/Co/MoS$_2$/C	P = 100 bar H$_2$/CO = 1 [a]	118	1.31	-0.65	0.05	Present work
K/Co/MoS$_2$/C [b]	P = 40-70 bar	106.5	-0.52	-0.03	-	[17]
Co/MoS$_2$/γ-Al$_2$O$_3$	P = 8.59 bar H$_2$/CO = 3 [a]	79.7	1.21	0.14	-	[406]
K/MoS$_2$/C [c]	P = 1 atm H$_2$/CO = 1 [a]	75	-	-	-	[407]
Co/MoS$_2$/TiO$_2$	P = 31 bar H$_2$/CO = 1 [a]	99.8	0.42	0	0.17	[403]
MoS$_2$/γ-Al$_2$O$_3$ [d]	P = 1 atm	31	0.5	1	0.5	[404]

[a] This is the molar H$_2$/CO ratio used in the determination of the activation energy. [b] These parameters from Gunturu et al. [17] do not constitute a dedicated rate expression for methane, but rather a lumped model for the entire hydrocarbon production, where methane is the main constituent. [c] This result is for a catalyst with 2 % K. [d] Hou and Wise [404] use a Langmuir-Hinshelwood type expression of the form $R_{CH_4} = \frac{k p_{H_2S}^{0.5} p_{H_2}^{0.5} p_{CO}}{1+K p_{CO_2}}$, so their rate expression would only correspond to equation (5.1) in situations with a negligible CO$_2$ concentration.

Apart from a comparison of the reaction kinetics it is also valuable to evaluate the operating characteristics of the presently used K$_2$CO$_3$/Co/MoS$_2$/C catalysts in relation to other alcohol synthesis catalysts reported in the literature. Table 5.5 on the next page contains a comparison of various alcohol synthesis catalysts including non-sulfide catalysts.

Table 5.5 Reported operating characteristics for different alcohol synthesis catalysts.

Catalyst	STY $\left[\frac{g}{g\ cat.\cdot h}\right]$	S_{Alc} [a] [mol%]	X_{CO} [mol%]	$\frac{C_{2+}OH}{C_1OH}$ [wt/wt]	P [bar]	T [°C]	GHSV [h^{-1}]	$\frac{H_2}{CO}$ [b]	Ref.
KCoMo-1 [c]	0.079	65	5	2.01	100	326	5418	1.0	
KCoMo-1 [d]	0.085	90	3	0.57	100	327	5247	1.0	This
KCoMo-3 [e]	0.194	79	8	0.65	100	325	5353	1.0	work
KCoMo-3 [f]	0.276	65	18	0.90	100	350	5244	1.0	
K$_2$CO$_3$/Co/MoS$_2$	0.189	84.6	15.3	0.72	50	310	4800	2.0	[196]
K$_2$CO$_3$/Co/MoS$_2$/C	0.39	80.0	14.0 [g]	0.34	138	290	1744	1.1	[188]
K$_2$CO$_3$/Co/MoS$_2$ [h]	-	75.7	39.0	2.56	104.5	305	1300	0.98	[18]
K$_2$CO$_3$/Ni/MoS$_2$	0.15 [i]	62.7	34.1	4.12	80	300	2500	1.0	[197]
K$_2$CO$_3$/MoS$_2$	0.11 [i]	74.5	11.4	0.79	80	300	2500	1.0	[197]
Cs/MoS$_2$	0.308	76 [j]	-	0.52	83	295	7750 [k]	0.96	[75]
K$_2$CO$_3$/β-Mo$_2$C [l]	0.122 [i]	52.6	23.4	1.54	80	300	2000	1.0	[121]
K$_2$CO$_3$/Co/β-Mo$_2$C [m]	0.156 [i]	42.6	40.8	1.75	80	300	2000	1.0	[119]
Co/Cu/Zn/Na/Al$_2$O$_3$	0.13-0.15	65-70	21-24	1.44	60	290	4000	2	[72]
Cs/Cu/ZnO/Cr$_2$O$_3$ [n]	0.309	79.4 [o]	22.0	0.50	76	310	5330 [k]	0.45	[408]
Cs/Cu/ZnO/Al$_2$O$_3$ [p]	0.433	91.2	12.5	0.07	76	310	5330 [k]	0.45	[408]
K/ZnO/Cr$_2$O$_3$ [q]	0.159	88	12	0.74	103	400	12000	1	[409]
Rh/Mn/Li/SiO$_2$ [r]	0.332 [s]	39.4 [t]	6.7 [t]	19.32	30	320	12000	2	[410]
Rh/Fe/TiO$_2$ [u]	-	42 [v]	6.2 [g]	5.57 [v]	20.3	270	8000 [k]	1	[411]
Rh/Fe/SiO$_2$ [x]	-	50 [v]	4.5 [g]	2.55 [v]	20	270	8000 [k]	1	[412]
Rh/Mn/Li + Cu/Zn	0.20	80-85	1.5	[y]	50	260-280	30-45000	1.4	[35]

[a] Alcohol selectivity on a CO$_2$-free basis. [b] Molar ratio in the syngas feed. [c] The experiment is conducted with 218 ppmv of H$_2$S in the syngas feed. [d] After 30 h on stream with an H$_2$S free syngas. [e] After 27.5 h on stream with an H$_2$S free syngas. [f] After 24 h on stream with an H$_2$S free syngas. [g] Excluding CO converted to CO$_2$. [h] The experiment is conducted with 50 ppmv of H$_2$S in the syngas feed. [i] The space time yield has the unit g/mL cat./h. [j] Estimated from figure 2 in the original paper. [k] The unit of the space velocity is L/kg cat./h. [l] This is for a catalyst with a molar ratio of K to Mo of 0.2. [m] This is for a catalyst with a molar ratio of Co to Mo of 1/8. [n] This is for a catalyst containing 3.0 mol% Cs. [o] Much of the remainder of the product is oxygenates – esters, aldehydes and ketones. The hydrocarbon selectivity is 10.6 C%. [p] This is for a catalyst containing 2.5 mol% Cs. [q] This is for a catalyst containing 3 wt% K. [r] The Rh:Mn:Li weight ratio is 1:1:0.075, and the Rh loading is 1 wt% [s] This is the total space time yield of C$_{2+}$ oxygenates. Ethanol is the dominant oxygenated product with a selectivity of 35.5 C%. [t] It is not quite clear, if this value is on a CO$_2$-free basis. The CO$_2$-formation is not reported, but the uncharacterized products only amount to 1.8 C%. The hydrocarbon selectivity is 41.9 C%. [u] Catalyst contains 2 wt% Rh and 5 wt% Fe. The catalyst bed also contains inert SiC, which is not included in the GHSV above. [v] Calculated using only methanol and ethanol. [x] Catalyst contains 2 wt% Rh, 1 wt% Fe. [y] Alcohol product is reported to be 100 % EtOH/Ethyl acetate. This is a double bed system where a Cu/ZnO catalyst reduces C$_2$ oxygenates produced by the Rh-based catalyst.

The results in table 5.5 illustrate various important aspects of the alcohol synthesis. Most importantly the table illustrates that it is a tremendous challenge to achieve both a high alcohol selectivity and a high fraction of higher alcohols in the product. In terms of alcohol selectivity the system, which currently looks most promising, must be the modified methanol synthesis catalysts based upon Alkali/Cu/ZnO or Alkali/ZnO/Cr$_2$O$_3$. Among the molybdenum based systems the cobalt promoted sulfide looks like the best choice with respect to selectivity. Table 5.5 shows that the alcohol productivity of the reported catalysts most commonly is found in the 0.1-0.3 $\frac{g}{g\ cat.\cdot hr}$ range. The table also shows that high productivities commonly are associated with a large fraction of methanol in the product. As it is reflected by the very large C$_{2+}$OH/C$_1$OH-ratios shown in table 5.5 rhodium based catalysts are able to produce a large fraction of higher oxygenates – particularly a large fraction of ethanol and other C$_2$-oxygenates [33, 36]. However even at relatively low conversion levels the Rh-based catalysts in table 5.5 show a modest alcohol selectivity. When comparing the entries in table 5.5 it is clear that some of the catalyst samples used in the present study have a relatively low activity in the relevant temperature range, however this must largely be ascribed to the low metal contents of at least the samples KCoMo-1 and KCoMo-2. In fact most of the catalysts presented in table 5.5 are unsupported systems that consist purely of the active phase. However table 5.5 also shows that the catalyst KCoMo-3, which has a significantly larger molybdenum content than KCoMo-1, is considerably more active. The results in table 5.5 show that KCoMo-3 at comparable conditions is more than twice as active as KCoMo-1 in a sulfur free syngas. The influence of the metal loading is discussed in more detail in the subsequent section.

5.4   Effect of the metal content

As it is mentioned above, the catalyst used for the kinetic investigations (KCoMo-2) has a fairly low content of the active materials (see table 4.4), and for a potential industrial application it might be desirable to raise the space time yield to lower the amount of catalyst needed. It should however be mentioned that in the aforementioned system study by Phillips [322] the economic analysis of the process was quite insensitive to the space time yield of the catalyst. An obvious way to improve the space time yield would be to increase the metal content of the catalyst, and for this reasons we have briefly investigated the effect of an increased metal content in the catalyst formulation. This investigation is conducted using the catalyst KCoMo-3 (see table 4.4). We have performed a temperature sweep with the catalyst, and the results are presented in figure 5.10, which shows the CO conversion and the alcohol selectivity as functions of the temperature.
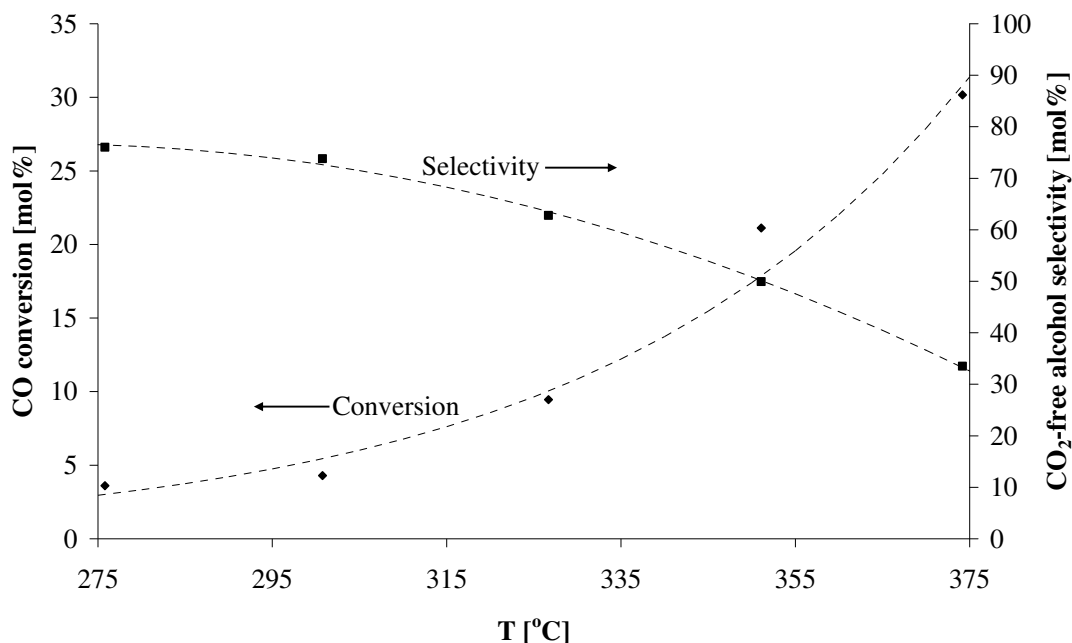
Figure 5.10 The CO conversion and alcohol selectivity as functions of the reactor temperature. The experimental conditions are P = 100 bar, GHSV = 5600 h^{-1}, Feed: 48.6 vol% H_2, 51.3 vol% CO, 219 ppmv H_2S. Time on stream is +25 h. The catalyst is KCoMo-3.

Figure 5.10 shows that while the conversion increases with increasing temperature the selectivity follows the opposite tendency, since hydrocarbon selectivity is increased by increasing temperature. As figure 5.10 shows the CO_2-free alcohol selectivity it might be added that the overall, carbon based CO_2-selectivity increases with increasing temperature from 17 mol% at 276 ºC to 43 mol% at 374 ºC. The increase in CO_2 selectivity is probably due to the increased hydrocarbon formation at higher temperature. Furthermore the water gas shift reaction may not cause as rapid a CO_2 formation at the lower temperatures.

The conditions at the data point at 326 ºC in figure 12 correspond to the conditions of the experiment presented in figure 5.2. These conditions can thus be utilized to compare the two catalysts KCoMo-1 and KCoMo-3 to assess the influence of the metal content. Such a comparison is presented in table 5.6.

Table 5.6 Comparison of the catalytic properties of KCoMo-1 and KCoMo-3. Conditions 326 ºC, 100 bar, GHSV = 5400±200 h^{-1}. Feed: 49±1 vol% H_2, 51±1 vol% CO, 219±1 ppmv H_2S. Time on stream +25 h.

Catalyst	KCoMo-1	KCoMo-3
Mo content [wt%]	4.23	13.60
STY $\left[\frac{g}{g\ cat.\cdot h}\right]$	0.079	0.145
CO conversion [mol%]	5	9
Alcohol selectivity [mol%]	65	62
C_{2+}/C_1 ratio [wt/wt]	2.01	1.88

The data in table 5.6 illustrate that in the investigated conversion range the catalyst with the higher Mo loading shows an STY and a CO conversion that are increased by a factor of 1.9 compared to the catalyst with lower metal content. As it was described in 5.3, the results in table 5.5 show that the difference in activity between the two catalysts is slightly larger, when an H_2S free feed is used. When looking at table 5.6 it can be seen that there are small differences in alcohol selectivity and product distribution. These variations could be the result of both the subtle dissimilarities in catalyst composition and the result of the different conversion levels. With the small change in selectivity and the larger variation in conversion it is somewhat difficult to make definite conclusions about the influence of metal loading upon the alcohol selectivity. table 5.6 also shows that the more active catalyst with the higher metal loading converts more H_2S than the catalyst with the lower metal content. Something that also should be noted is that the general increase in activity is less than the increase in metal loading.

In the patent literature [18, 103] it is typically recommended to use a catalyst with a high content of the active materials – preferably in the 50-70 wt% range, and on both carbon [243] and alumina [228] supports it has generally been observed that the selectivity as well as the activity increases with increasing metal loading. This reported increase in selectivity with increasing metal loading is most likely related to changes in the morphology of the active phase. Under the assumption that the sulfide does constitute the active phase, the relationship between metal loading and selectivity could potentially be rationalized on the basis of the fundamental knowledge of this system. Molybdenum sulfide has a layered structure, where a single MoS_2 slab is composed of a layer of molybdenum between two layers of sulfur [139]. While molybdenum sulfide has been the subject of substantial research due to its use as a catalyst for the important hydrotreating reactions in the oil industry [98], much less research has been done on the catalyst with respect to syngas reactions. In highly active hydrotreating catalysts the sulfide is mainly present as single S-Mo-S slabs lying flat on the support surface [208]. The hydrogenation activity of the MoS_2 slab is believed to be related to the brim along the top edge of the sulfide slab [151, 153]. If the slabs grow larger, or the stacking of the slabs increases, which would be expected results of an increased metal loading, the relative amount of hydrogenation sites at the brim should decrease. In relation to the alcohol synthesis a decreased hydrogenation activity would be expected to result in a reduced hydrocarbon formation, and it might thus not be unreasonable to expect an increased alcohol selectivity, when the metal loading is increased. The previous studies of the effect of the metal content [228, 243] have however used catalysts with significantly higher metal loadings and lower surface areas of the support, than it is the case in the present study. In our studies we only have a relatively modest increase in metal content and a support with a rather high surface area (see table 4.4). For this reason we are not likely to see a severe change in sulfide particle morphology between KCoMo-1 and KCoMo-3, and this could well be an important part of the explanation for the observed shift in activity with only a minor change in selectivity.

The data depicted in figure 5.10 can also be used to illustrate another important point about the alcohol synthesis, namely that a close relationship exits between conversion and selectivity. This is illustrated in figure 5.11, which shows the selectivity as a function

of the conversion, and this figure shows an approximately linear decrease in selectivity with increasing conversion.
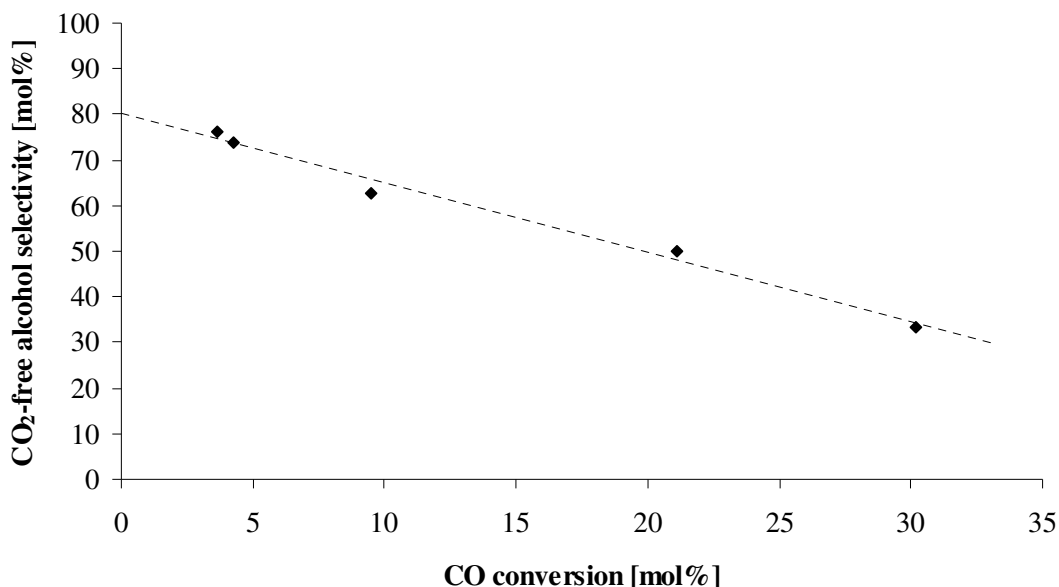
Figure 5.11 The alcohol selectivity depicted as a function of the CO conversion at the conditions given in figure 5.10. It should be noted that the variation in the CO conversion has been achieved by changing the reaction temperature.

A linear decrease in selectivity with increasing conversion has previously been reported by Quarderer [74]. However the shape of the S_{Alc}-X_{CO}-curve must be expected to reflect the method by which the conversion is manipulated. An increased conversion through an increased residence time at a relatively low constant temperature must be expected to have a less detrimental effect upon the selectivity compared to the present increase in conversion through an increased reaction temperature.

It seems quite reasonable that the selectivity is lowered, when the conversion is increased. In the preceding text the possible conversion of already formed alcohols has been mentioned several times, and since there is a noteworthy risk of chain termination to a hydrocarbon, the selectivity should of course suffer from an increased conversion of the already formed alcohols.

5.5 Incorporation of sulfur into the liquid product

The last part of this investigation concerns the incorporation of sulfur species into the condensed reaction product. The objective here is to quantify the amount of sulfur that is present in the alcohol product and to ascertain the nature of this sulfur. The experiments related to this examination are conducted using the catalyst KCoMo-1 (see table 4.4).

Figure 5.12 shows the weight fraction of sulfur in the collected alcohol product as a function of the H_2S concentration in the syngas feed. Prior to the first condensation the

catalyst has been on stream for 14.5 hours in a syngas containing 460 ppmv H_2S, and an evaluation of the effluent gas from the reactor has indicated that the catalytic properties have stabilized. Subsequent condensation experiments have been conducted with the same catalyst and have all been initiated after at least 7 hours with the respective H_2S levels in the feed. For the lowest H_2S concentration in figure 5.12, namely 46 ppmv, one must in light of the results in figure 5.3 expect that the distribution of the alcohol product changes over time. The main objective in these investigations is however to evaluate the product sulfur content, and less significance is in this investigation ascribed to the distribution of the alcohol product.

Figure 5.12 shows that the sulfur content in the liquid product increases linearly with an increasing H_2S level in the feed. The results in figure 5.12 clearly show that sulfur species are incorporated into the liquid product. In all the experiments the sulfur content in the liquid product can even be seen to be well above the US and EU limits for sulfur in automotive fuels that were mentioned in section 2.7. It should be mentioned that if all the H_2S, which is observed to be converted in the experiments in figure 5.12, had been incorporated into the liquid product, the sulfur content of the product would have been roughly 10 times higher, than it is the case. Part of the hydrogen sulfide is therefore clearly converted into gaseous sulfur species, but these species are not determined in the present investigations.

The incorporation of sulfur species into the liquid product also continues after H_2S is removed from the feed stream, but in this case the product sulfur content decreases over time. This is illustrated in figure 5.13, which shows the sulfur content in the liquid reaction product as a function of the catalyst age in a sulfur free syngas.

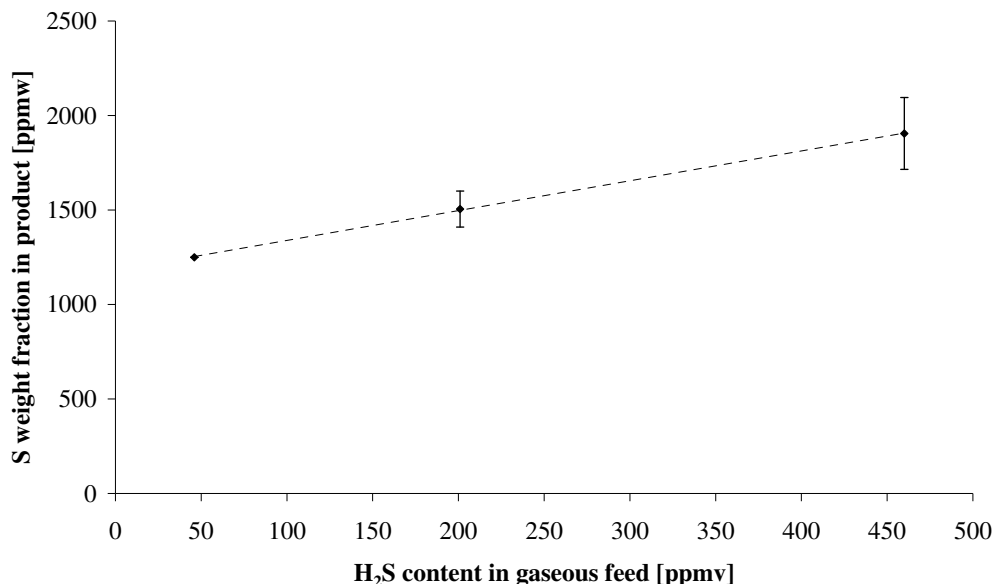**Figure 5.12** The weight fraction of sulfur in the condensed alcohol product as a function of the H_2S concentration in the syngas feed. The experimental conditions are T = 345 ºC, P = 100 bar, GHSV = 5100±200 h^{-1}, Feed: 50±1 vol% H_2, 50±1 vol% CO. The condensation of the liquid product is conducted at atmospheric pressure and dry ice temperature (-78.5 °C). The catalyst is KCoMo-1.
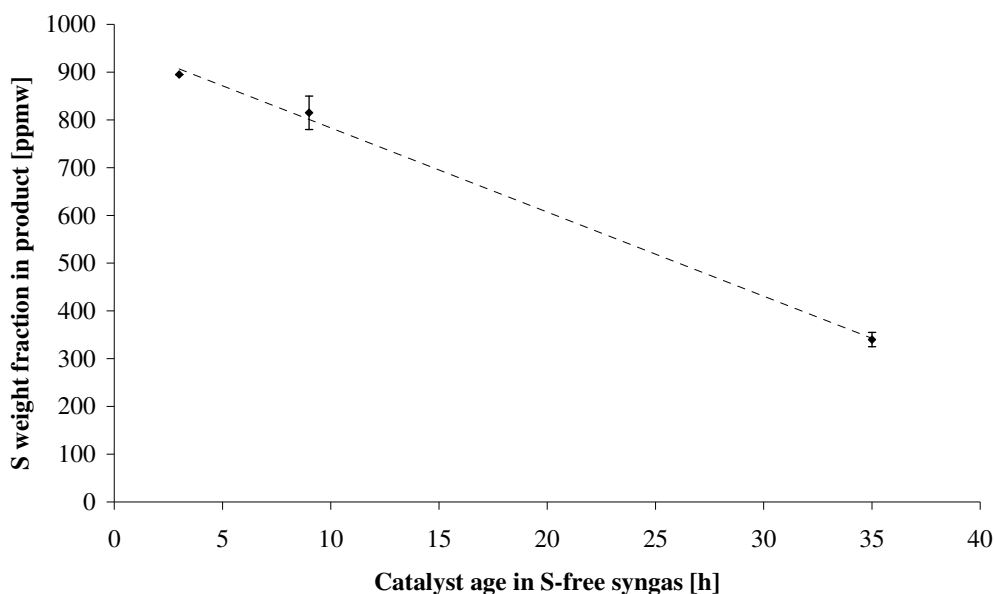
Figure 5.13 The weight fraction of sulfur in the condensed reaction product as a function of the catalyst age in sulfur free syngas. The experimental conditions are T = 345 °C, P = 100 bar, GHSV = 5261 h^{-1}, Feed: 49.9 vol% H$_2$, 50.1 vol% CO. The condensation of the liquid product is conducted at atmospheric pressure and dry ice temperature (-78.5 °C). The catalyst is KCoMo-1.

Figure 5.13 shows that during the experiment, there is a linearly decreasing relationship between the sulfur content in the alcohol product and the catalyst age in a sulfur free syngas. This must imply that the catalyst itself gradually is losing sulfur in the syngas atmosphere, and that the sulfur, which is lost, becomes incorporated into the condensed reaction product. From figure 5.13 it can be seen that even if the decreasing linear tendency continues all the way to zero sulfur content in the product, it will take a substantial period of time, before the sulfur content is below the 10 ppmw EU limit for sulfur in gasoline.

The above results indicate that at least if H$_2$S is present in the syngas feed, it will be necessary to perform a cleaning operation to remove sulfur from the final product. To assess the complications associated with such a cleaning operation we have performed a qualitative GC-AED analysis of the sulfur compounds present in the condensed alcohol product. This analysis indicates that thiols are the dominant sulfur species. Interestingly; there are essentially no traces of dissolved H$_2$S or COS in the product, although it cannot be fully excluded that these dissolved gases had been present, but had evaporated before the analysis of the sulfur species. However analysis of the effluent gas from the reactor before and during the condensation indicated that little or no H$_2$S was captured in the condensation. Figure 5.12 shows that when the catalyst is operated with H$_2$S in the feed, there is a substantial amount of sulfur in the condensed product, and the analysis of the nature of the sulfur species also reveals that a multitude of sulfur compounds are present in the alcohol product. Apart from thiols the analysis also indicates the presence of dimethyl sulfide and even traces of various thiophenes. When H$_2$S is removed from the

feed, the number of sulfur containing compounds in the liquid product decreases over time. For the liquid product condensed after 35 hours of operation with a sulfur free syngas the GC-AED analysis only shows the presence of ethanethiol, 1-propanethiol and 2-methyl-1-propanethiol. GC-AED spectra illustrating the sulfur speciation in two representative liquid samples are shown in appendix E.

The fact that the catalyst forms thiols is not entirely unexpected. The formation of 1-heptanethiol from 1-heptanol over $Ni/MoS_2/\gamma-Al_2O_3$ has previously been observed by Krause et al. [413, 414]. These authors [413, 414] found that the alcohol was converted into the thiol in the absence of H_2S, but the thiol formation was increased in the presence of H_2S. Chen et al. [415] have previously employed $Alkali/Co/MoS_2$ catalysts to synthesize methanethiol from H_2S containing syngas, and in their case COS and CH_3SH were the dominant reaction products. However it must be added that these authors [415] used a feed, where H_2S was the main constituent.

The incorporation of sulfur species into the alcohol product is certainly a clear disadvantage for the sulfide catalyst. If the catalyst is used with a sulfur-free syngas the problem of sulfur compounds incorporated into the product should of course disappear, when all sulfur or at least all detachable sulfur has been removed from the catalyst. If the catalyst on the other hand is operated with a sulfur containing feed, it seems certain that measures would have to be taken to remove the thiols and other sulfur species from the product in order to ensure that the alcohol product is usable.

5.6 Effects of H_2S upon the alcohol synthesis catalyst

The preceding text has illustrated several effects of H_2S upon the alcohol synthesis catalyst, and the purpose of the following two sections is to provide a general discussion of the results. In short the presence of hydrogen sulfide favors chain growth for both alcohols and hydrocarbons, but H_2S lowers the alcohol selectivity by enhancing the hydrocarbon production. Furthermore there is a significant shift in the effect of hydrogen sulfide, which at the presently used conditions occurs at an H_2S level between 57 and 103 ppmv (see figure 5.3). Above this concentration range the product distribution stabilizes relatively fast, and the higher alcohols are the dominant reaction products. Below 57 ppmv of H_2S the effect of hydrogen sulfide appears to be quite limited, methanol is the dominant reaction product, and the development of a stabilized product distribution is much slower.

In a discussion of the effects of H_2S it is a clear complication that the active phase of the stabilized catalyst is not unambiguously determined. The present results indicate that the catalyst is loosing sulfur in the syngas atmosphere. On the basis of the available information it is however difficult to say, whether the observed loss of sulfur from the sulfide is accompanied by a complete or partial phase change into what could be a carbide. This discussion should be especially relevant, when an H_2S free syngas is used. Højlund Nielsen et al. [403] studied the conversion of syngas to hydrocarbons over a $Co/MoS_2/TiO_2$ catalyst, and these authors [403] speculated that a carbide might constitute

the stabilized phase of the catalyst. Saito and Anderson [416] studied CO methanation over MoS_2 in a sulfur free syngas, and these authors observed a slowly increasing catalyst carbon content with time on stream, but they also reported that the sulfur content was quite constant. One could envision a partial carburization that is limited to the formation of an MoS_xC_y-like phase at the exterior surface of the sulfide cluster, while the interior of the cluster remains sulfided. Such a structure has in fact also been proposed for catalysts used in hydrodesulfurization processes [245, 417]. Although there is insufficient evidence to clarify the issue of a possible phase change, it can not be excluded that the initial development in activity and selectivity, which we observe in the first hours on stream (see figure 5.1 and figure 5.2), to some extent could be related to a change in the active phase of the catalyst. Alkali promoted molybdenum carbides have been reported to possess activity for alcohol formation [116, 119, 121], and at least a partial carburization of the sulfide catalyst is certainly a possibility in the present experiments. As previously mentioned it could be speculated that the strong shift in the effect of H_2S, which we observe between H_2S levels of 57 and 103 ppmv (see figure 5.3) is related to, whether the concentration is sufficient to uphold the sulfide as the active phase.

To obtain a further understanding of the changes that the sulfide catalyst undergoes, it seems prudent to compare the presently used catalyst to molybdenum carbide catalysts described in the literature. When alkali promoted molybdenum carbide is used as an alcohol synthesis catalyst, the alcohol selectivity is commonly reported to be lower than for catalysts based on molybdenum sulfide, as the carbide generally causes a larger hydrocarbon formation (see the examples in table 5.5) [115]. In the first hours on stream the alcohol selectivity obtained with MoS_2-based catalysts gradually increases (see figure 5.1). The development in selectivity does therefore not seem to indicate a carburization of the catalyst, but as previously mentioned this gradual increase in selectivity could also be due to other factors such as spreading of the alkali promoter or blocking of hydrocarbon forming sites by carbonaceous deposits. An indication of a partial carburization of the catalyst does however come from the distribution of the alcohol product. We have compared the product distribution obtained with the presently used $K_2CO_3/Co/MoS_2/C$ catalyst to results obtained by Woo et al. [115], with K_2CO_3/β-Mo_2C catalysts. Although the carbide catalysts employed by Woo et al. [115] do not contain cobalt it is a large advantage that these carbide catalysts yield conversion levels similar to the ones obtained in the present investigations. For a chain growth reaction such as the alcohol synthesis the product distribution will be a function of the conversion level [74], as already formed alcohols may readsorb and extend their carbon chains. It therefore seems appropriate to compare product distributions obtained at similar conversion levels although the operating conditions and catalyst compositions are somewhat different.

Figure 5.14 shows the detailed distribution of the alcohol product obtained with the presently used $K_2CO_3/Co/MoS_2/C$ catalyst (KCoMo-1). Also shown in the figure is the product distribution obtained by Woo et al. [115], with a K_2CO_3/β-Mo_2C catalyst operated with and without sulfur in the syngas feed. Interestingly; figure 5.14 shows how the product distribution obtained with a Co-Mo sulfide catalyst operated in a sulfur-free syngas is very similar to the distribution obtained with a molybdenum carbide catalyst operated in a sulfur containing syngas. The carbide operated in a sulfur free atmosphere yields a product distribution that is further away from the distribution obtained with the sulfide catalyst, but there are also larger differences in the CO conversion. These results

could suggest that when an MoS_2 based catalyst is operated in a sulfur free syngas, the stabilized phase of the catalyst is a combined phase containing both carbon and sulfur, and a similar phase is formed, when an Mo_2C based catalyst is operated in a sulfur containing atmosphere. It must however be emphasized that while the conversion levels are similar for the different results in figure 5.14 there are differences in catalyst compositions and operating conditions. Additionally figure 5.14 also illustrates how the addition of H_2S to the syngas passed over the MoS_2 catalyst shifts the product distribution towards the higher alcohols.
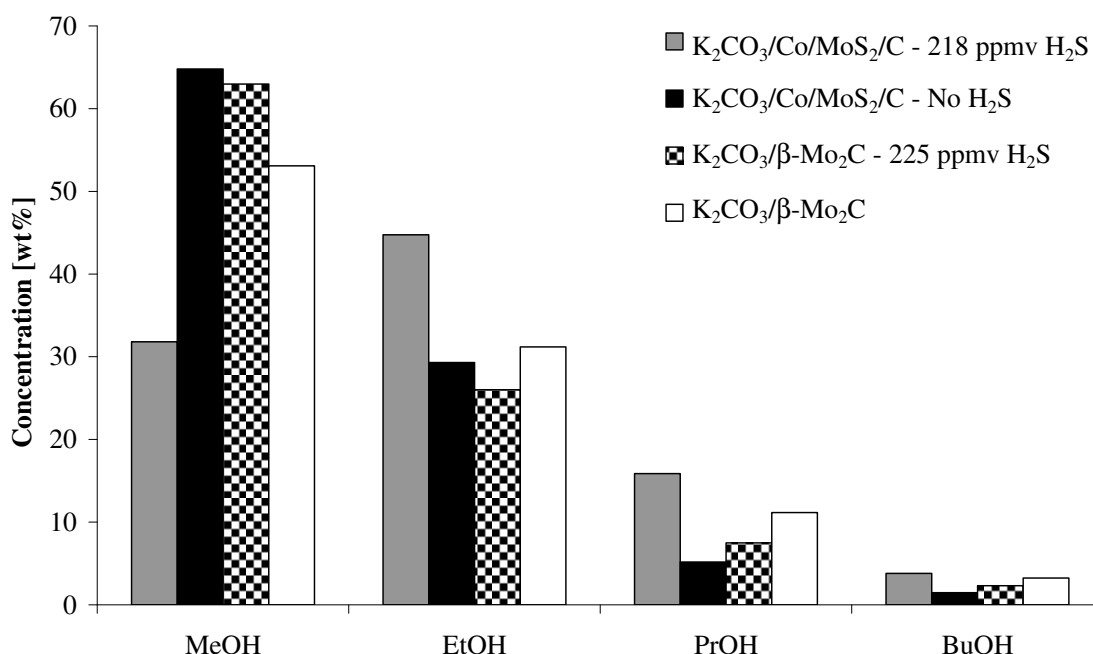
Figure 5.14 The steady state distribution of the alcohol product obtained with the sulfide catalyst (KCoMo-1) operated with and without H_2S in the syngas feed. Also shown are results from Woo et al. [115] using a K_2CO_3/β-Mo_2C catalyst. Notice the similarity of the two columns in the middle. The experimental conditions are (CO conv.):
$K_2CO_3/Co/MoS_2$: 327 °C, 100 bar, H_2/CO = 1.0, 42 hr on stream, (3 %)
$K_2CO_3/Co/MoS_2$ – 218 ppmv H_2S: 326 °C, 100 bar, H_2/CO = 1.0, 67 hr on stream, (5 %)
K_2CO_3/β-Mo_2C: 300 °C, 80 bar, H_2/CO = 0.98, 20 hr on stream (10.3 %)
K_2CO_3/β-Mo_2C – 225 ppmv H_2S: 300 °C, 80 bar, H_2/CO = 0.98, 35 hr on stream, (5.2 %)

At both high and low H_2S levels we observe the same general development in the first hours on stream, where the conversion gradually decreases, and the alcohol selectivity gradually increases (see figure 5.1 and figure 5.2). In section 5.2 it has been mentioned that a spreading of the alkali promoter might be part of the cause of this development. Based upon the gradually increasing carbon level observed by Saito and Anderson [416] one might as previously mentioned also speculate that a gradual blocking of the catalyst by carbonaceous deposits could contribute to the development in activity and selectivity, which we observe in the first hours on stream.

5.7 Effect of H$_2$S at higher concentrations

The results in sections 5.2 and 5.3 illustrate that even at H$_2$S levels, where the product distribution is stabilized, the concentration of hydrogen sulfide has an influence upon the reaction kinetics. Under the assumption that the H$_2$S level in this case is sufficient to sustain the sulfide, these effects might be rationalized in terms of the properties of the sulfide. EXAFS investigations of Mo-S and Mo-Mo bond lengths show that the sulfide in supported MoS$_2$ and Co/MoS$_2$ catalysts exists as a phase that resembles well-crystallized, bulk MoS$_2$ [131, 132], and similar results from investigations of supported K/MoS$_2$ alcohol synthesis catalysts indicate that this is also the case for the alkali promoted system [133, 134, 418]. It has previously been mentioned that the structure of MoS$_2$ is like a sandwich with a layer of Mo atoms between two layers of sulphur atoms. MoS$_2$ can potentially be terminated by two low Miller-index planes, namely the the Mo($10\bar{1}0$) edge and the S($\bar{1}010$) edge [139, 140]. These edges are commonly described as the Mo edge and the S edge respectively due to the element nominally exposed at the respective edges. However both edges might, depending upon the chemical potential of sulfur and the reductive potential of the gas, be covered with sulfur [140, 143, 156]. Investigations of pure MoS$_2$ without the alkali promoter have indicated that hydrogen is adsorbed as S-H groups [154, 155], and that these S-H groups are located on the outermost sulfur atoms along the edges of the sulfide [135, 140, 156]. In a reducing gas these outermost sulfur atoms can be removed to the gas phase, whereby sulfur vacancies are formed at the edge of the sulfide [419]. Such vacancy formation is believed to play an important role in hydrodesulfurization reactions, and vacancy formation has been illustrated by STM investigations, where molecular hydrogen has been dosed to sulfide clusters [147]. If the outermost sulfur atoms constitute the hydrogen adsorption sites, then their disappearance would also mean a loss of hydrogenation activity. The role of H$_2$S in the syngas could therefore be to replenish the hydrogen adsorption sites. This notion that H$_2$S serves to form hydrogen adsorption sites is supported by the results of Hou and Wise [404], who found that the hydrogen chemisorption capacity of MoS$_2$ increased with the H$_2$S/H$_2$ ratio in the preceding treatment of the catalyst. The formation of an increased number of hydrogen adsorption sites and the enhanced hydrogenation activity, which should ensue, could explain the increased hydrocarbon formation, when H$_2$S is added to the syngas feed. Moses et al. [419] used density functional theory to calculate the relative amount of vacancies along the S edge at various partial pressures of H$_2$ and H$_2$S, and judging from these results the amount of vacancies should, with the presently used amounts of H$_2$S in the syngas, be quite significant.

A loss of sulfur and a corresponding loss of hydrogenation activity could even in the absence of a phase change be contributing to the developments in activity and selectivity, when the catalyst is first exposed to syngas. If the catalyst is gradually loosing hydrogen adsorption sites, the result should be a gradually increasing alcohol selectivity, since the hydrogenation activity, and with it the hydrocarbon formation, decreases. This is the tendency observed in figure 5.2, which show the developments in selectivity and conversion with time on stream in a syngas with a relatively high H$_2$S level of 218 ppmv.

The idea that the presence of hydrogen sulfide influences the number of S-H hydrogen adsorption sites can potentially explain the enhanced hydrocarbon formation in the presence of H$_2$S, but some hydrogenation activity arising from the presence of Mo-H

groups can not be completely excluded. Such groups have reportedly [420] never been observed experimentally, although some computational studies have indicated their existence [420-422]. On the other hand it is quite likely that the formation of vacancies apart from a loss of hydrogenation sites simultaneously serves to provide new CO adsorption sites. Using infrared spectroscopy Travert et al. [148] observed that the intensity of bands related to CO adsorbed on MoS_2 decreased with increasing exposure of the catalyst to H_2S, while the band intensity increased with H_2 treatment. This result could suggest that the amount of CO adsorption sites is related to the number of vacancies, which would be increased by reducing treatment and decreased through blocking with sulfur derived from for example H_2S. It should be emphasized that the study of Travert et al. [148] deals with a sulfide without the alkali promoter, and the alkali promoter might also affect the CO adsorption. However if H_2S serves to lower the amount of adsorbed CO by blocking sulfur vacancies this could certainly also contribute to the lowering of the oxygenate selectivity that is observed in the presence of H_2S.

The kinetic parameters in table 5.1 and table 5.2 illustrate that there are two effects of H_2S at higher (≥ 260 ppmv) concentrations, namely that H_2S shifts the selectivity towards hydrocarbons and that H_2S favors chain-growth. That H_2S serves to replace hydrogen adsorption sites and thereby enhance the hydrogenation activity seems to be consistent with the increased hydrocarbon formation.

Concerning the promotional effect of H_2S upon the chain-growth it might have been expected that an increased hydrogenation activity would enhance the chance of chain-termination and lead to shorter products, but a quite recent DFT study can perhaps explain, why this is not the case. Chen et al. [423] studied the formation of ethanol by addition of CO to methanol on MoS_2 by means of density functional theory, and their investigations suggested that the C-O bond breakage in methanol preferably occurs through an attack of hydrogen on the hydroxyl group of methanol:

$$CH_3OH + H \rightleftharpoons CH_3 + H_2O \qquad\qquad\qquad R37$$

If the hydrogenation activity is increased it would presumably enhance the hydrogenation of CO into methanol and via R37 lead to more CH_3-groups. As discussed in section 2.5 methyl groups are chain growth precursors to which CO can be added to extend the C-C chain. At the present conditions, where the CO coverage appears to be high, it is thus possible that an increased hydrogenation activity could favor the chain-growth by increasing the formation of CH_3-groups available for CO addition. This could explain the effect of H_2S, which favors hydrocarbon formation, but also chain-growth.

6 Coupling of alcohols over alkali promoted cobalt-molybdenum sulfide

The pure and simple truth is rarely pure and never simple
- Oscar Wilde

6.1 Abstract

A newly observed route to chain growth for alkali promoted cobalt-molybdenum sulfide seems to be the coupling of alcohols. It is observed that addition of ethanol to the syngas fed to the reactor especially enhances the formation of 1-butanol. It seems quite likely that the mechanism for the coupling reaction over $K_2CO_3/Co/MoS_2$ resembles a classical aldol condensation. The aldol condensation pathway is known in the alcohol synthesis over Alkali/Cu catalysts, but while ethanol coupling over Alkali/Cu can result in both 2-butanol and 1-butanol, the coupling over the sulfide catalyst yields almost no 2-butanol. Alcohol coupling reactions proceeding via aldol condensation pathways can explain the presence of branched alcohols in the product obtained with Alkali/MoS$_2$ and Alkali/Co/MoS$_2$ catalysts. While ethanol addition boosts the production of higher alcohols, the ethanol is also partly converted into higher hydrocarbons, and overall there is a slight decrease in alcohol selectivity, when ethanol is added to the feed.

6.2 Coupling of alcohols

In section 2.5 it was described how experiments with isotopic labeling [75] have indicated that an important route to chain growth over MoS$_2$-based catalysts is the addition of CO to a growing alkyl group (RCH$_2$) to form an acyl species (RCH$_2$CO). The formed acyl species can then be hydrogenated into the corresponding alcohol or to a new, now longer alkyl group. Hydrocarbons are believed to be formed from hydrogenation of the alkyl goups. This route to formation of alcohols and hydrocarbons is illustrated in figure 2.7 on page 55.

In this chapter it will be shown that another route to chain growth for the sulfide catalyst is the coupling of alcohols – here exemplified by the self-coupling of ethanol into 1-butanol. A way to boost the production of the desirable higher alcohols could be to co-feed lower alcohols along with the syngas (see perhaps section 2.6). Previous work has clearly shown that methanol co-fed along with syngas is converted into higher alcohols [13, 75]. Here we are investigating the co-feeding of ethanol along with the syngas sent to the reactor. The catalyst used in this chapter is KCoMo-3 in table 4.4 on page 85.

The results in chapter 5 illustrated that the sulfide catalyst is affected by the presence of sulfur sources like H$_2$S in the syngas. The presence of H$_2$S in the syngas shifts the distribution of the alcohol product from methanol towards the higher alcohols, but the presence of H$_2$S also leads to an increased production of hydrocarbons and to incorporation of sulfur species into the alcohol product.

Due to the negative effects of H_2S in the syngas the present experiments have been conducted with a sulfur free syngas. It was previously observed (see figure 5.1 on page 93) that the catalyst in an S-free syngas requires a stabilization period of around 30 hours on stream to achieve steady state. The present addition of ethanol to the syngas is therefore commenced after the catalyst has been given 30 hours to stabilize in a sulfur free syngas (conditions are given in figure 6.1). Figure 6.1 shows the alcohol production rates as functions of the molar fraction of ethanol in the syngas feed.
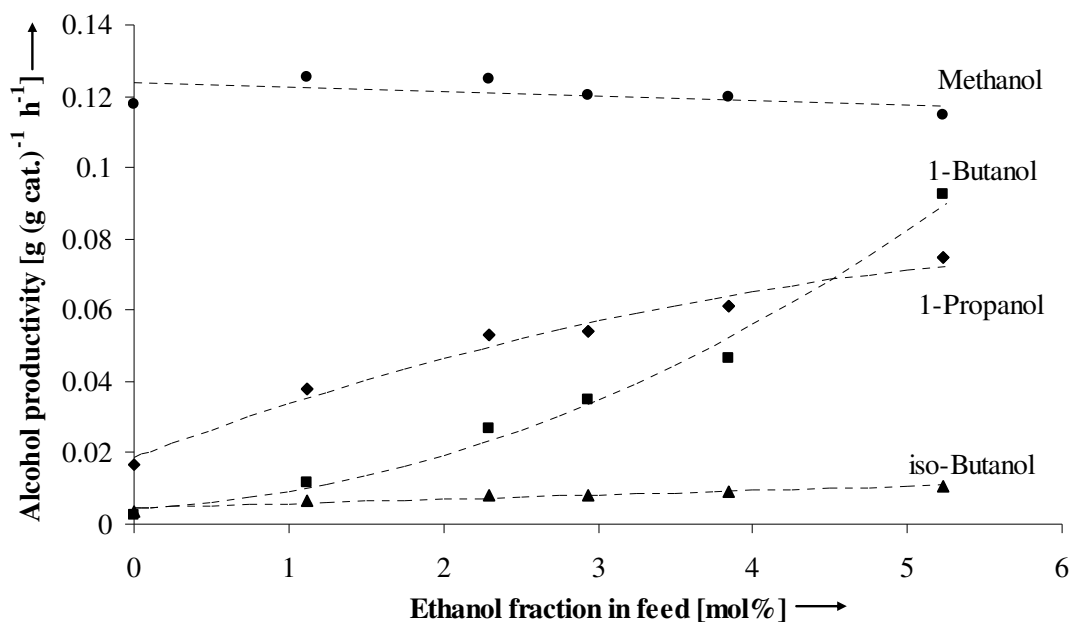
Figure 6.1 The production rates of various alcohols as functions of the ethanol fraction in the syngas feed. Experimental conditions: $T = 325.3$ °C; $P = 100$ bar; GHSV $= 5500$ h^{-1}. Feed excl. EtOH : 49.1 vol% H_2; 50.9 vol% CO; +30 h on stream.

Based upon the aforementioned CO addition mechanism it would be expected that the main result of the ethanol addition would be an increased production of the single CO addition product – propanol. Figure 6.1 shows that the production of 1-propanol indeed increases, when ethanol is added to the feed. However figure 6.1 also shows that the production of 1-butanol is even more strongly enhanced by the ethanol addition than the production of 1-propanol. The observed results could suggest that another route to chain growth for this catalyst is the coupling of alcohols, as there in this specific case seems to be a coupling of ethanol or ethanol-derived species into 1-butanol.

The observed results raise the question of the mechanism through which the coupling progresses. Such alcohol couplings have not previously been reported for molybdenum based alcohol synthesis catalysts. However in alcohol synthesis over Alkali/Cu based systems it has been observed that higher alcohols, especially alcohols with more than one C-C bond, are formed from alcohol coupling reactions – particularly couplings involving methanol [70, 424]. In the case of Alkali/Cu catalysts the coupling is believed to occur via a mechanism resembling an aldol condensation of the aldehydes corresponding to the

involved alcohols [70, 424]. Previously it has been observed [183] that addition of acetaldehyde to the syngas passed over a K/Co/MoS$_2$ catalyst generally enhances the production of higher alcohols, but causes the largest relative increase in the production of butanol (see perhaps section 2.6). Acetaldehyde is an intermediate in the aldol condensation route from ethanol to 1-butanol, so this result might indicate that the coupling reaction over Alkali/Co/MoS$_2$ also occurs through an aldol condensation pathway. The coupling pathway via a classical aldol condensation is illustrated in figure 6.2.
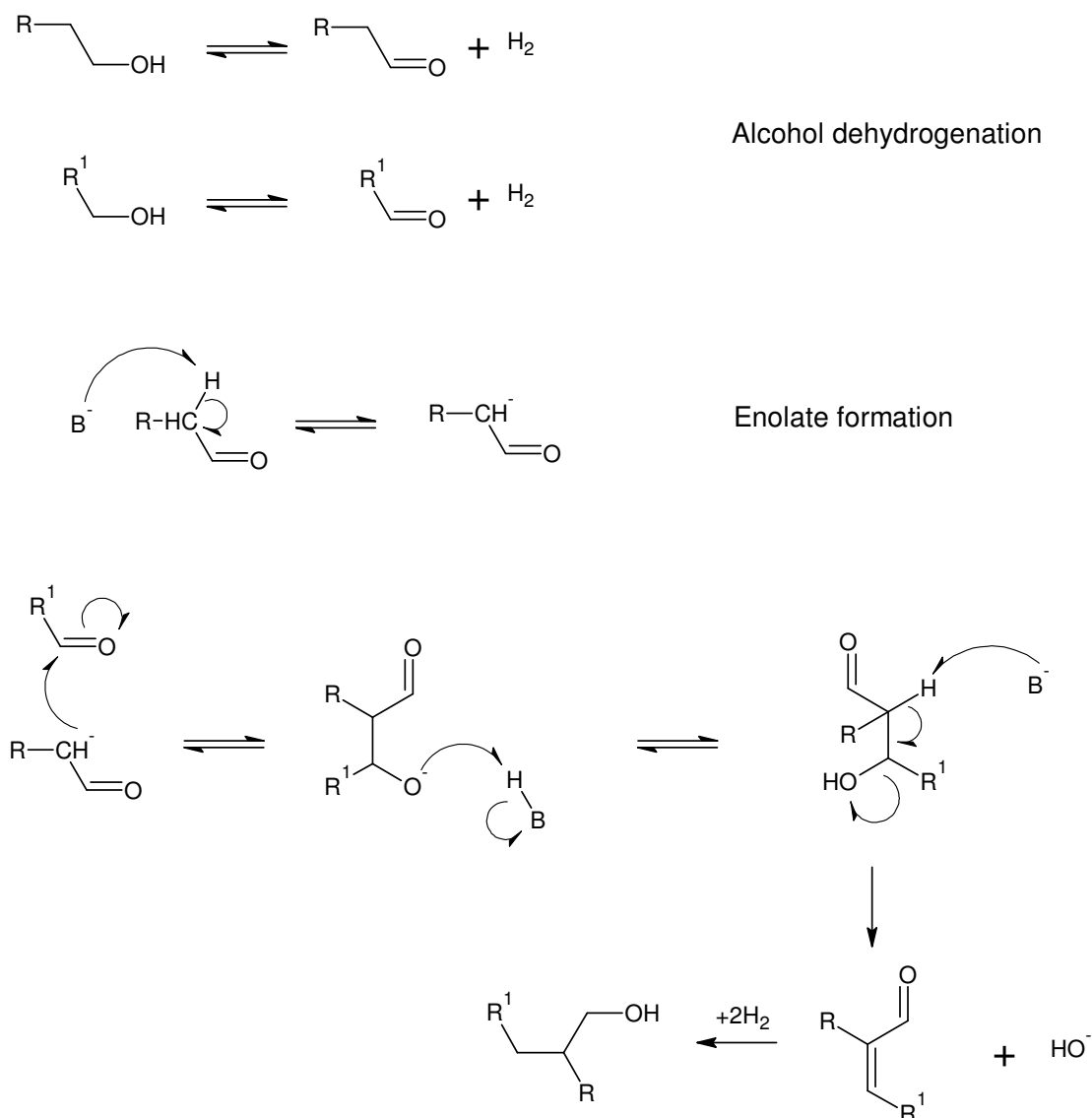
Figure 6.2 Alcohol coupling via a base catalyzed aldol condensation between the aldehydes corresponding to the involved alcohols. Here B⁻ would denote a basic functionality of the catalyst. In the specific case of ethanol coupling we have $R^1 = CH_3$, R = H.

An aldol condensation occurs through a β-hydroxy aldehyde (a so-called aldol). In a classical aldol condensation the oxygen atom in the carbonyl group of the β-hydroxy aldehyde is retained in the product (see figure 6.2). However in alcohol couplings over Alkali/Cu/ZnO catalysts Nunan et al. [70] observed another possible reaction pathway that occurs in parallel to the classical aldol condensation. In the alternative pathway it is instead the oxygen atom associated with the hydroxy group, which is retained in the product. Nunan et al. [70] described the alternative pathway as an "aldol condensation with oxygen retention reversal". In the case of ethanol condensation the classical pathway yields 1-butanol, while the "oxygen retention reversal" pathway yields 2-butanol. The distribution of the butanols can therefore provide some insight into the specific coupling pathway. In the present experiments 2-butanol is almost absent in the reaction product, and while there seems to be a slight increase in the 2-butanol production with increasing ethanol addition, the effect is not as dramatic, as it is the case for the production of 1-butanol. At the conditions of figure 6.1 without ethanol in the feed the 1-BuOH:2-BuOH ratio in the reaction product is 1:6.6 (2-BuOH production $4 \cdot 10^{-4}$ g (g cat.)$^{-1}$ h^{-1}), but with 5.23 mol% ethanol in the feed the marked rise in 1-butanol production means that the 1-BuOH:2-BuOH ratio has increased to 1:79.6 (2-BuOH production $1.2 \cdot 10^{-3}$ g (g cat.)$^{-1}$ h^{-1}). This observation indicates that the oxygen retention reversal pathway is of very limited importance in the case of ethanol coupling over $K_2CO_3/Co/MoS_2$, and the prevailing coupling mechanism will most likely resemble that of a classical aldol condensation (see figure 6.2). That the $K_2CO_3/Co/MoS_2$ catalyst shows such a significant preference for the formation of 1-butanol compared to 2-butanol in the coupling of ethanol constitutes a major departure from the behavior that Nunan et al. [70] report for Alkali/Cu/ZnO catalysts.

Figure 6.1 shows that iso-butanol and 1-butanol are formed in similar amounts, when no ethanol is added to the feed. Alcohol couplings via aldol condensations offer an explanation for the presence of branched alcohols like iso-butanol in the product. As an example the coupling between 1-propanol and methanol will, if it occurs through the pathway outlined in figure 6.2, result in iso-butanol. The production of methanol is hardly affected by the ethanol addition to the syngas feed, although a slightly decreased methanol production may be seen at higher ethanol concentrations. The slight decrease in methanol formation could be related to increased rates of other reactions, which consume CO and hydrogen that could otherwise have formed methanol. Additionally it cannot in light of the presented results be excluded that methanol is consumed in the coupling with ethanol to form 1-propanol.

While the co-feeding of ethanol along with syngas has the positive effect of boosting the production of higher alcohols, the ethanol addition also has the undesired effect of increasing the formation of higher hydrocarbons. Figure 6.3 shows the production rates of various hydrocarbons as functions of the ethanol fraction in the feed.
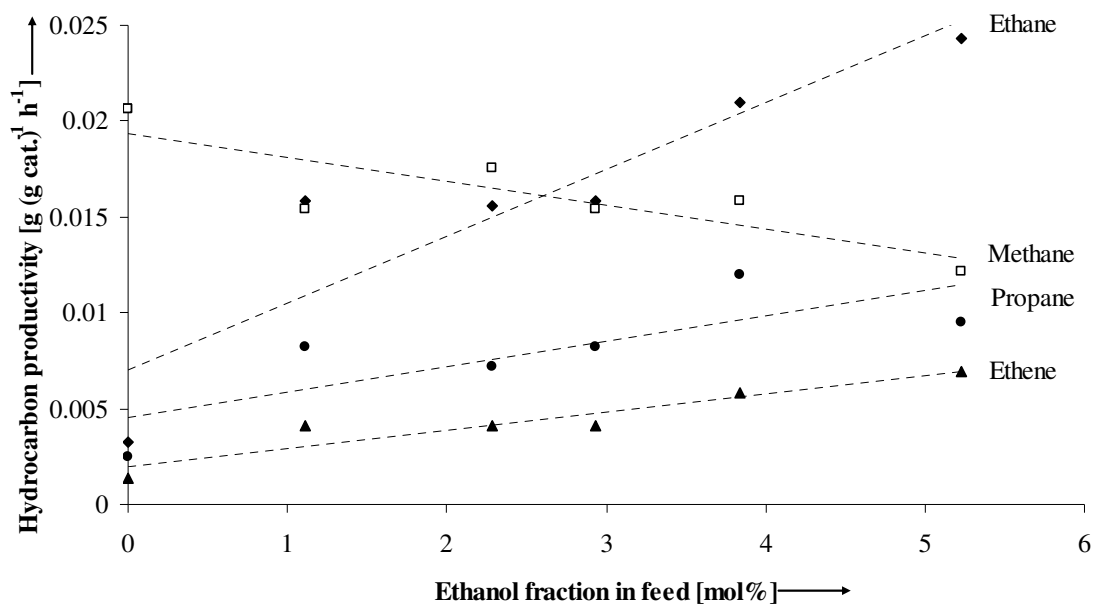
**Figure 6.3** The production rates of methane (open symbols) and higher hydrocarbons as functions of the ethanol fraction in the syngas feed. The experimental conditions are given in connection with figure 6.1.

Without ethanol in the syngas methane constitutes 75 wt% of the total production of the four hydrocarbons in figure 6.3, but the production of methane actually decreases, when ethanol is added to the feed. However the production of higher hydrocarbons, like ethane, ethene and propane, increases, when ethanol is added to the syngas. These higher hydrocarbons could all be formed from ethanol. Figure 6.4 shows the CO_2-free alcohol selectivity as well as the net conversion of CO and ethanol as functions of the ethanol fraction in the syngas.
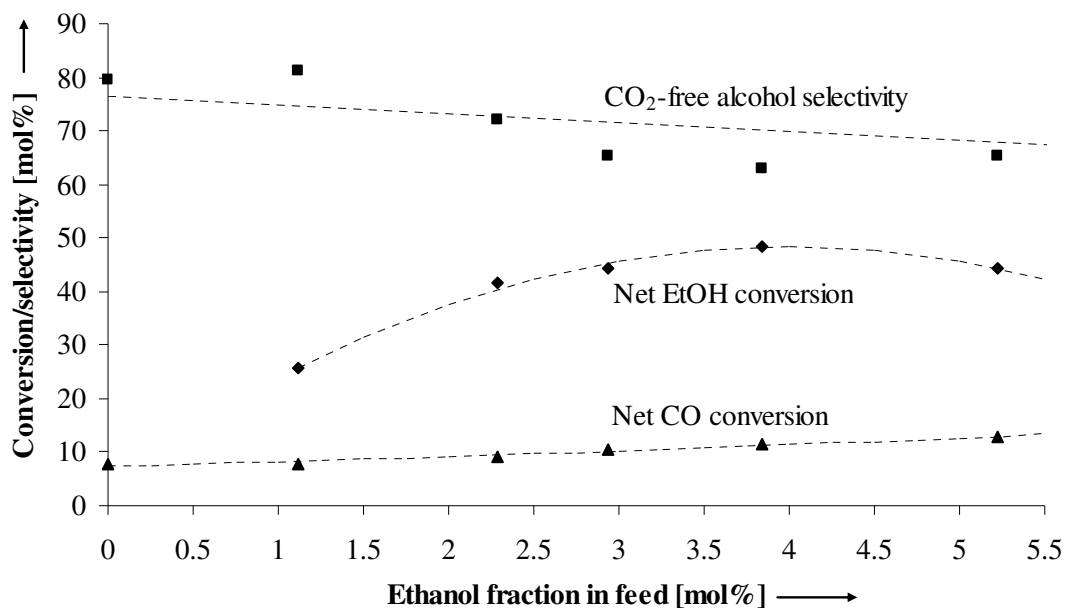
Figure 6.4 The CO_2-free alcohol selectivity (relative to the total amount of carbon fed to the reactor) and the net conversion of CO and ethanol as functions of the ethanol fraction in the feed. The experimental conditions are given in connection with figure 6.1.

Figure 6.4 shows that the CO_2-free alcohol selectivity relative to the total amount of carbon fed to the reactor (as ethanol and CO) decreases, when ethanol is added to the feed. This must be ascribed to the increasing production of higher hydrocarbons, but there may also be an increased production of uncharacterized oxygenates such as acetaldehyde. From these observations it is however difficult to determine, if ethanol is especially prone to hydrocarbon formation compared to CO. It can be seen in figure 6.4 that the net conversion of ethanol is markedly higher than the net conversion of CO. We have previously observed [244] that the alcohol selectivity decreases with increasing CO conversion, and this might also be the case in ethanol conversion. The loss in alcohol selectivity, when ethanol is added to the feed, might simply reflect a larger feed conversion rather than an inherently stronger disposition of ethanol to hydrocarbon formation.

That the increased formation of 1-butanol observed in figure 6.1 is due to the self-coupling of ethanol and not due to CO addition reactions is supported by the observation that ethanol conversion in a nitrogen atmosphere also yields 1-butanol as an important product. However in a nitrogen atmosphere ethyl acetate, formed in the dehydrogenation of ethanol (R36), becomes the dominant reaction product.

$$2CH_3CH_2OH \rightleftharpoons CH_3COOCH_2CH_3 + 2H_2 \qquad \text{(R36)}$$
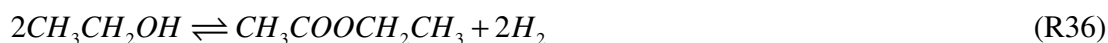
Figure 6.5 illustrates yields (on a carbon basis) of various products, when ethanol is converted in a nitrogen atmosphere at 250 °C. The yield, Y_i, of product i is defined in equation (6.1).

$$Y_i = \frac{n_i F_i^{Out}}{2F_{EtOH}^{In}} \qquad (6.1)$$

Here n_i is the number of carbon atoms in product i, F_i^{Out} is the molar flow rate of product i out of the reactor, and F_{EtOH}^{In} is the molar flow rate of ethanol into the reactor.
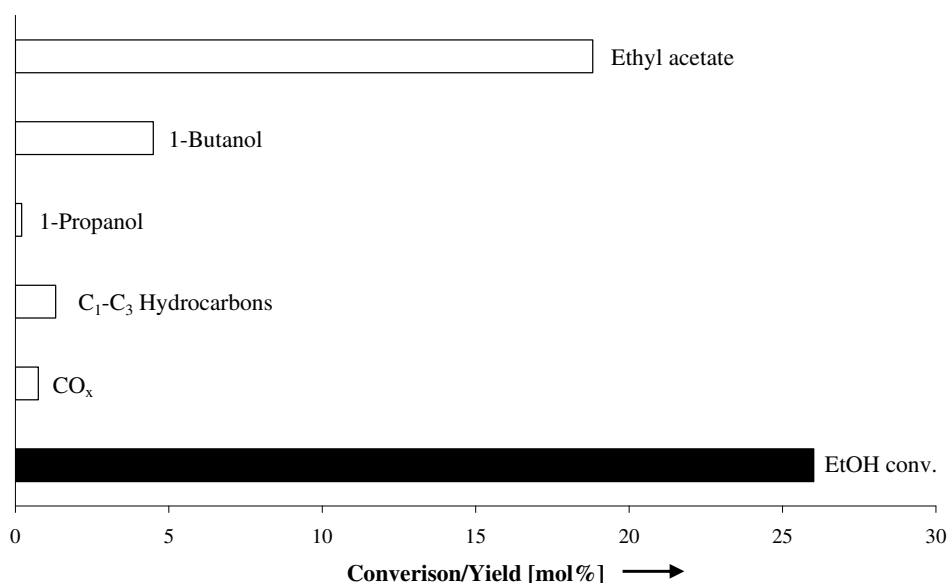
Figure 6.5 The ethanol conversion (dark bar) and the yields of various products from ethanol work-up in N_2. No 2-BuOH was detected in this experiment. Experimental conditions: $T = 250$ °C; $P = 100$ bar; GHSV = 2900 h^{-1}. Feed: 7.22 vol% EtOH; 92.78 vol% N_2; +35 h on stream.

Figure 6.5 illustrates that dehydrogenation to ethyl acetate is an important reaction, when ethanol is converted in a nitrogen atmosphere. This is different from the typical alcohol synthesis conditions, where the high hydrogen pressure serves to displace the dehydrogenation reaction towards ethanol. At the conditions of figure 1 without ethanol added to the syngas the CO_2-free selectivity towards ethyl acetate is 0.75 mol%.

In summary a newly observed route to chain growth for alkali promoted cobalt-molybdenum sulfide seems to be the coupling of alcohols. We have observed that addition of ethanol to the syngas fed to the reactor especially enhances the formation of 1-butanol. It seems quite likely that the mechanism for the coupling reaction over K_2CO_3/Co/MoS_2 resembles a classical aldol condensation. The aldol condensation pathway is known in the alcohol synthesis over Alkali/Cu catalysts, but while ethanol coupling over Alkali/Cu can result in both 2-butanol and 1-butanol, the coupling over the sulfide catalyst yields almost no 2-butanol. While ethanol addition boosts the production

of higher alcohols, the ethanol is also partly converted into higher hydrocarbons, and overall there is a slight decrease in alcohol selectivity, when ethanol is added to the feed.

Figure 6.1 shows that without ethanol added to the feed the production rates of branched iso-butanol and linear 1-butanol are very similar. As discussed in section 2.5 Bian et al. [14] have also observed that iso-butanol and n-butanol are formed in similar amounts over a K/MoS_2 catalyst without cobalt. The occurrence of alcohol coupling reactions progressing via aldol condensation pathways can explain the presence of branched alcohols like iso-butanol in the reaction product. A GC-MS analysis of the condensed liquid product obtained over the presently used $K_2CO_3/Co/MoS_2/C$ catalyst also reveals that the branched alcohols in the product essentially all are β-branched alcohols. Such β-branched alcohols are characteristic of the aldol condensation pathway illustrated in figure 6.2, if more than three carbon atoms are present in the final alcohol. The available evidence therefore suggests that the established reaction mechanism must be augmented with the aldol condensation type coupling reactions. Figure 6.6 illustrates a proposed, complete reaction mechanism for the sulfide catalyst that includes both CO addition reactions and alcohol coupling reactions.

Figure 6.6 Proposed, complete reaction mechanism for the formation of alcohols and hydrocarbons over MoS_2-based alcohol synthesis catalysts. In this proposal the established mechanism i.e. the CO addition reactions illustrated in figure 2.7 has been augmented with the presently observed alcohol coupling reactions that presumably occur via an aldol condensation pathway.
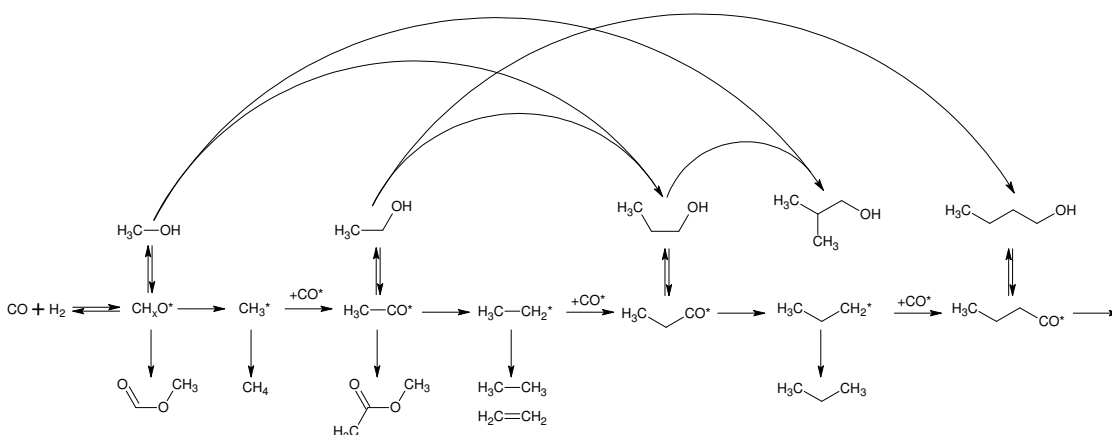
127

7 The role of the feed stream in the catalytic conversion of syngas to higher alcohols over alkali-promoted cobalt-molybdenum sulfide

Even the best of horses cannot carry two saddles
- Chinese proverb

Strive not to be a success, but rather to be valuable
- Albert Einstein

7.1 Abstract

In this work it is investigated, how the feed composition influences the catalytic conversion of syngas into higher alcohols over a $K_2CO_3/Co/MoS_2/C$ catalyst. This includes, what bearing the water content in the syngas has on the catalytic properties, and how NH_3, a potential impurity in syngas, affects the activity of the sulfide. Furthermore it is investigated, how the H_2/CO ratio in a sulfur free syngas influences the catalytic properties. The effect of the H_2/CO ratio has been evaluated at the conditions: $P = 100$ bar, $T = 326 \pm 1$ °C, GHSV = 2600 h^{-1}. In the sulfur free syngas it is observed that the production rate of C_2-C_4 alcohols is optimal with an equimolar mixture of CO and H_2, while the production rate of methanol increases with an increasing H_2/CO ratio. The increasing methanol production leads to a gradual increase in the overall alcohol selectivity with an increasing hydrogen content in the feed. The influence of the H_2O content in the feed has been evaluated at the conditions: $P = 100$ bar, $T = 326$ °C, GHSV = 2765-2795 h^{-1}, Feed (excl. H_2O): 49 vol% H_2, 51 vol% CO, 0 or 222 ppmv H_2S. Both with and without H_2S in the syngas it is observed that addition of water to the feed lowers the production rates of both hydrocarbons and higher alcohols. The presence of H_2O especially hampers the production of higher species, and this shifts the selectivity towards the C_1-products methanol and methane. The synthesis activity declines with H_2O added to the feed, but the CO conversion is actually increased by the co-fed water, since the H_2O in the feed undergoes an essentially complete shift into H_2/CO_2. Ammonia causes a general and largely reversible deactivation of the catalyst. Without H_2S in the syngas, at the conditions: $T = 326$ °C, $P = 100$ bar, GHSV = 5525 h^{-1}, 49 $\pm$ 1 vol% H_2, 51 $\pm$ 1 vol% CO, it is observed that addition of 741 ppmv NH_3 to the feed causes a 41 % reduction in the production rates of both alcohols and hydrocarbons (the total alcohol production rate drops from 0.194 g $g_{cat.}^{-1}$ h^{-1} to 0.116 g $g_{cat.}^{-1}$ h^{-1}). The original activity is largely restored, once NH_3 is removed from the feed. Similar effects of ammonia are seen with H_2S present in the syngas, but the loss of activity is less severe in a sulfur containing atmosphere. At the conditions: $T = 327$ °C, $P = 100$ bar, GHSV = 5350 h^{-1}, 49 $\pm$ 1 vol% H_2, 51 $\pm$ 1 vol% CO, 144 ppmv H_2S, it is observed that the total alcohol production rate decreases by 19 % (the total alcohol production rate drops from 0.135 g $g_{cat.}^{-1}$ h^{-1} to 0.110 g $g_{cat.}^{-1}$ h^{-1}), while the production rate of hydrocarbons decreases by 15 %, and the production rate of higher alcohols decreases by 23 %. Also in an S-containing atmosphere is the original behavior restored, once ammonia is removed from the feed.

Since the presence of NH_3 essentially causes the same relative drop in the production rates of both alcohols and hydrocarbons the selectivity is largely unaffected by the NH_3 poisoning.

7.2 The role of the H_2/CO ratio

The topic of this section is how the feed stream influences the properties of the sulfided alcohol synthesis catalyst. All the results in this chapter are obtained with the catalyst denoted KCoMo-3 in table 4.4 on page 85. Because of the negative effect of H_2S in the syngas i.e. the possible incorporation of sulfur species into the alcohol product (see section 5.5 on page 111) the focus in the current investigations is the use of an S-free syngas. In some cases the studies are however augmented with investigations carried out in the presence of H_2S. In these cases the H_2S content employed is higher than the 103 ppmv, which previously has been observed to stabilize the product distribution (see figure 5.3 on page 96). Presently it is investigated how the H_2/CO ratio in a sulfur free syngas feed influences the properties of the sulfide catalyst, it is investigated how H_2O/CO_2 in the feed influences the catalyst, and it is investigated how NH_3 in the syngas influences the catalytic properties.

The first part of the present investigations concerns the influence of the H_2/CO ratio in the feed, when the sulfide catalyst is operated in a sulfur free syngas. In section 5.2 it is described how the fraction of higher alcohols decreases over time during operation in an S-free syngas. The variations in the H_2/CO ratio are therefore not commenced, until the catalyst has been given an initiation period of 48 hours at the conditions provided in the legend of figure 7.1. Figure 7.1 shows the production rates of alcohols and hydrocarbons in a $H_2/CO = 0.96$ mol/mol feed during various stages of the experiment.
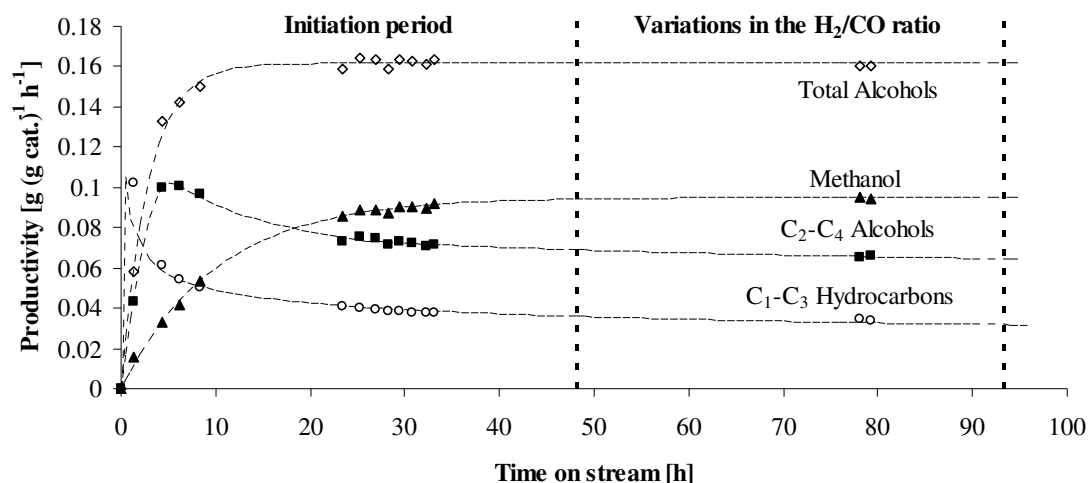
Figure 7.1 The production rates of various product classes as functions of the time on stream during the initiation and the variations in the H_2/CO ratio. The figure shows the productivities obtained at a molar H_2/CO ratio of 0.96 during both of these periods. The objective of the figure is to provide an indication of the degree of deactivation occurring during the variations in the H_2/CO ratio. The experimental conditions are: P = 100 bar; T = 326 °C; GHSV = 2600 h^{-1}, 49.0 vol% H_2, 51.0 vol% CO.

Figure 7.1 shows that the total alcohol production stabilizes, but this covers the fact that the methanol production gradually increases at the expense of the higher alcohols. The results in figure 7.1 also indicate that although the changes in the production rates of alcohols and hydrocarbons have slowed down considerably during the initiation period, there still seems to be a slight time dependency of the activity during the period with variations of the H_2/CO ratio (48-93 h on stream). If the data points in figure 7.1 are extrapolated by power law or exponential functions, those functions indicate that the total production rate of C_2-C_4 alcohols may vary by up to 3 % from the average value during the period of 48-93 h on stream. The total production rate of C_1-C_3 hydrocarbons may on the other hand vary by up to 6 % compared to the average value during the period of 48-93 h on stream. The time dependency of the activity may thus for some components introduce a minor uncertainty (3-6 %) in the evaluation of the effect of the feed composition Contrary to the case for higher alcohols and hydrocarbons there are no indications of discernible variations in the methanol production rate during the variations in the H_2/CO ratio.

Figure 7.2 shows the space time yields of methanol, higher alcohols and C_1-C_3 hydrocarbons as functions of the H_2/CO ratio in the syngas feed.
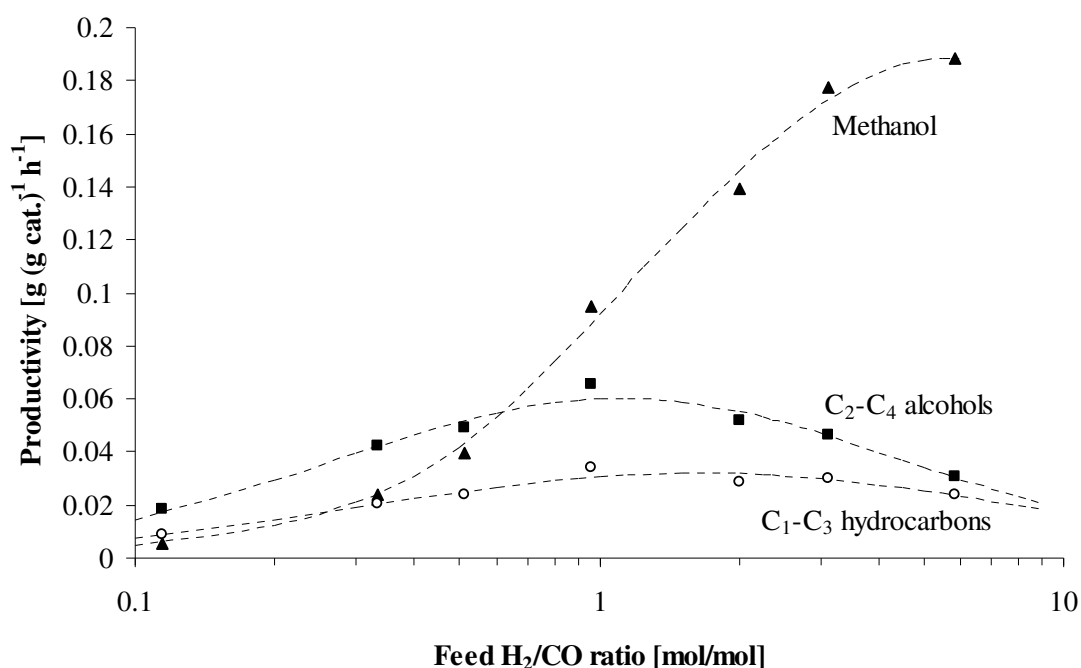
Figure 7.2 The production rates of methanol, higher alcohols and hydrocarbons as functions of the H_2/CO ratio in the syngas feed. The experimental conditions are: P = 100 bar; T = 326 ± 1 °C; GHSV = 2600 ± 25 h^{-1}, +48 h on stream.

Figure 7.2 illustrates that the methanol production increases with an increasing hydrogen content in the feed, while the production of higher alcohol is optimal with an equimolar mixture of CO and H_2. An equimolar mixture of CO and H_2 also constitutes the

stoichiometric feed for the synthesis of ethanol, the dominant higher alcohol, if it is assumed that all water co-produced in the ethanol synthesis is shifted into CO_2 in the water-gas shift reaction (R12 + R13). The production of hydrocarbons generally follows the production of higher alcohols, but at higher H_2/CO ratios the production of hydrocarbons is clearly approaching the production of higher alcohols. It is interesting to observe how the production rates of hydrocarbons and higher alcohols follow the same general tendency, while the production of methanol exhibits a completely different response to variations in the H_2/CO ratio. It is also interesting to observe that the dominant effect of an increased feed hydrogen content is an increased hydrogenation of CO to form methanol. It thus appears that the catalyst favors C-O bond retention. It might have been expected that an increased hydrogen content in the syngas feed especially would favor the hydrocarbon production, but at the presently employed conditions this is not the case.

The present observations agree quite well with previously reported results from the literature. Park et al. [425] studied a K_2CO_3/MoS_2 catalyst, and they also observed that the methanol production increased with an increasing feed hydrogen content, while the production of higher alcohols peaked around a molar H_2/CO ratio of 1. In a related investigation Youchang et al. [159] also observed that an increase in the partial pressure of H_2 at a fixed partial pressure of CO primarily enhanced the methanol selectivity. Furthermore it is in the patent literature [104, 129, 183] typically recommended that the sulfide catalyst is operated with a molar H_2/CO ratio of around 1 in the feed. In an H_2S containing syngas we [244] have previously determined experimental rate equations for the production of various alcohols and hydrocarbons from syngas, and based upon these rate equations one would expect that an increased H_2/CO ratio especially would benefit the production of methane (see table 5.1 and table 5.2). For an H_2S containing feed Zhang et al. [426] also observed that an increasing H_2/CO ratio boosted the methane selectivity. It is possible that it is the presence of H_2S, which modifies the catalytic properties in such a way that hydrogenation without retention of a C-O bond becomes a more favorable pathway.

Previous investigations suggest that chain-growth for the sulfide catalyst occurs by addition of CO to an alkyl group to form an acyl species that can be hydrogenated into the corresponding alcohol [75, 187]. Alternatively chain-growth can take place by alcohol coupling reactions, which presumably occur via an aldol condensation pathway [215]. For the higher alcohols it is most likely that it is the shared need for CO addition and hydrogenation reactions that creates an optimum in the production of higher alcohols around an H_2/CO molar ratio of 1. It is also quite likely that an increased chance of hydrogenation of the alkyl intermediates into hydrocarbons is the reason, why the production rate of hydrocarbons approaches the production rate of higher alcohols at higher H_2/CO ratios. Methanol may couple with ethanol or higher alcohols via an aldol condensation pathway, but it is quite likely that aldol condensation type couplings, which would involve aldehyde intermediates, become increasingly disfavored by an increase in the partial pressure of H_2, which serves to displace the alcohol/aldehyde equilibria towards the alcohols.

That the methanol production increases so significantly with an increasing H_2/CO ratio has the implication that the overall alcohol selectivity also increases with an increasing H_2/CO ratio in the syngas feed. This is illustrated in figure 7.3, which shows

131

the CO conversion, the CO_2-free alcohol selectivity, and the CO_2 selectivity as functions of the H_2/CO ratio in the feed.
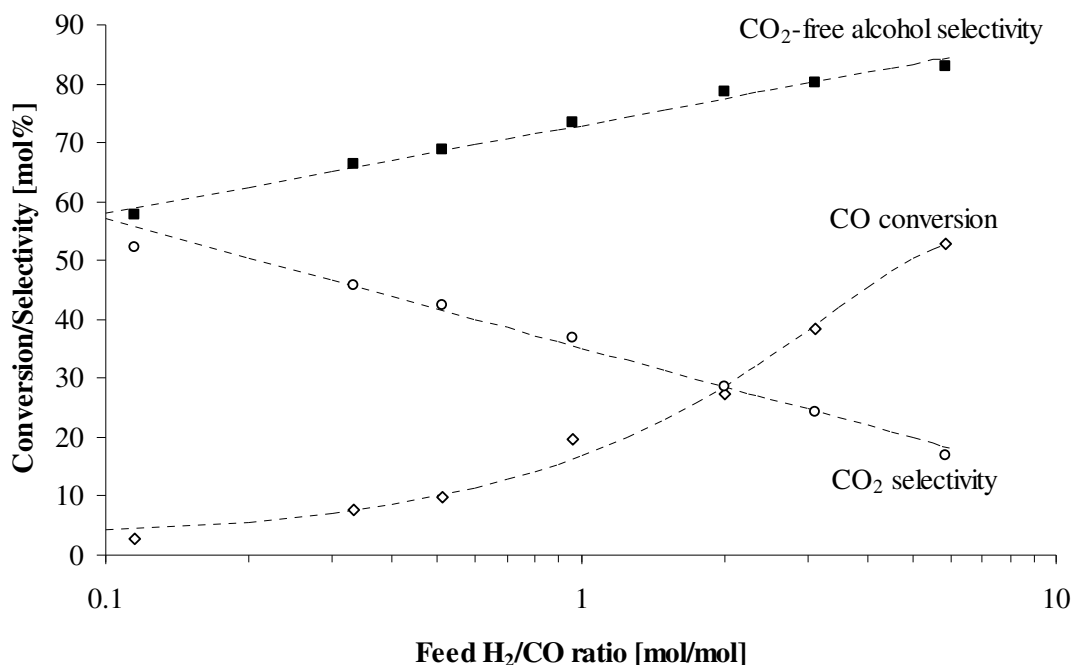
Figure 7.3 The CO conversion, the CO_2 selectivity and the CO_2-free alcohol selectivity as functions of the H_2/CO ratio in the feed. The experimental conditions are given in the legend of figure 7.2.

From figure 7.3 it can be seen that the CO conversion increases markedly, when the H_2/CO ratio is increased. This is related to the strong increase in the methanol production rate, but it should also be kept in mind that the feed becomes increasingly CO deficient at the higher H_2/CO ratios. Figure 7.3 also shows that the CO_2 selectivity decreases with increasing hydrogen content in the feed. This is due to the fact that the water gas shift reaction (R13) is displaced towards the left with increasing hydrogen content in the gas, and due to the fact that the dominant reaction in a hydrogen rich syngas becomes the direct hydrogenation of CO into methanol (R11), which does not result in a co-production of H_2O/CO_2.

The effect of the feed composition upon the CO conversion and the product selectivitites is also consistent with previous investigations. The results of Park et al. [425] with a K_2CO_3/MoS_2 catalyst also indicated a declining CO_2 selectivity and a weakly increasing alcohol selectivity with an increasing H_2/CO ratio, but Park et al. [425] did not observe as strong an increase in the CO conversion with increasing H_2/CO ratio, as it is seen in the present experiments.

Table 2.1 illustrates the CO_2-free product selectivities for selected H_2/CO ratios. The results clearly show how methanol is the product that benefits from an increasing hydrogen content in the feed.

Table 7.1 CO_2-free product selectivities for H_2/CO ratios in the feed. The experimental conditions are given in the legend of figure 7.2.

H_2/CO [mol/mol]	CO_2-free CO conv. [mol%] [a]	CO_2-free, carbon based selectivity [mol%] [b]								
		CH_4	C_2H_4	C_2H_6	C_3H_8	MeOH	EtOH	1-PrOH	1-BuOH	iso-BuOH
0.11	1.7	14.3	3.5	9.0	6.1	9.7	26.3	14.0	5.6	5.0
0.96	13.2	19.5	1.1	3.1	2.4	35.6	17.6	12.5	2.1	5.7
5.83	44.8	15.2	0.2	1.1	0.8	66.4	7.6	5.9	0.4	2.4

[a] The CO conversion into products other than CO_2. The total CO conversion can be seen in figure 7.3.
[b] For the lowest H_2/CO ratio it is an element of uncertainty that the GC spectra show signs of uncharacterized products – presumably compounds like higher alcohols/hydrocarbons, aldehydes and esters.

An evaluation of the equilibrium for the overall methanol synthesis reaction (R11) suggests that the beginning stagnation, which is seen in the methanol production at the highest H_2/CO ratios in figure 7.2, is due to the fact that the methanol synthesis here draws near to its equilibrium boundary. With thermodynamic data from Barin [65] one obtains a value of $K_{f,599.15K} = 1.19 \cdot 10^{-4} bar^{-2}$ for the equilibrium constant at the reaction temperature of 326 °C. Figure 7.4 shows the quantity $\frac{f_{MeOH}}{K_f f_{H_2}^2 f_{CO}}$ at the reactor exit depicted as a function of the H_2/CO ratio in the feed. As described in chapter 3, the quantity $\frac{f_{MeOH}}{K_f f_{H_2}^2 f_{CO}}$ is a measure of the degree of equilibration for the methanol synthesis reaction.

Figure 7.4 The quantity $\frac{f_{MeOH}}{K_f f_{H_2}^2 f_{CO}}$ at the reactor exit depicted as a function of the H_2/CO ratio in the feed. The experimental conditions are given in the legend of figure 7.2.

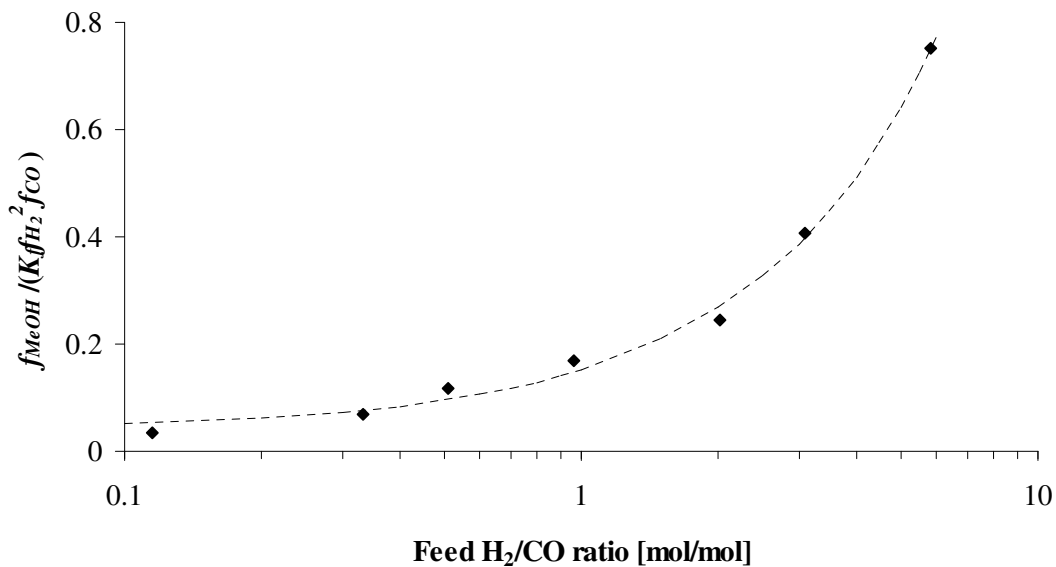The results in figure 7.4 illustrate that the methanol synthesis at higher H_2/CO ratios comes quite near to the equilibrium boundary ($\frac{f_{MeOH}}{K_f f_{H_2}^2 f_{CO}} = 1$).There is a significant scattering in the literature [359, 361, 427-430] concerning the exact location of the methanol synthesis equilibrium, and it is possible to find equilibrium constants both above and below the value used in the present case. There is thus some uncertainty regarding the exact degree of equilibration for the methanol synthesis, but in light of the results in figure 7.4 it does seem most likely that the beginning stagnation of the methanol synthesis rate at the highest H_2/CO ratios in figure 7.2 can be ascribed to the growing importance of the reverse reaction of R11 i.e. the methanol decomposition. As described in chapter 3 the fugacity coefficients have been determined by means of the SRK equation of state. Generally the compressibility factor and all the individual fugacity coefficients are within 5 % of unity in all the experiments seen in figure 7.4. The deviations from ideality are thus not large, but the accumulated deviation in products of fugacities can have a more significant impact on the equilibrium. For the experiments presented in figure 7.4 one quite consistently has $K_\varphi = 0.890 \pm 0.006$ (see perhaps eq. 3.17), and the deviations from ideality thus have a significant impact upon the location of the methanol synthesis equilibrium.

The equilibrium for the synthesis of the higher alcohols should generally be more favorable than the methanol synthesis equilibrium [36, 431, 432], and the synthesis of higher alcohols is therefore less likely to be equilibrium controlled. An evaluation of the equilibrium for the synthesis of higher alcohols would necessitate an evaluation of the water-gas shift equilibrium. Such an evaluation has not been attempted, since the water content in the product stream has not been determined in the present investigations.

7.3   The role of H_2O/CO_2 in the syngas

As it is illustrated in table 2.5 on page 26 the raw syngas from the gasifier may contain significant amounts of water and CO_2. It is therefore also important to clarify how these components may influence the properties of the sulfide catalyst and the synthesis process. Water and CO_2 are as noted in section 2.3.6 on page 41 largely parallel products in the synthesis reactor, because the water gas shift reaction (R13) proceeds rapidly over the alcohol synthesis catalyst. Gang et al. [15] used a $K/Co/MoS_2/C$ catalyst and observed that the water gas shift reaction generally is very close to equilibrium at typical alcohol synthesis conditions. Since the water-gas shift reaction appears to be relatively rapid compared to the synthesis reactions it is thus also difficult to distinguish between the effects of H_2O and CO_2.

In these investigations water is co-fed along with the syngas sent to the reactor. Because the increased water content in the syngas feed could result in some degree of oxidation of the sulfide, and because such an oxidation could depend upon the sulfur level in the syngas, the investigations are conducted both with and without 222 ppmv H_2S in the syngas. These investigations are performed with an approximately equimolar mixture of CO and H_2, since such a mixture as discussed in section 7.2 provides the optimal production of higher alcohols.

Figure 7.5 shows the production rates of alcohols and hydrocarbons as functions of the time on stream in a sulfur free syngas with a progressively increasing addition of water to the syngas feed ($H_2/CO = 0.96$ mol/mol).
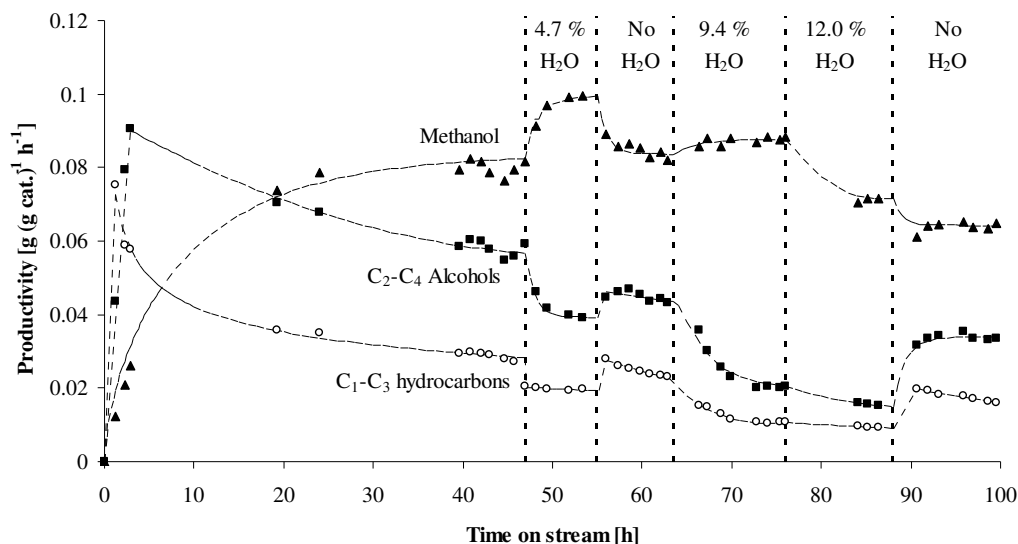
Figure 7.5 The production rates of methanol, C_2-C_4 alcohols and C_1-C_3 hydrocarbons as functions of the time on stream with progressively increasing addition of H_2O to the syngas feed. The water content in the syngas feed in mol% is noted for each segment of the experiment. The experimental conditions are: P = 100 bar, T = 326 °C, GHSV = 2765 ± 80 h^{-1}. Excl. H_2O the feed contains 48.9 vol%H_2, 51.1 vol% CO, No H_2S.

Figure 7.5 illustrates that the addition of water to the syngas feed causes a decline in the production of hydrocarbons and especially in the production of the higher alcohols. Figure 7.5 also illustrates that the methanol production benefits from a modest water content in the feed (4.7-9.4 mol%). This may be related to a reduced consumption of methanol as a precursor for the production of higher alcohols. Another factor that may contribute to the increased methanol production is that the shift of the H_2O co-fed with the syngas raises the hydrogen content in the gas from the original ratio of $H_2/CO = 0.96$ mol/mol. From section 7.2 it is known that the methanol production in the region of an equimolar H_2/CO mixture benefits strongly from an increased hydrogen content in the syngas. From figure 7.2 it can be seen that the production of higher alcohols has a relatively broad optimum in the region of a molar H_2/CO ratio around 1, but the increasing H_2/CO ratio should also provide a minor contribution to the decline in the production of higher alcohols.

Additionally the available evidence for Cu-based methanol synthesis catalysts suggests that CO_2 is the dominant source of carbon in methanol formed over such catalysts [433-436]. A minor addition of H_2O to H_2/CO also enhances the methanol production over Cu/ZnO, in the same way as it in figure 7.5 is seen for the sulfide catalyst [31]. If the sulfide catalyst also has a favorable reaction pathway from CO_2 to methanol, then the increased CO_2 level arising from the shift of co-fed water could boost the methanol production.

135

It might look, as if the catalyst at the highest water level (12.0 mol%) undergoes an irreversible change. In the final period with a water free feed in figure 7.5 the production rates of both methanol and C_2-C_4 alcohols have decreased by 24 % compared to the activity before exposure to the higher water contents (9.4 -12.0 mol%). With the declining production of hydrocarbons and higher alcohols and the increasing production of methanol the overall alcohol selectivity actually increases with the addition of water to the syngas feed. This is illustrated in figure 7.6, which shows the CO_2-free alcohol selectivity, the CO_2 selectivity, and the CO conversion during the experiment presented in figure 7.5.

Figure 7.6 The CO_2-free alcohol selectivity, the CO_2 selectivity and the CO conversion as functions of the time on stream with progressively increasing addition of H_2O to the S-free syngas feed. The water content in the syngas feed in mol% is noted for each segment of the experiment. The experimental conditions are given in the legend of figure 7.5.

With thermodynamic data from Barin [65] the equilibrium constant for the water-gas shift reaction at 326 °C is K_{WGS} = 27.9. At equilibrium the dominant part of the added water will therefore be shifted into CO_2. Figure 7.6 illustrates that the CO conversion, despite the decreasing production of the synthesis products, increases significantly, when water is added to the feed. The increase in the CO conversion corresponds relatively well to an essentially complete shift of the added water. From figure 7.6 it can also be seen how the contribution from the shift reaction causes a marked increase in the CO_2 selectivity. Even with the lowest feed water level (4.7 mol%) the CO_2 selectivity has increased to 57 mol%, and with 12.0 mol% water in the syngas feed the CO_2 selectivity has increased to 84 mol%.

Table 7.2 summarizes the individual product selectivites and the CO conversion into products other than CO_2 for various H_2O levels in the feed. The results in table 7.2 emphasize that especially the production of higher species is hampered by water.

Table 7.2 The CO_2-free product selectivities for various water levels in the H_2S-free feed. The experimental conditions are given in the legend of figure 7.5.

H_2O in feed [vol%] [a]	CO_2-free CO conv. [mol%] [b]	CO_2-free, carbon based selectivity [mol%]								
		CH_4	C_2H_4	C_2H_6	C_3H_8	MeOH	EtOH	1-PrOH	1-BuOH	iso-BuOH
0	10.3	20.0	1.1	3.0	2.2	34.7	19.3	11.5	2.6	5.0
4.7	7.8	16.9	0.7	1.3	1.1	50.1	15.6	8.8	1.2	4.1
9.4	5.9	13.3	0.6	0.7	0.7	62.8	12.6	6.0	0.7	2.4
12.0	4.9	13.5	1.2	0.9	0.9	63.2	12.0	5.6	0.8	1.9

[a] H_2O fraction in the feed. The value for H_2O-free syngas corresponds to the value after 40-47 h on stream.
[b] The CO conversion into products other than CO_2. The total CO conversion can be seen in figure 7.6.

With 222 ppmv H_2S in the syngas the qualitative effects of the water addition are largely similar to the effects in an H_2S-free syngas. As the presence of H_2S boosts the production rates of hydrocarbons and higher alcohols and lowers the production rate of methanol, the starting point is however quite different in the H_2S containing syngas. Figure 7.7 illustrates the production rates of alcohols and hydrocarbons as functions of the time on stream with a progressively increasing addition of water to the syngas feed ($H_2/CO = 0.96$ mol/mol).
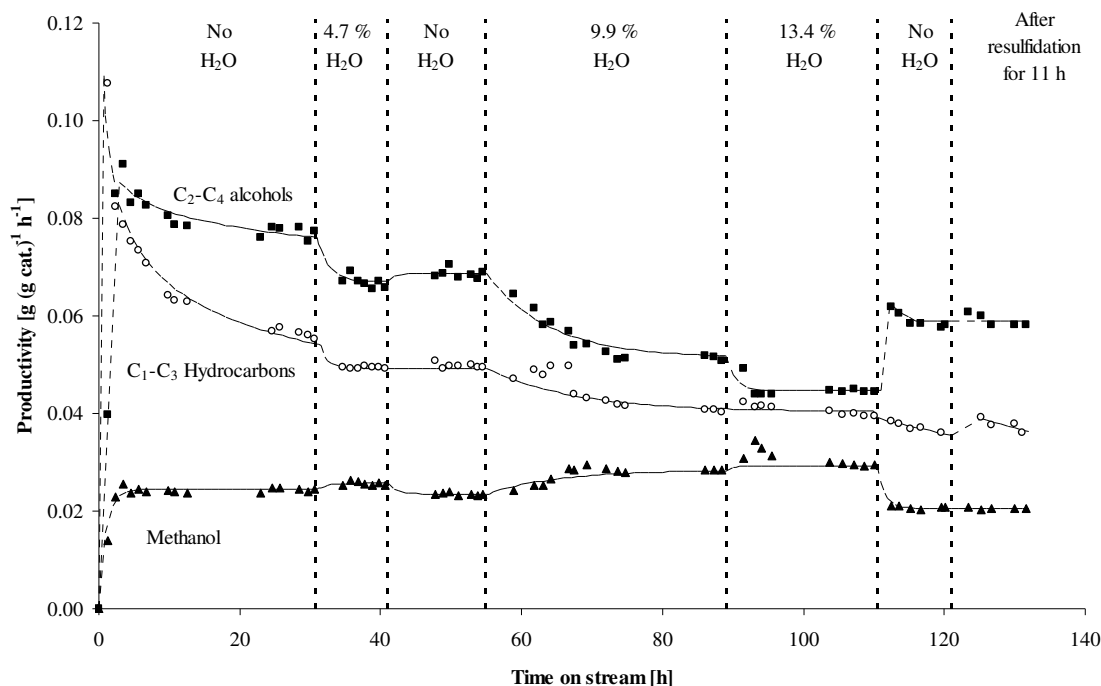
Figure 7.7 The production rates of methanol, C_2-C_4 alcohols and C_1-C_3 hydrocarbons as functions of the time on stream with progressively increasing addition of H_2O to the H_2S containing syngas feed. The water content in the syngas feed in mol% is noted for each segment of the experiment. The experimental conditions are: P = 100 bar, T = 326 °C, GHSV = 2795 ± 90 h^{-1}. Excl. H_2O the feed contains 49.1 vol%H_2, 50.9 vol% CO, 222 ppmv H_2S. Before the last stage of the experiment the catalyst is resulfided for 11 h at 325 °C and atmospheric pressure in an 80 NmL/min flow of 2 mol% H_2S in H_2.

Figure 7.7 again illustrates how the how the production rates of hydrocarbons and higher alcohols are progressively lowered by the increasing co-feeding of water. The exposure to 4.7 mol% H_2O appears to cause a permanent loss of activity for the production of hydrocarbons and higher alcohols. The exposure of the catalyst to 9.9 mol% and 13.4 mol% of H_2O lowers the production of hydrocarbons/higher alcohols further, but the removal of water from the feed restores part of the activity. With 222 ppmv of H_2S in the syngas the methanol production rate benefits from the co-feeding of H_2O in the entire 0-13.4 mol% range. This is contrary to the situation with an S-free syngas, where exposure to 12.0 mol% H_2O causes a permanent loss of methanol synthesis activity. This difference may be related to the fact that the methanol production rate is significantly lower in the H_2S containing syngas. Figure 7.7 also shows that 11 h of resulfidation at 325 °C and atmospheric pressure does not alter the properties of the catalyst, which has been exposed to syngas containing 0-13.4 mol% H_2O. The fact that a resulfidation is without influence on the catalytic properties is an argument against a partial oxidation of the sulfide as the reason for the loss of activity. If a partial oxidation of the catalyst occurs it certainly leaves the catalyst in a state that is not resulfided with the normal sulfiding procedure. With 222 ppmv H_2S in the syngas, where higher alcohols and hydrocarbons are the dominant products, the co-feeding of water along with the syngas is virtually without an effect upon the alcohol selectivity. This is illustrated in figure 7.8, which shows the CO_2-free alcohol selectivity, the CO_2 selectivity, and the CO conversion during the experiment with H_2O co-feeding in an H_2S containing atmosphere.
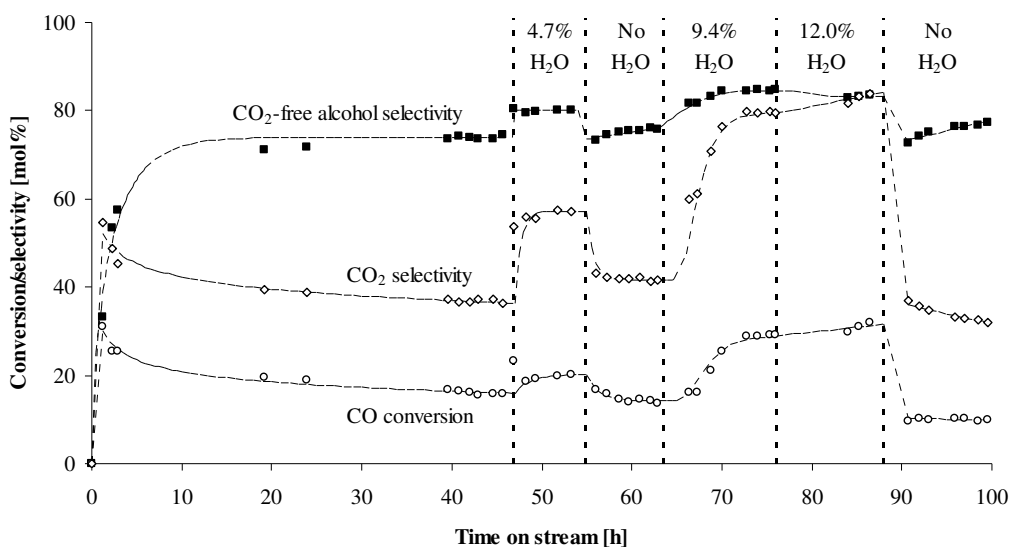

Figure 7.8 The CO_2-free alcohol selectivity, the CO_2 selectivity and the CO conversion as functions of the time on stream with progressively increasin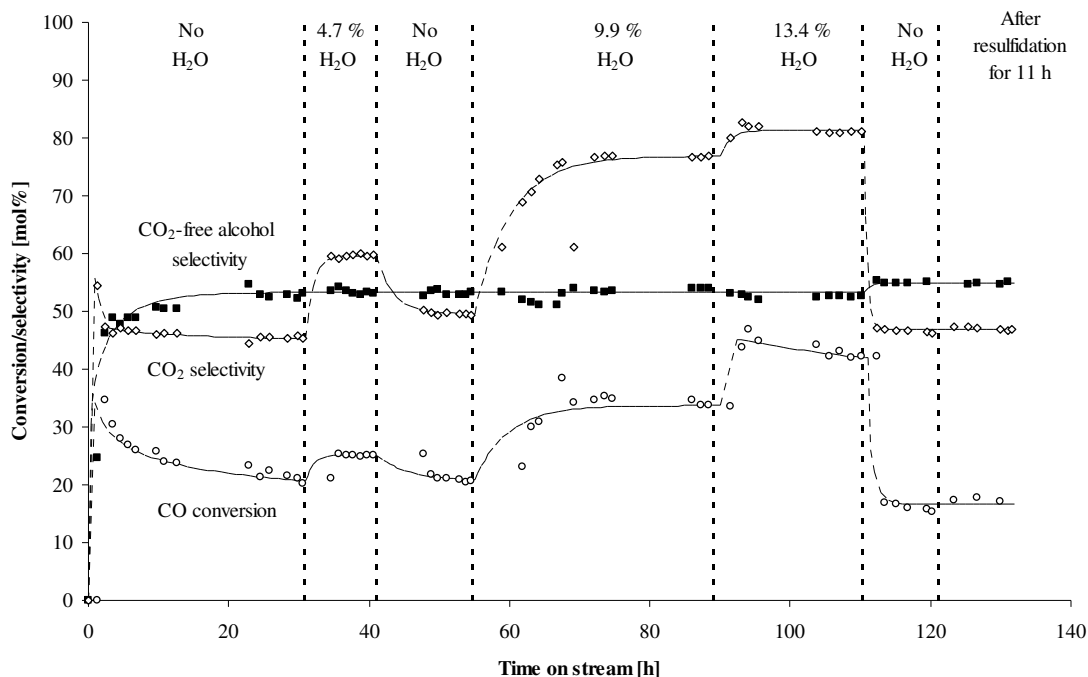g addition of H_2O to the H_2S containing syngas feed. The water content in the syngas feed in mol% is noted for each segment of the experiment. The experimental conditions are given in the legend of figure 7.7.

Figure 7.8 illustrates how the alcohol selectivity is unaltered through the H_2O co-feeding experiment, although the selectivity increases slightly, when water is finally removed from the feed stream. Furthermore figure 7.8 shows that the CO conversion also in an H_2S containing syngas increases, when H_2O is added to the feed. The increase in the CO conversion corresponds reasonably well to an essentially full shift of the co-fed water, and figure 7.8 also shows how the CO_2 selectivity increases substantially, when water is added to the syngas feed. For the part of the experiment with 13.4 vol% H_2O in the feed the increase in the CO conversion is actually observed to be slightly higher, than it would be expected – even for a full shift of the co-fed water. This must be ascribed to experimental uncertainty, which is difficult to avoid, when such a high fraction of a normally liquid component is co-fed along with the gaseous feed.

Table 7.3 summarizes the individual product selectivites and the conversion into products other than CO_2 for various H_2O levels in the feed. The results in table 7.3 also illustrate how water lowers the synthesis activity and shifts the product towards the C_1-species methane and methanol.

Table 7.3 The CO_2-free product selectivities for various water levels with 222 ppmv H_2S in the feed. The experimental conditions are given in the legend of figure 7.7.

H_2O in feed [vol%] [a]	CO_2-free CO conv. [mol%] [b]	CO_2-free, carbon based selectivity [mol%]								
		CH_4	C_2H_4	C_2H_6	C_3H_8	MeOH	EtOH	1-PrOH	1-BuOH	iso-BuOH
0	12.5	28.3	1.1	9.3	4.4	9.3	25.2	12.0	3.2	3.5
4.7	9.2	29.6	1.0	8.6	4.2	11.0	25.5	10.6	3.0	3.1
9.9	8.3	31.0	0.9	7.1	4.0	14.8	24.8	9.3	2.3	2.7
13.4	7.8	33.3	0.8	6.9	3.8	16.4	23.9	8.6	2.2	1.6

[a] H_2O fraction in the feed. The value for H_2O-free syngas corresponds to the value after 23-31 h on stream.
[b] The CO conversion into products other than CO_2. The total CO conversion can be seen in figure 7.8.

Due to the parallel nature of water and CO_2 in the synthesis reactor it is highly relevant to compare the effects of water in the feed to the effect of CO_2 in the feed. The presence of CO_2 in the syngas feed is generally reported as having a detrimental effect upon the alcohol synthesis over MoS_2 based catalysts. In the patent literature [18, 103] it is recommended that the partial pressure of carbon dioxide is kept below 1 bar at the reactor entry. Herman [31] have reported results from experiments made by the British Coal Research Establishment [248], where the CO_2 level in the syngas passed over a $K_2CO_3/MoS_2/C$ catalyst has been varied. These results are summarized in table 7.4 and table 7.5 [31, 248], which shows the production rates and carbon based selectivities for various reaction products with different CO_2 levels in the syngas feed.

The results in table 7.4 and table 7.5 illustrate that there in terms of the alcohol/hydrocarbon synthesis are strong similarities between the reported effect of CO_2 and the presently observed effect of H_2O. The presence of CO_2 lowers the production rates for alcohols and hydrocarbons and especially the production of the higher species. This shifts the selectivity towards the C_1-products methane and methanol. This is the same effect that is observed with H_2O in the syngas feed.

Table 7.4 The effect of the feed CO_2 level on the production rates of various reaction products [31, 248]. The experimental conditions are: $K_2CO_3/MoS_2/C$ (5/19/76 wt%), T = 305 °C, 101 bar, $H_2/CO = 1$.

CO_2 fraction in feed [vol%]	CO conversion [mol%]	GHSV [h^{-1}]	Product STY $\left[\frac{g}{kg\ cat \cdot h} \right]$					
			MeOH	EtOH	1-PrOH	CH$_4$	C$_2$H$_6$	H$_2$O
0.0	24.5	2000	166.9	70.4	22.9	64.2	19.9	7.1
6.7	22.5	1600	145.7	40.6	10.4	58.8	7.1	12.8
15.0	18.9	1900	144.0	33.5	7.2	42.1	0.0	17.1
30.3	12.0	1800	81.5	25.1	5.9	25.1	4.3	21.8

Table 7.5 The effect of the feed CO_2 level on the selectivities of various products [31, 248]. The experimental conditions are given in the legend of table 7.4.

CO_2 fraction in feed [vol%]	CO_2-free CO conversion [mol%]	GHSV [h^{-1}]	CO_2-free, carbon based selectivity [mol%]				
			MeOH	EtOH	1-PrOH	CH$_4$	C$_2$H$_6$
0.0	12.2	2000	35.4	20.7	7.8	27.2	9.0
6.7	13.2	1600	41.4	16.1	4.7	33.4	4.3
15.0	10.1	1900	50.3	16.3	4.0	29.4	0.0
30.3	6.2	1800	44.0	18.9	5.1	27.1	4.9

Gang et al. [15] have also reported that the selectivity to higher alcohols is lowered, when CO_2 is added to the feed. The methanol production is only modestly affected by CO_2 levels in the 0-15 mol% range, but at a high feed CO_2 level of 30.3 mol% the production of methanol is significantly diminished. This behavior bears some qualitative resemblance to the behavior seen in figure 7.5, where the methanol production is enhanced at lower H_2O levels in the feed (0-9.4 mol%), but significantly diminished at a higher water level (12.0 mol%). Since CO_2 is the product favored by the water-gas shift equilibrium, the presence of CO_2 in the feed does not give rise to an increased CO conversion due to the shift reaction, as it is seen, when H_2O is added to the feed. When CO_2 is added to the feed there is thus only a lowering of the conversion due to the poisoning of the synthesis reactions.

Figure 7.5-figure 7.8 indicate that the deactivation of the synthesis reactions, which is caused by water, is partially irreversible. Unfortunately no spectroscopic or compositional analyses were obtained for the present catalysts exposed to elevated water concentrations. It is therefore not possible to establish, if changes in the structure and composition of the catalytically active phase are part of the reason for the reduced synthesis activity seen in the presence of elevated water levels. The partly irreversible nature of the deactivation does however indicate that such changes in the active phase do occur. One type of alteration in the active phase that might be envisioned is a partial oxidation of the sulfide. It has previously been discussed how the structure of MoS_2 is like a sandwich with a layer of Mo atoms between two sheets of sulphur atoms. MoS_2 can potentially be terminated by two low Miller-index planes, namely the the $Mo(10\bar{1}0)$ edge and the $S(\bar{1}010)$ edge [139, 140]. Badawi et al. [437] investigated the effect of water upon the structure of MoS_2 by means of density functional theory, and these authors [437] observed that especially the S-edge of the sulfide is susceptible to replacement of

sulfur with oxygen, if the H_2O/H_2S ratio is of sufficient magnitude. Furthermore the investigations of Karolewski and Cavell [169] on $Cs/MoS_2(0001)$ suggested that the alkali promoted sulfide could be more susceptible to oxidation by H_2O than the bare sulfide. Laurent and Delmon [438] studied the effect of water upon a $Ni/MoS_2/\gamma-Al_2O_3$ catalyst employed for hydrodeoxygenation reactions. These authors [438] observed no signs of oxidation of the MoS_2-phase, but they [438] did observe a partial oxidation of nickel. As one possible option Laurent and Delmon [438] suggested that the oxidation of Ni could be related to a formation of an inactive layer of nickel sulfate species that blocked the sulfide lowered the catalytic activity.

Without H_2S in the syngas it appears to be especially the highest employed water level (12.0 mol%) that causes a rather general permanent deactivation with only minor changes in selectivity and alcohol distribution. Judging from the relatively general effect it might be simple sintering, which lowers the activity. It possible that the elevated water levels could accelerate the sintering of the system. With 222 ppmv H_2S in the syngas the permanent deactivation caused by the elevated water levels is also rather general in its effect, and this could perhaps also point to a general sintering. In the presence of H_2S the deactivation of the higher alcohol production is slightly more significant, than the deactivation of the methanol synthesis. This could be related to an effect upon the cobalt chain-growth promoter, but since a resulfidation of the catalyst is without any significant effect the deactivation is not necessarily related to a partial oxidation.

While the permanent deactivation, which remains after H_2O has been removed from the feed, is a relatively general effect, the presence of elevated H_2O/CO_2 levels in the feed primarily causes a diminished production of the higher species. There are several factors that should be contributing to this negative influence of H_2O/CO_2 upon the chain-growth. It is described in section 3.1 how one of the available routes to chain-growth is the coupling of alcohols, which appears to occur via an aldol condensation pathway. It is well established [63, 439, 440] that base catalyzed aldol condensation reactions are poisoned by water or CO_2, and this poisoning effect could very well be a significant part of the explanation for the declining production of higher alcohols. For the other possible route to chain-growth, namely the CO addition reactions, the presence of cobalt appears to be very important. Calafat and Laine [216, 217] have observed that addition of Co to carbon supported MoS_2 greatly benefits the addition of CO to methanol to form C_2 oxygenates. If Co in the presence of increased water levels to any extent becomes partially oxidized, in the same way as H_2O may oxidize Ni added to MoS_2, then this oxidation could also mean an alteration of the activity for the CO addition reactions that contribute to the chain growth. Chen et al. [423] also studied the formation of ethanol by addition of CO to methanol on MoS_2 by means of density functional theory, and their investigations might suggest that the initial step is a C-O bond breakage in methanol through an elementary reaction of the type given in R37:

$$CH_3OH + H \rightleftharpoons CH_3 + H_2O \qquad\qquad\qquad \text{R37}$$

It is quite likely that the rate of such an elementary reaction would be adversely affected by an elevated presence of water on the catalyst surface. There are thus several kinetic and structural effects that could hamper the chain-growth in the presence of H_2O/CO_2.

141

Gang et al. [15] have previously also mentioned the adverse effect of elevated water levels upon the equilibrium for the synthesis of higher species (R12 and R14) as a possible reason for the declining production of higher alcohols with H_2O/CO_2 in the feed.

In light of the preceding discussion it seems fairly reasonable that the synthesis activity, and especially the production of higher species, is adversely effected by the presence of H_2O/CO_2 in the syngas feed.

When larger amounts of water are added to the syngas, it is also likely that the synthesis reactions in general are hampered by a significant consumption of CO in the water gas shift reaction, which removes available carbon monoxide from the surface of the catalyst. As illustrated by the CO_2 selectivity in figure 7.6 and figure 7.8 the water-gas shift reaction becomes very dominant at higher water levels.

7.4 The role of NH_3

As mentioned in section 2.1 ammonia is a potential impurity in syngas derived from gasification. Currently the impact that 730-745 ppmv NH_3 has upon the catalytic activity is evaluated. The typical ammonia level in syngas has been discussed in section 2.1, and on the basis of that discussion the presently employed NH_3 level should correspond to an intermediate level for wood gasification, while the investigated NH_3 level is slightly low compared to the concentration typically found in the syngas derived from coal gasification.

The $K_2CO_3/Co/MoS_2/C$ catalyst has been allowed to stabilize for 27.7 h in a sulfur free syngas, and ammonia is then added to the syngas to a content of 741 ppmv. Figure 7.9 illustrates the developments in the production rates of alcohols and hydrocarbons as functions of the time on stream for this experiment.
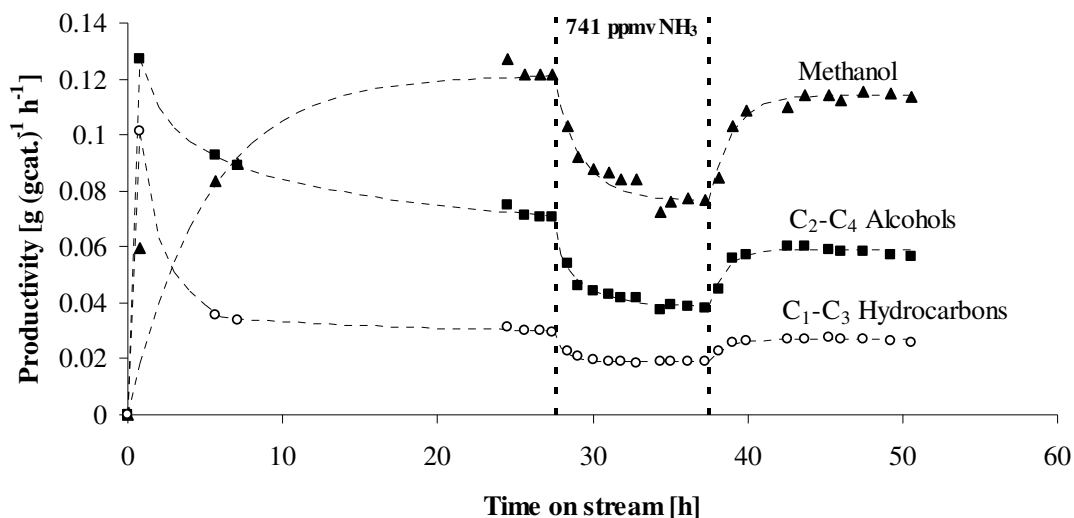
Figure 7.9 The production rates of methanol, C_2-C_4 alcohols and C_1-C_3 hydrocarbons as functions of the time on stream in an H_2S free syngas. After 27.7 h on stream 741 ppmv NH_3 is added to the syngas feed, and the NH_3 addition is maintained for 10 h. The experimental conditions are: T = 326 °C, P = 100 bar, GHSV = 5525 h^{-1}, Feed: 49 ± 1 vol% H_2, 51 ± 1 vol% CO.

Figure 7.9 illustrates that the addition of 741 ppmv of NH_3 to the feed severely poisons the catalyst. This NH_3 level causes a 41 % reduction in activity (the total alcohol production rate drops from 0.194 g $g_{cat.}^{-1}$ h^{-1} to 0.116 g $g_{cat.}^{-1}$ h^{-1}). The relative loss of activity is the same for both methanol and higher alcohols. Figure 7.9 also shows that the poisoning is largely reversible. Once the ammonia is removed from the feed, the catalyst regains a significant portion of its original activity. The original production rates for especially the higher alcohols are not completely restored, but judging from the trend in the activity prior to the ammonia addition there might also be an inherent decline in the production of higher alcohols (see figure 7.1), and the reduced alcohol production after the exposure to ammonia may therefore not only be an effect of NH_3, but also an effect of time. Although it is somewhat difficult to see with the scaling of figure 10 the relative decline in the production rate upon exposure to ammonia is the same for both alcohols and hydrocarbons. The selectivity is thus essentially unaffected by the presence of ammonia. This is illustrated in figure 7.10, which shows the development in the CO conversion and the CO_2-free alcohol selectivity as a function of the time on stream

Figure 7.10 The CO conversion and the CO_2-free alcohol selectivity as functions of the time on stream in a sulfur free syngas. After 27.7 h on stream 741 ppmv NH_3 is added to the syngas feed, and the NH_3 addition is maintained for 10 h. The experimental conditions are given in the legend of figure 7.9.

Figure 7.10 illustrates the deactivation of the catalyst, when ammonia is present in the syngas, but in addition to this figure 7.10 shows how the alcohol selectivity is unaffected by the presence of ammonia.

A reversible poisoning is also the result, when the freshly sulfided catalyst at 325 °C and 1 atm is exposed to an 80 NmL/min flow of 6115 ppmv NH_3 in H_2 for 90 minutes prior to the catalytic test. Figure 7.11 shows a comparison between the alcohol production rates for the ammonia treated catalyst and an untreated sulfide.

143
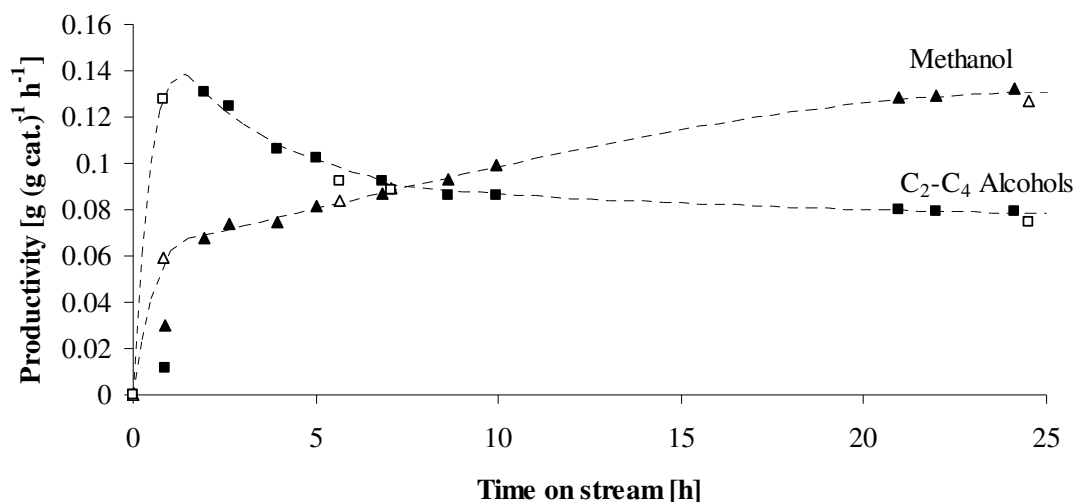
Figure 7.11 The production rates of methanol and C_2-C_4 alcohols over the $K_2CO_3/Co/MoS_2/C$ catalyst as a function of time on stream. The open symbols are for a freshly sulfided catalyst. The filled symbols are for a freshly sulfided catalyst, which at 325 °C and 1 atm has been exposed to 6115 ppmv NH_3 in H_2 for 90 minutes prior to the catalytic test. The experimental conditions are: T = 326 ± 1 °C, P = 100 bar, GHSV = 5525 h^{-1}, Feed: 49 ± 1 vol% H_2, 51 ± 1 vol% CO.

Figure 7.11 illustrates that the catalyst, which has been pretreated with NH_3 in H_2 initially suffers from a reduced activity compared to the catalyst without ammonia treatment, but the NH_3 treated catalyst soon reaches the level of the untreated catalyst, and from around 5 h on stream the properties of the two catalysts are virtually indistinguishable. This result again points to an essentially reversible deactivation caused by ammonia.

The effect of ammonia has also been evaluated with 144 ppmv H_2S in the syngas. Figure 7.12 shows the production rates of alcohols and hydrocarbons as functions of the time on stream during an ammonia poisoning experiment in the presence of H_2S.
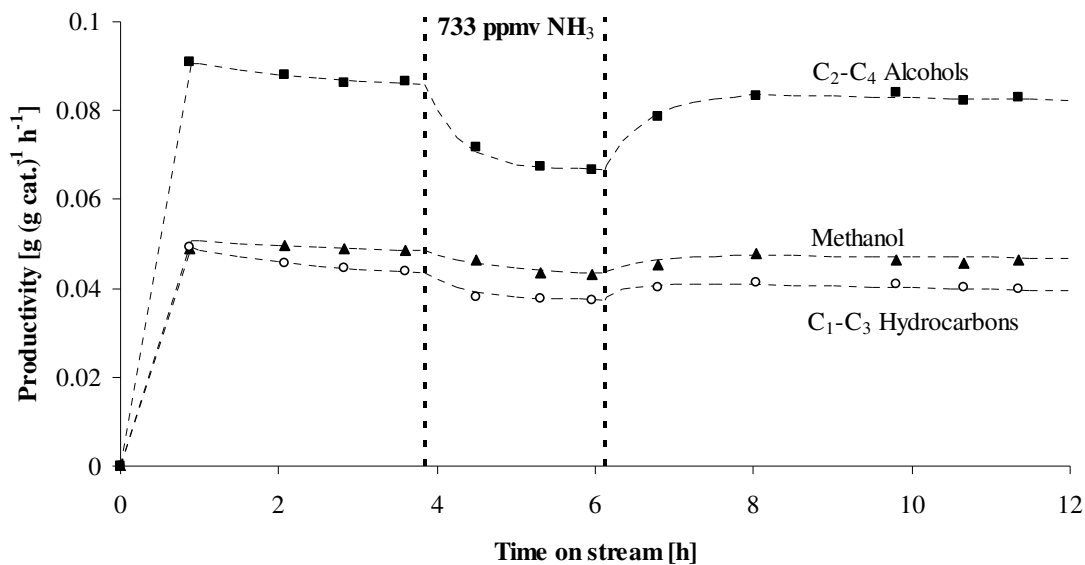
Figure 7.12 The production rates of methanol, C_2-C_4 alcohols and C_1-C_3 hydrocarbons as functions of the time on stream with 144 ppmv H_2S in the syngas. After 3.9 h 733 ppmv NH_3 is added to the syngas feed, and the NH_3 addition is maintained for 2.3 h. The experimental conditions are: T = 327 °C, P = 100 bar, GHSV = 5350 h^{-1}, Feed: 49 ± 1 vol% H_2, 51 ± 1 vol% CO, 144 ppmv H_2S.

Figure 7.12 illustrates that ammonia also in the presence of H_2S causes a pronounced deactivation of the catalyst. The total alcohol production decreases by 19 % (the total alcohol production rate drops from 0.135 g $g_{cat.}^{-1}$ h^{-1} to 0.110 g $g_{cat.}^{-1}$ h^{-1}), and the production of ethanol and higher alcohols decreases by 23 %. The relative decline in the hydrocarbon production rate is 15 %, which is similar to the drop in the total alcohol production rate. The investigations in a sulfur containing atmosphere also indicate a largely reversible effect of ammonia. Figure 7.12 indicates that two hours after the NH_3 exposure has been discontinued the production rates of alcohols and hydrocarbons fall on the trajectory found by extrapolation of the data points obtained before the NH_3 exposure. It should be pointed out that the exposure to ammonia is shorter in the experiment conducted with H_2S in the syngas than in the experiment without H_2S, but it appears that the deactivation caused by ammonia is less severe in the presence of H_2S. As previously discussed the presence of H_2S in the syngas modifies the activity of the catalyst, and it is also possible the presence of hydrogen sulfide modulates the effect that ammonia has upon the catalyst. With H_2S in the syngas the selectivity is also largely unaffected by the ammonia poisoning. This is illustrated in figure 7.13, which shows the CO conversion and the CO_2-free alcohol selectivity as functions of the time on stream during the NH_3-poisoning experiment in an H_2S containing syngas.
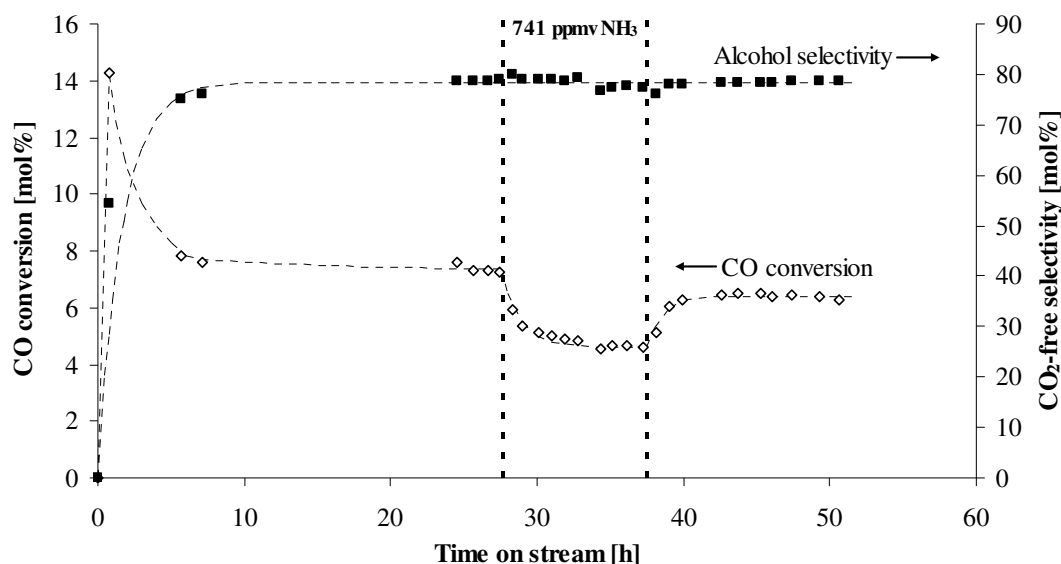
145
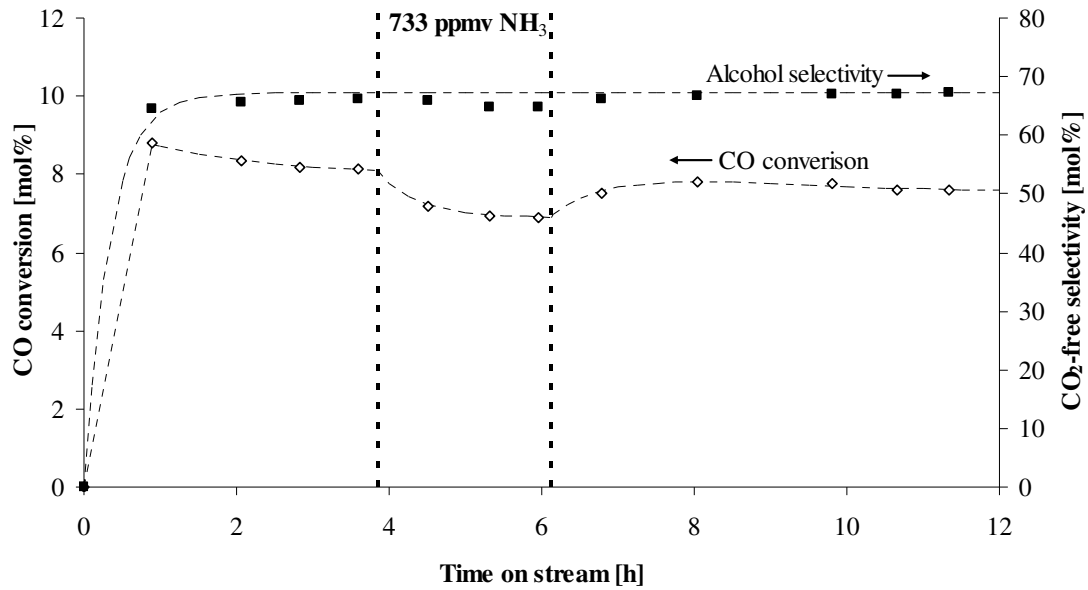
Figure 7.13 The CO conversion and the CO_2-free alcohol selectivity as functions of the time on stream with 144 ppmv H_2S in the syngas. After 3.9 h 733 ppmv NH_3 is added to the syngas feed, and the NH_3 addition is maintained for 2.3 h. The experimental conditions are given in the legend of figure 7.12.

Figure 7.13 illustrates that there is only a slight reduction in the alcohol selectivity, when the catalyst is exposed to ammonia. The slight decrease in the alcohol selectivity stems from the fact that the hydrocarbon production is slightly less affected by ammonia than the alcohol production. This situation differs slightly from operation in an S-free syngas, where the deactivation is observed to be completely without impact on the selectivity.

   LaVopa and Satterfield [157] studied the poisoning effect of basic nitrogen compounds on the hydrotreating activity of a $Ni/MoS_2/Al_2O_3$ catalyst. These authors [157] observed that the fractional loss of activity, θ, could be determined with the same expression as the expression derived from a Langmuir isotherm describing the fractional surface coverage of the basic inhibitor. In this way the fractional loss of activity can be described in terms of the partial pressure of ammonia, p_{NH_3}, and the ammonia adsorption equilibrium constant, K_{NH_3}:

$$\theta = \frac{p_{NH_3} K_{NH_3}}{1 + p_{NH_3} K_{NH_3}} \tag{7.1}$$

For ammonia LaVopa and Satterfield [157] determined a value of $K_{NH_3} = 0.048 kPa^{-1}$ for the adsorption equilibrium constant. With the presently employed partial pressure of ammonia, this would correspond to a fractional activity loss of 26 %. For the experiment with 144 ppmv H_2S in the syngas the predicted decline in the activity corresponds relatively well to the observed loss of activity (23 % for C_2-C_4 alcohols, 19 % for C_1-C_4 alcohols and 15 % for C_1-C_3 hydrocarbons). This may be related to the fact that the

poisoning experiments by LaVopa and Satterfield [157] also were conducted in the presence of hydrogen sulfide. The present results could certainly suggest that the presence of H_2S in the syngas influences the catalysts response to ammonia. The 41 % activity loss observed in the absence of H_2S would correspond to an ammonia adsorption coefficient of $K_{NH_3} = 0.094 kPa^{-1}$, but it would be imprudent to rely on a coefficient determined with only one data point. It is difficult to know, if the fractional decline in the catalytic activity actually does correspond to the surface coverage of ammonia, although the fact that the loss of activity can be expressed in the same way as for a Langmuir isotherm does support this notion. If this is the case, the poisoning effect of ammonia on the alcohol synthesis catalyst can be explained by a general and largely reversible site-blocking.

The observed deactivation is presumably not limited to ammonia. It is quite likely that other basic nitrogen compounds would have a qualitatively similar effect upon the catalyst, although the poisoning by other basic N-compounds may not be as reversible as it is observed for ammonia. For thiophene hydrodesulfurization LaVopa and Satterfield [157] observed that the poisoning effect of numerous basic nitrogen compounds (including ammonia) correlated well with the gas phase proton affinities of the nitrogen compounds. In line with this observation it has for pyridine been observed [158, 441] that the adsorption on MoS_2 is related to strongly bound pyridinum ions formed in a protonation of pyridine. It is very likely that the poisoning effect of ammonia in the same way stems from adsorbed ammonium ions formed by a protonation of ammonia. In hydrotreating reactions it has been reported [158] that it is especially the hydrogenation pathway, which is poisoned by basic nitrogen compounds. Such a poisoning with pyridine has even been actively used to selectively diminish the olefin hydrogenation during hydrodesulfurization reactions [442]. In the alcohol synthesis the ammonia poisoning appears to have only a very limited bearing on the selectivity, and the inhibition of the hydrogenation pathway does not appear to favor the production of neither alcohols nor hydrocarbons. It is possible that poisoning with another base like pyridine could affect the selectivity, but the NH_3 poisoning does not favor a specific product through a selective poisoning. This may be related to the fact that the alcohol formation and the hydrocarbon formation both require hydrogenation reactions.

The present work has focused on how NH_3 affects the catalytic activity. Another potentially problematic issue related to operation in ammonia containing syngas is however that nitrogen species (for example amines) could be incorporated into the liquid alcohol product. Such an incorporation of nitrogen compounds might be problematic for the use of the alcohol product. Since no experiments were made with condensation and analysis of the liquid alcohol product, it is not possible to say whether and to what extent such an incorporation of nitrogen species occurs.

147

8 Changes in a potassium promoted cobalt-molybdenum sulfide catalyst during the conversion of syngas into higher alcohols

If you are finished changing, then you are finished
- Benjamin Franklin

8.1 Abstract

Activity evaluations have been combined with spectroscopy and microscopy investigations in an attempt to determine the origin of the gradual decline in the production of higher alcohols, which is occurring, when cobalt-molybdenum sulfide is operated in a sulfur free syngas. The results indicate that a change in the state of the cobalt chain-growth promoter is a significant part of the reason for the gradual changes in the activity. The distribution of methanol and higher alcohols in the product after 25 hours on stream is largely independent of the cobalt content in the catalyst, although the fraction of higher alcohols initially benefits strongly from an increased presence of cobalt. TEM and XAS investigations indicate that cobalt in the spent catalyst is incorporated into larger, more sulfur-deficient, coagulated structures that are absent in the freshly sulfided catalyst. The XRD spectrum of the freshly sulfided catalyst contains diffraction peaks that previously have been linked to improved properties in cobalt promoted catalysts, but these diffraction peaks are absent in the spent catalysts, and crystalline Co_9S_8, which previously have been reported not to yield a promotional effect, has emerged. It is hypothesized that cobalt is expelled from the active phase (possibly a mixed cobalt-molybdenum sulfide) and incorporated into larger, coagulated, inactive structures. The XAS investigations have however in neither the fresh nor the spent catalyst samples provided clear evidence for a Co-Mo coordination, so this suggestion will so-far have to remain speculative. The change in the state of the cobalt promoter is most likely caused by a loss of sulfur from the active phase, since the presence of ≥ 103 ppmv H_2S in the feed previously was observed to stabilize the original prodct distribution and thus possibly the original active phase.

8.2 Developments in the catalytic activity

The results in chapters 5 and 7 illustrated that when a supported K_2CO_3/Co/MoS_2/C catalyst is operated in sulfur free or sulfur poor syngas, there is a gradual decline in the fraction of higher alcohols in the product.

This chapter combines activity evaluations with spectroscopy and microscopy investigations in an attempt to determine, if structural changes in the active phase are the cause of the changes in the activity. Due to time constraints this chapter does not constitute as finalized an investigation as the other chapters. It is particularly the XAS investigations presented in section 8.5 that require further treatment. If possible it is the

intention that the present results, when supplemented with further XAS results and with further treatment of the XAS results, should be incorporated into a manuscript that can be submitted to Journal of Catalysis.

It was illustrated in section 5.2 that when the sulfide catalyst is operated in an H_2S-free syngas the total alcohol production becomes relatively stable, but at least initially this covers the fact that the methanol production gradually increases at the expense of the higher alcohols. This is illustrated in figure 8.1, which shows the production rates of methanol, C_2-C_4 alcohols and C_1-C_3 hydrocarbons as functions of the time on stream in an H_2S-free syngas.
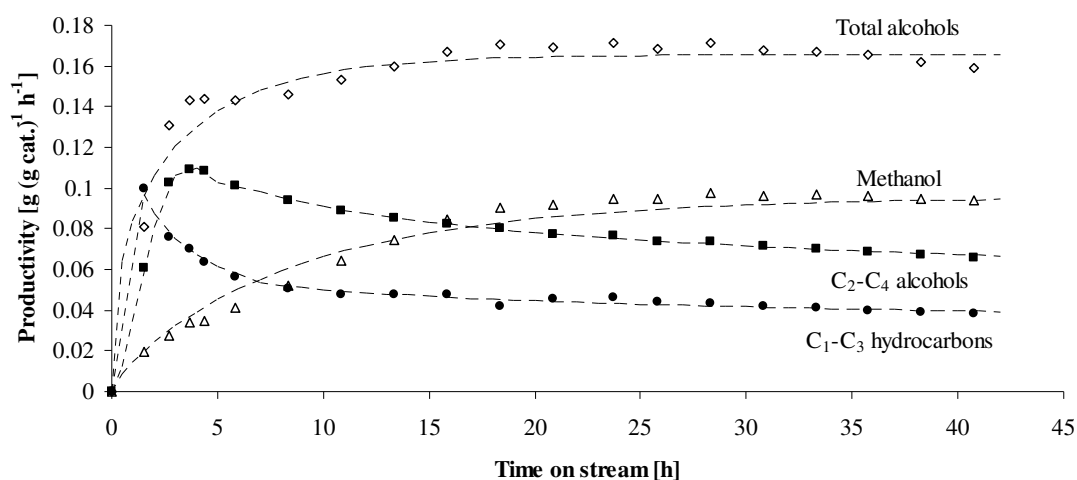
Figure 8.1 The production rates of methanol, C_2-C_4 alcohols and C_1-C_3 hydrocarbons as functions of the time on stream in a sulfur free syngas. The experimental conditions are: P = 100 bar, T = 325 °C, GHSV = 2980 h^{-1}, Feed: 49.5 vol% H_2, 50.5 vol% CO. The catalyst is KCoMo-3.

Additionally figure 8.1 shows that the hydrocarbon production also undergoes a gradual decline. The decline in the production rates of hydrocarbons and higher alcohols seems to be slowing down over time, and the production rates may over time begin to stabilize. In section 5.2 we have previously with a similar catalyst, although at a higher space velocity, observed a more rapid stabilization of the production of higher alcohols. Apart from the fact that the lower space velocity could affect the stabilization rate, the syngas is in present experiment diluted with nitrogen during the first hour of operation in order to limit the initial temperature rise, which occurs, when the catalyst is first exposed to syngas. It is quite possible that such an initial temperature rise can accelerate the effects that lead to the initial decline in activity.

The alcohol selectivity increases during the first 10-15 hours on stream, while the CO conversion gradually decreases. This is illustrated in figure 8.2, which shows the gradual development in the CO conversion, the CO_2 selectivity and the CO_2-free selectivities to methanol and to alcohols in general.

149
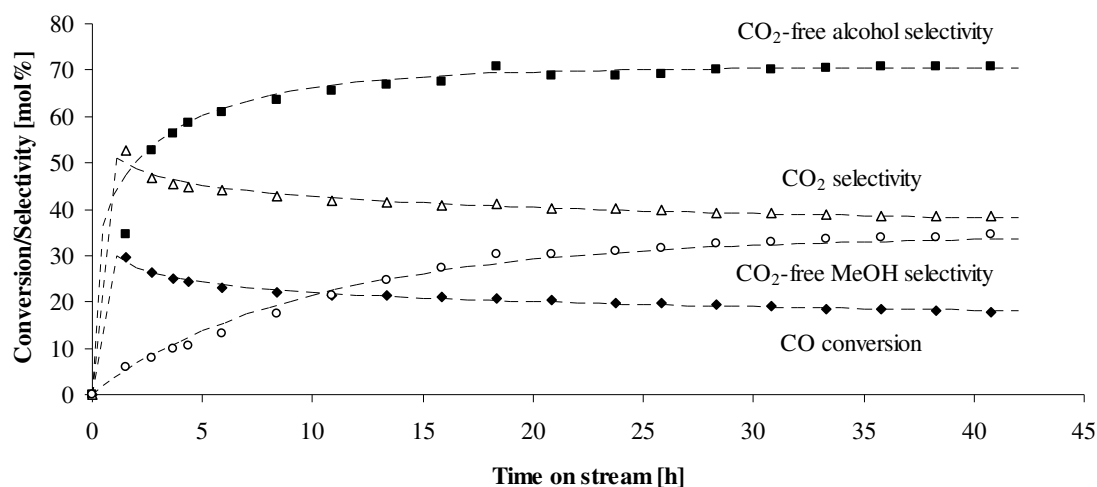
Figure 8.2 The CO conversion and selected carbon based selectivities as functions of the time on stream in an H_2S-free syngas. The experimental conditions are given in the legend of figure 8.1. The catalyst is KCoMo-3.

Figure 8.2 also shows that the CO_2 selectivity undergoes a gradual decline. The decreasing CO_2 selectivity must be ascribed to the increasing importance of the direct hydrogenation of CO into methanol, which, unlike the synthesis of hydrocarbons/higher alcohols, does not result in a co-production of CO_2/H_2O.

In an H_2S free syngas Alkali/MoS_2 catalysts without the Co promoter also undergo a gradual shift in the product distribution from higher alcohols towards methanol [13, 443]. Sections 5.6 and 5.7 contained a discussion of various factors that can contribute to these changes in the catalytic properties of the sulfide. One such factor is a loss of sulfur from the catalyst in the reducing atmosphere. As discussed in section 5.6 a partial carburization could be another factor that may influence the properties of the catalyst in a sulfur free atmosphere.

For the Co-promoted catalysts there is however the added possibility that a change in the state of the cobalt chain-growth promoter can contribute to the gradual changes in the catalytic properties. That this could be the case is illustrated in figure 8.3, which for two sulfide catalysts with different Co/Mo ratios shows the weight ratio of higher alcohols to methanol as a function of the time on stream.
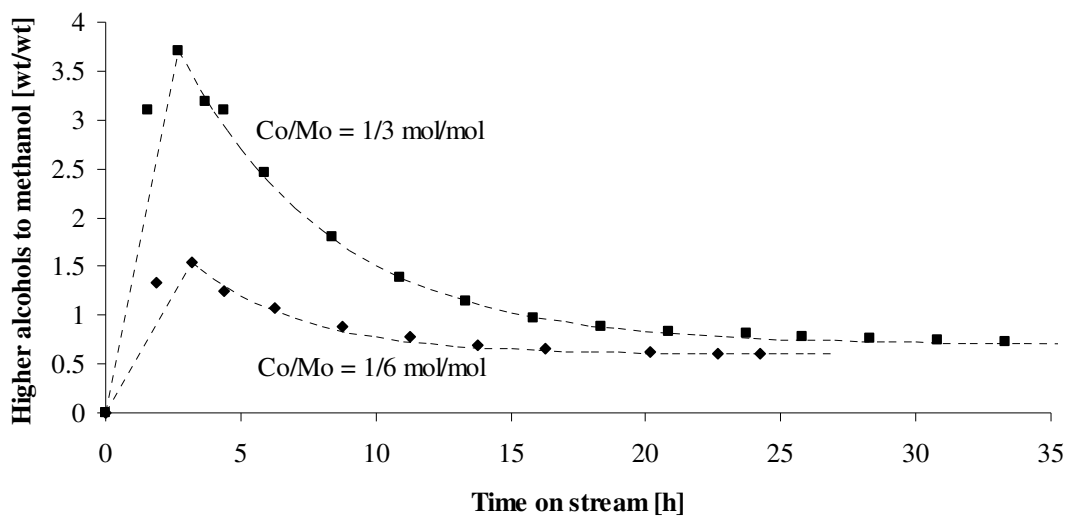
Figure 8.3 The ratio of higher alcohols to methanol as a function of the time on stream for two otherwise identical $K_2CO_3/Co/MoS_2/C$ catalysts with different Co/Mo ratios. The experimental conditions are given in the legend of figure 8.1. The catalysts are respectively KCoMo-3 and KCoMo-4 in table 4.4 on page 77.

As it is described in section 4.9.1, the Co/Mo = 1/3 catalyst is provided by Haldor Topsøe A/S, while the Co/Mo = 1/6 catalyst is prepared by the author through incipient wetness impregnation. There can thus be differences in the sample preparation, but the tendecies in figure 8.3 could nevertheless suggest that a change in the state of the cobalt chain-growth promoter is a significant part of the explanation for the initial decline in the fraction of higher alcohols in the product. A very interesting thing to observe in figure 8.3 is that the two catalysts regardless of the cobalt content ultimately approache the same approximate distribution of methanol and higher alcohols. As it is illustrated in figure 8.4 below the two catalysts ultimately reach the same methanol production rate, so the only difference between the two catalysts is the slightly increased production of higher alcohols for the more cobalt-rich catalyst.
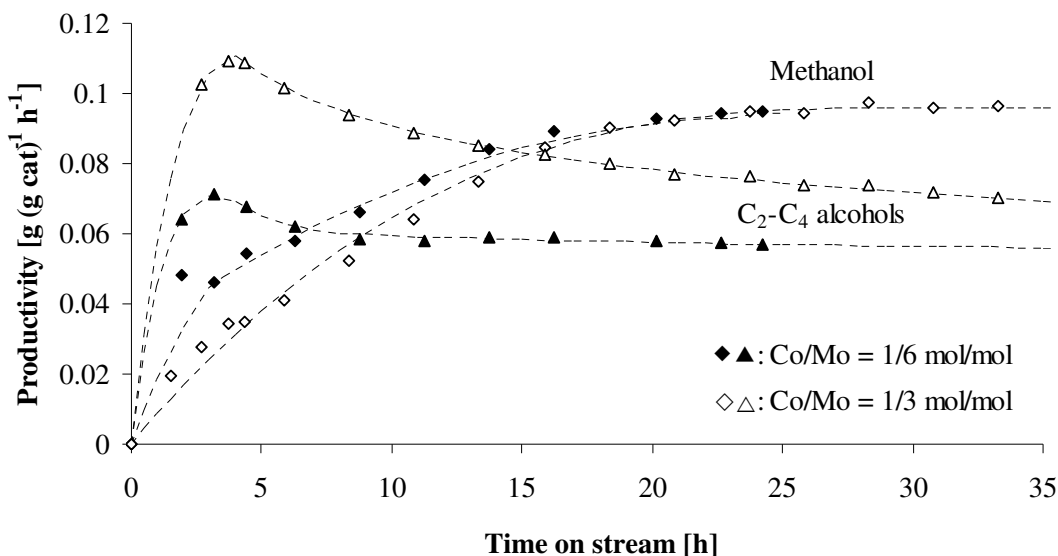
Figure 8.4 The production rates of methanol ($\blacklozenge$, $\diamond$) and C_2-C_4 alcohols ($\blacktriangle$, $\triangle$) for the cobalt-molybdenum sulfide catalyst with Co/Mo = 1/3 mol/mol and the catalyst with Co/Mo = 1/6 mol/mol. The experimental conditions are given in the legend of figure 8.1. The catalysts are respectively KCoMo-3 and KCoMo-4 in table 4.4.

The tendecies in figure 8.3 suggest that a primary cause for the intial changes in the catalytic properties is a change in the state of the cobalt chain-growth promoter, and as it will be shown subsequently this notion is also supported by the spectroscopy/microscopy investigations.

8.3   TEM investigations

After the experiment presented in figure 8.1 and figure 8.2 samples of the spent catalyst (KCoMo-3, Co/Mo = 1/3 mol/mol) from the front and rear ends of the catalyst bed have been removed from the reactor and compared to a freshly sulfided catalyst using various spectroscopic techniques. Something that should be emphasized in connection with the spectroscopic studies is that sulfide samples could be affected by the exposure to air during handling and storage. For MoS_2 there are varying reports concerning the air sensitivity of the sulfide. It has been observed [444] that even a few minutes of air exposure may influence the structure of supported MoS_2 nanoparticles. Furthermore Karolewski and Cavell [169] investigated $Cs/MoS_2(0001)$ and observed that the alkali promoted sulfide could be more susceptible to oxidation by H_2O or O_2 than the bare sulfide. Other studies with electron microscopy [219, 445] or scanning tunneling microscopy [446] have on the other hand indicated that the at least a brief air exposure is without significant effects upon the structure of MoS_2 nanoparticles. The oxidation of MoS_2 nanoparticles during extended air exposure reportedly makes the active phase appear more blurred in TEM images [445]. Previous investigations [447, 448] have also indicated that mixed cobalt-molybdenum sulfides are susceptible to room-temperature

oxidation, and it seems that the cobalt component is particularly sensitive to the exposure to oxygen. Based upon the reports in the literature it can thus not be ruled out that there is an effect of the air exposure. As stated in section 4.9.2 the samples were kept in closed containers, and the spectroscopy investigations were conducted within 1 week after the removal from the reactor, while the microscopy investigations were conducted 2-3 weeks after the removal of the sample from the reactor. Due to the possible influence of the air exposure a final verification of the presently reported results will require full in-situ experiments.

Figure 8.5 shows TEM images of the freshly sulfided catalyst, while figure 8.6 shows TEM images of the spent catalyst from the front end of the catalyst bed.
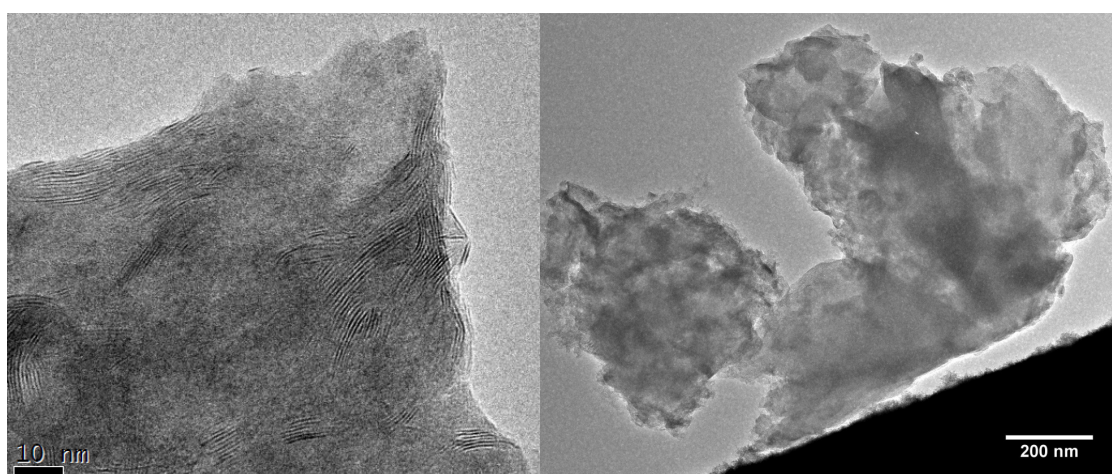
Figure 8.5 TEM images of the freshly sulfided catalyst (KCoMo-3). The images were recorded without a reducing pretreatment. In-situ reduction for several hours in 1.5 mbar H_2 at 325 °C did not cause any significant changes to the images.
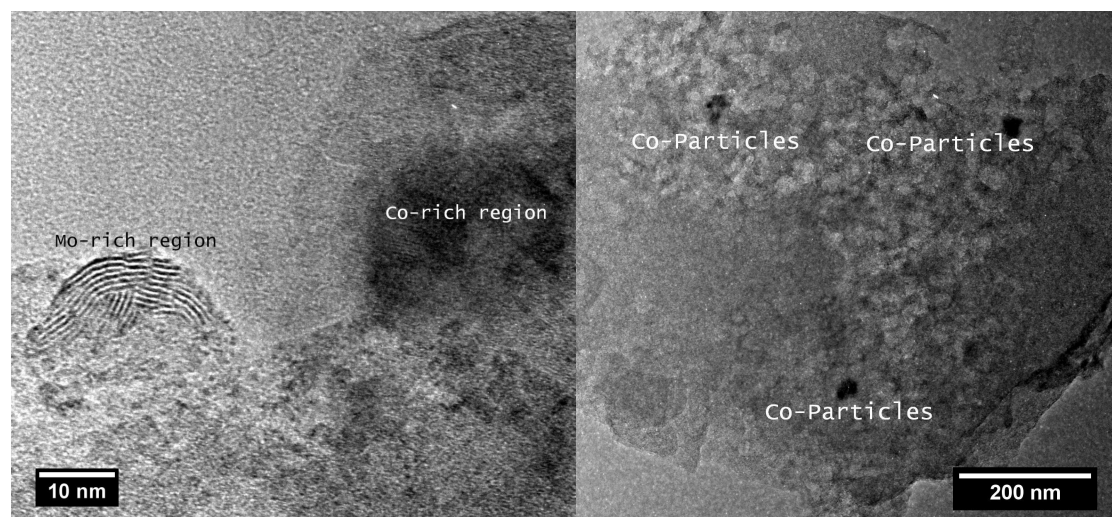
Figure 8.6 TEM images of the spent catalyst (KCoMo-3) from the front end of the catalyst bed. This catalyst has been operated for 42 h at the conditions given in the legend of figure 8.1. The images were recorded without a reducing pretreatment.

MoS$_2$ has a layered structure with a sheet of Mo atoms between two sheets of sulfur atoms (see perhaps figure 2.1 on page 31). In TEM individual S-Mo-S slabs are typically only imaged, when they are oriented edge-on towards the electron beam [219]. The TEM images of both the fresh and the spent catalysts clearly show these MoS$_2$ slabs, and the images thus indicate that the bulk MoS$_2$ structure is preserved during the 42 hours in syngas. The most interesting observation in figure 8.5 and figure 8.6 is however that darker regions have emerged in the spent catalyst, where a simultaneous EDX analysis reveals a strongly increased presence of Co. Figure 8.7 shows EDX spectra for the Co-rich and Mo-rich regions in the small-scale image in figure 8.6.
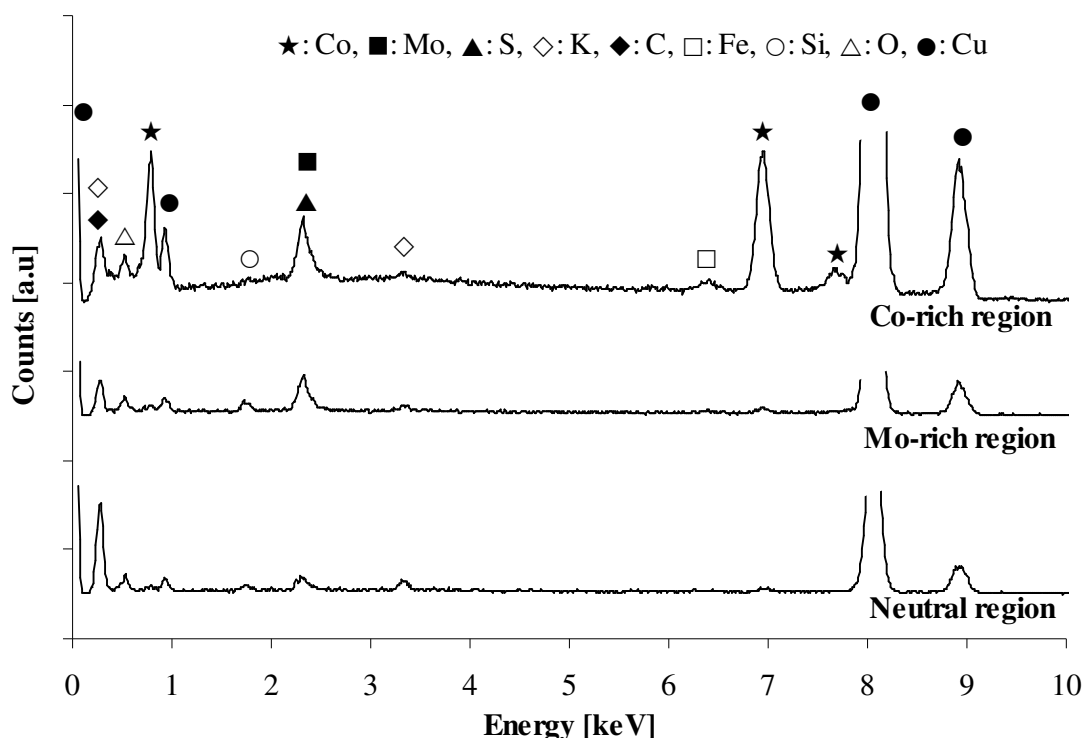
Figure 8.7 Energy dispersive X-ray (EDX) analyses of the composition in the "Co-rich region" and the "Mo-rich region" in the small-scale image in figure 8.6. For comparison a compositional analysis of the "neutral" region between the two metal-rich regions in the small-scale image in figure 8.6 is also shown. The strongest cupper signals from the TEM grid are cut off to obtain a better scaling of the EDX spectra. The catalyst is KCoMo-3.

The local nature of the TEM investigation must of course be remembered, but on the larger scale images in figure 8.5 and figure 8.6 it is possible to observe several such Co-rich regions in the spent catalyst, while no cobalt rich regions are clearly discernible in the freshly sulfided catalyst. These observations suggest a change in the state of cobalt during operation, where cobalt is incorporated into larger, coagulated structures.

Since the samples are dispersed on the TEM grid in dry form the Co-rich regions in the spent catalyst are presumably not formed by redisperison of soluble cobalt during the

sample preparation. That an air oxidation could affect the catalyst structure can however not be completely excluded.

8.4 XRD studies

The X-ray diffraction patterns of the fresh and spent catalyst samples could also support the notion of a change is the state of the cobalt promoter. Figure 8.8 show the XRD patterns for the fresh and spent catalyst samples.
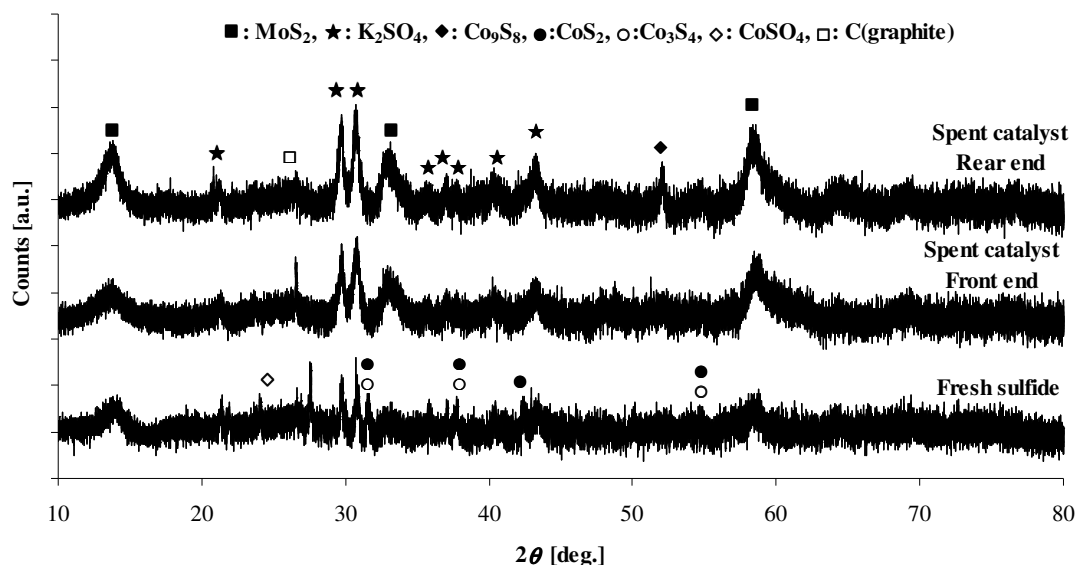
Figure 8.8 X-ray diffraction patterns for the freshly sulfided catalyst (KCoMo-3) and for samples of the catalyst that has been on stream for 42 h at the conditions given in the legend of figure 8.1.

Generally the catalyst samples are relatively amorphous – especially the freshly sulfided sample. The spectra seen in figure 8.8 are collected over a period of 7 hours, but the diffraction peaks are still rather weak. Based upon reported spectral features for potassium sulfate [449-451] the dominant diffraction peaks in both the fresh and the spent catalysts have been ascribed to K_2SO_4. It is however difficult to determine, if the potassium sulfate phase is native to the working catalyst or formed by air oxidation of the catalyst after its removal from the reactor. Woo et al. [172, 174, 182] have previously observed that K_2SO_4 is formed in air oxidation of K_2CO_3/MoS_2 at room temperature, and this could also occur for the presently investigated catalysts. On a molar basis potassium is actually the dominant active material (see table 4.4 on page 85), and it is therefore not unexpected that relatively large, potassium rich structures exist. Apart from K_2SO_4 both the fresh and spent samples show clear signs of MoS_2. With respect to cobalt, there are however significant differences between the fresh and spent samples. Murchison et al. [13] observed that cobalt promoted sulfides with improved catalytic properties exhibited diffraction peaks at approximately $2\theta = \{38.0°, 42.6°, 65.2°\}$, which the authors [13]

155

ascribed to CoS_2 (the CoS_2 assignments in figure 8.8 are largely based upon this suggestion). Murchison et al. [13] also observed that cobalt promoted catalysts, for which the XRD patterns showed clear signs of Co_9S_8, were less efficient and behaved much like regular MoS_2 without the Co promoter. The diffraction peaks that can be linked to the improved properties in a cobalt promoted catalyst are, although they are very faint, present in the freshly sulfided catalyst, but these diffraction peaks are absent in the catalyst samples that have been on stream for 42 h. The diffraction pattern of at least the spent sample from the rear end of the bed also shows a clear sign of Co_9S_8. The disappearance of the signs of the reportedly benign form of cobalt and the appearance of a Co_9S_8 phase, which reportedly does not provide a promotional effect, again supports the idea of a change in the state of the cobalt chain-growth promoter as part of the reason for the decline in the production of higher alcohols. That a Co_9S_8 phase emerges or becomes more prominent in the spent catalyst is something that also has been reported by other authors [188, 452].

Cobalt sulfate, which has a significant diffraction peak around $2\theta = 25.2°$ [453], may be formed in air oxidation of cobalt molybdenum sulfide [445]. There do not appear to be strong signs of $CoSO_4$ in the catalysts, although the fresh sulfide does seem to exhibit a minor diffraction peak at $2\theta = 24.5°$.

It seems that the ~20 nm large Co-rich regions, which are observed in the spent catalyst from the front of the bed (see figure 8.6), are not likely to be 20 nm large unified crystalline structures. If this was the case, then the cobalt rich structures should be visible in the XRD-spectrum, but this does not appear to be the case.

A comparison of the diffraction patterns for the fresh and spent catalyst samples in figure 8.8 reveals a clear sintering of the catalyst during operation, as the diffraction peaks have become significantly more pronounced for the spent samples. The sintering appears to be slightly more severe in the rear end of the catalyst bed. The primary difference between the conditions in the two ends of the catalytic bed is that an appreciable concentration of CO_2/H_2O is present in the rear end of the bed. Water and CO_2 are formed in connection with the synthesis reactions and the water-gas shift reaction. It was shown in section 7.3 that addition of water to the syngas feed causes a permanent, general deactivation that could be related to sintering. This is consistent with the present observation of a slightly accelerated sintering in the rear end of the catalyst bed, where appreciable amounts of H_2O and CO_2 are present in the gas.

8.5   XAS investigations

Additional investigations of the catalyst samples have been carried out by means of of X-ray absorption spectroscopy.

Table 8.1 shows the EXAFS fitting results for the spectra recorded at the Co K-edge for fresh and spent catalysts samples (KCoMo-3) before any in-situ pretreatment, while table 8.2 shows the EXAFS fitting results for the spectra recorded at the Co K-edge after an in-situ treatment in 5 mol% H_2 in He at 325 °C for 1 hour.

Table 8.1 and table 8.2 show that the cobalt species generally have high Co-S coordination numbers. This is in qualitative agreement with other reports for similar catalysts [214, 454]. That the Co-S coordination numbers in certain cases exceed 6,

which is even higher than the expectation for CoS_2 [209, 214] or a mixed Co-Mo-S phase [208], must be ascribed to the uncertainty, but it is also possible that Co_9S_8, which has been used to obtain the dampening factor, is not the ideal model compound for the cobalt species actually present in the catalyst.

Table 8.1 EXAFS fitting results for the fresh and spent catalyst samples (KCoMo-3) before the in-situ treatment in reducing gas. All data were fitted with a dampening factor of $S_0^2 = 0.45$ obtained from the Co_9S_8 reference.

Shell	N	R [Å]	σ^2 [Å^{-2}]	ΔE_0 [eV]
Fresh sulfided catalyst, $k = 3\text{-}15$ Å^{-1}, fitted between 1.2-2.4 Å; residual 2.2				
Co-S	7.8	2.22	0.0081	-3.2
Co-Co	1.9	2.48	0.0097	-3.2
Spent catalyst, front end, $k = 3\text{-}13.5$ Å^{-1}, fitted between 1.0-2.6 Å; residual 1.6				
Co-O	3.7	1.97	0.0078	-8.2
Co-S	1.6	2.27	0.011	-6.7
Co-Co	5.9	2.45	0.0095	-6.7
Spent catalyst, rear end, $k = 3\text{-}13$ Å^{-1}, fitted between $1.4 - 2.4$ Å; residual 0.9				
Co-S	7.3	2.21	0.013	-8.3
Co-Co	4.3	2.47	0.012	-2.4
Co_9S_8, $k = 3\text{-}13$ Å^{-1}, fitted between 1.2 Å - 2.6 Å; residual 0.7				
Co-S	4.2 [a]	2.19	0.0060	-1.8
Co-Co	2.7 [a]	2.47	0.0043	-1.8

[a] Enforced value.

Table 8.2 EXAFS fitting results for the fresh and spent catalyst samples (KCoMo-3) after in-situ treatment in 5 mol% H_2 in He at 325 °C for 1 hour. All data were fitted with a dampening factor of $S_0^2 = 0.45$ obtained from the Co_9S_8 reference.

Shell	N	R [Å]	σ^2 [Å^{-2}]	ΔE_0 [eV]
Fresh sulfided catalyst, $k = 3\text{-}15$ Å^{-1}, fitted between 1.4-2.6 Å; residual 1.9				
Co-S	6.5	2.20	0.0060	-1.3
Co-Co	3.3	2.50	0.0090	-1.3
Spent catalyst, front end, $k = 3 - 13.5$ Å^{-1}, fitted between 1.6-3.8 Å; residual 1.1				
Co-S	5.8	2.21	0.013	1.5
Co-Co	5.1	2.49	0.0066	1.5
Spent catalyst, rear end, $k = 3\text{-}13.5$ Å^{-1}, fitted in the range 1.6-2.8 Å, residual 0.65				
Co-S	4.4	2.20	0.0067	0.3
Co-Co	4.5	2.50	0.0058	0.3

The results in table 8.1 indicate that the spent catalyst from the front end of the bed has been partially oxidized – possibly during passivation and handling after the reaction. As discussed in section 8.3 the sulfide might be susceptible to oxidation, and it does not seem unreasonable that the spent catalyst, where the reducing atmosphere can have created more anion vacancies, is more prone to incorporation of oxygen. The EXAFS spectra for the freshly sulfided catalyst and the spent catalyst from the rear end of the bed can be fitted satisfactorily without inclusion of a Co-O coordination. The results in table 8.2 indicate that the oxygen in the sulfide structure is removed by the reducing in-situ

157

treatment. The Co-Co coordination numbers are observed to be significantly increased in the spent catalyst samples from both the front and rear ends of the catalyst bed. These observations of an increased Co-Co coordination in the spent catalyst are consistent with the TEM results, which show that larger Co-rich structures have emerged in the spent catalysts. Generally the Co-S coordination numbers seem to have decreased in the spent catalyst samples, and the larger, more Co-rich structures may therefore be more sulfur-deficient, than the Co-species in the freshly sulfided catalyst. Although the possibility was investigated, it was for neither the fresh nor the spent catalysts possible to fit a Co-Mo coordination. The present XAS results can therefore not provide any information about the presence and role of a mixed cobalt-molybdenum sulfide phase in the alcohol synthesis catalyst.

Compared to the significant changes in the cobalt environment during operation there are less marked changes in the molybdenum environment during the reaction. This is illustrated in table 8.3, which shows the EXAFS fitting results for the spectra recorded at the Mo K-edge after an in-situ treatment in 5 mol% H_2 in He at 325 °C for 1 hour.

Table 8.3 EXAFS fitting results at the Mo K-edge for the fresh and spent catalyst samples (KCoMo-3) after in-situ treatment in 5 mol% H_2 in He at atmospheric pressure and 325 °C for 1 hour. All data were fitted with a dampening factor of $S_0^2 = 0.9$ obtained from the MoS_2 reference.

Shell	N	R [Å]	σ^2 [Å^{-2}]	ΔE_0 [eV]
Fresh sulfided catalyst, $k = 3\text{-}15$ Å^{-1}, fitted in the range 1.7-3.3 Å, residual 0.8				
Mo-S	6.1	2.41	0.0037	7.9
Mo-Mo	3.9	3.17	0.0046	6.4
Spent catalyst, front end, $k = 3 - 14$ Å^{-1}, fitted in the range 1.6-3.2 Å, residual 1.4				
Mo-S	5.0	2.41	0.0030	9.3
Mo-Mo	3.2	3.17	0.0032	6.3
Spent catalyst, rear end, $k = 3\text{-}15$ Å^{-1}, fitted in the range 1.6-3.2 Å, residual 1.5				
Mo-S	5.2	2.41	0.0029	9.1
Mo-Mo	3.7	3.17	0.0036	6.3
MoS_2 reference, $k = 3.5\text{-}17$ Å^{-1}, fitted in the range 1.8 Å-3.6 Å, residual 3.5				
Mo-S	6 [a]	2.41	0.0021	2.7
Mo-Mo	6 [a]	3.16	0.0026	0.2

[a] Enforced value.

The structural parameters obtained for the different catalysts from the EXAFS fits at the Mo K-edge indicate that the MoS_2-phase is retained during the 42 hours of operation, as the fitted bond distances correspond to those of MoS_2. This is consistent with the results from the TEM and XRD investigations. Satisfactory fits to the spectra for the in-situ reduced catalysts could be obtained by including only Mo-Mo and Mo-S coordinations. A comparison of the fitting results for the fresh and spent catalysts in tables 3 and 4 shows that the catalyst loses sulfur in the reducing syngas atmosphere. This loss of sulfur could also influence the structure and the catalytic properties of the sulfide catalyst.

Apart from structural changes another possible reason for the gradual decline in the production of higher alcohols could in principle be a poisoning effect arising from impurities in the syngas - for example deposition of Fe and Ni in the catalyst bed from

decomposition of carbonyls. For this reason the presence of iron in the catalyst samples was probed in the fluorescence mode. This investigation revealed that both the fresh and spent catalysts (as well as the oxide precursor) contained minor amounts of iron. The strength of the Fe signal is approximately 1/18 of the Co signal for both fresh and spent samples. The iron present is presumably either an impurity in the carbon carrier or introduced during the catalyst preparation. Since oxidized, freshly sulfided and spent catalysts contain the same approximate amount of iron the metal deposition from carbonyls is estimated not to be a significant issue in the present case. This is consistent with the results of Bogdan et al. [455], who observed that the sulfides unlike metallic catalysts were rather unsusceptible to metal deposition from carbonyl decomposition. It might be added that the first few times the presently employed experimental setup was used for syngas conversion in the early part of 2007 metal deposition in the catalyst bed was observed, but during the experimental campaigns presented in this thesis no such depositions have been observed.

8.6 Changes in the state of the cobalt chain-growth promoter duing operation

The present results indicate that the initial, gradual decline in the production of higher alcohols, which the supported cobalt-molybdenum sulfide undergoes in sulfur-free or sulfur-poor syngas, to a significant extent is related to a change in the state of the cobalt chain-growth promoter. Figure 8.3 illustrates that the distribution of methanol and higher alcohols in the product after 25 hours on stream is largely independent of the cobalt content in the catalyst, although the fraction of higher alcohols initially benefits considerably from an increased presence of cobalt. TEM and XAS investigations indicate that cobalt in the spent catalyst is incorporated into larger, more sulfur-deficient, coagulated structures that are absent in the freshly sulfided catalyst. The XRD spectrum for the spent catalyst from the rear end of the bed, where sintering generally seems to be accelerated, is also exhibiting signs of crystalline Co_9S_8. The Co_9S_8 phase is reported not to yield a promotional effect in the alcohol synthesis. It is possible that it is from the sintered cobalt-rich structures that the rearrangement into Co_9S_8 occurs.

On the other hand the XRD spectrum for the fresh catalyst exhibit the diffraction peaks, which previously have been correlated to improved properties in cobalt containing catalysts. It is tempting to suggest that the active form of cobalt during operation is expelled from the active phase and incorporated into larger structures and in the end possibly rearranged into Co_9S_8, which is known not to provide a promotional effect.

As it has been described in section 2.3.3, the active form of cobalt in the alcohol synthesis catalyst is not completely clarified. Although a mixed cobalt-molybdenum sulfide phase may contribute the promotional effect, it seems quite clear that also isolated cobalt species, if they are present in the right form, could benefit the chain-growth over the sulfide catalyst. The results from TEM and XAS illustrate that cobalt in the spent catalyst has been incorporated into larger, coagulated, more sulfur deficient and quite possibly less active structures. It seems very likely that this change in the state of the Co

chain-growth promoter contributes to the declining production of more long-chained products.

The results in figure 5.3 on page 96 illustrates that the original product distribution is stabilized by inclusion of 103 ppmv or more of H_2S in the syngas feed. This could also suggest that the original active phase, namely the sulfide, is stabilized by the inclusion of ≥ 103 ppmv H_2S in the feed. The results in section 5.5 illustrated that sulfur is lost from the catalyst during operation in the reducing syngas atmosphere, and it is possible that it is this loss of sulfur from the catalyst, which drives the coagulation of the cobalt species into larger, but more sulfur-poor structures and drives the formation of Co_9S_8. In line with a previous suggestion by Iranmahboob and Hill [188] it could be the loss of sulfur that drives the conversion of the more sulfur rich Co-containing phases (CoS_2, Co_3S_4, Co-Mo-S) into the relatively more sulfur deficient Co_9S_8 phase according to reactions of the type given in R38 and R39:

$$9CoS_2 + 10H_2 \rightarrow Co_9S_8 + 10H_2S \qquad\qquad \text{R38}$$
$$3Co_3S_4 + 4H_2 \rightarrow Co_9S_8 + 4H_2S \qquad\qquad \text{R39}$$

If it is necessary to include a sulfur source in the feed to stabilize the active cobalt species this introduces a dilemma for the operator, since the presence of H_2S in the syngas previously was shown to lead to incorporation of sulfur species into the alcohol product.

As it is reported for Co-free, MoS_2-based, alcohol synthesis catalysts [13] (see section 2.3.5), bulk cobalt-molybdenum sulfides also appear to be more stable than supported systems. Bogdan et al. [455] observed that a bulk cobalt-molybdenum sulfide catalyst yielded relatively stable production rates of the higher alcohols over several hundred hours. The methanol production was observed [455] to increase over the first 50-100 h and then stabilize. As it was also discussed in section 2.3.5, it is however difficult to know, if the bulk sulfide yields a better stability or simply a longer period of stability, because the bulk sulfide acts as a sulfur storage and counteracts the loss of sulfur from the catalyst surface.

An important factor is presumably the stability of the mixed sulfide vs. the stability of isolated cobalt sulfides, and this relative stability could well be influenced by the support or by the use of an unsupported bulk sulfide. The use of a more strongly interacting support like alumina may provide a greater resistence towards sintering, but, as it is discussed in section 2.3.4 on page 38, the use of a more strongly interacting support like alumina is less attractive in terms of the alcohol selectivity.

9 Catalytic conversion of syngas into higher alcohols over carbide catalysts

It doesn't matter if you try and try and try, and fail. It matters if you try and fail, and fail to try again.
- Charles F. Kettering

Just because something doesn't do, what you planned it to do, doesn't mean it's useless
- Thomas Edison

9.1 Abstract

Various catalysts based upon the bulk carbides Mo_2C, WC and NbC have been synthesized and evaluated with respect to the catalytic behavior in high-pressure CO hydrogenation. The generally applied reaction conditions were 100 bar, GHSV = 5000 h^{-1}, H_2/CO = 1.0 mol/mol. The catalytic activity of a K_2CO_3/Mo_2C (10 wt% K_2CO_3, 2.4 m^2/g) catalyst was observed to stabilize at a temperature 250 °C, but at 276 °C and 300 °C the catalyst underwent a gradual deactivation. The cause of the deactivation is most likely the build-up of carbonaceous deposits on the catalyst. On a carbon basis ethanol was the dominant alcohol formed over the K_2CO_3/Mo_2C catalyst. At 276 °C the catalyst yielded a CO conversion of 9.3 mol% and a CO_2-free, carbon based ethanol selectivity of 20.6 mol% (total alcohol selectivity 53 mol%). A K_2CO_3/WC (5.5 wt% K_2CO_3, 1.1 m^2/g) catalyst primarily produced methanol and had a low activity. At 350 °C the K_2CO_3/WC catalyst gave a CO conversion of 2.7 mol% with a CO_2-free, carbon based selectivity to methanol of 49.5 mol%. NbC (8.1 m^2/g) was almost without activity, and at 350 °C niobium carbide gave a CO conversion of only 0.5 mol% with methane being the only important product. The role of the choice of alkali cation in Mo_2C promoted by an alkali salt has also been evaluated at a promoter level of Alkali/Mo = 0.164±0.001 mol/mol. At 275 °C-300 °C the behavior of catalysts promoted by Cs_2CO_3 and K_2CO_3 was qualitatively similar, with K providing a 31 % better activity and a better selectivity at identical conditions. At 275 °C an $Li(CH_3COO)$ promoted catalyst was very active and produced only hydrocarbons. If the effect of the different alkali promoters was compared at the same general activity level, corresponding to the Li containing catalyst being operated at a lower temperature of 250 °C, the Li promoted catalyst is however only slightly inferior to the K promoted catalyst in terms of the selectivity. Finally different multiply promoted Mo_2C catalysts have been evaluated in terms of the CO hydrogenation properties. Addition of Re (1 wt%) or Mn (1 or 5 wt%) to the K_2CO_3/Mo_2C system results in a slight reduction in the catalytic activity. The addition of Cu (0.84 wt%) was on the other hand observed to improve the activity by 33 % and improve the selectivity of the K_2CO_3/Mo_2C system without altering the distribution of the alcohol product. Mo_2C modified with La (5 wt%) and V (3 wt%) produces mainly hydrocarbons.

9.2 Introduction

The preceding text has revealed several problematic issues related to the use of the sulfides as alcohol synthesis catalysts. Section 5.5 illustrated the risk of incorporating sulfur species into the alcohol product, when the catalyst is operated in a sulfur containing atmosphere. The results in section 5.2 on the other hand illustrated that the production of the desired higher alcohols undergoes a slow decline in a sulfur free atmosphere. The results in chapter 8 illustrated that this at least in part could be related to a change in the state of the cobalt chain-growth promoter. Due to these problematic issues with the sulfides the use of various bulk carbides, namely Mo_2C, WC and NbC, has been investigated in an attempt to find an alternative catalyst. The reason behind the choice of these 3 carbides is presented in section 2.4.3, and a detailed description of the preparation of the carbide catalysts is presented in section 4.9.3. In this chapter the structural and catalytic properties of promoted carbides are presented. As for the rest of this work the treatment is focued on Mo-based systems.

9.3 Catalyst structure

Figure 9.1 shows the XRD diffractograms of the oxide precursors used in the carburization processes. The observed diffraction peaks can, as it would be expected, be ascribed to MoO_3, WO_3 and Nb_2O_5 respectively. Figure 9.2 shows the X-ray diffraction patterns of various fresh and spent carbide samples.
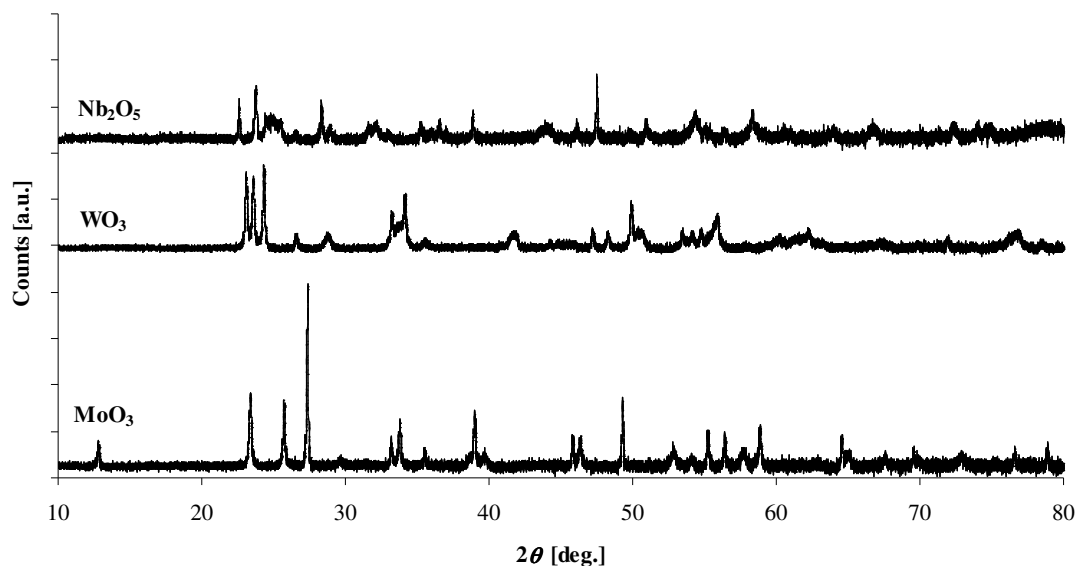
Figure 9.1 X-ray diffraction patterns of the oxide precursors used in the preparation of the carbides.
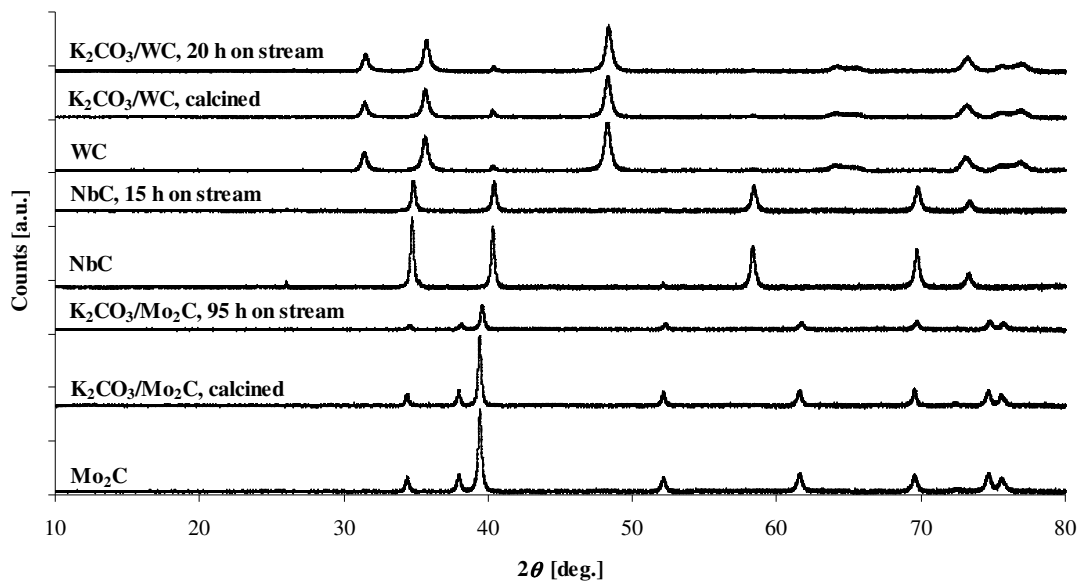
Figure 9.2 X-ray diffraction patterns of the fresh and spent carbide samples.

The XRD patterns of the carbide samples in figure 9.2 reveal that the carburization procedures have been successful in the sense that the desired carbide phases Mo_2C, NbC and WC essentially are the only crystalline phases, which are observed. The diffraction patterns seem to be most consistent with hexagonally structured α-WC (simple hexagonal structure) and β-Mo_2C (*hcp*-structure) and with NbC in a cubic structure (an NaCl structure). The presence of some orthorhombic α-Mo_2C can however not be completely excluded on the basis of the XRD data. For the molybdenum carbide sample Mo_2C is the only crystalline phase that is observed. For the freshly carburized (and passivated) NbC sample the XRD pattern reveal minute traces of an NbO_2 phase, which is indicated by the diffraction peaks at $2\theta = \{26°, 36°, 52°\}$. NbO_2 is thought to constitute an intermediate phase in the carburization of Nb_2O_5 [394]. No trace of NbO_2 is observed in the spent NbC sample, which has been on stream for 15 h. The XRD diffractograms for the WC samples also indicate a minor trace of an intermediate phase. Apart from the diffraction peaks arising from WC, the tungsten carbide samples all exhibit a weak diffraction at $2\theta = 40.4°$. This diffraction feature may be ascribed to W_2C, which has been observed to be an intermediate phase in the synthesis of WC [456]. The diffraction patterns for the promoted and calcined carbides do not exhibit any new traces of oxides indicating that no bulk oxidation occurs during the catalyst preparation. Figure 9.2 also shows that no new crystalline phases have emerged in the spent catalysts, which have been on stream for varying amounts of time. Table 9.1 summarizes the BET surface areas and estimated average particle diameters of selected carbide samples.

Table 9.1 BET surface areas and estimated particle diameters for selected carbide samples.

Sample	S_g [m²/g]	$d_{p,XRD}$ [a)] [nm]	$d_{p,BET}$ [nm]
Mo₂C	11.5	28.5	56.8
K₂CO₃/Mo₂C, calcined	2.4	35.5	268.5
K₂CO₃/Mo₂C, spent, 95 h on stream [b)]	0.2	32.5	2712.0
NbC	8.1	31.7	94.7
NbC, spent, 15 h on stream [c)]	8.1	27.0	95.1
WC	1.2	20.0	333.3
K₂CO₃/WC, calcined	1.1	21.0	338.9
K₂CO₃/WC, spent, 20 h on stream [c)]	0.5	20.2	821.8

[a)] The average crystal size determined from X-ray line broadening. The value of $d_{p,XRD}$ has been determined as an average of the particle sizes determined from the major diffraction peeks, which all yielded similar values. [b)] Tested at 100 bar, H_2/CO = 1.0 mol/mol, GHSV = 4975 h⁻¹ at temperatures up to T = 300 °C. [c)] Tested at 100 bar, H_2/CO = 1.0 mol/mol, GHSV = 5000 ± 25 h⁻¹ at temperatures up to T = 375 °C

The results in table 9.1 illustrate that the present carburization conditions yield bulk carbides with relatively low surface areas. Although the present surface areas generally are comparable to those obtained by other researchers [388, 392, 394, 395, 457], it should be mentioned that bulk carbides with considerably larger surface areas have been obtained [122, 254, 392, 457]. The low surface areas of the presently synthesized carbides must to a significant extent be ascribed to the fact that the present carburizations in terms of temperatures require somewhat harsher conditions than the general reports in the literature. There are several factors that should be contributing to the requirement of more severe carburization conditions. First and foremost the present investigations are performed with oxide granulates, while fine powders typically are utilized in dedicated investigations of the carburization process. Secondly the arrangement, where the carburizing gas passes over the sample rather than through a packed bed of sample, may introduce mass transport limitations that result in a slower carburization. Thirdly the sample amounts used for the present catalyst preparations are generally higher than what is normally used in dedicated investigations of carburization behavior.

It is known from previous studies of CO hydrogenation over Mo₂C catalysts that the addition of significant amounts of potassium is necessary to shift the product distribution towards alcohols [115, 121, 122]. The choice of the alkali content in the catalysts is based upon the results of Woo et al. [115], who observed that the alcohol selectivity increases with increasing K₂CO₃ content in a K₂CO₃/Mo₂C catalyst up to a level of about 10 wt% K₂CO₃ and then stagnates (see perhaps figure 2.3 on page 44). For this reason the following promoter levels were chosen: 10 wt % K₂CO₃ in the K₂CO₃/Mo₂C catalyst and 5.50 wt% K₂CO₃ in the K₂CO₃/WC catalyst (corresponding to 0.16 mol K/mol Me, Me = W/Mo). The results in table 9.1 illustrate that the addition of the potassium promoter to the carbide catalyst causes a significant reduction in the surface area of especially the Mo₂C catalyst. This must be ascribed to plugging of the catalyst pores by the alkali salt.

In the present investigations the alkali promoter is added by aqueous impregnation of the prepared carbide rather than by addition of alkali to the oxide precursor prior to the carburization. This choice of adding alkali after the carburization is based upon the results of Kojima and Aika [262] who observed that addition of an alkali salt to the MoO₃

precursor prior to the carburization hampered the carburization in 20 vol% CH_4 in H_2. Instead the attempted carburization of Alkali/MoO_3 only resulted in the formation of metallic Mo [262]. Bengaard et al. [458] observed that the adsorption of potassium on nickel surfaces led to a dramatic reduction in the methane sticking probability on the K/Ni surfaces. Through DFT calculations Bengaard et al. [458] determined that the methane molecule during adsorption passes through a transition state with a relatively large dipole moment. It is the repulsive interaction between potassium and the inducted dipole moment of the methane transition state complex that raises the energy barrier for methane dissociation and lowers the sticking probability of methane [458]. It seems likely that a similar effect of alkali reduces the sticking probability of methane during the carburization of an alkali promoted precursor, and this reduced sticking probability will hamper or prohibit the carburization by limiting the amount of carbon available on the surface of the material. It should be mentioned that Kojima and Aika [262] were able to convert the Alkali/MoO_3 precursor into a molybdenum nitride by treatment in a flow of NH_3, and the nitride could subsequently be carburized in a flow of 20 vol% CH_4 in H_2. It is however difficult to determine, how the nitridation influences the state and location of the alkali promoter.

The data in table 9.1 also clearly illustrate that the spent K_2CO_3/WC catalyst and especially the K_2CO_3/Mo_2C catalysts have considerably lower surface areas than the fresh catalysts. As it will be shown below these catalysts also experience a gradual loss of activity. Within the uncertainty the particle sizes estimated from the XRD diffractograms are identical for the fresh and spent carbides indicating that sintering is not a significant problem for the carbide catalysts at these conditions. The carbides have very high melting points [459], and this should signify a low propensity towards sintering. Another possibility might be that carbonaceous deposits formed during the CO hydrogenation blocks the pores of the catalyst and lowers the available surface area. For the spent K_2CO_3/Mo_2C catalyst, which has been on stream of 95 h and has been used in the experiments presented in section 3.2, the mass of the sample in the reactor has increased by approximately 11 % during the experiment. This could be an indication that the catalyst has taken up carbon. Judging from the mass balance the unidentified products of the CO hydrogenation are very carbon rich. This is consistent with the notion of carbon deposition occurring during the reaction. Previously several other authors [260, 261, 274, 416] have reported an increased catalyst carbon content in Mo_2C catalysts used for CO hydrogenation. There are thus good indications that the carbide catalysts loose surface area as a result the build-up of carbonaceous deposits during CO hydrogenation. The possible problems with carbon deposition may be reduced by operating at a higher H_2/CO ratio than the ratio of H_2/CO $\cong$ 1, which has been utilized in the present investigations. In the determination of the surface area of the spent catalysts an element of uncertainty is however that minor amounts of long-chained products are formed in the reaction. This may lead to the formation of waxy deposits in the pores of the catalyst, and if these deposits are not removed in the evacuation procedure this would influence the surface area measurement. The surface area of the evaluated NbC catalyst is unchanged after the CO hydrogenation experiment. As it will be shown subsequently this catalyst is also essentially inactive in syngas conversion.

Table 9.1 shows that there in general are quite significant differences between the average particle diameters predicted from the XRD and BET results. This is something

that also has been reported by other authors [258]. The greatest similarity between the particle size estimates are observed for the fresh samples of Mo_2C and NbC. The blocking of pores by the promoter salt or by carbonaceous deposits formed during carburization and CO hydrogenation diminishes the apparent surface area, and this will lead to an increased estimate of the particle size on the basis of the surface area. This fact is presumably a significant part of the explanation for the discrepancies in the particle size estimates for potassium promoted and spent catalysts.

A TEM analysis of the carbides can provide the rest of the explanation for the discrepancies in the particle size estimates. Figure 9.3 shows the particle size distribution obtained from TEM for different catalyst samples.
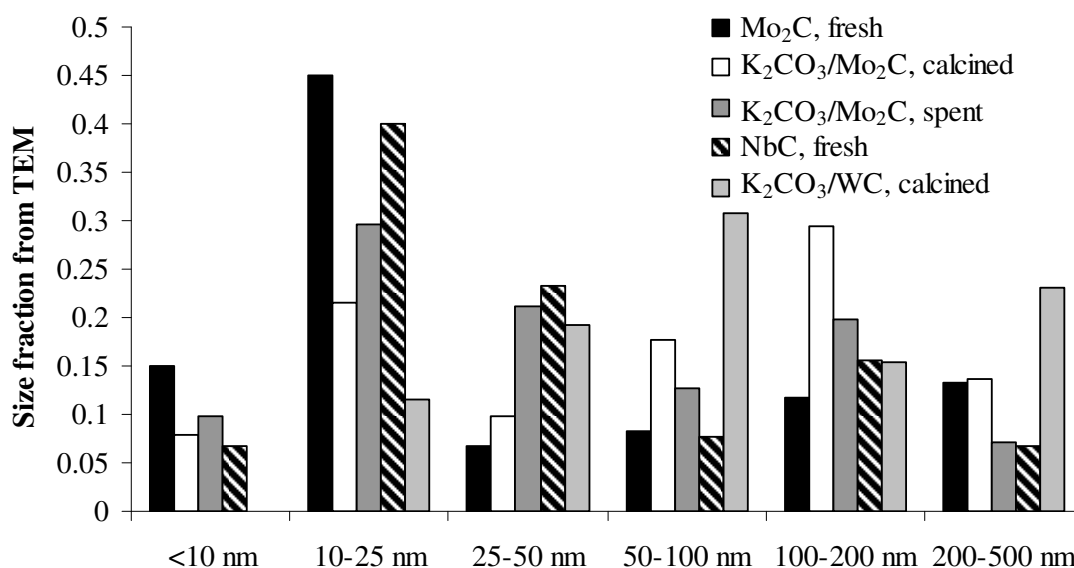
Figure 9.3 The number based particle size distribution from TEM for various carbide catalysts. For the Mo_2C-based catalyst the distribution is based upon 51-71 particles, for NbC 90 particles are used, and for K_2CO_3/WC 26 particles are used.

Figure 9.3 illustrates that the catalysts have a large fraction of their particles in the 10-25 nm range, which is relatively consistent with the size estimate from XRD, but figure 9.3 also shows that the catalysts contain a significant fraction of larger particles (> 100 nm). These larger particles are however not monocrystalline, but composed of many smaller crystalline domains. This is illustrated in figure 9.4, which shows bright- and darkfield TEM images of a freshly carburized, unpromoted Mo_2C particle.

167
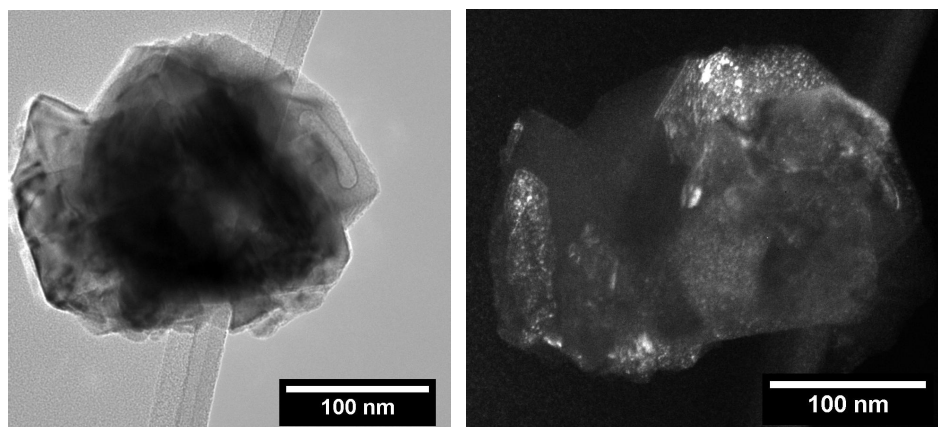
Figure 9.4 Left: Brigthfield TEM image of a freshly carburized NbC particle. Right: Darkfield image of the same particle obtained from primarily a single diffraction spot, whereby all the regions with a crystal direction corresponding to that diffraction spot are illuminated.

In the darkfield image in figure 9.4 the regions with the same crystal orientation are lit up, and the extent of these crystalline domains are in the range of 5-30 nm, which also is consistent with the particle size estimate from XRD. That the larger particles are composed of smaller crystalline domains, which are similar in size to the predominant smaller particles could suggest that the larger particles are formed from coagulation of the smaller particles at the high temperatures of the carburization process. The differences in the particle size estimates from XRD and BET thus arise from the fact that XRD provides an estimate of the size of the crystalline domains, while at least some of the particles are polycrystalline and considerably larger than the individual crystalline domains.

In the the particle size distribution from TEM there is of course and element of uncertainty due to the limited number of particles considered, but based upon the data in figure 9.3 there does not seem to be any discernible sintering of the Mo_2C catalyst during use.

9.4 Catalytic properties of carbides

Figure 9.5 shows the developments in CO conversion and CO_2-free alcohol selectivity as functions of the time on stream with stepwise changes in temperature for the K_2CO_3/Mo_2C catalyst.
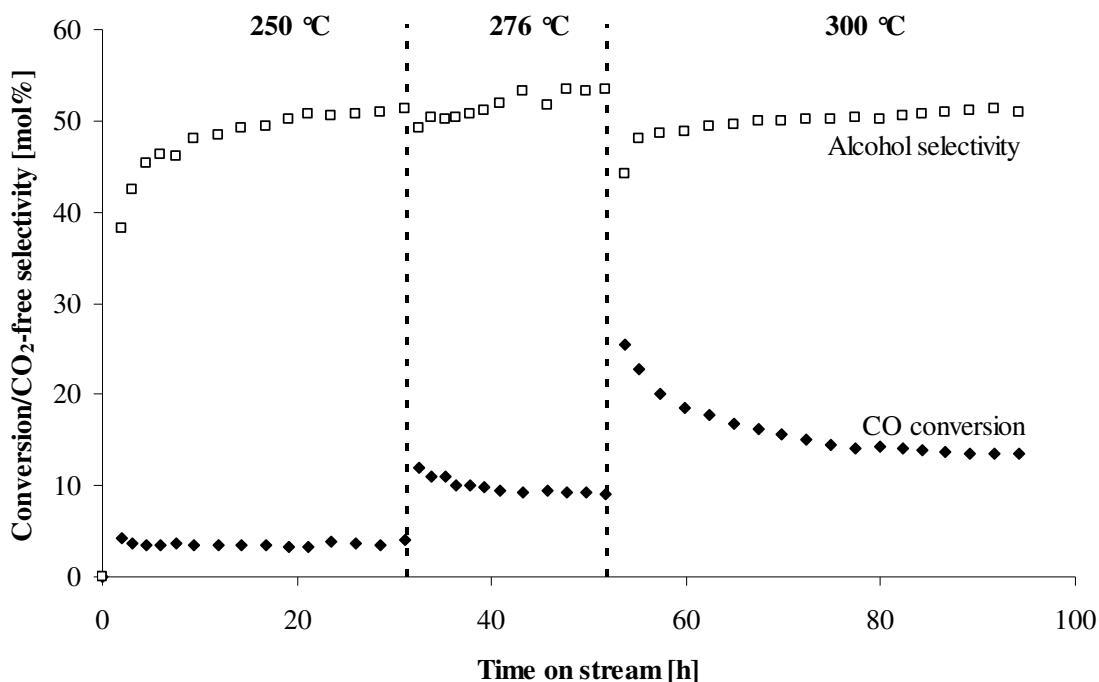
Figure 9.5 The CO conversion and the alcohol selectivity as functions of the time on stream with stepwise changes in temperature for the K_2CO_3/Mo_2C catalyst. The experimental conditions are: P = 100 bar, GHSV = 4975 h^{-1}, Feed: 49.7 vol% H_2, 50.3 vol% CO.

Figure 9.5 illustrates that the activity under these conditions is stable at 250 °C, while a gradual decline in activity can be observed at higher temperatures. It is quite reasonable to assume that the gradual decline in activity is linked to the significant loss of surface area in the K_2CO_3/Mo_2C catalyst (see table 9.1). This gradual decline in activity with time on stream is a common observation for molybdenum carbide catalysts [115, 274]. Figure 9.5 illustrates that the alcohol selectivity gradually increases to a stabilized level. An increase in temperature lowers the selectivity, but over time the selectivity increases and approaches the same stabilized level. The reason for the increasing selectivity is that the gradual decline in the production rate of hydrocarbons is greater than the decline in the production rate of alcohols. Figure 9.6 shows the space time yields of alcohols and hydrocarbons during the experiment presented in figure 9.5.
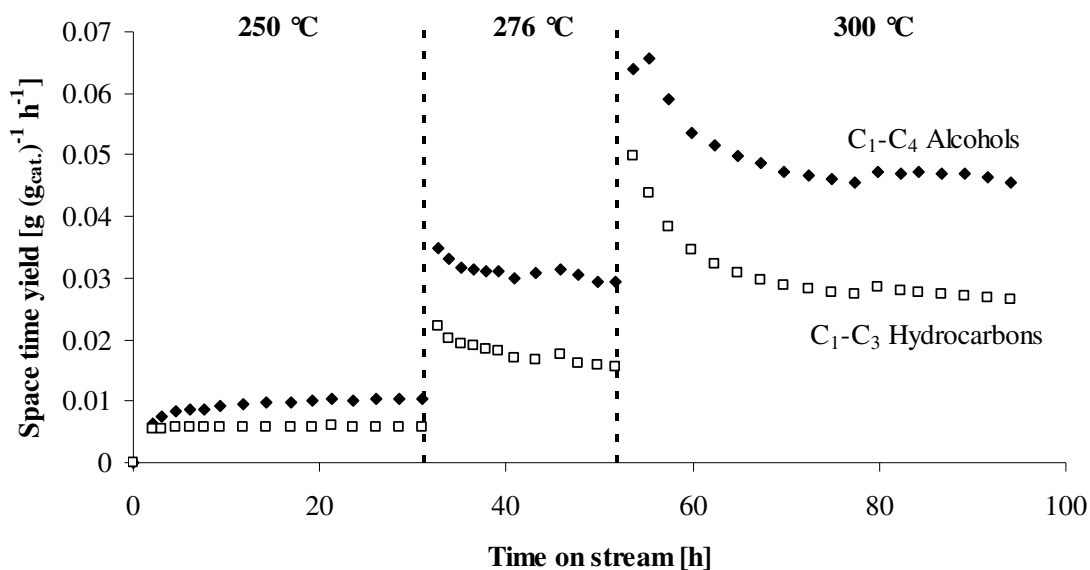
Figure 9.6 The space time yields of C_1-C_4 alcohols and C_1-C_3 hydrocarbons as functions of the time on stream with stepwise changes in temperature for the K_2CO_3/Mo_2C catalyst. The experimental conditions are given in the legend of figure 9.5.

Figure 9.6 also illustrates that the production rates of alcohols and hydrocarbons appear to stabilize at 250 °C, while a gradual deactivation is observed at higher temperatures. The gradual decline in the alcohol production, which is observed at higher temperatures, is the result of a decreasing production of higher alcohols. This is illustrated in figure 9.7, which shows the development in the production rates of methanol and higher alcohols as functions of time on stream.
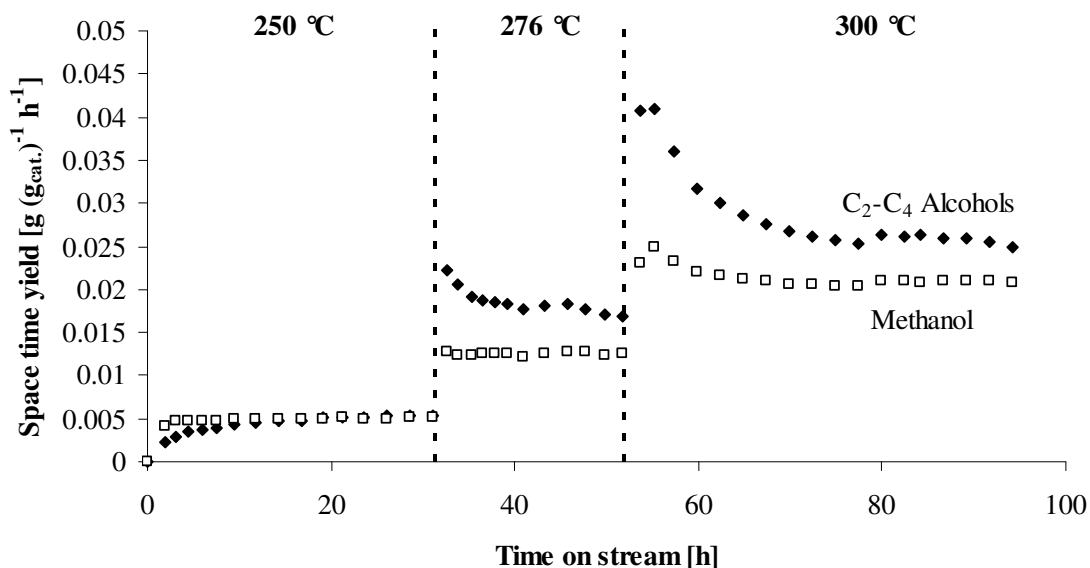
Figure 9.7 The space time yields of methanol and higher alcohols as functions of the time on stream with stepwise changes in temperature for the K_2CO_3/Mo_2C catalyst. The experimental conditions are given in the legend of figure 9.5.

Figure 9.7 shows that the methanol production rate is fairly stable - even at the higher temperatures the decline in the production of methanol is less marked than the decline in the production of higher alcohols. A comparison of figure 9.6 and figure 9.7 illustrates that the development in the production of higher alcohols parallels the production of hydrocarbons.

At the two higher temperatures (276 °C and 300 °C) investigated in figure 9.5-figure 9.7 there seems to be a gradual decline in the activity of the K_2CO_3/Mo_2C catalyst throughout the experiment, although the rate of deactivation seems to slow down over time. As stated above, the gradual decline in catalytic activity is most likely linked to the observed loss of surface area. In section 9.3 it is discussed how the most probable cause for the loss of surface area is the build-up of carbonaceous deposits on the catalyst. The build-up of larger carbonaceous deposits could well be related to the sites related to chain growth, and these sites may therefore be blocked first. This could explain the observed development, where the production of higher alcohols declines, while the methanol production seems more stable. As the catalyst gradually becomes blocked by carbonaceous deposits it does however seem likely that also the methanol production eventually will begin to decline.

Table 9.2 summarizes the activity and selectivity of K_2CO_3/Mo_2C, K_2CO_3/WC and NbC at various conditions.

Table 9.2 Behavior of various carbide catalysts in CO hydrogenation. Experimental conditions: P = 100 bar, H_2/CO = 1.0 mol/mol GHSV = 5000 ± 25 h^{-1}.

Catalyst	T [°C]	TOS [a] [h]	X_{CO} [mol%]	Carbon based, CO_2-free selectivity [mol%]							
				MeOH	EtOH	1-PrOH	1-BuOH	CH_4	C_2H_4	C_2H_6	C_3H_8
K_2CO_3/Mo_2C	250	31	3.8	20.1	19.2	7.6	2.9	26.1	9.4	5.0	8.5
K_2CO_3/Mo_2C	276	48	9.3	17.5	20.6	10.2	3.3	24.4	8.9	5.1	7.9
K_2CO_3/Mo_2C	300	55	22.8	13.9	19.3	10.1	2.9	27.6	8.7	6.7	8.4
K_2CO_3/Mo_2C	300	94	13.4	18.4	18.5	10.1	2.5	27.7	7.1	6.7	7.1
K_2CO_3/WC	350	11	2.7	49.5	4.0	5.0	0.5	22.9	9.6	2.8	3.5
K_2CO_3/WC	375	15	3.8	39.3	5.0	6.7	0.8	27.6	10.3	3.5	4.3
NbC	350	10	0.5	0.1	0	0	0	91.4	0.3	6.8	1.5

[a] The time on stream.

Table 9.2 shows that the K_2CO_3/Mo_2C catalyst at 276 °C is able to provide a selectivity to ethanol, which is very close to the methane selectivity. This is a reasonably good result, but the overall alcohol selectivity, which only amounts to 53 mol%, leaves room for further improvements. The catalysts based upon WC and NbC are observed to possess a low activity in CO hydrogenation. For these carbides the temperature had to be increased significantly, before a catalytic activity was observed. As part of the background for the low activity one should remember the limited surface areas of the carbides prepared in the present investigations (see table 9.1). It is also well established that carbonaceous deposits formed during the carburization can further reduce the area of the catalytically active surface [250, 254]. Niobium carbide is observed to be essentially inactive in CO hydrogenation. At 350 °C only a slight CO conversion is observed with methane being the only important product. The tested K_2CO_3/WC catalyst primarily produces C_1 species, namely methane and methanol, with a low activity. The K_2CO_3/WC catalyst produces minor amounts of the higher alcohols ethanol, 1-propanol and iso-butanol. This behavior is similar to alkali modified methanol synthesis catalysts over

171

which chain-growth primarily occurs via aldol condensation reactions [70, 71]. No deactivation of the K_2CO_3/WC catalyst is observed during a 12 h run at 350 °C, but this is somewhat uncertain due to the low activity. At 375 °C a slight, gradual deactivation is observed, and the specific surface area of this catalyst has also decreased from 1.1 m^2/g to 0.5 m^2/g during the catalytic test (see table 9.1).

A source of uncertainty in the determination of the alcohol selectivity, particularly for the K_2CO_3/Mo_2C catalyst, is that minor amounts of C_{4+} hydrocarbons and C_{5+} alcohols are formed. Judging from the trend in the characterized products the amount of the higher species is not large, but over time the production of very high boiling products might also cause problems in the CO hydrogenation. For the K_2CO_3/Mo_2C catalyst, which has been on stream for 95 h it is possible to observe traces of waxy deposits at the end of the catalytst bed. If oil gradually is formed in the pores of the catalyst that could in principle introduce mass transport limitations, which will hamper the reaction rate, in the same way as it is observed in the Fischer-Tropsch reaction [460].

An issue, which deserves a comment, is the CO_2 production arising from the shift of water formed in the synthesis reaction. In this work the selectivity is generally expressed on a CO_2-free basis. Molybdenum carbide is however known to exhibit an activity for the water gas shift reaction [461, 462], and CO_2, which inevitably is formed in the shift reaction, is a major part of the reaction product. Table 9.3 presents the carbon based selectivities to alcohols, hydrocarbons and CO_2 for the experiments described in table 9.2.

Table 9.3 Behavior of various carbide catalysts in CO hydrogenation. The experimental conditions are given in the legend of table 9.2.

Catalyst	T	TOS [a]	X_{CO}	Carbon based selectivity [mol%]		
	[°C]	[h]	[mol%]	Alcohols	Hydrocarbons	CO_2
K_2CO_3/Mo_2C	276	48	9.3	27.4	23.7	48.7
K_2CO_3/Mo_2C	300	55	22.8	24.4	26.1	49.2
K_2CO_3/Mo_2C	300	94	13.4	26.0	27.3	46.6
K_2CO_3/WC	350	11	2.7	39.0	24.6	36.6
K_2CO_3/WC	375	15	3.8	32.0	26.9	41.1
NbC	350	10	0.5	0.1	67.8	32.2

[a] The time on stream.

The CO_2 selectivity observed for the K_2CO_3/Mo_2C catalyst is quite consistent with previous observations for this system [115]. The CO_2 selectivity for the WC based catalyst is similar to what has been observed in some studies of tungsten carbide [388], but in other cases only a negligible CO_2 production has been observed for tungsten carbide [251]. For all the presently evaluated catalysts except NbC it is observed that the CO_2 selectivity is larger than what would be expected from the characterized products – even with full shift of all the water formed in the synthesis reaction. It is discussed above that carbonaceous deposits gradually may be formed on the catalyst, and the removal of the oxygen from the C-O dissociation steps giving rise to the carbonaceous deposits may account for part of the CO_2 produced over the carbide catalyst. As discussed above there is also a production of uncharacterized, larger alcohols and hydrocarbons, which may lead to CO_2 production.

Table 9.4 contains a comparison of the presently evaluated carbide catalysts and carbide catalysts investigated in the literature with respect to the alcohol productivity and

selectivity. The comparison in table 9.4 illustrates that the behavior of the presently investigated K_2CO_3/Mo_2C catalyst is quite similar to the behavior observed in previous reports on this system at similar conditions. When behavior of the presently evaluated K_2CO_3/WC catalyst is compared to the behavior reported for unmodified WC, it is clear that the alkali promoter lowers the overall activity, but shifts the selectivity from hydrocarbons towards alcohols. This is consistent with the influence that potassium promotion is observed to have upon Mo_2C [115, 121, 122].

Table 9.4 shows that the presently achieved alcohol production rates are in the same order as the previously results, but the achieved space time yields are quite low. This must in no small part be ascribed to the fact that the surface areas of the final, potassium promoted carbides are quite small (see table 9.1). Considering that the surface area of the spent K_2CO_3/Mo_2C catalyst, after the 95 h of operation in figure 9.6, has dropped to 0.2 m^2/g, the activity per surface area actually seems quite good for the Mo_2C-based catalyst. A possibility for enhancing the available carbide surface area and thereby the activity might be to employ supported systems instead of the presently used bulk carbides. Judging from the results with WC presented in table 9.4 TiO_2 might be a promising support for carbide based alcohol synthesis catalysts.

Table 9.4 Comparison of the presently evaluated carbide catalysts to reports in the literature.

Catalyst	$STY^{a)}$ $\left[\frac{g}{mL\ cat.\cdot h}\right]$	$X_{CO}{}^{b)}$ [mol%]	$S_{Alc}{}^{c)}$ [mol%]	$S_{C_{2+},Alc}{}^{d)}$ [mol%]	P [bar]	T [°C]	GHSV [h^{-1}]	$\frac{H_2}{CO}$	Ref.
K$_2$CO$_3$/WC	0.020 $^{e)}$	2.7	61.1	11.7	100	350	5020	1.0	
K$_2$CO$_3$/WC	0.027 $^{e)}$	3.8	54.1	14.8	100	375	5020	1.0	This work
NbC	0	0.5	0.1	0	100	350	4975	1.0	
K$_2$CO$_3$/Mo$_2$C	0.086 $^{e)}$	13.4	51.0	32.6	100	300	4975	1.0	
K$_2$CO$_3$/β-Mo$_2$C		10.3	50.5	28.6	80	300	3460 $^{f)}$	0.98	[115]
K$_2$CO$_3$/β-Mo$_2$C	0.122	23.4	52.6	33.8	80	300	2000	1.0	[121, 122]
K$_2$CO$_3$/α-MoC$_{1-x}$	0.021	15.5	41.5	21.6	80	300	2000	1.0	[122]
K$_2$CO$_3$/α-MoC$_{1-x}$		7.9	44.5	27.9	80	300	4870 $^{f)}$	0.98	[115]
β-Mo$_2$C		59.0	3.8	1.3	80	300	3460 $^{f)}$	0.98	[115]
α-MoC$_{1-x}$		70.3	1.3	0.16	80	300	2000	1.0	[122]
Mo$_2$C		7.8	10.8	4.5	50	220	3150	2	[395]
α-WC		6.9	18.8	10.3	50	300		2	[251]
WC/TiO$_2$		14.4	51.3	15.7	50	300		2	[251]
WC/Al$_2$O$_3$		2.4	8.2 $^{g)}$	0	50	300		2	[251]
α-WC		2	37.4 $^{h)}$		50	200	6000	2	[388]
α-WC		16	3.8		50	260	6000	2	[388]
α-W$_2$C		9.8	0	0	50	300		2	[251]
Effect of anion in alkali salt at K/Mo = 0.4 mol/mol									
K$_2$CO$_3$/β-Mo$_2$C		10.6	33.1	27.6	10	300	2400 $^{f)}$	1	[116]
KOH/β-Mo$_2$C		8.3	34.7	27.6	10	300	2400 $^{f)}$	1	[116]
CH$_3$COOK/β-Mo$_2$C		10.4	31.3	25.6	10	300	2400 $^{f)}$	1	[116]
KCl/β-Mo$_2$C		25.0	1.4	0.3	10	300	2400 $^{f)}$	1	[116]
K$_2$SO$_4$/β-Mo$_2$C		28.3	2.1	0.4	10	300	2400 $^{f)}$	1	[116]
Effect of transition metal promoters Me/Mo = 1/8 mol/mol (Me = Fe, Ni, Co), K/Mo = 0.2 mol/mol									
K$_2$CO$_3$/Co/β-Mo$_2$C	0.156	40.8	42.6	29.9	80	300	2000	1.0	[118, 119]
K$_2$CO$_3$/Ni/β-Mo$_2$C	0.324	73.0	44.9	32.9	80	300	2000	1.0	[117, 118]
K$_2$CO$_3$/Fe/β-Mo$_2$C	0.075	22.0	42.0	29.0	80	300	2000	1.0	[118, 120]

$^{a)}$ The space time yield of alcohols. $^{b)}$ The CO conversion. $^{c)}$ Overall carbon based alcohol selectivity on a CO$_2$-free basis. $^{d)}$ Carbon based selectivity to ethanol and higher alcohols on a CO$_2$-free basis. $^{e)}$ This is the alcohol production relative to the entire volume of the catalytic bed (particles + voids). $^{f)}$ The unit of the gas hourly space velocity is L(STP)/(kg cat.·h). $^{g)}$ This is the combined selectivity to methanol and DME. No higher alcohols are observed. $^{h)}$ The exact distribution is of the alcohol product is not reported, but it is stated that methanol is the dominant alcohol.

9.5 Effect of the alkali promoter

As discussed in sections 2.4.1, 9.3 and 9.4 the use of an alkali promoter is of great importance in achieving a reasonable alcohol selectivity in CO hydrogenation over carbide catalysts. It would therefore be valuable to establish how the nature of the alkali cation influences the alcohol synthesis over the carbide catalysts. For this reason the promoting effect that K_2CO_3, Cs_2CO_3 and $Li(CH_3COO)$ have on the alcohol synthesis over Mo_2C has been evaluated. The choice of lithium acetate is based upon the solubility of the lithium salts. Lee et al. [116] have previously evaluated the role of the anion in potassium promoted Mo_2C, and found that the use of carbonate and acetate salts gave catalysts with similar properties (see table 9.4). Table 9.5 summarizes the activity and selectivity of Mo_2C promoted with Li, K and Cs.

The results in table 9.5 on the following page illustrate that the heavier alkali metals K and Cs behave similarly with potassium providing the better performance, when Cs_2CO_3/Mo_2C and K_2CO_3/Mo_2C are compared at the same conditions. It is difficult to operate the lithium promoted catalyst at the same conditions as the catalysts promoted with cesium or potassium. When the Li promoted carbide at the conditions given in the legend of table 9.5 is operated at elevated temperatures ($\geq$275 ºC) there is a tendency for the catalyst to "ignite" and cause a large feed conversion with hydrocarbons as the only important products. In this case the Li promoted carbide behaves more like unpromoted Mo_2C, which at similar conditions produces hydrocarbons at a high feed conversion (see table 9.5). With the presently employed experimental setup the heat evolved in the exothermic synthesis reaction makes it difficult to maintain the desired reactor temperature, when the reaction "ignites" over the Li promoted catalyst. For the entry in table 9.5, where it is attempted to operate a Li promoted catalyst at a nominal temperature of 275 ºC, the temperature in the front end of the bed, where most of the conversion presumably takes place, is actually 281 ºC. Given that the temperature as described in section 2.3 is measured on the outside of the quartz tube holding the catalyst, the actual temperature in the front end of the catalyst bed might be even higher than the measured temperature of 281 ºC. The temperature in the rear end of the bed is on the other hand only 271 ºC. At identical conditions lithium therefore appears to be inferior to cesium or potassium as a promoter for the alcohol synthesis. However the results in table 9.5 also illustrate that if the three alkali promoters are compared at the same general activity level (X_{CO} = [5.6-9.3]), corresponding to the Li promoted catalyst being operated at a lower temperature than the K or Cs promoted catalysts, there is actually not a very large difference between the behaviors achieved with the three promoters. In this case the Li promoted carbide gives only a slightly lower alcohol selectivity than the K-promoted carbide.

Table 9.5 Behavior of Alkali/Mo_2C (Alkali/Mo = 0.164±0.001 mol/mol) catalysts in CO hydrogenation. Experimental conditions: P = 100 bar, GHSV = 5000 ± 25 h^{-1}, H_2/CO = 1.0 mol/mol.

Catalyst	T [ºC]	TOS [a] [h]	X_{CO} [mol%]	Carbon based, CO_2-free selectivity [mol%]							
				MeOH	EtOH	1-PrOH	1-BuOH	CH_4	C_2H_4	C_2H_6	C_3H_8
K_2CO_3/Mo_2C	276	48	9.3	17.5	20.6	10.2	3.3	24.4	8.9	5.1	7.9
K_2CO_3/Mo_2C	300	94	13.4	18.4	18.5	10.1	2.5	27.7	7.1	6.7	7.1
Cs_2CO_3/Mo_2C	275	40 [b]	5.6	21.3	18.4	9.1	2.5	28.3	6.4	4.9	5.5
Cs_2CO_3/Mo_2C	301	34	11.7	15.3	16.6	10.1	2.2	32.8	7.2	6.1	6.3
$Li(CH_3COO)$/Mo_2C	250	25	7.4	13.9	18.5	9.5	3.5	28.0	3.6	9.5	10.8
$Li(CH_3COO)$/Mo_2C	275 [c]	5	90.7	0.8	0.1	0.1	0	53.2	0.4	27.7	16.0

[a] The time on stream. b) The catalyst has been operated at 300 ºC for the first 34 h, and the temperature was then reduced to 275 ºC. [c] This is an average of the temperature along the catalyst bed. In this case the temperature in the front end of the catalyst bed is 281 ºC, while the temperature in the rear end of the bed is only 271 ºC.

At 250 °C the Li(CH$_3$COO)/Mo$_2$C catalyst, just like the K$_2$CO$_3$/Mo$_2$C catalyst, appears to be quite stable. This is illustrated in figure 9.8, which shows various properties of the Li(CH$_3$COO)/Mo$_2$C catalyst as functions of the time on stream. No investigations were made of the long-terms stability of the Li promoted carbide at elevated temperatures, where the conversion is very high.

Figure 9.8 The CO conversion, alcohol selectivity and the space time yields of alcohols and hydrocarbons as functions of the time on stream for the Li(CH$_3$COO)/Mo$_2$C catalyst. The experimental conditions are T = 250 °C, P = 100 bar, GHSV = 4990 h^{-1}, Feed: 49.3 vol% H$_2$, 50.7 vol% CO.

The behavior of the Cs$_2$CO$_3$ promoted carbide is very similar to the behavior of the K$_2$CO$_3$/Mo$_2$C catalyst described in section 3.2. At a temperature of 300 °C the production rates of both alcohols and hydrocarbons undergo a slow decline. This is illustrated in figure 9.9, which shows the development in the catalytic properties of the Cs$_2$CO$_3$/Mo$_2$C with time on stream. The entry for the Cs$_2$CO$_3$/Mo$_2$C catalyst at 300 °C in table 9.5 is after 34 h on stream, where the decline in activity has slowed down considerably.
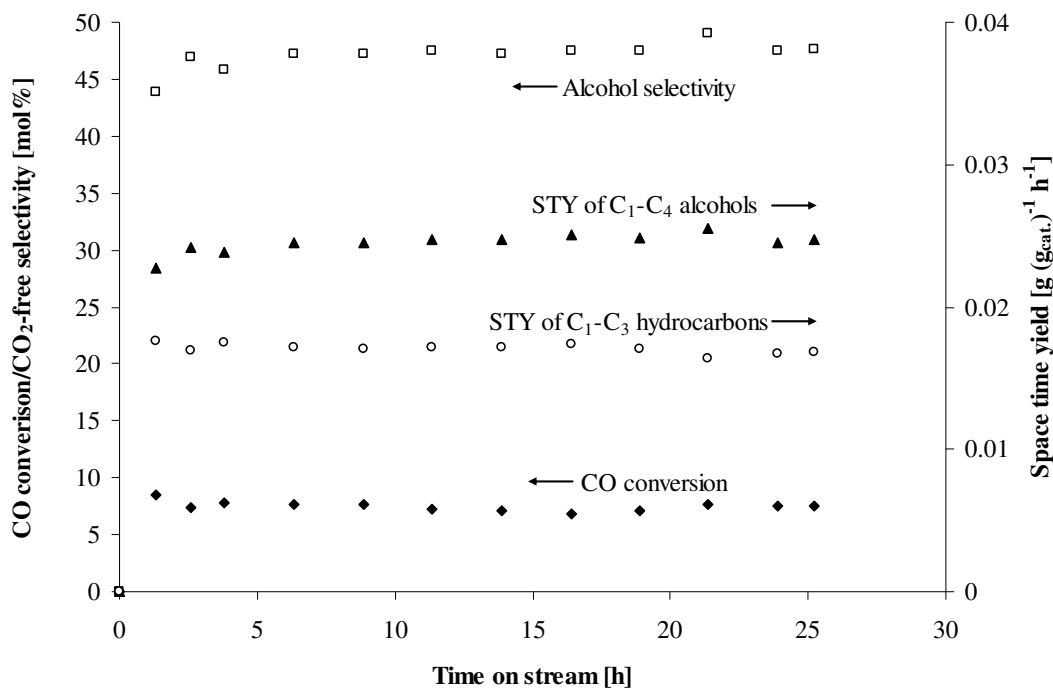
177
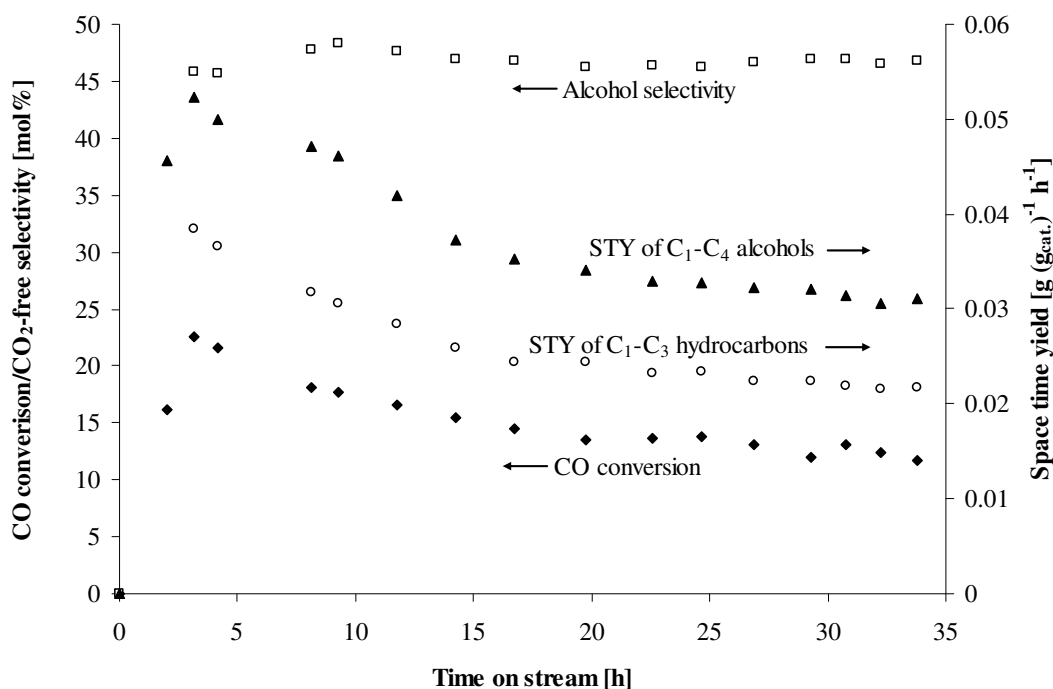
Figure 9.9 The CO conversion, alcohol selectivity and the space time yields of alcohols and hydrocarbons as functions of the time on stream for the Cs_2CO_3/Mo_2C catalyst. The experimental conditions are T = 301 °C, P = 100 bar, GHSV = 4980 h^{-1}, Feed: 49.4 vol% H_2, 50.6 vol% CO.

Figure 9.10 illustrates the space time yields of different product classes for the Mo_2C catalysts promoted by different alkali cations.

The space time yields shown in figure 9.10 emphasize the previously discussed results. At the same conditions the potassium promoted catalyst behaves somewhat better than the cesium promoted carbide, and at the same general activity level there is not a huge difference between Mo_2C promoted by $Li(CH_3COO)$ and K_2CO_3. Here it should however be emphasized that the concentration of the alkali promoter is based upon the level that Woo et al. [115] found to be sufficient for K_2CO_3. For alcohol synthesis over alkali promoted molybdenum sulfide the ranking of the alkali cations has been observed [184] to depend upon the Alkali/Mo ratio, and this may also be the case for Mo_2C. It is therefore possible that a comparison at a different promoter concentration might yield different results. With the current promoter level the large molar mass of cesium means that quite a large amount of Cs_2CO_3 must be added to the carbide (see table 4.7 on page 88), and this migth be prohibitive for the activity of the catalyst. For the experiment with the Cs promoted catalyst at 275 °C it must also be remembered that the catalyst previously has been operated for a long period at 301 °C, where a significant deactivation occurs (see figure 9.9), and this is a significant part of the reason for the low acticity. That being stated the conclusion on the basis of the present results must be that potassium, at a promoter level of Alkali/Mo = 0.164±0.001 mol/mol, seems to be the best choice for the alkali cation in the promoter salt.
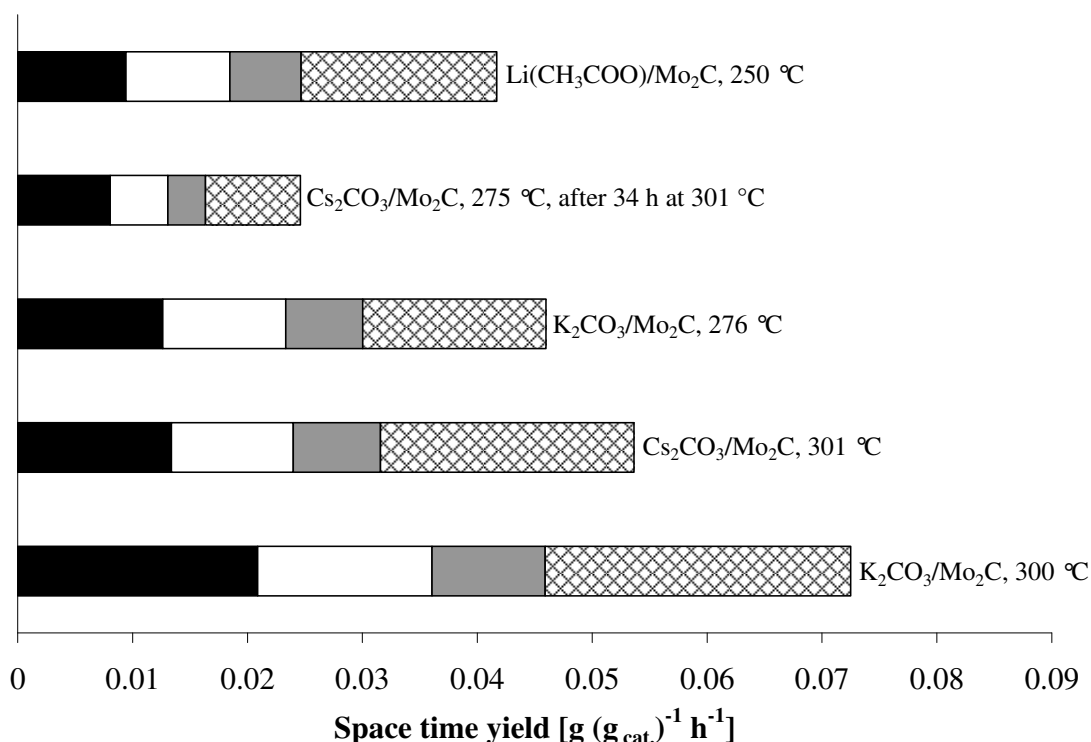
Figure 9.10 The space time yields of methanol (dark bar), C_2-C_4 alcohols (white bar) and C_1-C_3 hydrocarbons (hatched bar) for Mo_2C promoted with different alkali cations. The experimental conditions and the time for which the catalysts have been on stream are given in table 9.5.

9.6 Properties of promoted K_2CO_3/Mo_2C catalysts

As described in the preceding sections molybdenum carbide is the only one of the three tested carbides with a significant propensity towards the production of higher alcohols. While the alcohol product formed over K_2CO_3/Mo_2C is reasonably well shifted towards the higher alcohols, the carbide catalyst is nevertheless only able to provide a moderate alcohol selectivity and a relatively low alcohol space time yield. One way to further boost the alcohol production over the K_2CO_3/Mo_2C catalyst might be through promotion of the catalyst with further additives. Presently it has been attempted to improve the K_2CO_3/Mo_2C catalyst by modification with a few additives that previously have been observed to exert a beneficial effect upon alcohol synthesis catalysts, namely Cu, Re, Mn and La + V. There are various factors that have led to the selection of these additives. Cupper is active for the methanol synthesis, and an improvement in the methanol synthesis activity could improve the production of higher alcohols, since methanol might be a precursor in the production of higher alcohols. The use of manganese as a support or promoter has been reported to benefit the alcohol synthesis over a wide variety of catalytic systems [16, 463-466]. Promotion by rhenium has been reported to benefit the

179

ethanol selectivity in CO hydrogenation over Co based catalysts [82, 467]. Recently promotion by La and V were reported to boost the ethanol selectivity of rhodium [87]. Table 9.6 summarizes the activities and selectivities of various multiply promoted carbide catalysts.

Figure 9.11 illustrates the space time yields of various product classes for the promoted Mo_2C catalysts. A few conclusions can be drawn on the results presented in table 9.6 and figure 9.11. The performances of the catalysts promoted by Re and Mn are very similar to the performance of the unmodified K_2CO_3/Mo_2C catalyst. With the presently employed experimental conditions and catalyst preparation procedures Re and Mn thus appear to have a very limited influence on the catalytic activity. As illustrated in figure 9.11 the main effect of the Re/Mn addition is a slight decrease in the alcohol production rate. The catalyst with 5 wt% Mn provides a larger conversion than the basic K_2CO_3/Mo_2C system, but the production rates of the characterized compounds are similar for the two systems. This is mainly related to a larger CO_2 production for the $K_2CO_3/Mn(5)Mo_2C$ system. Apart from experimental uncertainty the increased CO_2 production may be the result of an increased production of unidentified products like carbonaceous deposits and higher alcohols/hydrocarbons. The gradual decline in the production rates of hydrocarbons and higher alcohols, which is observed for the unmodified K_2CO_3/Mo_2C catalyst is also observed for the catalysts promoted with Re and Mn. The activity levels presented in table 9.6 and figure 9.11 are again the values after prolonged exposure to syngas, where the deactivation has slowed down considerably.

Table 9.6 CO conversion and selectivity for various multiply promoted carbide catalysts. Experimental conditions: P = 100 bar, GHSV = 4980 ± 25 h^{-1}, H$_2$/CO = 1.00 ± 0.04 mol/mol.

Catalyst	T [ºC]	TOS [h] [a]	X_{CO} [mol%]	Carbon based, CO$_2$-free selectivity [mol%]							
				MeOH	EtOH	1-PrOH	1-BuOH	CH$_4$	C$_2$H$_4$	C$_2$H$_6$	C$_3$H$_8$
K$_2$CO$_3$/Mo$_2$C	300	94	13.4	18.4	18.5	10.1	2.5	27.7	7.1	6.7	7.1
K$_2$CO$_3$/Re(1)/Mo$_2$C	301	50	13.4	19.0	18.4	7.7	1.4	29.7	7.3	7.5	7.2
K$_2$CO$_3$/Mn(1)/Mo$_2$C	300	28	13.3	17.9	18.3	8.4	1.9	28.6	7.8	7.2	8.3
K$_2$CO$_3$/Mn(5)/Mo$_2$C	300	36	15.7	13.6	18.9	9.2	2.9	27.9	7.5	8.3	9.4
K$_2$CO$_3$/Mo$_2$C	276	48	9.3	17.5	20.6	10.2	3.3	24.4	8.9	5.1	7.9
K$_2$CO$_3$/Mn(5)/Mo$_2$C	275	44 [b]	4.6	19.5	18.5	9.8	2.7	25.1	5.6	6.9	7.5
Cu(0.84)/K$_2$CO$_3$/Mo$_2$C	275	28	11.8	18.0	21.8	10.3	4.1	22.9	7.8	5.1	7.7
La(CH$_3$COO)$_3$/V/Mo$_2$C	275	6	12.2	9.7	11.2	5.3	0.4	35.9	3.5	16.5	14.4

[a] The time on stream. [b] The catalyst has been operated at 300 ºC for the first 36 h, and the temperature was then reduced to 275 ºC.
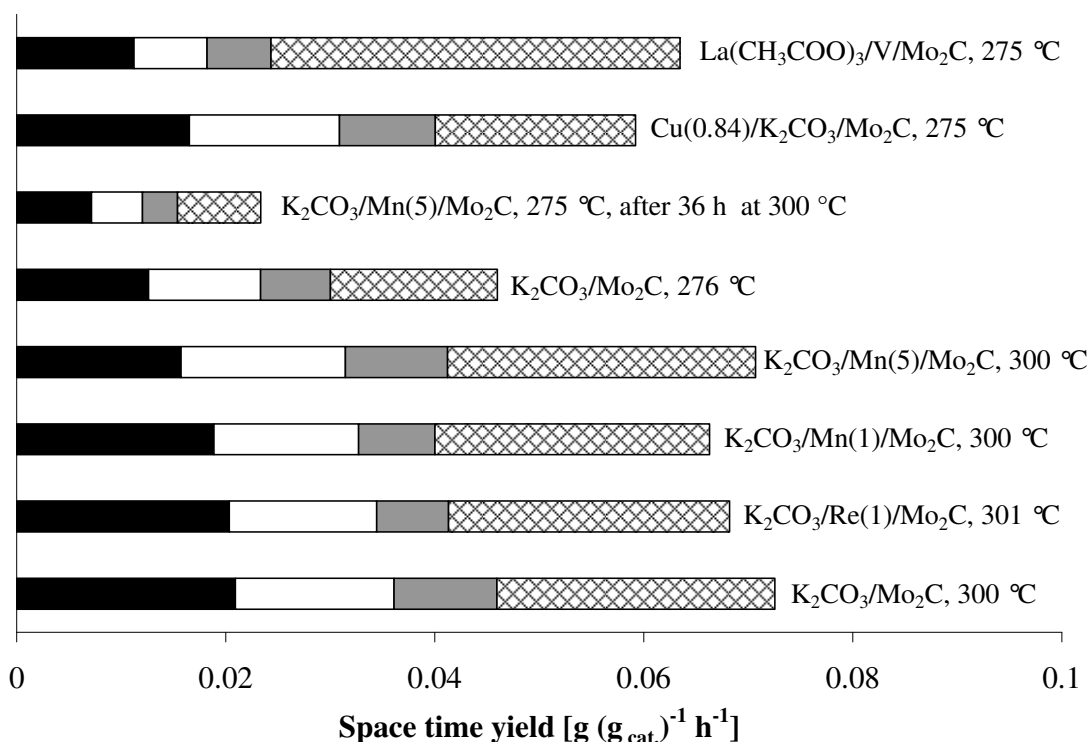
Figure 9.11 The space time yields of methanol (dark bar), C_2-C_4 alcohols (white bar) and C_1-C_3 hydrocarbons (hatched bar) for Mo_2C with different promoters. The experimental conditions and the time for which the catalysts have been on stream are given in table 9.6.

The catalyst promoted by lanthanum and vanadium exhibits a modest alcohol selectivity and a considerable hydrocarbon selectivity. The mass balance fulfillment for the experiment with the $La(CH_3COO)_3/V/Mo_2C$ catalyst is relatively poor, and there seems to be a considerable amount of uncharacterized products. Judging from the trends in the product distribution shown in table 9.6 it seems that a considerable amount of C_{4+} hydrocarbons is formed.

The only multiply promoted system, which behaves better than the unmodified K_2CO_3/Mo_2C catalyst is the $Cu(0.84)/K_2CO_3/Mo_2C$ system. The Cu containing catalyst provides a better alcohol productivity and selectivity than the Cu free catalyst, while the $Cu(0.84)/K_2CO_3/Mo_2C$ and K_2CO_3/Mo_2C catalysts provide similar distributions of the alcohol products. As previously discussed cupper particles may contribute to the formation of methanol, which can act as a precursor in the formation of higher alcohols.

Figure 9.11 shows that at 275 °C the $Cu(0.84)/K_2CO_3/Mo_2C$ catalyst exhibits a significantly higher alcohol production rate than the Cu-free catalyst. This is however partly due to the fact that the K_2CO_3/Mo_2C catalyst looses 16 % of its activity during the operation at 275 °C (see figure 9.5), while no appreciable deactivation is observed in the 28 hours that the $Cu(0.84)/K_2CO_3/Mo_2C$ was kept on stream. It is possible that the Cu containing catalyst over time will begin to undergo a deactivation similar to what is

observed for the basic K_2CO_3/Mo_2C system, and the differences in catalytic activity could thus to some extent be related to differences in the sample history. The differences in activity between the two catalysts should therefore be regarded with some caution due to the different durations of the two experiments.

Based upon the present results it cannot be excluded that the impregnation sequence can influence the effect of the promoter. The addition of Mn and Re before the addition of the alkali promoter resulted in catalyst with slightly diminished activity compared to the basic K_2CO_3/Mo_2C system, while cupper, which was added after the introduction of the alkali salt, improved the catalytic properties.

9.7 Similarities between metal carbides and more noble metals in the context of CO hydrogenation

In section 2.4.3 it was discussed how the carbides may bear a resemblance to more noble metals. It was discssued how WC and Mo_2C in terms of catalytic properties and electronic structure resemble respectively Pt and Ru. It was also described that the electronic structure of NbC holds some parallels to the electronic structure of the coinage metals – particularly silver.

The presently evaluated carbide catalysts also exhibit some qualitative similarities with the more noble metals that have a similar electronic structure. At the present conditions the K_2CO_3/WC catalyst primarily produces C_1 species, namely methanol and methane with a relatively low activity (see table 9.2). The same qualitative behavior is reported for platinum in CO hydrogenation, where C_1 species are the dominant products [83, 468-472]. The literature reports for CO hydrogenation on unpromoted WC generally corroborates that methane and methanol are respectively the dominant hydrocarbon and the dominant alcohol [251, 388, 473]. Leclercq et al. [251] do however report a significantly larger fraction of C_{2+}-hydrocarbons in CO hydrogenation over a WC catalyst. The differences in the observed catalytic behavior for WC are perhaps related to the complexity of the catalytic material. Factors like the extent of carburization and the amount of oxygen incorporated into the surface could, as it is mentioned above, influence the catalytic activity of the carbide materials. The results in table 9.2 illustrate that the present use of an alkali promoted K_2CO_3/WC catalyst yields methanol as the dominant product. Similarly Watling et al. [468] found that addition of an alkaline earth promoter (Ca) to a Pt/SiO_2 catalyst shifted the selectivity from methane to methanol. The present results with a K_2CO_3/WC catalyst are thus broadly in line with the previously reported similarity between platinum and tungsten carbide.

Alkali promoted Mo_2C is the only one of the presently evaluated carbides that produces significant amounts of higher alcohols. As it is described above previous authors have reported a "ruthenium-like" behavior for unmodified Mo_2C. Ruthenium based catalysts have been observed to exhibit an activity for the synthesis of alcohols - typically when Ru is present in combination with alkali and Mo [81, 109, 474-476]. Thus the catalytic behavior of the presently evaluated Mo_2C catalysts does at least not contradict the previously proposed "Ru-like" behavior of molybdenum carbide.

It can also be argued that the catalytic properties of NbC to some extent resembles those of the noble metal with the most similar electronic structure, namely silver. The absence of significant activity for CO hydrogenation is close to what would be expected for a "silver-like" material. At relatively similar conditions Shaw et al. [477] observed no CO hydrogenation activity for Ag/CeO_2 catalysts with Ag particles in the size range of 5-40 nm – particle dimensions comparable to the smaller particles in the present NbC catalyst (see table 9.1 and figure 9.3). Frost [478] did observe methanol syntesis activity for Ag/ThO_2 and Au/ThO_2 catalysts, and silver may, in the same way as it is observed for gold [479], exhibit CO hydrogenation activity, if the particles become sufficiently small. In conclusion also the CO hydrogenation behavior of NbC is quite consistent with the behavior of the more noble metal having a similar electronic structure – namely silver.

The investigation of carbide catalysts was partly motivated by a search for a replacement for the expensive, but promising metal rhodium. None of the presently evaluated carbides showed the desired "Rh-like" properties, although the alcohol product obtained over the K_2CO_3/Mo_2C catalysts was displaced towards ethanol. A high ethanol selectivity in CO hydrogenation is as previously discussed a "rhodium-like" trait. Of course the identification of a material that to a certain extent emulates the electronic structure of metallic rhodium, might not even be sufficient to duplicate the attractive catalytic properties of rhodium. Previous investigations have suggested that the formation of C_2 oxygenates may require a combination of Rh^+ and Rh^0 species [480], and a carbide catalyst would not necessarily be able to duplicate this kind of behavior. In terms of structural effects on the catalytic activity there could also be differences between a carbide and a noble metal like rhodium. However carbides could potentially become attractive alcohol synthesis catalysts in their own right. As discussed in section 9.4 especially Mo_2C exhibits a good activity per surface area, and the alcohol product is reasonably well shifted towards the desired higher alcohols. The use of supported carbides with higher surface areas could therefore potentially provide a highly active system for CO hydrogenation. It could therefore be fruitful to investigate the use of supported carbides for syngas conversion.The present investigations of promoters added to the prepared carbide were in most cases unsuccessful. An integration of a promoter within the carbide, structure might be preferable to addition of promotors to the prepared carbide. A possibility for continuation of the present work could be to investigate supported, bimetallic carbides such as Co_3Mo_3C/Co_6Mo_6C [481-483] (or in principle Co_3W_3C/Co_6W_6C [484-486]). These are known bimetallic carbide structures, which by analogy to cobalts effect on sulfide systems might possess interesting properties as alcohol synthesis catalysts. In the course of the present experiments it was attempted to prepare bimetallic cobalt-molybdenum carbides from carburization of $CoMoO_4$, but a suitable set of carburizing conditions that could yield a mixed carbide and not just isolated Co- and Mo-phases was not identified.

10 Conclusion

I have worked for a good many years on this subject, and every theory that I have put forward I have been able to destroy, and I have never met anybody who was in any better position.
- Sir Richard Threlfall on the topic of CO hydrogenation at high pressure in 1930

This work has dealt with the catalytic conversion of syngas into higher alcohols over Mo-based catalysts. The main focus has been on the use of potassium promoted cobalt-molybdenum sulfide as a catalyst for the alcohol synthesis. Because it has been established that the sulfide systems can provide a good alcohol selectivity and an alcohol product, which is reasonably well shifted towards the higher alcohols, the sulfides are promising alcohol synthesis catalysts. The present investigations have however revealed some important issues that must be considered, if the sulfides are used as alcohol synthesis catalysts.

It is observed that the sulfide catalyst is able to operate both with and without a sulfur source in the syngas feed, but the presence of a sulfur source like H_2S can exert a significant influence on the catalytic properties. The presence of 103 ppmv or more of H_2S in the syngas feed stabilizes a large fraction of higher alcohols in the product formed over a $K_2CO_3/Co/MoS_2/C$ catalyst. With 57 ppmv or less of H_2S in the feed the production of the desired higher alcohols is however gadually declining, while the methanol production is increasing. Loss of sulfur from the catalyst, and perhaps incorporation of carbon into the sulfide structure may contribute to this development. Furthermore the present investigations could suggest that these changes in the product distribution, which occur in sulfur-free or sulfur-poor syngas, especially are related to changes in the state of cobalt, which is added to the catalyst to promote chain-growth. The distribution of methanol and higher alcohols in the product after 25 hours on stream is largely independent of the cobalt content in the catalyst, although the fraction of higher alcohols initially benefits significantly from an increased presence of cobalt. In catalysts that have operated in sulfur free syngas, cobalt is incorporated into larger, coagulated structures, and signs of crystalline Co_9S_8, which is considered to be inactive, can be observed in the spent catalyst. It is hypothesized that loss of sulfur from the catalyst in the reducing atmosphere is driving the conversion of cobalt from its active form (possibly a mixed cobalt-molybdenum sulfide) into larger, more sulfur-deficient structures and into the more sulfur-deficient Co_9S_8-phase. That the presence of a sulfur source in the feed is necessary to stabilize the product distribution and possibly the catalyst introduces an important dilemma, because it is observed that the presence of a sulfur source like H_2S in the syngas feed can lead to incorporation of sulfur species into the condensed alcohol product. It is observed that the sulfur content in the condensed alcohol product increases linearly with the H_2S level in the syngas feed from 1250 ppmw S with 46 ppmv H_2S to 1905 ppmw S with 460 ppmv H_2S. Without H_2S in the feed sulfur species are also incorporated into the condensed reaction product, but in this case the products sulfur content decreases over time. The primary sulfur species in the alcohol product are short-chained thiols. With the increasingly stringent regulations for sulfur in motor fuels, often with regulatory limits in the order of 10 ppmw, this incorporation of sulfur into the

alcohol product is an important issue for the use of the alcohol product as a fuel additive/substitute.

On a fundamental level the present investigations have revealed a chain-growth pathway, which was unknown for the sulfide catalysts. In addition to the established CO addition reactions it has been discovered that alcohol coupling reactions, presumably occurring via aldol condensation pathways, contribute to the chain-growth over the sulfide catalyst. Such coupling reactions occurring via aldol condensation pathways can explain the observed presence of branched alcohols (e.g. iso-butanol) in the product. The discovery of the coupling reactions comes from the observation that ethanol co-fed along with the syngas especially causes an increased production of 1-butanol.

Various investigations have been carried out to clarify the effect of the feed composition on the catalytic properties of the sulfide catalyst. In a sulfur free syngas it is observed that the production of higher alcohols is optimal with an equimolar mixture of CO and H_2 in the feed, while the methanol production benefits from an increasing hydrogen content in the feed. It has been argued that the sulfides ability to operate in a sulfur containing atmosphere may enable the user to employ a less thorough and therefore less costly syngas cleaning. To evaluate to which extent a removal of other components in the raw syngas is necessary, the influence of NH_3 and H_2O in the feed has also been evaluated. An ammonia impurity (741 ppmv) in the feed is observed to cause a general and largely reversible deactivation of the catalyst. Operation with elevated water levels in the syngas feed (4.7-13.4 mol%) is observed to cause a deactivation of the catalyst, and it is especially the chain-growth, which is affected. A permanent, general deactivation is observed once the water is removed from the feed – a deactivation which could be caused by an accelerated sintering in the presence of water.

Since the use of the sulfide catalyst encompasses the risk of sulfur being incorporated into the alcohol product, carbide catalysts have been investigated as a possible non-sulfided alternative. Various catalysts based upon the bulk carbides Mo_2C, WC and NbC have been synthesized and evaluated with respect to the catalytic behavior in high-pressure CO hydrogenation. NbC is largely inactive, K_2CO_3/WC produces mainly methanol and methane with a low activity, and K_2CO_3/Mo_2C produces a mixture of methanol and higher alcohols, but also significant amounts of hydrocarbons. It is also observed that K_2CO_3/Mo_2C at the higher temperatures evaluated (276 °C and 300 °C) undergoes a gradual deactivation, which most likely is related to the formation of carbonaceous deposits on the catalyst. After a 95 h experimental run at temperatures up to 300 °C the mass of a K_2CO_3/Mo_2C catalyst had for example increased by 11 %.

The role of the choice of alkali cation in Mo_2C promoted by an alkali salt has also been evaluated at a promoter level of Alkali/Mo = 0.164±0.001 mol/mol, and it is observed that K is preferable to Li and Cs.

Finally different multiply promoted Mo_2C catalysts have been evaluated in terms of the CO hydrogenation properties, but only the addition of Cu (0.84 wt%) has been observed to improve the activity (by 33 % at 275 °C, 100 bar, 5000 h^{-1}). The addition of Cu was also observed to improve the selectivity of the basic K_2CO_3/Mo_2C system, and the addition of Cu was observed not to cause a significant alteration of the alcohol distribution.

187

11 References

A little knowledge is a dangerous thing. Drink deeply from the source or not at all
- Alexander Pope

[1] L.R. Lynd, Annu. Rev. Energy Environ. 21 (1996) 403-465.
[2] L.R. Lynd, J.H. Cushman, R.J. Nichols, C.E. Wyman, Science 251 (1991) 1318-1323.
[3] A.E. Farell, R.J. Plevin, B.T. Turner, A.D. Jones, M. O'Hare, D.M. Kammen, Science 11 (2006) 506-508.
[4] J.R. Regalbuto, Science 325 (2009) 822-824.
[5] D. Rotman, Technol. Rev. 111 (2008) 42-51.
[6] C. Somerville, H. Youngs, C. Taylor, S.C. Davis, S.P. Long, Science 329 (2010) 790-792.
[7] C. Higman, M. van der Burgt, Gasification, 1st ed., Gulf Professional Publishing, USA, 2003.
[8] J. Rezaiyan, N.P. Cheremisinoff (Eds.), Gasification Technologies, 1st ed., CRC Press, USA, 2005.
[9] R.G. Herman, Catal. Today 55 (2000) 233-245.
[10] J.L. Keller, Hydrocarbon Process 58 (1979) 127-138.
[11] I. Wender, Fuel. Proc. Technol. 48 (1996) 189-297.
[12] Z. Liu, X. Li, M.R. Close, E.L. Kugler, J.L. Petersen, D.B. Dadyburjor, Ind. Eng. Chem. Res. 36 (1997) 3085-3093.
[13] C.B. Murchison, M.M. Conway, R.R. Stevens, G.J. Quarderer, in: M.J. Phillips, M. Ternan (Eds.), Proceedings of the 9th International Congress of Catalysis, Vol. 2, Calgary, Chemical Institute of Canada, Ottawa, (1988) pp. 626-633.
[14] G. Bian, L. Fan, Y. Fu, K. Fujimoto, Ind. Eng. Chem. Res. 37 (1998) 1736-1743.
[15] L. Gang, Z. Chengfang, C. Yanqing, Z. Zhibin, N. Yianhui, C. Linjun, Y. Fong, App. Catal. A 150 (1997) 243-252.
[16] H. Qi, D. Li, C. Yang, Y. Ma, W. Li, Y. Sun, B. Zhong, Catal. Commun. 4 (2003) 339-342.
[17] A.K. Gunturu, E.L. Kugler, J.B. Cropley, D.B. Dadyburjor, Ind. Eng. Chem. Res. 37 (1998) 2107-2115.
[18] R.R. Stevens, M.M. Conway, US Patent 4,831,060 (1989), to Dow Chemical Company.
[19] W.P. Dianis, App. Catal. 30 (1987) 99-121.
[20] P.J. Alsum, E.M. Wilcox, J.E. Hensley and K. Kharas, US Patent 2010/0076228 A1 (2010), to Range Fuels, Inc.
[21] K. Kharas, US Patent 2010/0099925 A1 (2010), to Range Fuels, Inc.
[22] G. Meitzner, US Patent 2010/0022806 A1 (2010), to Range Fuels, Inc.
[23] G. Meitzner, K. Kharas, US Patent 2010/0075837 A1 (2010), to Range Fuels, Inc.
[24] H.J. Robota, K. Kharas, E.M. Wilcox, US Patent 2010/0152498 A1 (2010), to Range Fuels, Inc.
[25] R.C. Stites, US Patent 2010/0152497 A1 (2010), to Range Fuels, Inc.
[26] K. Kharas, US Patent 2009/0156393 A1 (2009), to Range Fuels, Inc.
[27] K. Kharas, US Patent 2009/0156697 A1 (2009), to Range Fuels, Inc.

[28] S.H. Tirmizi, R.E. Klepper, F.M. Ferraro, US Patent 2009/0018372 A1 (2009), to Range Fuels, Inc.

[29] R.B. Anderson, J. Feldman, H.H. Storch, Ind. Eng. Chem. 44 (1952) 2418-2424.

[30] P. Forzatti, E. Tronconi, I. Pasquon, Catal. Rev. 33 (1991) 109-168.

[31] R.G. Herman, Stud. Surf. Sci. Catal. 64 (1991) 265-349.

[32] X. Xiaoding, E.B.M. Doesburg, J.J.F. Scholten, Catal. Today 2 (1987) 125-170.

[33] J.J. Spivey, A. Egbebi, Chem. Soc. Rev. 36 (2007) 1514-1528.

[34] K.J. Smith, K. Klier, Prepr. - Div. Petr. Chem., Am. Chem Soc. 37 (1992) 214-224.

[35] P. Courty, P. Chaumette, C. Rimbault, P. Travers, Oil Gas Sci. Technol. 45 (1990) 561-578.

[36] V. Subramani, S.K. Gangwal, Energy & Fuels 22 (2008) 814-839.

[37] G.A. Mills, Fuel 73 (1994) 1243-1279.

[38] J.A. Moulijn, M. Makkee and A. Van Diepen, Chemical process technology, 1st ed., John Wiley & Sons, Great Britain, 2001.

[39] M.E. Dry, Catal. today 6 (1990) 183-206.

[40] L.H. Cohen, H.L. Muller, Oil Gas J. 83 (1985) 119-124.

[41] P.L. Rogerson, in: R.A. Meyers (Ed.), Handbook of Synfuels Technology, 1st ed., McGraw-Hill, USA, 1985, pp. 2/45-2/73.

[42] A.Y. Kam, M. Schreiner, S. Yurchak, in: R.A. Meyers (Ed.), Handbook of Synfuels Technology, 1st ed., McGraw-Hill, USA, 1984, pp. (2)75-(2)111.

[43] N.M. Laurendeau, Prog. Energy Combust. Sci. 4 (1978) 221-270.

[44] D.R. Lide, Handbook of Chemistry and Physics, 78th ed., CRC Press, USA, 1997.

[45] H. Watanabe, M. Otaka, Fuel 85 (2006) 1935-1943.

[46] G.T. Austin, Shreve's Chemical process industries, 5th ed., McGraw-Hill, Singapore, 1984.

[47] D.F. Spencer, M.J. Gluckman, S.B. Alpert, Science 215 (1982) 1571-1576.

[48] E.D. Larson, R. Tingjin, Energy Sust. Dev. 7 (2003) 79-102.

[49] R.H. Williams, E.D. Larson, R.E. Katofsky, J. Chen, Energy Sust. Dev. 1 (1995) 18-34.

[50] M.J.A. Tijmensen, A.P.C. Faaij, C.N. Hamelinck, van Hardeveld, M. R. M., Biomass Bioenergy 23 (2002) 129-152.

[51] D.S. Newsome, Catal. Rev. 21 (1980) 275-318.

[52] M. Kantschewa, F. Delannay, H. Jeziorowski, E. Delgado, S. Eder, G. Ertl, H. Knözinger, J. Catal. 87 (1984) 482-496.

[53] C.R.F. Lund, Ind. Eng. Chem. Res. 35 (1996) 2531-2538.

[54] K. Salo, A. Horvath, J. Patel, Pressurized Gasification of Biomass, International Gas Turbine & Aeroengine Congress & Exhibition, Stockholm, Sweden, 1998.

[55] W. Torres, S. Pansare, J.G. Goodwin Jr, Catal. Rev. Sci. Eng. 49 (2007) 407-456.

[56] E. Supp, How to Produce Methanol from Coal, 1st ed., Springer-Verlag, Germany, 1990.

[57] J. Leppälahti, T. Koljonen, Fuel Proc. Tech. 43 (1995) 1-45.

[58] J. Leppälahti, Biores. Technol. 46 (1993) 65-70.

[59] Anonymous, Deutsches Reich Patent 293787 (1916), to Badische Anilin & Soda-Fabrik.

[60] Anonymous, Deutsches Reich Patent 295202 (1916), to Badische Anilin & Soda-Fabrik.

[61] A. Mittasch, C. Schneider, US Patent 1,201,850 (1916), to Badische Anilin & Soda-Fabrik.

[62] F. Fischer, H. Tropsch, Deutsches Reich Patent 411216 (1923), to Hans Tropsch and Franz Fischer.

[63] H. Machemer, Angew. Chem. 64 (1952) 213-220.

[64] Range Fuels, Inc., www.rangefuels.com, Accessed December 2010.

[65] I. Barin, G. Platzki, Thermochemical Data of Pure Substances, 3rd ed., VCH Verlag, Weinheim, 1995.

[66] E. Tronconi, L. Lietti, P. Forzatti, I. Pasquon, App. Catal. 47 (1989) 317-333.

[67] E. Tronconi, L. Lietti, G. Groppi, P. Forzatti, I. Pasquon, J. Catal. 135 (1992) 99-114.

[68] V. Fattore, B. Notari, A. Paggini, V. Lagana, US Patent 4,513,100 (1985), to Snamprogetti S.p.A.

[69] K.J. Smith, R.B. Anderson, Can. J. Chem. Eng. 61 (1983) 40-45.

[70] J.G. Nunan, C.E. Bogdan, K. Klier, K.J. Smith, C.-W. Young, R.G. Herman, J. Catal. 116 (1989) 195-221.

[71] J.G. Nunan, C.E. Bogdan, K. Klier, K.J. Smith, C.-W. Young, R.G. Herman, J. Catal. 113 (1988) 410-433.

[72] P. Courty, D. Durand, E. Freund, A. Sugier, J. Mol. Catal. 17 (1982) 241-254.

[73] J.A. Dalmon, P. Chaumette, C. Mirodatos, Catal. Today 15 (1992) 101-127.

[74] G.J. Quarderer, Mixed alcohols from synthesis gas, AIChE Spring National Meeting, New Orleans, USA, (1986) Paper 25a.

[75] J.G. Santiesteban, C.E. Bogdan, R.G. Herman, K. Klier, in: M.J. Phillips, M. Ternan (Eds.), Proceedings of the 9th International Congress of Catalysis, Vol. 2, Calgary, Chemical Institute of Canada, Ottawa, (1988) 561-568.

[76] M.M. Bhasin, W.J. Bartley, P.C. Ellgen, T.P. Wilson, J. Catal. 54 (1978) 120-128.

[77] M. Ichikawa, Bull. Chem. Soc. Jpn. 51 (1978) 2273-2277.

[78] H. Arakawa, K. Takeuchi, T. Matsuzaki, Y. Sugi, Chem. Lett. 13 (1984) 1607-1610.

[79] Y. Kintaichi, Y. Kuwahara, H. Hamada, T. Ito, K. Wakabayashi, Chem. Lett. 14 (1985) 1305-1306.

[80] Y. Kuwahara, H. Hamada, Y. Kintaichi, T. Ito, K. Wakabayashi, Chem. Lett. 14 (1985) 205-206.

[81] H. Hamada, Y. Kuwahara, Y. Kintaichi, T. Ito, K. Wakabayashi, H. Iijima, K. Sano, Chem. Lett. 13 (1984) 1611-1612.

[82] Y. Sugi, K. Takeuchi, T. Matsuzaki, H. Arakawa, Chem. Lett. (1985) 1315-1318.

[83] T. Matsuzaki, K. Takeuchi, T. Hanaoka, H. Arakawa, Y. Sugi, Catal. Today 28 (1996) 251-259.

[84] T. Matsuzaki, T. Hanaoka, K. Takeuchi, H. Arakawa, Y. Sugi, K. Wei, T. Dong, M. Reinikainen, Catal. Today 36 (1997) 311-324.

[85] M. Van Der Riet, D. Copperthwaite, R. Hunter, G.J. Hutchings, J. Chem. Soc., Chem. Commun. (1988) 687-688.

[86] J. Hu, Y. Wang, C. Cao, D.C. Elliott, D.J. Stevens, J.F. White, Catal. Today 120 (2007) 90-95.

[87] N.D. Subramanian, J. Gao, X. Mo, J.G. Goodwin Jr, W. Torres, J.J. Spivey, J. Catal. 272 (2010) 204-209.

[88] T. Hanaoka, H. Arakawa, T. Matsuzaki, Y. Sugi, K. Kanno, Y. Abe, Catal. Today 58 (2000) 271-280.

[89] G.V. Schulz, Zeit. Phys. B. 30 (1935) 379-398.

[90] R.A. Friedel, R.B. Anderson, J. Am. Chem. Soc. 72 (1950) 1212-1215.

[91] P.J. Flory, J. Am. Chem. Soc. 58 (1936) 1877-1885.

[92] G.C. Chinchen, K.C. Waugh, J. Catal. 97 (1986) 280-283.

[93] J.R. LeBlanc, R.V. Schneider III, R.B. Strait, in: W.H. Cheng, H.H. Kung (Eds.), Methanol Production and Use, 1st ed., CRC Press, USA, 1990, pp. 51-132.

[94] P.J.A. Tijm, D.M. Waller, D.M. Brown, App. Catal. A 221 (2001) 275-282.

[95] J.-P. Lange, Catal. today 64 (2001) 3-8.

[96] H.H. Kung, Catal. Rev. 22 (1980) 259.

[97] K.C. Waugh, Catal. Today 15 (1992) 51-75.

[98] H. Topsøe, B.S. Clausen, F.E. Massoth, Hydrotreating Catalysis, Catalysis - Science and Technology, Vol. 11, Springer, Berlin, 1996.

[99] O. Weisser, S. Landa, Sulfide Catalysts. Their Properties and Applications, 1st ed., Pergamon, New York, 1973.

[100] R. Prins, Adv. Catal. 46 (2002) 399-459.

[101] D.D. Whitehurst, T. Isoda, I. Mochida, Adv. Catal. 42 (1998) 345-467.

[102] R. Prins, De Beer, V. H. J., G.A. Somorjai, Catal. Rev. Sci. Eng. 31 (1989) 1-41.

[103] G.J. Quarderer, G.A. Cochran, Eur. Patent 0 119 609 (1984), to DOW Chemical Company.

[104] G.J. Quarderer, G.A. Cochran, US Patent 4,749,724 (1988), to DOW Chemical Company.

[105] N.E. Kinkade, WO Patent 85/03073 (1985), to Union Carbide Corporation.

[106] N.E. Kinkade, WO Patent 85/03074 (1985), to Union Carbide Corporation.

[107] N.E. Kinkade, Eur. Patent 0149255A2 (1985), to Union Carbide Corporation.

[108] N.E. Kinkade, Eur. Patent 0149256A2 (1985), to Union Carbide Corporation.

[109] M. Inoue, T. Miyake, S. Yonezawa, D. Medhanavyn, Y. Takegami, T. Inui, J. Mol. Catal. 45 (1988) 111-126.

[110] E.C. Alyea, D. He, J. Wang, App. Catal. A 104 (1993) 77-85.

[111] K. Fujimoto, T. Oba, App. Catal. 13 (1985) 289-293.

[112] T. Tatsumi, A. Muramatsu, H. Tominaga, App. Catal. 34 (1987) 77-88.

[113] Y. Avila, C. Kappenstein, S. Pronier, J. Barrault, App. Catal. A 132 (1995) 97-109.

[114] G.J. Quarderer, G.A. Cochran, Eur. Patent 0119609 (1984), to Dow Chemical Company.

[115] H.C. Woo, K.Y. Park, Y.G. Kim, I.S. Nam, J.S. Chung, J.S. Lee, App. Catal. 75 (1991) 267-280.

[116] J.S. Lee, S. Kim, Y.G. Kim, Top. Catal. 2 (1995) 127-140.

[117] M. Xiang, D. Li, H. Xiao, J. Zhang, W. Li, B. Zhong, Y. Sun, Catal. Today 131 (2008) 489-495.

[118] M. Xiang, D. Li, H. Xiao, J. Zhang, H. Qi, W. Li, B. Zhong, Y. Sun, Fuel 87 (2008) 599-603.

[119] M. Xiang, D. Li, W. Li, B. Zhong, Y. Sun, Catal. Commun. 8 (2007) 503-507.

[120] M. Xiang, D. Li, W. Li, B. Zhong, Y. Sun, Catal. Commun. 8 (2007) 88-90.

[121] M. Xiang, D. Li, H. Qi, W. Li, B. Zhong, Y. Sun, Fuel 86 (2007) 1298-1303.

[122] M. Xiang, D. Li, W. Li, B. Zhong, Y. Sun, Fuel 85 (2006) 2662-2665.

[123] A. Calafat, F. Vivas, J.L. Brito, App. Catal. A 172 (1998) 217-224.

[124] S.F. Zaman, K.J. Smith, Molec. Simul. 34 (2008) 1073-1084.

[125] S.F. Zaman, K.J. Smith, Catal. Comm. 10 (2009) 468-471.

[126] S.F. Zaman, K.J. Smith, Molec. Simul. 36 (2010) 118-126.

[127] S.F. Zaman, K.J. Smith, App. Catal. A 378 (2010) 59-68.

[128] R.R. Stevens, US Patent 4,752,622 (1988), to Dow Chemical Company.

[129] R.R. Stevens, US Patent 4,752,623 (1988), to Dow Chemical Company.

[130] R.R. Stevens, EU Patent 0 172 431 (1986), to Dow Chemical Company.

[131] S.M.A.M., Bouwens, R. Prins, V.H.J., de Beer, D.C. Koningsberger, J. Phys. Chem. 94 (1990) 3711-3718.

[132] B.S. Clausen, H. Topsøe, R. Candia, J. Villadsen, B. Lengeler, J. Als-Nielsen, F. Christensen, J. Phys. Chem. 85 (1981) 3868-3872.

[133] G. Bian, Y. Fu, M. Yamada, App. Catal. A 144 (1996) 79-91.

[134] M. Jiang, G. Bian, Y. Fu, J. Catal. 146 (1994) 144-154.

[135] J.V. Lauritsen, M. Nyberg, R.T. Vang, M.V. Bollinger, B.S. Clausen, H. Topsøe, K.W. Jacobsen, E. Lægsgaard, J.K. Nørskov, F. Besenbacher, Nanotech. 14 (2003) 385-389.

[136] M. Salmeron, G.A. Somorjai, A. Wold, R. Chianelli, K.S. Liang, Chem. Phys. Lett. 90 (1982) 105-107.

[137] S.J. Tauster, T.A. Pecoraro, R.R. Chianelli, J. Catal. 63 (1980) 515-519.

[138] H. Topsøe, R. Candia, N.Y. Topsøe, B.S. Clausen, Bull. Soc. Chem. Belg. 93 (1984) 783-806.

[139] J.V. Lauritsen, J. Kibsgaard, S. Helveg, H. Topsøe, B.S. Clausen, E. Lægsgaard, F. Besenbacher, Nature Nanotechnol. 2 (2007) 53-58.

[140] J.V. Lauritsen, M.V. Bollinger, E. Lægsgaard, K.W. Jacobsen, J.K. Nørskov, B.S. Clausen, H. Topsøe, F. Besenbacher, J. Catal. 221 (2004) 510-522.

[141] L.S. Byskov, J.K. Nørskov, B.S. Clausen, H. Topsøe, J. Catal. 187 (1999) 109-122.

[142] P. Raybaud, J. Hafner, G. Kresse, H. Toulhoat, Surf. Sci. 407 (1998) 237-250.

[143] P. Raybaud, J. Hafner, G. Kresse, S. Kasztelan, H. Toulhoat, J. Catal. 189 (2000) 129-146.

[144] L.S. Byskov, J.K. Nørskov, B.S. Clausen, H. Topsøe, Catal. Lett. 64 (2000) 95-99.

[145] J. Lipsch, G.C.A. Schuit, J. Catal. 15 (1969) 179-189.

[146] S. Kolboe, Can. J. Chem. 47 (1969) 352-355.

[147] S. Helveg, J.V. Lauritsen, E. Lægsgaard, I. Stensgaard, J.K. Nørskov, B.S. Clausen, H. Topsøe, F. Besenbacher, Phys. Rev. Lett. 84 (2000) 951-954.

[148] A. Travert, C. Dujardin, F. Maugé, S. Cristol, J.F. Paul, E. Payen, D. Bougeard, Catal. Today 70 (2001) 255-269.

[149] M.V. Bollinger, J.V. Lauritsen, K.W. Jacobsen, J.K. Nørskov, S. Helveg, F. Besenbacher, Phys. Rev. Lett. 87 (2001) 196803-1-4.

[150] J.V. Lauritsen, M. Nyberg, J.K. Nørskov, B.S. Clausen, H. Topsøe, E. Lægsgaard, F. Besenbacher, J. Catal. 224 (2004) 94-106.

[151] H. Topsøe, B. Hinnemann, J.K. Nørskov, J.V. Lauritsen, F. Besenbacher, P.L. Hansen, G. Hytoft, R.G. Egeberg, K.G. Knudsen, Catal. Today 107-108 (2005) 12-22.

[152] J. Kibsgaard, J.V. Lauritsen, E. Lægsgaard, B.S. Clausen, H. Topsøe, F. Besenbacher, J. Am. Chem. Soc. 128 (2006) 13950-13958.

[153] M. Daage, R.R. Chianelli, J. Catal. 149 (1994) 414-427.

[154] N.Y. Topsøe, H. Topsøe, J. Catal. 139 (1993) 641-651.

[155] E. Payen, S. Kasztelan, J. Grimblot, J. Mol. Struct. 174 (1988) 71-76.

[156] M.V. Bollinger, K.W. Jacobsen, J.K. Nørskov, Phys. Rev. B 67 (2003) 085410-1-17.

[157] V. LaVopa, C.N. Satterfield, J. Catal. 110 (1988) 375-387.

[158] Á. Logadóttir, P.G. Moses, B. Hinnemann, N.Y. Topsøe, K.G. Knudsen, H. Topsøe, J.K. Nørskov, Catal. Today 111 (2006) 44-51.

[159] X. Youchang, B.M. Naasz, G.A. Somorjai, App. Catal. 27 (1986) 233-241.

[160] C. Papageorgopoulos, M. Kamaratos, S. Kennou, D. Vlachos, Surf. Sci. 251/252 (1991) 1057-1061.

[161] S. Kennou, S. Ladas, C. Papageorgopoulos, Surf. Sci. 152/153 (1985) 1213-1221.

[162] F.S. Ohuchi, W. Jaegermann, C. Pettenkofer, B.A. Parkinson, Langmuir 5 (1989) 439-442.

[163] K.T. Park, J. Kong, Top. Catal. 18 (2002) 175-181.

[164] K. Klier, M. Neiman, Q. Ma, J. Spirko, Modeling of Syngas Reactions and Hydrogen Generation Over Sulfides, Annual Technical Progress Report, US DoE Research Project No. DE-FG26-01NT41276, 2004. Available from: http://www.osti.gov/bridge/servlets/purl/836407-FMjxEI/native/836407.pdf

[165] K.T. Park, J.S. Hess, K. Klier, J. Chem. Phys. 111 (1999) 1636-1649.

[166] K.T. Park, M. Richards-Babb, M.S. Freund, J. Weiss, K. Klier, J. Phys. Chem. 100 (1996) 10739-10745.

[167] K.T. Park, M. Richards-Babb, J.S. Hess, J. Wiss, K. Klier, Phys. Rev. B 54 (1996) 5471-5479.

[168] M.A. Karolewski, R.G. Cavell, Surf. Sci. 274 (1992) 421-429.

[169] M.A. Karolewski, R.G. Cavell, Surf. Sci. 219 (1989) 261-276.

[170] A.B. Anderson, J. Yu, J. Catal. 119 (1988) 135-145.

[171] H.C. Woo, I.S. Nam, J.S. Lee, J.S. Chung, Y.G. Kim, J. Catal. 142 (1993) 672-690.

[172] H.C. Woo, J.C. Kim, I.S. Nam, J.S. Lee, J.S. Chung, Y.G. Kim, App. Catal. A 104 (1993) 199-214.

[173] J.S. Lee, S. Kim, K.H. Lee, I.S. Nam, J.S. Chung, Y.G. Kim, H.C. Woo, App. Catal. A 110 (1994) 11-25.

[174] H.C. Woo, I.S. Nam, J.S. Lee, J.S. Chung, K.H. Lee, Y.G. Kim, J. Catal. 138 (1992) 525-535.

[175] F. Maugé, J.C. Lavalley, J. Catal. 137 (1992) 69-76.

[176] Elst, L. P. A. F., S. Eijsbouts, A.D. van Langeveld, J.A. Moulijn, J. Catal. 196 (2000) 95-103.

[177] B. Müller, A.D. van Langeveld, J.A. Moulijn, H. Knözinger, J. Phys. Chem. 97 (1993) 9028-9033.

[178] N. Koizumi, G. Bian, K. Murai, T. Ozaki, M. Yamada, J. Mol. Catal. A 207 (2004) 171-180.

[179] T. Zeng, X.D. Wen, Y.W. Li, H. Jiao, J. Phys. Chem. B 109 (2005) 13704-13710.

[180] T. Zeng, X.D. Wen, G.S. Wu, Y.W. Li, H. Jiao, J. Phys. Chem. B 109 (2005) 2846-2854.

[181] J. Iranmahboob, H. Toghiani, D.O. Hill, App. Catal. A 247 (2003) 207-218.

[182] H.C. Woo, T.Y. Park, Y.G. Kim, I.S. Nam, J.S. Lee, A. Muramatsu, Stud. Surf. Sci. Catal.75 (1993) 2749-2752.

[183] L.V. Bolton, B.P. Gracey, WO Patent 2007/138300A1 (2007), to BP Chemicals Ltd.

[184] N. Koizumi, K. Murai, T. Ozaki, M. Yamada, Catal. Today 89 (2004) 465-478.

[185] J. Iranmahboob, D.O. Hill, H. Toghiani, App. Catal. A 231 (2002) 99-108.

[186] X. Li, L. Feng, Z. Liu, B. Zhong, D.B. Dadyburjor, E.L. Kugler, Ind. Eng. Chem. Res. 37 (1998) 3858-3863.

[187] K. Klier, R.G. Herman, J.G. Nunan, K.J. Smith, C.E. Bogdan, C.-W. Young, J.G. Santiesteban, Stud. Surf. Sci. Catal. 36 (1988) 109-125.

[188] J. Iranmahboob, D.O. Hill, Catal. Lett. 78 (2002) 49-55.

[189] Anonymous, GB Patent 315,439 (1929), to I. G. Farbenindustrie.

[190] H. Beuther, R.A. Flinn, J.B. McKinley, Ind. Eng. Chem. 51 (1959) 1349-1350.

[191] G.C.A. Schuit, B.C. Gates, AIChE J. 19 (1973) 417-438.

[192] J.T. Richardson, Ind. Eng. Chem. Fundam. 3 (1964) 154-158.

[193] P.R. Wentrcek, H. Wise, J. Catal. 51 (1978) 80-85.

[194] Z. Li, Y. Fu, J. Bao, M. Jiang, T. Hu, T. Liu, Y. Xie, App. Catal. A 220 (2001) 21-30.

[195] G. Bian, Y. Fu, Y. Ma, Catal. Today 51 (1999) 187-193.

[196] J. Bao, Y. Fu, G. Bian, Catal. Lett. 121 (2008) 151-157.

[197] D. Li, N. Zhao, H. Qi, W. Li, Y.H. Sun, B. Zhong, Catal. Commun. 6 (2005) 674-678.

[198] D. Li, C. Yang, W. Li, Y. Sun, B. Zhong, Top. Catal. 32 (2005) 233-239.

[199] D. Li, C. Yang, N. Zhao, H. Qi, W. Li, Y. Sun, B. Zhong, Fuel Proc. Tech. 88 (2007) 125-127.

[200] D. Li, C. Yang, H. Qi, H. Zhang, W. Li, Y. Sun, B. Zhong, Catal. Commun. 5 (2004) 605-609.

[201] H. Topsøe, B.S. Clausen, R. Candia, C. Wivel, S. Mørup, J. Catal. 68 (1981) 433-452.

[202] C. Wivel, R. Candia, B.S. Clausen, S. Mørup, H. Topsøe, J. Catal. 68 (1981) 453-463.

[203] H. Topsøe, B.S. Clausen, N.Y. Topsøe, E. Pedersen, Ind. Eng. Chem. Fundam. 25 (1986) 25-36.

[204] N.Y. Topsøe, H. Topsøe, J. Catal. 84 (1983) 386-401.

[205] H. Topsøe, App. Catal. A 322 (2007) 3-8.

[206] L.S. Byskov, B. Hammer, J.K. Nørskov, B.S. Clausen, H. Topsøe, Catal. Lett. 47 (1997) 177-182.

[207] J.V. Lauritsen, S. Helveg, E. Lægsgaard, I. Stensgaard, B.S. Clausen, H. Topsøe, F. Besenbacher, J. Catal. 197 (2001) 1-5.

[208] J.V. Lauritsen, J. Kibsgaard, G.H. Olesen, P.G. Moses, B. Hinnemann, S. Helveg, J.K. Nørskov, B.S. Clausen, H. Topsøe, E. Lægsgaard, F. Besenbacher, J. Catal. 249 (2007) 220-233.

[209] G.U. Kulkarni, C.N.R. Rao, Catal. Lett. 9 (1991) 427-440.

[210] W. Niemann, B.S. Clausen, H. Topsøe, Catal. Lett. 4 (1990) 355-364.

[211] J. Kibsgaard, A. Tuxen, K.G. Knudsen, M. Brorson, H. Topsøe, E. Lægsgaard, J.V. Lauritsen, F. Besenbacher, J. Catal. 272 (2010) 195-203.

[212] F. Baksh, Synthesis Gas Conversion to Aliphatic Alcohols: Study of MoS_2 catalytic systems, MSc-Thesis, University of Kansas, 2010.

[213] J. Iranmahboob, D.O. Hill, H. Toghiani, App. Surf. Sci. 185 (2001) 72-78.
[214] S.M.A.M., Bouwens, J.A.R., van Veen, D.C. Koningsberger, V.H.J., de Beer, R. Prins, J. Phys. Chem. 95 (1991) 123-134.
[215] J.M. Christensen, P.A. Jensen, N.C. Schiødt, A.D. Jensen, ChemCatChem 2 (2010) 523-526.
[216] A. Calafat, J. Laine, App. Catal. A 133 (1995) 67-79.
[217] A. Calafat, J. Laine, Catal. Lett. 28 (1994) 69-77.
[218] K.W. Wang, X.Z. Jiang, W.C. Zhang, Chinese Chem. Lett. 15 (2004) 1497-1500.
[219] M. Brorson, A. Carlsson, H. Topsøe, Catal. Today 123 (2007) 31-36.
[220] M. Breysse, J.L. Portefaix, M. Vrinat, Catal. Today 10 (1991) 489-505.
[221] J.P.R. Vissers, B. Scheffer, de Beer, V. H. J., J.A. Moulijn, R. Prins, J. Catal. 105 (1987) 277-284.
[222] M. Xu, J.H. Lunsford, D.W. Goodman, A. Bhattacharyya, App. Catal. A 149 (1997) 289-301.
[223] J.J. Spivey, Chem. Eng. Commun. 110 (1991) 123-142.
[224] A.F. Pérez-Cadenas, J. Maldonado-Hódar, C. Moreno-Castilla, Carbon 41 (2003) 473-478.
[225] P.K. Doolin, S. Alerasool, D.J. Zalewski, J.F. Hoffman, Catal. Lett. 25 (1994) 209-223.
[226] X. Wang, U.S. Ozkan, J. Mol. Catal. A 232 (2005) 101-112.
[227] X. Wang, U.S. Ozkan, J. Catal. 227 (2004) 492-501.
[228] G. Bian, L. Fan, Y. Fu, K. Fujimoto, App. Catal. A 170 (1998) 255-268.
[229] R. Candia, O. Sørensen, J. Villadsen, N.Y. Topsøe, Bull. Soc. Chim. Belg. 93 (1984) 763-773.
[230] E. Diemann, T. Weber, A. Müller, J. Catal. 148 (1994) 288-303.
[231] R.G. Leliveld, A.J. van Dillen, J.W. Geus, D.C. Koningsberger, J. Catal. 165 (1997) 184-196.
[232] E.J.M. Hensen, V. H. J., de Beer, J. A. R., van Veen, R.A. van Santen, Catal. Lett. 84 (2002) 59-67.
[233] E.G. Derouane, E. Pedersen, B.S. Clausen, Z. Gabelica, R. Candia, H. Topsøe, J. Catal. 99 (1986) 253-261.
[234] B. Hinnemann, J.K. Nørskov, H. Topsøe, J. Phys. Chem. B 109 (2005) 2245-2253.
[235] Y. Okamoto, K. Ochiai, M. Kawano, K. Kobayashi, T. Kubota, App. Catal. A 226 (2002) 115-127.
[236] J.M. Solar, F.J. Derbyshire, de Beer, V. H. J., L.R. Radovic, J. Catal. 129 (1991) 330-342.
[237] B.M. Reddy, V.S. Subrahmanyam, App. Catal. 27 (1986) 1-8.
[238] S.J. Moon, S.K. Ihm, App. Catal. 42 (1988) 307-324.
[239] S.M.A.M., Bouwens, F.B.M., von Zon, M.P. van Dijk, A. M., van der Kraan, V.H.J., de Beer, J.A.R., van Veen, D.C. Koningsberger, J. Catal. 146 (1994) 375-393.
[240] M. Sun, D. Nicosia, R. Prins, Catal. Today 86 (2003) 173-189.
[241] L. Medici, R. Prins, J. Catal. 163 (1996) 38-49.
[242] B. Scheffer, P. Arnoldy, J.A. Moulijn, J. Catal. 112 (1988) 516-527.
[243] Z. Li, Y. Fu, M. Jiang, T. Hu, T. Liu, Y. Xie, J. Catal. 199 (2001) 155-161.
[244] J.M. Christensen, P.M. Mortensen, R. Trane, P.A. Jensen, A.D. Jensen, App. Catal. A 366 (2009) 29-43.

[245] S.P. Kelty, G. Berhault, R.R. Chianelli, App. Catal. A 322 (2007) 9-15.

[246] G. Berhault, A. Mehta, A.C. Pavel, J. Yang, L. Rendon, M.J. Yäcaman, L.C. Araiza, A.D. Moller, R.R. Chianelli, J. Catal. 198 (2001) 9-19.

[247] R.R. Chianelli, G. Berhault, Catal. Today 53 (1999) 357-366.

[248] British Coal Research Establishment, Synthesis of Chemical Feedstocks and Intermediates, Final Report ECSC No. 7220-EC/824, 1987.

[249] M.M. Conway, C.B. Murchison, R.R. Stevens, US Patent 4,675,344 (1989), to Dow Chemical Company.

[250] S.T. Oyama, Catal. Today 15 (1992) 179-200.

[251] L. Leclercq, A. Almazouari, M. Dufour, G. Leclercq, in: S.T. Oyama (Ed.), The chemistry of transition metal carbides and nitrides, 1st ed., Blackie Academic & Professional Glasgow, Great Britain, 1996, 345-361.

[252] N. Wang, K. Fang, D. Jiang, D. Li, Y. Sun, Catal. Today 158 (2010) 241-245.

[253] N. Wang, K. Fang, M. Lin, D. Jiang, D. Li, Y. Sun, Catal. Lett. 136 (2010) 9-13.

[254] J.S. Lee, S.T. Oyama, M. Boudart, J. Catal. 106 (1987) 125-133.

[255] J.S. Lee, L. Volpe, F.H. Ribeiro, M. Boudart, J. Catal. 112 (1988) 44-53.

[256] J.S. Lee, S. Locatelli, S.T. Oyama, M. Boudart, J. Catal. 125 (1990) 157-170.

[257] S.T. Oyama, J.C. Schlatter, J.E. Metcalfe III, J.M. Lambert Jr, Ind. Eng. Chem. Res. 27 (1988) 1639-1648.

[258] K.Y. Park, W.K. Seo, J.S. Lee, Catal. Lett. 11 (1991) 349-356.

[259] I. Barin and O. Knacke, Thermochemical properties of inorganic substances, 1st ed., Springer-Verlag, Berlin, 1973.

[260] G.S. Ranhotra, G.W. Haddix, A.T. Bell, J.A. Reimer, J. Catal. 108 (1987) 24-39.

[261] G.S. Ranhotra, A.T. Bell, J.A. Reimer, J. Catal. 108 (1987) 40-49.

[262] R. Kojima, K. Aika, App. Catal. A 219 (2001) 141-147.

[263] R.B. Levy, M. Boudart, Science 181 (1973) 547-549.

[264] N.I. Ilchenko, Y.I. Pyatnitsky, in S.T. Oyama (Ed.), The Chemistry of Transition Metal Carbides and Nitrides, 1st ed., Blackie Academic & Professional Glasgow, Great Britain, 1996, 311-326.

[265] L. Leclercq, M. Prigent, F. Daubrege, L. Gengembre, G. Leclercq, Stud. Surf. Sci. Catal. 30 (1987) 417-426.

[266] R.J. Colton, J.T.J. Huang, J.W. Rabalais, Chem. Phys. Lett. 34 (1975) 337-339.

[267] L.H. Bennett, J.R. Cuthill, A.J. McAlister, N.E. Erickson, R.E. Watson, Science 184 (1974) 563-565.

[268] L.H. Bennett, J.R. Cuthill, A.J. McAlister, N.E. Erickson, R.E. Watson, Science 187 (1975) 858-859.

[269] S.J. Peppernick, K.D. Gunaratne, A.W. Castleman, PNAS 107 (2010) 975-980.

[270] M. Orita, I. Kojima, E. Miyazaki, Bull. Chem. Soc. Jpn. 59 (1986) 689-695.

[271] J.S. Lee, M. Boudart, Catal. Lett. 8 (1991) 107-114.

[272] L. Leclercq, K. Imura, S. Yoshida, T. Barbee, M. Boudart, in: B. Delmon, P. Grange, P.A. Jacobs, G. Poncelet (Eds.), Preparation of Catalysts II, Elsevier, Amsterdam, 1978, pp. 627.

[273] J.S. Lee, M.H. Yeom, D.S. Lee, J. Mol. Catal. 62 (1990) L45-L51.

[274] H.G. Kim, K.H. Lee, J.S. Lee, Res. Chem. Intermed. 26 (2000) 427-443.

[275] J.C. Fuggle, T.E. Madey, M. Steinkilberg, D. Menzel, Phys. Lett. A 51 (1975) 163-164.

[276] J.R. Kitchin, J.K. Nørskov, M.A. Barteau, J.G. Chen, Catal. Today 105 (2005) 66-73.

[277] M.E. Eberhart and J.M. MacLaren, in: T. Oyama (Ed.), The Chemistry of Transition Metal Carbides and Nitrides, 1st ed., Blackie Academic & Professional, Great Britain, 1996, pp. 107-120.

[278] J.E. Houston, G.E. Laramore, R.L. Park, Science 185 (1974) 258-260.

[279] B. Hammer, J.K. Nørskov, Surf. Sci. 343 (1995) 211-220.

[280] A. Vojvodic, C. Ruberto, J. Phys.: Condens. Matter. 22 (2010) 375501.

[281] I. Kojima, M. Orita, E. Miyazaki, S. Otani, Surf. Sci. 160 (1985) 153-163.

[282] D.J. Chadi, M.L. Cohen, Phys. Rev. B 10 (1974) 496-500.

[283] B. Hammer, J.K. Nørskov, Adv. Catal. 45 (2000) 71-129.

[284] N.V. Smith, G.K. Wertheim, S. Hüfner, M.M. Traum, Phys. Rev. B 10 (1974) 3197-3206.

[285] S. Hüfner, G.K. Wertheim, N.V. Smith, M.M. Traum, Solid State Commun. 11 (1972) 323-326.

[286] L.F. Mattheiss, D.R. Hamann, Phys. Rev. B 30 (1984) 1731-1738.

[287] M. Xiang, D. Li, J. Zou, W. Li, Y. Sun, X. She, J. Nat. Gas Chem. 19 (2010) 151-155.

[288] M. Huang, K. Cho, J. Phys. Chem. C 113 (2009) 5238-5243.

[289] P. Liu, Y.M. Choi, Y. Yang, M.G. White, J. Phys. Chem. A . 114 (2010) 3888-3895.

[290] X.R. Shi, H. Jiao, K. Hermann, J. Wang, J. Mol. Catal. A 312 (2009) 7-17.

[291] X.R. Shi, S.G. Wang, J. Hu, H. Wang, Y.Y. Chen, Z. Qin, J. Wang, App. Catal. A 365 (2009) 62-70.

[292] G.J. Quarderer, R.R. Stevens, G.A. Cochran, C.B. Murchison, US Patent 4,825,013 (1989), to Dow Chemical Company.

[293] G.M. Loudon, Organic Chemistry, 4th ed., Oxford University Press, USA, 2002.

[294] R.C. Brady III, R. Pettit, J. Am. Chem. Soc. 103 (1981) 1287-1289.

[295] R.C. Brady III, R. Pettit, J. Am. Chem. Soc. 102 (1880) 6182-6184.

[296] W.A.A., van Barneveld, V. Ponec, J. Catal. 88 (1984) 382-387.

[297] L.M. Tau, H.A. Dabbagh, B.H. Davis, Energy Fuels 5 (1991) 174-179.

[298] C.K. Rofer-DePoorter, Chem. Rev. 81 (1981) 447-474.

[299] M.E. Dry, Catal. Today 71 (2002) 227-241.

[300] M.E. Dry, App. Catal. A 138 (1996) 319-344.

[301] K.J. Smith, R.G. Herman, K. Klier, Chem. Eng. Sci. 45 (1990) 2639-2646.

[302] T. Tatsumi, A. Muramatsu, K. Yokota, H. Tominaga, J. Catal. 115 (1989) 388-398.

[303] T. Tatsumi, A. Muramatsu, K. Yokota, H. Tominaga, J. Mol. Catal. 41 (1987) 385-389.

[304] E.I. Ko, R.J. Madix, Surf. Sci. 112 (1981) 373-385.

[305] A.P. Farkas, A. Koós, L. Bugyi, F. Solymosi, J. Phys. Chem. C 112 (2008) 18502-18509.

[306] A.P. Farkas, F. Solymosi, Surf. Sci. 602 (2008) 1475-1485.

[307] A.P. Farkas, F. Solymosi, Surf. Sci. 602 (2008) 1497-1506.

[308] R. Barthos, A. Széchenyi, Á. Koós, F. Solymosi, App. Catal. A 327 (2007) 95-105.

[309] A.P. Farkas, L. Bugyi, Á. Koós, F. Solymosi, Surf. Sci. 601 (2007) 3736-3739.

[310] A.P. Farkas, F. Solymosi, Surf. Sci. 601 (2007) 193-200.

197

[311] A.P. Farkas, Á. Koós, L. Bugyi, F. Solymosi, Surf. Sci. 600 (2006) 2355-2363.

[312] F. Solymosi, T. Bánsági, T.S. Zakar, J. Mol. Catal. A 225 (2005) 217-223.

[313] J. Cserenyi, L. Ovari, T. Bansagi, F. Solymosi, J. Mol.Catal. A 162 (2000) 335-352.

[314] F. Solymosi, L. Bugyi, Catal. Lett. 66 (2000) 227-230.

[315] F. Solymosi, L. Bugyi, A. Oszko, I. Horvath, J. Catal. 185 (1999) 160-169.

[316] C. Pistonesi, A. Juan, A.P. Farkas, F. Solymosi, Surf. Sci. 602 (2008) 2206-2211.

[317] H.H. Hwu, J.G. Chen, Chem. Rev. 105 (2005) 185-212.

[318] H.H. Hwu, M.B. Zellner, J.G. Chen, J. Catal. 229 (2005) 30-44.

[319] J. Eng, B.E. Bent, B. Fruehberger, J.G. Chen, Langmuir 14 (1998) 1301-1311.

[320] P. Courty, A. Forestiere, N. Kawata, T. Ohno, C. Raimbault and M. Yoshimoto, in: D.R. Fahey (Ed.), Industrial Chemicals via C_1 Processes, 1st ed., ACS Publications, USA, 1987, pp. 42-60.

[321] R. Rapier, http://www.globalsubsidies.org/en/subsidy-watch/commentary/diminishing-expectations-broken-promises-development-cellulosic-ethanol-, Accessed December 2010.

[322] S.D. Phillips, Ind. Eng. Chem. Res. 46 (2007) 8887-8897.

[323] R.J. Dry, Ind. Eng. Chem. Res. 27 (1988) 616-624.

[324] E. Supp, R.F. Quinkler, in: R.A. Meyers (Ed.), Handbook of Synfuels Technology, 1st ed., McGraw-Hill, USA, 1984, pp. 2/113-2/131.

[325] A. Cybulski, Catal. Rev. 36 (1994) 557-615.

[326] S. Lee, A. Sardesai, Top. Catal. 32 (2005) 197-207.

[327] S. Lee, Methanol Synthesis Technology, 1st ed., CRC Press, USA, 1990.

[328] D.M. Brown, G.R. Jackson, Ecalene^{TM} An Ethanol-Rich Fuel Additive from Syngas, Cat Con 2005, 2005.

[329] G.R. Jackson and D. Mahajan, US Patent 6,753,353 (2004), to PowerEnerCat, Inc.

[330] G.R. Jackson and D. Mahajan, US Patent 6,248,796 (2001), to PowerEnerCat, Inc.

[331] J. Haggin, Chem. Eng. News 62 (1984) 29-30.

[332] BP Chemicals Ltd., Eur. Patent 1862443A1 (2006), to BP Chemicals Ltd.

[333] H. Mahy, C. Szabo, L. Woods, in: G. Hund, K. Laverty (Eds.), 200 Proof Transportation: The Potential for Ethanol as an Alternative Fuel, Report No. ENVIR 550/BBUS 550, University of Washington, USA, 2003, pp. 1-39.

[334] B. Kovarik, Automot. Hist. Rev. 32 (1998) 7-27.

[335] J.B. Hansen, in: G. Ertl, H. Knözinger and J. Weitkamp (Eds.), Handbook of Heterogeneos Catalysis, 1st ed., Wiley-VCH, France, 1997, pp. 1856-1876.

[336] G.A. Olah, Catal. Lett. 93 (2004) 1-2.

[337] G.A. Olah, Angew. Chem. Int. Ed. 44 (2005) 2636-2639.

[338] G.A. Olah, A. Goeppert, G.K.S. Prakash, Beyond Oil and Gas: The Methanol Economy, 1st ed., Wiley-VCH, Germany, 2006.

[339] H.L. MacLean, L.B. Lave, Prog. Energy Combust. Sci. 29 (2003) 1-69.

[340] S. Mintner (Ed.), Alcoholic Fuels, 1st ed., CRC Press, USA, 2006.

[341] T. Ogawa, N. Inoue, T. Shikada, Y. Ohno, J. Nat. Gas Chem. 12 (2003) 219-227.

[342] X.-D. Peng, B.A. Toseland, P.J.A. Tijm, Chem. Eng. Sci. 54 (1999) 2792.

[343] T.A. Semelsberger, R.L. Borup, H.L. Greene, Journal of Power Sources 156 (2006) 497-511.

[344] S.T. Sie, M.M.G. Senden, H.M.H., van Wechem, Catal. Today 8 (1991) 371-394.

[345] DOE Alternative Fuels Data Center, http://afdcmap2.nrel.gov/locator/findpane.asp, Accessed March 2007.

[346] M. Gautam, D.W. Martin II, Proc. Instn. Mech. Engrs. Part A 214 (2000) 497-511.

[347] Y. Yacoub, R. Bata, M. Gautam, Proc. Instn. Mech. Engrs. Part A 212 (1998) 363-379.

[348] R.H. Thring, Automot. Eng. 92 (1984) 60-64.

[349] R.H. Thring, SAE paper 831685 (SP-559), Vol. 92, Section 4, 1983.

[350] M.L. Poulton, Alternative fuels for road vehicles, 1st ed., Computational Mechanics Publications, Great Britain, 1994.

[351] X. Nie, X. Li,D.O. Northwood, Materials Science Forum 546-549 (2007) 1093-1100.

[352] R.F. Service, Science 329 (2010) 784-785.

[353] M.D. Jackson, C.B. Moyer, Alcohol Fuels, Kirk-Othmer Encyclopedia of Chemical Technology, Wiley-VCH, 2000.

[354] E.S. Olson, T.R. Aulich, R.K. Sharma, R.C. Timpe, Appl. Biochem. Biotechnol. 108 (2003) 843-851.

[355] L. Lave, H. MacLean, C. Hendrickson, R. Lankey, Env. Sci. Technol. 34 (2000) 3498-3606.

[356] M. Gautam, D.W. Martin II, D. Carder, Proc. Inst. Mech. Eng. A 214 (2000) 165-182.

[357] C. Song, Catal. Today 86 (2003) 211-263.

[358] Directive 2003/17/EC of the European Parliament and of the Council of 3 March 2003 amending Directive 98/70/EC relating to the quality of petrol and diesel fuels, Available from: http://europa.eu/scadplus/leg/en/lvb/l28077.htm.

[359] W.J. Thomas, S. Portalski, Ind. Eng. Chem. 50 (1958) 967-970.

[360] T. Chang, R.W. Rousseau, P.K. Kilpatrick, Ind. Eng. Chem. Process Des. Dev. 25 (1986) 477-481.

[361] G.H. Graaf, P.J.J.M., Sijtsema, E.J. Stamhuis, G.E.H. Joosten, Chem. Eng. Sci. 41 (1986) 2883-2890.

[362] O. Redlich, J.N.S. Kwong, Chem. Rev. 44 (1949) 233-244.

[363] G. Soave, Chem. Eng. Sci. 27 (1972) 1197-1203.

[364] D.-Y. Peng, D.B. Robinson, Ind. Eng. Chem. Fundam. 15 (1976) 59-64.

[365] K.S. Pitzer, J. Am. Chem. Soc. 77 (1955) 3427-3433.

[366] K.S. Pitzer, D.Z. Lippmann, R.F. Curl Jr, C.M. Huggins, D.E. Petersen, J. Am. Chem. Soc. 77 (1955) 3433-3440.

[367] J.M. Smith, H.C. Van Ness, M.M. Abbott, Introduction to Chemical Engineering Thermodynamics, 5th ed., McGraw-Hill, USA, 1996.

[368] R.C. Reid, J.M. Prausnitz, T.K. Sherwood, Properties of Gases and Liquids, 3rd ed., McGraw–Hill, New York, 1977.

[369] P.L. Chueh, J.M. Prausnitz, Ind. Eng. Chem. Fund. 6 (1967) 492-498.

[370] C. Tsonopoulos, AIChE J. 20 (1974) 263-272.

[371] J.R. Elliot, C.T. Lira, Introductory Chemical Engineering Thermodynamics, 1st ed. (corrected), Prentice Hall, Upper Saddle River, NJ, 1998.

[372] C.L. Rasmussen, K.H. Wassard, K. Dam-Johansen, P. Glarborg, Int. J. Chem. Kin. 40 (2008) 423-441.

[373] C.L. Rasmussen, A.E. Rasmussen, P. Glarborg, Combust. Flame 154 (2008) 529-545.

[374] C.L. Rasmussen, J.G. Jakobsen, P. Glarborg, Int. J. Chem. Kin. 40 (2008) 778-807.

[375] C.L. Rasmussen, J. Hansen, P. Marshall, P. Glarborg, Int. J. Chem. Kin. 40 (2008) 454-480.

[376] C.L. Rasmussen, P. Glarborg, Ind. Eng. Chem. Res. 47 (2008) 6579-6588.

[377] C.L. Rasmussen, Direct Partial Oxidation of Natural Gas to Liquid Chemicals, PhD-Thesis, Technical University of Denmark, 2007.

[378] C.L. Rasmussen, A.E. Rasmussen, J. Hansen, P. Glarborg, 045-12 High Pressure Flow Reactor - Operations Manual, CHEC Report No. R0604, Technical University of Denmark, Lyngby, 2006.

[379] J.A. Shaeiwitz, W.B. Whiting, R. Turton, F. Torries, J. Saymansky, M. Tandon, R.W. Maier, B. Haught, J. Dodd, The Economical Production of Alcoholic Fuels from Coal-Derived Synthesis Gas, Chapters 7-14, US DoE Contract No. DE-AC22-91PC91034-25 West Virginia University, USA, 1999. Available from: http://www.fischer-tropsch.org/DOE/DOE_reports/91034/91034_25 /91034_25_toc.htm

[380] J.D. Seader, E.J. Henley, Separation Process Principles, John Wiley & Sons, USA, 1998.

[381] H.H. Rachford, J.D. Rice, Petrol. Trans., AIME 195 (1952) 327-328.

[382] D.E. Mears, Ind. Eng. Chem. Process. Des. Develop. 10 (1971) 541-547.

[383] P.B. Weisz, Science 179 (1973) 433-440.

[384] P.B. Weisz, C.D. Prater, Adv. Catal. Related Subj. 6 (1954) 143-196.

[385] R.B. Bird, W.E. Stewart, E.N. Lightfoot, Transport Phenomena, 2nd ed., John Wiley & Sons, USA, 2001.

[386] T. Xiao, A.P.E. York, K.S. Coleman, J.B. Claridge, J. Sloan, J. Charnock, M.L.H. Green, J. Mater. Chem. 11 (2001) 3094-3098.

[387] K.T. Jung, W.B. Kim, C.H. Rhee, J.S. Lee, Chem. Mater. 16 (2004) 307-314.

[388] A. Griboval-Constant, J.M. Giraudon, I. Twagishema, G. Leclercq, M.E. Rivas, J. Alvarez, M.J. Pérez-Zurita, M.R. Goldwasser, J. Mol. Catal. A 259 (2006) 187-196.

[389] G. Leclercq, M. Kamal, J.M. Giraudon, P. Devassine, L. Feigenbaum, L. Leclercq, A. Frennet, J.M. Bastin, A. Löfberg, S. Decker, J. Catal. 158 (1996) 142-169.

[390] V.L.S., Teixeira da Silva, M. Schmal, V. Schwartz, S.T. Oyama, J. Mater. Res. 13 (1998) 1977-1988.

[391] V.L.S., Teixeira da Silva, M. Schmal, S.T. Oyama, J. Solid State Chem. 123 (1996) 168-182.

[392] V.L.S., Teixeira da Silva, E.I. Ko, M. Schmal, S.T. Oyama, Chem. Mater. 7 (1995) 179-184.

[393] J.B. Claridge, A.P.E. York, A.J. Brungs, M.L.H. Green, Chem. Mater. 12 (2000) 132-142.

[394] H.S. Kim, G. Bugli, G. Djéga-Mariadassou, J. Solid State Chem. 142 (1999) 100-107.

[395] A. Griboval-Constant, J.-M. Giraudon, G. Leclercq, G. Leclercq, App. Catal. A 260 (2004) 35-45.

[396] F. Solymosi, T. Bansagi, J. Phys. Chem. 96 (1992) 1349-1355.

[397] J.-D. Grunwaldt, S. Hannemann, J. Göttlicher, S. Mangold, M.A. Denecke, A. Baiker, Phys. Scripta T115 (2005) 769-772.

[398] J.-D. Grunwaldt, M. Caravati, S. Hannemann, A. Baiker, Phys. Chem. Chem. Phys. 6 (2004) 3037-3047.

[399] T. Ressler, J. Synchrotron Rad. 5 (1998) 118-122.

[400] S.I. Zabinsky, J.J. Rehr, A. Ankudinov, R.C. Albers, M.J. Eller, Phys. Rev. B 52 (1995) 2995-3009.

[401] A.L. Ankudinov, J.J. Rehr, Phys. Rev. B 56 (1997) 1712-1716.

[402] R.J. Matyi, L.H. Schwartz, J.B. Butt, Catal. Rev. Sci. Eng. 29 (1987) 41-99.

[403] P.E. Højlund Nielsen, K. Pedersen, J.R. Rostrup-Nielsen, Top. Catal. 2 (1995) 207-221.

[404] P.Y. Hou, H. Wise, J. Catal. 93 (1985) 409-416.

[405] V.R. Surisetty, A.K. Dalai, J. Kozinski, Energy & Fuels 24 (2010) 4130-4137.

[406] L.T. Thompson Jr, J. Schwank, M.D. Curtis, AIChE J. 35 (1989) 109-119.

[407] R.D. Oades, S.R. Morris, R.B. Moyes, Catal. Today 7 (1990) 199-208.

[408] J.G. Nunan, R.G. Herman, K. Klier, J. Catal. 116 (1989) 222-229.

[409] W.S. Epling, G.B. Hoflund, W.M. Hart, D.M. Minahan, J. Catal. 169 (1997) 438-446.

[410] H. Yin, Y. Ding, H. Luo, H. Zhu, D. He, J. Xiong, L. Lin, App. Catal. A 243 (2003) 155-164.

[411] M.A. Haider, M.R. Gogate, R.J. Davis, J. Catal. 261 (2009) 9-16.

[412] R. Burch, M.I. Petch, App. Catal. A 88 (1992) 39-60.

[413] E.-M. Ryymin, M.L. Honkela, T.-R. Viljava, A. Outi, I. Krause, App. Catal. A 358 (2009) 42-48.

[414] O.I. Senol, E.-M. Ryymin, T.-R. Viljava, I. Krause, J. Mol. Catal. A 268 (2007) 1-8.

[415] A. Chen, Q. Wang, Q. Li, Y. Hao, W. Fang, Y. Yang, J. Mol. Catal. A 283 (2008) 69-76.

[416] M. Saito, R.B. Anderson, J. Catal. 63 (1980) 438-446.

[417] G. Berhault, L.C. Araiza, A.D. Moller, A. Mehta, R.R. Chianelli, Catal. Lett. 78 (2002) 81-90.

[418] J.T. Miller, W.J. Reagan, J.A. Kaduk, C.L. Marshall, A.J. Kropf, J. Catal. 193 (2000) 123-131.

[419] P.G. Moses, B. Hinnemann, H. Topsøe, J.K. Nørskov, J. Catal. 248 (2007) 188-203.

[420] S. Cristol, J.F. Paul, E. Payen, D. Bougeard, S. Clémendot, F. Hutschka, J. Phys. Chem. B 106 (2002) 5659-5667.

[421] S. Cristol, J.F. Paul, E. Payen, D. Bougeard, S. Clémendot, F. Hutschka, J. Phys. Chem. B 104 (2000) 11220-11229.

[422] M. Sun, A.E. Nelson, J. Adjaye, J. Catal. 233 (2005) 411-421.

[423] Y.Y. Chen, X. Zhao, X.D. Wen, X.R. Shi, M. Dong, J. Wang, H. Jiao, J. Mol. Catal. A 329 (2010) 77-85.

[424] M. Xu, E. Iglesia, J. Catal. 188 (1999) 125-131.

[425] T.Y. Park, I.-S. Nam, Y.G. Kim, Ind. Eng. Chem. Res. 36 (1997) 5246-5257.

[426] J. Zhang, Y. Wang, L. Chang, App. Catal. A 126 (1995) L205-L218.

[427] R.H. Ewell, Ind. Eng. Chem. 32 (1940) 147-153.

[428] E.F., von Wettberg Jr., B.F. Dodge, Ind. Eng. Chem. 22 (1930) 1040-1046.

[429] R.H. Newton, B.F. Dodge, J. Am. Chem. Soc. 56 (1934) 1287-1291.

[430] G.T. Morgan, W.A. Bone, C.N. Hinshelwood, M.P. Applebey, A. Michels, E.K. Rideal, S.J. Green, F.A. Freeth, F.G. Donnan, A.C. Egerton, Proc. Royal Soc. Lond. Series A 127 (1930) 240-267.

[431] S. Mawson, S. McCutchen, P.K. Lim, G.W. Roberts, Energy & Fuels 7 (1993) 257-267.

[432] Z. Qin, J. Liu, J. Wang, Fuel. Proc. Technol. 85 (2004) 1175-1192.

[433] G.C. Chinchen, P.J. Denny, D.G. Parker, G.D. Short, M.S. Spencer, K.C. Waugh, D.A. Whan, Preprints Am. Chem. Soc., Div. Fuel. Chem. 29 (1984) 178-188.

[434] G.C. Chinchen, P.J. Denny, D.G. Parker, M.S. Spencer, D.A. Whan, App. Catal. 30 (1987) 333-338.

[435] Y.B. Kagan, L.G. Liberov, E.V. Slivinskii, S.M. Loktev, G.I. Lin, A.Y. Rozovskii, A.N. Bashkirov, Dokl. Chem. (Engl. Transl.) 221 (1975) 254-256.

[436] Y.B. Kagan, A.Y. Rozovskii, L.G. Liberov, E.V. Slivinskii, G.I. Lin, S.M. Loktev, A.N. Bashkirov, Dokl. Chem. (Engl. Transl.) 224 (1975) 598-601.

[437] M. Badawi, S. Cristol, J.F. Paul, E. Payen, C. R. Chimie. 12 (2009) 754-761.

[438] E. Laurent, B. Delmon, J. Catal. 146 (1994) 281-291.

[439] A.M. Hilmen, M. Xu, M.J.L. Gines, E. Iglesia, App. Catal. A 169 (1998) 355-372.

[440] P.L. Burk, R.L. Pruett, K.S. Campo, J. Mol. Catal. 33 (1985) 1-14.

[441] B. Temel, A.K. Tuxen, J. Kibsgaard, N.-Y. Topsøe, B. Hinnemann, K.G. Knudsen, H. Topsøe, J.V. Lauritsen, F. Besenbacher, J. Catal. 271 (2010) 280-289.

[442] S. Hatanaka, Catalysis Surveys from Asia 9 (2005) 87-93.

[443] H. Xiao, D. Li, W. Li, Y. Sun, Fuel Process. Technol. 91 (2010) 383-387.

[444] P.J. Kooyman, J. A., Rob van Veen, Catal. Today. 130 (2008) 135-138.

[445] S. Eijsbouts, App. Catal. A 158 (1997) 53-92.

[446] J.H. Nielsen, L. Bech, K. Nielsen, Y. Tison, K.P. Jørgensen, J.L. Bonde, S. Horch, T.F. Jaramillo, I. Chorkendorff, Surf. Sci. 603 (2009) 1182-1189.

[447] B.S. Clausen, H. Topsøe, Hyperfine Interactions 47 (1989) 203-217.

[448] J.T. Miller, C.L. Marshall, A.J. Kropf, J. Catal. 202 (2001) 89-99.

[449] P. Engler, M.W. Santana, M.L. Mittleman, D. Balazs, Thermochimica Acta 130 (1988) 309-318.

[450] M.A. Bredig, J. Phys. Chem. 46 (1942) 747-764.

[451] S. Bin Anooz, R. Bertram, D. Klimm, Solid State Commun. 141 (2007) 497-501.

[452] V.R. Surisetty, Y. Hu, A.K. Dalai, J. Kozinski, App. Catal. A, In press, 2010.

[453] H. Tagawa, H. Saijo, Thermochimica Acta 91 (1985) 67-77.

[454] M.W.J. Craje, S.P.A. Louwers, V.H.J., de Beer, R. Prins, A.M., van der Kraan, J. Phys. Chem. 96 (1992) 5445-5452.

[455] C.E. Bogdan, J.G. Nunan, J.G. Santiesteban, R.G. Herman, K. Klier, Stud. Surf. Sci. Catal. 38 (1988) 745-760.

[456] A. Löfberg, A. Frennet, G. Leclercq, L. Leclercq, J.M. Giraudon, J. Catal. 189 (2000) 170-183.

[457] Y. Hara, N. Minami, H. Itagaki, App. Catal. A 323 (2007) 86-93.

[458] H.S. Bengaard, I. Alstrup, I. Chorkendorff, S. Ullmann, J.R. Rostrup-Nielsen, J.K. Nørskov, J. Catal. 187 (1999) 238-244.

[459] S.T. Oyama, in: S.T. Oyama (Ed.), The Chemistry of Transition Metal Carbides and Nitrides, 1st ed., Blackie Academic & Professional Glasgow, Great Britain, 1996, 1-27.

[460] M.F.M. Post, A.C. van't Hoog, J.K. Minderhoud, S.T. Sie, AIChE J. 35 (1989) 1107-1114.

[461] J. Patt, D.J. Moon, C. Phillips, L. Thompson, Catal. Lett. 65 (2000) 193-195.

[462] D.J. Moon, J.W. Ryu, Catal. Lett. 92 (2004) 17-24.

[463] P.C. Ellgen, M.M. Bhasin, US Patent 4,014,913 (1977), to Union Carbide Corporation.

[464] T.P. Wilson, P.H. Kasai, P.C. Ellgen, J. Catal. 69 (1981) 193-201.

[465] A.B. Stiles, F. Chen, J.B. Harrison, X. Hu, D.A. Storm, H.X. Yang, Ind. Eng. Chem. Res. 30 (1991) 811-821.

[466] T. Hayasaka, Y. Obayashi, S. Uchiyama, N. Kawata, Chem. Lett. 15 (1986) 1405-1408.

[467] H. Hachenberg, F. Wunder, E.I. Leupold and H.-J. Schmidt, Eur. Patent 0 021 330 (1983), to Hoechst Aktiengesellschaft.

[468] T.C. Watling, A.F. Gusovius, R. Prins, J. Catal. 188 (1999) 233-236.

[469] T. Inoue, T. Iizuka, J. Chem. Soc. Faraday Trans. 82 (1986) 1681-1686.

[470] M. Ichikawa, L.F. Rao, T. Kimura, A. Fukuoka, J. Mol. Catal. 62 (1990) 15-35.

[471] V.I. Kovalchuk, B.N. Kuznetsov, J. Mol. Catal. A 102 (1995) 103-110.

[472] G. Lu, T. Hoffer, L. Guczi, Catal. Lett. 14 (1992) 207-220.

[473] I. Kojima, E. Miyazaki, M. Inoue, I. Yasumori, Bull. Chem. Soc. Jpn. 58 (1985) 611-617.

[474] M. Inoue, T. Miyake, Y. Takegami, T. Inui, App. Catal. 11 (1984) 103-116.

[475] P.Z.M. Josefina, D. Muriel, H. Yann, G. Anne, L. Lucien, L. Ginette, G. Mireya, C.M. Luisa, B. Geoffrey, App. Catal. A 274 (2004) 295-301.

[476] A. Juan, D.E. Damiani, J. Catal. 137 (1992) 77-91.

[477] E.A. Shaw, T. Rayment, A.P. Walker, J.R. Jennings, R.M. Lambert, J. Catal. 126 (1990) 219-227.

[478] J.C. Frost, Nature 334 (1988) 577-580.

[479] H. Sakurai, M. Haruta, App. Catal. A 127 (1995) 93-105.

[480] M. Kawai, M. Uda, M. Ichikawa, J. Phys. Chem. 89 (1985) 1654-1656.

[481] M. Nagai, K. Matsuda, J. Catal. 238 (2006) 489-496.

[482] X.H. Wang, M.H. Zhang, W. Li, K.Y. Tao, Dalton Transact. 2007 (2007) 5165-5170.

[483] T.C. Xiao, A.P.E. York, H. Al-Megren, C.V. Williams, H.T. Wang, M.L.H. Green, J. Catal. 202 (2001) 100-109.

[484] H. Shao, E.L. Kugler, D.B. Dadyburjor, Prepr. Pap. - Am. Chem. Soc., Div. Fuel Chem. 49 (2004) 702-705.

[485] D.V. Suetin, I.R. Shein, A.L. Ivanovskii, Physica B 404 (2009) 3544-3549.

[486] S.L. Gonzalez-Cortes, T.C. Xiao, A.P.E. York, D. Ma, H. Al-Megren, M.L.H. Green, Reac. Kin. Catal. Lett. 84 (2005) 21-28.

[487] J.E. Connett, J. Chem. Thermodynamics 4 (1972) 233-237.

[488] NIST Chemistry WebBook, http://webbook.nist.gov/chemistry/, Accessed May 2007.

[489] J.M. Christensen, Catalytic conversion of syngas to mixed long chain alcohols, MSc-Thesis, Tehcnical University of Denmark, 2007.

[490] A. Hansen, Enhedsoperationer i den Kemiske Industri, 4th ed., 2nd print, Polyteknisk Forlag, Denmark, 2002.

[491] M.L. Michelsen, Fluid Phase Equilib. 158-160 (1999) 617-626.

[492] P.D. Neufeld, A.R. Janzen, R.A. Aziz, J. Chem. Phys. 57 (1972) 1100-1102.

[493] B.E. Poling, J.M. Prausnitz, O.C. John Paul, R.C. Reid, The properties of gases and liquids, 5th ed., McGraw-Hill New York, USA, 2001.

[494] J. Pardo, M.C. Lopez, J. Santafe, F.M. Royo, J.S. Urieta, Fluid Phase Equilib. 109 (1995) 29-37.

[495] A.K. Barua, M. Afzal, G.P. Flynn, J. Ross, J. Chem. Phys. 41 (1964) 374-378.

[496] G.L. Chierici, A. Paratella, AIChE J. 15 (1969) 786-790.

[497] C.R. Wilke, J. Chem. Phys. 18 (1950) 517-519.

[498] J. Kestin, S.T. Ro, Ber. Bunsen. Phys. Chem. 87 (1983) 600-602.

[499] J.O. Hirschfelder, R.B. Bird, E.L. Spotz, Chem. Rev. 44 (1949) 205-231.

[500] S. Gotoh, M. Manner, J.P. Sorensen, W.E. Stewart, J. Chem. Eng. Data 19 (1974) 169-171.

[501] H.S. Fogler, Elements of chemical reaction engineering, 4th ed., Prentice-Hall, Westford, MA, 2006.

Appendix A: Adiabatic temperature rise

If you can't make them see the light – make them feel the heat
- Ronald Reagan

Although the generated heat effect in all experiments is quite low, the heat capacity of the gas stream and the total molar flow rate are in all experiments also of a limited magnitude. Even the small amounts of heat generated can therefore in the adiabatic case heat the system to very high temperatures. The temperature rise of the gas phase in the adiabatic case can be calculated from the following expression:

$$\Delta T_{adiabatic} = \frac{m\sum_{j=1}^{n} -\Delta H_{ij}\left(r_{ij}{}'\right)}{\left.\sum_{\alpha=1}^{N} F_\alpha \tilde{C}_{P\alpha}\right|_{exit}} \tag{A.1}$$

Here m is the mass of catalyst, ΔH_{ij} is the heat of reaction j per mole of component i formed/converted in the reaction, and r_{ij}' is the reaction rate of reaction j per mass of catalyst with the stoichiometry normalized with respect to component i. The term in the numerator contains the product of the molar flow rate, F, and the molar heat capacity, $\tilde{C}_P$, summarized for all N chemical species present in the system. The term in the numerator is evaluated at the bed exit conditions. Table A.1 summarizes the molar heat capacities used in the calculations.

Table A.1 The molar heat capacities used in the calculations [65, 487, 488].

Component	$\tilde{C}_P$ $\left[\frac{J}{mol\cdot K}\right]$	Component	$\tilde{C}_P$ $\left[\frac{J}{mol\cdot K}\right]$
CO_2	47.323	1-Propanol	145.41
CO	30.444	1-Butanol	186.38
H_2	29.326	Methane	52.232
H_2O	36.322	Ethane	89.120
N_2	30.113	Ethene	70.663
Methanol	66.815	Propane	129.282
Ethanol	107.476		

For simplicity it is presently assumed that all co-produced water is shifted into CO_2. As previously discussed the water-gas shift reaction favors CO_2 at the reaction conditions, and the reaction is close to equilibration at typical alcohol synthesis conditions.

The overall reactions for the production of alcohols and hydrocarbons therefore become:

$$(2n-1)CO + (n+1)H_2 \rightleftharpoons C_nH_{2n+1}OH + (n-1)CO_2 \qquad \text{R40}$$
$$2nCO + (n+1)H_2 \rightleftharpoons C_nH_{2n+2} + nCO_2 \qquad \text{R41}$$
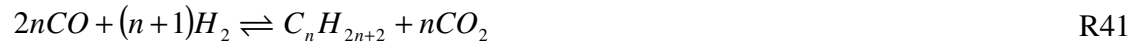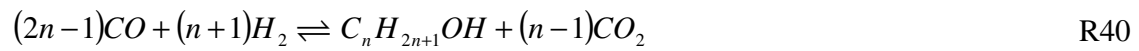
Table A.2 summarizes the calculated reaction enthalpies and the heat capacity changes for the considered alcohol/hydrocarbon forming reactions (R40+R41).

Table A.2 The calculated reaction enthalpies and the heat capacity changes for the considered alcohol/hydrocarbon forming reactions (R40+R41) [65, 487, 488].

Product	$\Delta H^{\circ}_{600K} \left[\frac{kJ}{mol}\right]$	$\Delta \tilde{C}_{P,600K} \left[\frac{J}{mol \cdot K}\right]$
Methanol	-100.44	-22.28
Ethanol	-286.65	-65.17
1-Propanol	-508.81	-29.47
1-Butanol	-717.33	-31.39
Methane	-256.77	-19.99
Ethane	-444.27	-25.99
Ethene	-302.62	-15.12
Propane	-640.11	-28.18

With equation (A.1), the known effluent gas composition, and the reaction enthalpies in table A.2 it is possible to calculate the adiabatic temperature rise. Table A.3 summarizes the adiabatic temperature rise for the experiments used in the kinetic investigations in section 5.3.

Table A.3 The adiabatic temperature rise for the experiments with the high metal content catalyst. All experiments are at P = 100 bar, GHSV = 5106 h^{-1}. The catalyst is KCoMo-2 (see perhaps section 5.3)

CO conv. [mol%]	Experiment used in the determination of	$\Delta T_{adiabatic}$ [°C]	$T_{nominal}$ [°C]	Feed y_{H_2}	y_{CO}	y_{N_2}	y_{H_2S} ($\cdot 10^{-6}$)
22	H₂S effect	348.0	350.7	0.50	0.50	0	260
1		15.0	277.1	0.50	0.50	0	260
3		44.0	300.2	0.50	0.50	0	260
6	T dependence	123.3	326.4	0.50	0.50	0	260
12		188.4	340.1	0.50	0.50	0	260
5		109.8	324.5	0.50	0.50	0	260
2	H₂ reaction order	44.3	324.8	0.22	0.50	0.28	260
7		34.8	324.5	0.19	0.51	0.31	260
16		122.5	324.8	0.50	0.19	0.31	260
25	CO reaction order	135.3	324.8	0.51	0.12	0.38	260
15		96.7	325.4	0.50	0.22	0.29	260
11	H₂S reaction order	106.4	324.5	0.50	0.50	0	1600
12		102.7	324.5	0.50	0.50	0	1000

What is evident from table A.3 is that the adiabatic temperature rise is quite significant for all the conducted experiments, and this could potentially have a substantial effect upon the results. This is however for the adiabatic case, and although small amounts of heat are sufficient to cause a significant adiabatic temperature rise, the flows involved are quite small, and small amounts of heat therefore also have to be transported away to remove this effect entirely.

Appendix B: Possible difference between measured and real temperature

A scholar, who cherishes comfort, is not worthy to be deemed a scholar
- Lao Tzu

In the presently used setup the temperature is measured in a thermo pocket inside the pressure shell and not inside the catalyst bed itself. This appendix describes the development of a model used to estimate the difference between the reactor temperature and the measured temperature. In this model heat transfer occurs by conduction through the quartz tube wall and through a stationary layer of nitrogen.

Model assumptions

- The reactor is isothermal both in the radial direction and along the length of the bed

- The reaction rates are constant through the length of the bed

- Pellets and gas phase will at all times be at the same temperature, and this is the temperature found at the inner wall of the quartz tube

- At steady state all heat formed in the chemical reactions are removed from the reactor by heat conduction in the radial direction along the 25 cm long catalytic bed

- The thermal conductivity of nitrogen is constant despite the presence of a temperature gradient across the nitrogen layer

- Reaction enthalpies are calculated at the nominal reaction temperature and are independent of the excess temperature in the catalytic bed

- Heat transfer limitations across the steel wall of the thermo couple are negligible

The nominal reaction temperature refers to the temperature measured in the thermo pocket inside the pressure shell.

Model derivation

In the following section an expression for the difference between the measured temperature and the actual temperature is derived. Figure B.1 shows a diagram illustrating the cross section of the pressure shell with the quartz tube and the thermo pocket separated by a layer of stationary nitrogen.
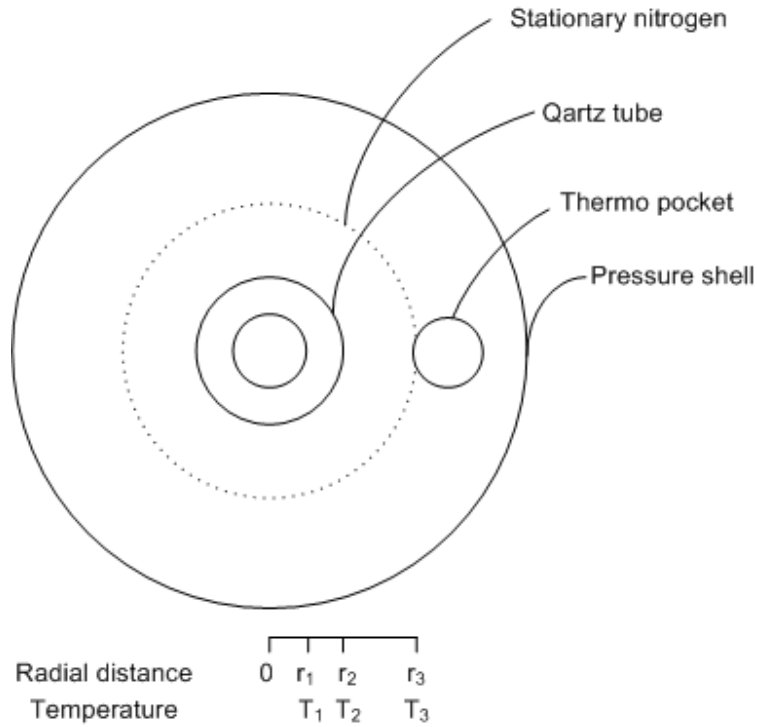
Figure B.1 The cross-section of the pressure shell showing quartz tube and the thermo-pocket separated by a stationary layer of nitrogen. See perhaps figure 4.4 on page 77.

The nominal reaction temperature is the temperature, T_3, measured inside the thermo pocket. Previous investigations [489] have shown that the pellet surface temperature is equal to the bulk gas temperature. In this calculation it will be assumed that the temperature of both pellets and gas is the same throughout the catalyst bed, and this is the temperature, T_1, found at the inner wall of the quartz tube:

$$T_1 = T_s = T_b \tag{B.1}$$

The purpose of this model is to estimate the temperature difference between the measured temperature, T_3, and the bed temperature, T_1,. The heat effect, Q, transported through the wall of the tube along the length of the catalytic bed, L, can be described from the wall area A_{wall} and Fourier's law for the heat flux q_r:

$$Q = A_{wall} q_r = -\lambda_{quartz} 2\pi\, rL \frac{dT}{dr} \tag{B.2}$$

Here λ is the thermal conductivity. Separation of the variables and subsequent integration yields:

$$Q\int_{r_1}^{r_2} \frac{1}{r} dr = -\lambda_{quartz} 2\pi L \int_{T_1}^{T_2} dT \Leftrightarrow$$

$$Q = \frac{2\lambda_{quartz}\pi L}{\ln\left(\dfrac{r_2}{r_1}\right)}(T_1 - T_2) \tag{B.3}$$

At steady state the heat passing through the quartz glass must also pass through the stationary nitrogen layer, and it is possible to derive the following analogous expression for heat transport through the nitrogen layer:

$$Q = \frac{2\lambda_{N_2}\pi L}{\ln\left(\dfrac{r_3}{r_2}\right)}(T_2 - T_3) \tag{B.4}$$

Addition of equation (B.3) to equation (B.4) eliminates the intermediate temperature T_2:

$$Q\frac{\ln\left(\dfrac{r_3}{r_2}\right)}{2\lambda_{N_2}\pi L} + Q\frac{\ln\left(\dfrac{r_2}{r_1}\right)}{2\lambda_{quartz}\pi L} = (T_2 - T_3) + (T_1 - T_2) \Leftrightarrow$$

$$T_1 - T_3 = \frac{Q}{2\pi L}\left(\frac{\ln\left(\dfrac{r_2}{r_1}\right)}{\lambda_{quartz}} + \frac{\ln\left(\dfrac{r_3}{r_2}\right)}{\lambda_{N_2}}\right) \tag{B.5}$$

At steady state the heat effect removed from the reactor must be equal to the heat effect generated in the chemical reactions, wherefore one has:

$$\Delta T_{real} = T_1 - T_3 = \frac{m\sum -\Delta H_{ij}(r_{ij}')}{2\pi L}\left(\frac{\ln\left(\dfrac{r_2}{r_1}\right)}{\lambda_{quartz}} + \frac{\ln\left(\dfrac{r_3}{r_2}\right)}{\lambda_{N_2}}\right) \tag{B.6}$$

Where m is the mass of catalyst, ΔH_{ij} is the heat of reaction j per mole of component i formed/converted in the reaction, and r_{ij}' is the reaction rate of reaction j per mass of

catalyst with the stoichiometry normalized with respect to component *i*. This is summarized for the *n* reactions taking place in the system. The heat generation term can be calculated from the measured reaction rates and the calculated reaction enthalpies. What remain to be determined is just the physical parameters for the system.

The dimensions of the system are given in table B.1 below:

Table B.1 The dimensions used in the calculation of the actual bed temperature

r_1	4 mm
r_2	5 mm
r_3	6.5 mm
L	250 mm

The thermal conductivity for the quartz glass is taken from Hansen [490]:

$$\lambda_{quartz} = 1.3 \frac{W}{m \cdot K} \tag{B.7}$$

The thermal conductivity for the pure nitrogen gas phase at 100 bar is taken from a temperature relation fitted to experimental data from the Handbook of Chemistry and Physics [44]:

$$\lambda_{N_2} \left[\frac{mW}{m \cdot K} \right] = 0.0548 \cdot T[K] + 14.66 \tag{B.8}$$

With the physical parameters presented above equation (B.6) can be used to determine the excess temperature in the reactor. The results of the temperature calculations are presented in the subsequent section.

Possible temperature differences

Table B.2 below summarizes the estimations of the actual excess temperature in the reactor calculated using equation B.6.

The results in table B.2 illustrate that if conduction through the stagnant nitrogen layer is the only mode of heat transfer, then there could be significant disparity between the temperature in the bed and the temperature measured in the thermo pocket. In the most relevant range of CO conversions from 3-15 mol% the temperature may, depending upon the conversion and the product distribution, differ by 4-15 °C. This is definitely a quite significant uncertainty. There are however some redeeming factors that should help to reduce the uncertainty on the temperature. The primary factor is that the thermo pocket is not completely straight, as it is depicted in figure 4.4 and figure 4.5. Instead the thermo pocket has some wriggles, and the pocket is in places brushing up against the quartz tube. This should ensure a greatly improved heat transfer compared to a stationary layer of nitrogen. If a temperature gradient does evolve across the stagnant nitrogen layer in the pressure shell this would also introduce motion in the gas, which again would help to improve heat transfer. Finally radiation, which is not considered in the simple model

above, would also contribute to the heat transfer and thereby reduce the temperature difference.

Table B.2 Estimation of the possible differences in temperature for the catalyst bed and the thermo pocket for the experiments used in the kinetic investigations in section 5.3.

CO conv. [mol%]	Experiment used in the determination of	ΔT_{real} [°C]	T_3 [°C] [a]	Feed			
				y_{H_2}	y_{CO}	y_{N_2}	y_{H_2S} ($\cdot 10^{-6}$)
22	H$_2$S effect	25.9	350.7	0.50	0.50	0	260
1		1.3	277.1	0.50	0.50	0	260
3		3.7	300.2	0.50	0.50	0	260
6	T dependence	10.0	326.4	0.50	0.50	0	260
12		15.4	340.1	0.50	0.50	0	260
5		9.1	324.5	0.50	0.50	0	260
2	H$_2$ reaction order	4.8	324.8	0.22	0.50	0.28	260
7		3.8	324.5	0.19	0.51	0.31	260
16		11.1	324.8	0.50	0.19	0.31	260
25	CO reaction order	11.9	324.8	0.51	0.12	0.38	260
15		8.6	325.4	0.50	0.22	0.29	260
11	H$_2$S reaction order	10.8	324.5	0.50	0.50	0	1600
12		9.9	324.5	0.50	0.50	0	1000

[a] The temperature measured in the thermo pocket. See figure B.1.

215

Appendix C: VLE calculations

Some people teach their troubles to swim instead of drowning them
- Mark Twain

PT Flash calculations

The PT-flash calculation is done by a modified version [380] of the Rachford-Rice [381] algorithm.

We let the parameter β denote the molar fraction of the feed that enters the vapor phase. If z_i denotes the molar fraction of component i in the feed mixture, then a mass balance for component i yields:

$$z_i = x_i \left(1 - \beta\right) + y_i \beta \qquad \text{(C.1)}$$

Here x_i and y_i are the molar fractions of component i in the gas phase and the liquid phase respectively. We let K_i denote the vapor-liquid equilibrium factor, which is defined by the relationship $y_i = x_i K_i$. If K_i is introduced into equation (C.1) we obtain:

$$x_i = \frac{z_i}{1 + \beta \left(K_i - 1\right)} \qquad \text{(C.2)}$$

$$y_i = \frac{z_i K_i}{1 + \beta \left(K_i - 1\right)} \qquad \text{(C.3)}$$

The equilibrium factor, K_i, represents the relative volatility and can be described in terms of the fugacity coefficients in the gas phase (φ_i^G) and in the liquid phase (φ_i^L)

$$K_i = \frac{\varphi_i^L}{\varphi_i^G} \qquad \text{(C.4)}$$

The methodology for calculation of the fugacity coefficients from a mixture of known composition is briefly described in chapter 3.

The molar fractions in the gas- and liquid phases must sum to one, wherefore we must have the following relationship:

$$\left(\sum_i x_i - \sum_i y_i \right) = 0 \qquad \text{(C.5)}$$

Introducing (C.2) and (C.3) into (C.5) yields the so-called Rachford-Rice equation [381]:

$$f(\beta) = \left(\sum_i x_i - \sum_i y_i \right) = \sum_i \frac{z_i(1-K_i)}{1-\beta(K_i-1)} = 0 \qquad \text{(C.6)}$$

For at set of K-values equation (C.7) can be solved iteratively with an initial guess of β between 0 and 1. This can be done numerically by the Newton-Raphson method, which requires the derivative of the objective function, $f(\beta)$:

$$f'(\beta) = \sum_i \frac{z_i(1-K_i)^2}{\left[1-\beta(K_i-1)\right]^2} = 0 \qquad \text{(C.7)}$$

Initially the unknown parameters are the molar fractions in the gas- and liquid phases and the K-values. These unknown parameters are solved iteratively. To initiate the iterative procedure one needs an initial guess of the K-values. A good estimate, which is used in the present case, is the Wilson K-factor approximation [491]:

$$\ln(K_i) = \ln\left(\frac{P_{Ci}}{P} \right) + 5.373(1+\omega_i)\left(1 - \frac{T_{Ci}}{T} \right) \qquad \text{(C.8)}$$

From the initial guess of the K-values the Rachford-Rice equation is solved to obtain β, and the x- and y-values are calculated by (C.2) and (C.3). The fugacity coefficients in the gas- and liquid phases are then calculated according to the procedure described in chapter 3, and a new set of K-values are determined by equation (C.4). The iterative procedure is continued until convergence. The calculation is conducted using MS Excel.

The dew point temperature of the reactor effluent

To obtain an estimate of the necessary heating of the tubing between the reactor and the analyses equipment the dew point temperatures of a representative product mixture have been evaluated as functions of the CO conversion from a $H_2/CO = 1$ mol/mol feed. This evaluation has been conducted at pressures of 100 bar and 1 atm. The representative composition of the product is taken from Shaeiwitz et al. [379] and it is shown in table C.1.

Table C.1 Typical composition of the product formed over a potassium promoted, sulfided cobalt-molybdenum catalyst according to Shaeiwitz et al. [379]

Component	Product selectivity (S_i) [†]
CO_2	32.9 %
CH_4	9.7 %
C_2H_6	0.8 %
MeOH	13.8 %
EtOH	28.9 %
1-PrOH	9.6 %
1-BuOH	3.2 %
EtAc	1.0 %

[†] Shaeiwith et al. [379] also assume minor fractions of other products, but the present calculation is based upon the products in the table.

The first stage in the calculation is to determine the composition of the gas mixture that leaves the reactor. The molar flow, F_i, of product i in the mixture calculated in the following way:

$$F_i = \frac{F_{CO,0} X_{CO} S_i}{N_{C,i}}$$
(C.9)

Here $F_{CO,0}$ is the initial flow of CO, X_{CO} is the degree of CO conversion, S_i is the selectivity to product i, and $N_{C,i}$ is the amount of carbon atoms in product i.
The remaining molar flow of CO becomes:

$$F_{CO} = F_{CO,0}\left(1 - X_{CO}\right)$$
(C.10)

While the remaining molar flow of H_2 becomes:

$$F_{H_2} = F_{H_2,0} - \sum_i \tfrac{1}{2} F_i N_{H,i}$$
(C.11)

Here $N_{H,i}$ is the number of hydrogen atoms in product i.

From the calculated molar flows of reactants and products it is possible to determine the composition of the gas mixture at a given degree of CO conversion. It is then possible to calculate the dew point temperature of the gas mixture.

The determination of the dew point for the product mixture at a known pressure can be done directly or indirectly. Presently an indirect method is used, as this is the easiest calculation to implement. The calculation procedure is that a dew point temperature is assumed and a PT-flash calculation is conducted to establish the phase composition. The procedure of the flash calculation is described in the preceding section. The dew point temperature is then manually adjusted to locate the point, where a liquid phase begins to develop, i.e. the point where β begins to deviate from 1. Alternatively one could have obtained the dew point temperature directly by simultaneously iteration in both temperature and composition.

Appendix D: Assessment of the diffusion limitations for the alcohol synthesis

Experience without reflection is useless
- Frederick the Great

The rate of catalytic reactions may be limited by the diffusion of reactants or products towards or away from the active site. It is important to establish, if the investigations are influenced by such mass transfer limitations. In the present investigations it is especially important that the kinetic investigations are free from mass transfer limitations in order to avoid a falsification of the observed kinetics. Especially for the more bulky long-chained species one could envision that diffusional limitations may be present. In this section the diffusional limitations in the production of alcohols and methane are estimated.

External diffusion limitations

To evaluate the influence of external diffusion i.e. the transport between the bulk gas phase and the surface of the catalyst pellet the Mears criterion [382] is used. The Mears criterion states that external mass transport limitations are absent, if the following condition is met:

$$C_{Mears} = \frac{-r'_{obs} \cdot \rho_b \cdot d_p \cdot n_A}{2 \cdot k_c \cdot C_{Ab}} < 0.15 \tag{D.1}$$

Here $-r'_{obs} \left[\frac{kmol}{kg\ cat.\cdot s} \right]$ is the observed reaction rate, $\rho_b \left[\frac{kg}{m^3} \right]$ is the density of the catalyst bed, $d_p [m]$ is the diameter of the catalyst pellets, n_A is the reaction order with respect to the key reactant (reactant A), $k_c \left[\frac{m}{s} \right]$ is the mass transfer coefficient, and $C_{Ab} \left[\frac{kmol}{m^3} \right]$ is the concentration of the key reactant (reactant A) in the bulk gas phase. H_2 and CO are generally present in the feed in the same concentration, and the two reactants are consumed with the same approximate rate. Reactant A in the Mears criterion is therefore presently defined as a pseudo-reactant, the concentration of which is identical to the concentrations of H_2 and CO. In this case the reaction rate equation can be simplified to a basic n^{th} order rate equation in a single reactant:

$$-r'_{obs} = k' C_{H_2}^{n_{H_2}} C_{CO}^{n_{CO}} = k' C_A^{n_{H_2}} C_A^{n_{CO}} = k' C_A^{n_{H_2}+n_{CO}} = k' C_A^{n_A} \tag{D.2}$$

In some of the kinetic investigations the flow of one reactant is replaced with an equal flow of N_2. In those cases the minority reactant is regarded as the key reactant to evaluate the worst-case scenario. In this case C_A and n_A are the values for the minority reactant. For the experiments conducted with H_2S in the gas the H_2S level is generally constant,

and the dependence of the reaction rate upon the H_2S concentration is therefore contained within the apparent rate constant k'. The Mears criterion is evaluated for the production rates of the linear C_1-C_4 alcohols and methane.

The observed, mass based reaction rate for the production of component i is determined as the molar flow rate of component i, F_i, and the mass of the catalyst bed, m_{cat}:

$$-r'_{obs} = \frac{F_i^{Out}}{m_{cat}}$$
(D.3)

The density of the catalyst bed, ρ_b, is determined from the mass of catalyst and the volume of the bed, V_{bed}:

$$\rho_b = \frac{m_{cat}}{V_{bed}} = \frac{m_{cat}}{R_{tube}^2 \pi L_{bed}}$$
(D.4)

For the reaction orders the experimentally determined values presented in table 5.1 and table 5.2 will be used. Since the experimentally determined reaction orders, which themselves could be influenced by mass transfer limitations, are used in the calculations, it is clear that the calculations only will be valid, if mass transfer limitations are found to be absent.

The average particle diameter varies slightly between the catalyst samples. For the catalyst sample used for the kinetic evaluations KCoMo-2 (see perhaps table 4.4 on page 85) the average diameter can with approximation be given as:

$$d_p = 1.3 \pm 0.2 mm$$
(D.5)

To determine the mass transfer constant the so-called Frössling equation has been used to determine the dimensionless Sherwood number, Sh:

$$Sh = 2 + 0.6 \, Re^{\frac{1}{2}} \, Sc^{\frac{1}{3}}$$
(D.6)

Where Re is the dimensionless Reynolds number, and Sc is the dimensionless Schmidt number, Sc. The dimensionless groups are defined in the following way:

$$Sh = \frac{k_c \cdot d_p}{D_{\alpha\beta}} \qquad Sc = \frac{\nu}{D_{\alpha\beta}} \qquad Re = \frac{v_0 \cdot d_p}{\nu}$$
(D.7)

The density of the gas is determined from the ideal gas law as:

$$\rho = \frac{P \cdot M}{R \cdot T}$$
(D.8)

The characteristic gas velocity, v_0, used to calculate the Reynolds number is given as:

221

$$v_0 = \frac{V_0}{A_{reactor}} = \frac{V_0}{\pi R_{tube}^2} \qquad (D.9)$$

Where V_0 is the volumetric gas flow rate at bed entry conditions, while $A_{reactor}$ is the cross sectional area of the reactor tube through which the gas flows. R_{tube} is the internal radius of the reactor tube. For all experiments conducted on the high metal catalyst the feed flow rate is very close to 1 NL. In this case v_0 becomes the following function of temperature:

$$v_0 = 10^{-3} \tfrac{m^3}{L} \cdot \frac{1 \min}{60 s} \frac{1 \frac{L}{\min} T}{273.15 K \cdot 98.69 atm} = 1.23 \cdot 10^{-5} \tfrac{m}{s \cdot K} T \qquad (D.10)$$

In the calculations of the system the actual flow rates are utilized.

In the dimensionless numbers v is the kinematic viscosity, which is defined as the viscosity, μ, divided by the density, ρ:

$$v = \frac{\mu}{\rho} \qquad (D.11)$$

$D_{\alpha\beta}$ in equation (D.7) is the diffusion coefficient for diffusion of component α in the surrounding gas β.

The viscosity of a mono-atomic gas at low densities can be determined using the theory of Chapman and Enskog, which states that the viscosity, μ, can be written as [385]:

$$\mu = \frac{5\sqrt{\pi m \kappa T}}{16\pi\sigma^2 \Omega_\mu} = 2.6693 \cdot 10^{-6} \frac{kg \cdot \mathring{A}^2 \sqrt{\frac{mol}{g \cdot K}}}{m \cdot s} \frac{\sqrt{MT}}{\sigma^2 \Omega_\mu} \qquad (D.12)$$

Where σ is a characteristic collision diameter for the molecule, m is the mass of the molecule, M is the molar mass of the molecule, and κ is the Boltzmann constant.
The parameter Ω_μ is a factor in the order of unity, which accounts for the deviation from rigid sphere behavior of the gas molecules. The value of Ω_μ at a given temperature is given by the expression [492]:

$$\Omega_\mu = \frac{1.16145}{\left(\frac{\kappa T}{\varepsilon}\right)^{0.14874}} + \frac{0.52487}{\exp\left(0.77320 \cdot \frac{\kappa T}{\varepsilon}\right)} + \frac{2.16178}{\exp\left(2.43787 \cdot \frac{\kappa T}{\varepsilon}\right)} \qquad (D.13)$$

The parameters σ and $\frac{\varepsilon}{\kappa}$ are the ones that appear in the Lennard-Jones potential. The values employed in the present calculations are the ones in table D.1.

Table D.1 Lennard-Jones parameters for the evaluated components.

Molecule	σ [Å]	$\frac{\varepsilon}{\kappa}$ [K]	Reference
H_2	2.915	38.0	[385]
CO	3.590	110	[385]
N_2	3.667	99.8	[385]
MeOH	3.626	481.8	[493]
EtOH	4.530	362.6	[493]
1-PrOH	4.549	576.7	[493]
1-BuOH	5.27	467	[494]
CH_4	3.758	148.6	[493]

The Chapman-Enskog expression is nominally valid only for mono-atomic gasses at low densities, but will nevertheless be used at the high reaction pressures. However the expression is known to yield a good description of the viscosity for polyatomic gases, and the pressure dependence of the viscosity is quite small at high temperatures, so this equation will be used throughout the calculations [385]. Barua et al. [495] have investigated the pressure dependence of the hydrogen, which is one of the two main components in the gaseous phase, and find that the viscosity in the 1-100 bar range shows virtually no pressure dependence at temperatures above 75 °C, so at the reaction temperatures it should be safe to used equation (D.12) for hydrogen at high pressure.

The viscosity of the other main component of the system, namely CO, does show a stronger pressure dependency although it like most gasses decreases with temperature [495]. In order to establish whether equation (D.12) is valid for CO the calculated CO viscosity is tested against a couple of high pressure measurements by Barua et al [495] and Chierici and Paratella [496]. Table D.2 shows a comparison of viscosities measured at high pressure to values calculated using equation (D.12).

Table D.2 Comparison of viscosity calculated using equation (D.12) compared to literature data.

Component	T [°C]	P [bar]	μ_{real} [µP]	μ_{calc} [µP]	$\frac{\mu_{real}-\mu_{calc}}{\mu_{real}}$ [%]	Reference
CO	50	100	206.4	188.0	8.91	[496]
CO	75	100[†]	218.36	200.2	8.25	[495]
N_2	326.85	100	304	288	5.26	[44]

[†]Extrapolated value calculated using a second order polynomial determined by Barua et al. [495] using isothermal pressure data in the 1-200 atm range

It can be seen that the error on the viscosity is reasonable, and given the weakening pressure dependence with temperature it should be safe to utilized equation (D.12) for CO at reaction conditions. N_2 and CO are isoelectric molecules and show strong parallels in physical properties [385, 496]. For this reason a viscosity measurement for N_2 at reaction conditions is included in table D.2, and it can be seen that at this temperature the relative error on the calculated viscosity is quite low.

The relation between the viscosity of a gas mixture and the viscosities of the individual components can at time be strongly non-linear. It is reported that good results

for mixture viscosity can be obtained with the following semi-empirical expression developed by Wilke [497]:

$$\mu_{mix} = \sum_{\alpha=1}^{N} \frac{y_\alpha \mu_\alpha}{\sum_\beta y_\beta \phi_{\alpha\beta}}$$

(D.14)

Where y_α is the molar fraction of component α having viscosity μ_α. The total number of components in the gas mixture is N. The denominator contains a summation over any component, β, by which component α can interact (including α itself) through a dimensionless interaction parameter $\phi_{\alpha\beta}$, which is given as:

$$\varphi_{\alpha\beta} = \frac{1}{\sqrt{8}} \left(1 + \left(\frac{M_\alpha}{M_\beta} \right) \right)^{-\frac{1}{2}} \left(1 + \left(\frac{\mu_\alpha}{\mu_b} \right)^{\frac{1}{2}} \left(\frac{M_\beta}{M_\alpha} \right)^{\frac{1}{4}} \right)^2$$

(D.15)

It can be verified that $\beta = \alpha$ yields $\phi_{\alpha\beta} = 1$. Equation (D.14) is derived for non-polar mixtures at low densities. It will however be assumed that the equation is able to determine the mixture viscosity at the high pressures found in the present case. This is at least coherent with the assumption of pressure independent viscosities. It is speculated that the weakly polar CO molecule (dipole moment 0.11 Debye [44]) might cause problems in the calculations. In order to verify equation (D.14) the calculated viscosities of a few CO containing gas mixtures are compared to experimental data by Kestin and Ro [498]:

Table D.3 Verification of equation (D.14) against experimental data from Kestin and Ro [498]

T [°C]	P [bar]	System	y_{CO}	$\mu_{mix,real}$ [μP]	$\mu_{mix,calc}$ [μP]	$\frac{\mu_{real}-\mu_{calc}}{\mu_{real}}$ [%]
200	1	CO(α)/CH$_4$(β)	0.3282	192.4	191.1	0.68
200	1	CO(α)/CO$_2$(β)	0.6859	246.0	252.4	2.6

It seems that the influence of the weak CO polarity at the conditions specified is without influence upon the viscosity and that the correlation for the mixture viscosity at least at the investigated conditions is quite good.

The theory of Chapman and Enskog can also be employed to determine the diffusion coefficient of component α in the surrounding gas β [385]:

$$D_{\alpha\beta}\left[\frac{cm^2}{s}\right] = 0.0018583 \sqrt{T[K]^3 \left(\frac{1}{M_\alpha\left[\frac{g}{mol}\right]} + \frac{1}{M_\beta\left[\frac{g}{mol}\right]} \right)} \frac{1}{P[atm] \cdot \sigma_{\alpha\beta}^2 \left[\mathring{A}^2 \right] \Omega_D}$$

(D.16)

In this expression the following mixing rules are employed [499, 500]:

$$\sigma_{\alpha\beta} = \frac{\sigma_\alpha + \sigma_\beta}{2} \tag{D.17}$$

$$\frac{\varepsilon_{\alpha\beta}}{\kappa} = \frac{\sqrt{\varepsilon_\alpha \varepsilon_\beta}}{\kappa} \tag{D.18}$$

The value of Ω_D at a given temperature is given by the expression [492]

$$\Omega_D = \frac{1.06036}{\left(\frac{\kappa T}{\varepsilon}\right)^{0.15610}} + \frac{0.19300}{\exp\left(0.47635 \cdot \frac{\kappa T}{\varepsilon}\right)} + \frac{1.03587}{\exp\left(1.52996 \cdot \frac{\kappa T}{\varepsilon}\right)} + \frac{1.76474}{\exp\left(3.89411 \cdot \frac{\kappa T}{\varepsilon}\right)} \tag{D.19}$$

Also the expression for the diffusion coefficient given in equation (D.16) is only valid at low pressure. Out of necessity the expression will nevertheless be utilized at the high reaction pressure. To determine the mass transport coefficient of a given component it is necessary to evaluate the diffusion coefficient of that component in the surrounding gas. The actual surrounding gas is a relatively complicated multi component mixture. To simplify the calculations the diffusion coefficient of a given component is approximated as the diffusion coefficient in a nitrogen atmosphere. The diffusion in CO will presumably be very similar to the diffusion in nitrogen, while the diffusion in the lighter hydrogen presumably occurs more readily. The estimated diffusion coefficients should therefore constitute a lower limit.

Once the physical properties of the system have been determined the dimensionless numbers in equation (D.7) can be determined. The mass transport coefficient can then be calculated from the Sherwood number:

$$k_c = \frac{\text{Sh} \cdot D_{\alpha\beta}}{d_p} \tag{D.20}$$

To perform the final evaluation against the Mears criterion it is also necessary to determine the bulk concentration of the pseudo component A, which is identical to the bulk concentration of both H_2 and CO:

$$C_{Ab} = \frac{y_A \cdot P}{RT} \tag{D.21}$$

The Mears criterion in equation (D.1) can then be tested. Table D.4 summarizes the calculated values of C_{Mears} in (D.1) for the kinetic investigations presented in section 5.3. The most important thing for the data in table D.4 is that we for all the experiments have $C_{Mears} \ll 0.15$. This indicates that external mass transfer limitations are negligible in the experiments used for the studies of the reaction kinetics.

In some of the studies the catalyst KCoMo-3 (see table 4.4 on page 85) is used. The catalyst KCoMo-3 has a higher metal content than KCoMo-1 or KCoMo-2 and is also more active (see table 5.6 on page 109). To complete the evaluation of the external mass transfer limitations the Mears criterion is evaluated for KCoMo-3 operated a 350 °C (the

catalytic properties are presented in table 5.5 on page 107). Among the present experiments this is the one where the highest activity is achieved, and if this experiment is without external mass transfer limitations, it is quite likely that this also goes for the rest of the presented experiments. The evaluation of the Mears criterion for KCoMo-3 operated a 350 °C is presented in table D.5.

Table D.4 The gas compositions and the calculated values of the Mears criterion for the kinetic investigations presented in section 5.3. The experiments are performed at 100 bar with 260 ppmv of H_2S in the feed.

T [°C]	y_{H_2}	y_{CO}	y_{N_2}	C_{Mears}				
				MeOH	EtOH	1-PrOH	1-BuOH	CH$_4$
277.1	0.500	0.500	0	$3.1 \cdot 10^{-5}$	$2.4 \cdot 10^{-5}$	$5.6 \cdot 10^{-6}$	$9.4 \cdot 10^{-7}$	$3.7 \cdot 10^{-6}$
300.2	0.500	0.500	0	$5.4 \cdot 10^{-5}$	$6.3 \cdot 10^{-5}$	$2.0 \cdot 10^{-5}$	$3.9 \cdot 10^{-6}$	$1.2 \cdot 10^{-5}$
326.4	0.500	0.500	0	$8.2 \cdot 10^{-5}$	$1.4 \cdot 10^{-4}$	$5.4 \cdot 10^{-5}$	$1.4 \cdot 10^{-5}$	$3.9 \cdot 10^{-5}$
340.1	0.500	0.500	0	$1.0 \cdot 10^{-4}$	$1.7 \cdot 10^{-4}$	$8.4 \cdot 10^{-5}$	$2.1 \cdot 10^{-5}$	$6.0 \cdot 10^{-5}$
324.5	0.500	0.500	0	$8.1 \cdot 10^{-5}$	$1.4 \cdot 10^{-4}$	$4.9 \cdot 10^{-5}$	$1.1 \cdot 10^{-5}$	$3.8 \cdot 10^{-5}$
324.8	0.505	0.118	0.378	$4.3 \cdot 10^{-4}$	$3.7 \cdot 10^{-4}$	$1.2 \cdot 10^{-4}$	$2.3 \cdot 10^{-5}$	$4.4 \cdot 10^{-4}$
324.5	0.187	0.510	0.303	$4.2 \cdot 10^{-5}$	$7.0 \cdot 10^{-5}$	$4.6 \cdot 10^{-5}$	$1.5 \cdot 10^{-5}$	$2.2 \cdot 10^{-5}$
324.8	0.220	0.500	0.280	$4.8 \cdot 10^{-5}$	$8.6 \cdot 10^{-5}$	$4.7 \cdot 10^{-5}$	$1.2 \cdot 10^{-5}$	$3.8 \cdot 10^{-5}$
324.8	0.500	0.190	0.310	$2.6 \cdot 10^{-4}$	$2.8 \cdot 10^{-4}$	$1.1 \cdot 10^{-4}$	$2.5 \cdot 10^{-5}$	$2.0 \cdot 10^{-4}$
325.4	0.500	0.220	0.280	$1.7 \cdot 10^{-4}$	$2.0 \cdot 10^{-4}$	$7.1 \cdot 10^{-5}$	$1.5 \cdot 10^{-5}$	$1.3 \cdot 10^{-4}$
324.5 [a)]	0.500	0.500	0	$4.4 \cdot 10^{-5}$	$7.6 \cdot 10^{-5}$	$4.1 \cdot 10^{-5}$	$1.5 \cdot 10^{-5}$	$4.1 \cdot 10^{-5}$
324.5 [b)]	0.500	0.500	0	$4.9 \cdot 10^{-5}$	$8.6 \cdot 10^{-5}$	$4.2 \cdot 10^{-5}$	$1.3 \cdot 10^{-5}$	$4.4 \cdot 10^{-5}$

[a)] With 1600 ppmv H_2S in the feed.
[b)] With 1000 ppmv H_2S in the feed.

Table D.5 The calculated Mears criterion and intermediary values for the experiment at 350 °C with KCoMo-3 presented in table 5.5.

Component (i)	MeOH	EtOH	1-PrOH	1-BuOH	CH$_4$
y_i^{out}	$1.73 \cdot 10^{-2}$	$4.15 \cdot 10^{-3}$	$2.77 \cdot 10^{-3}$	$0.40 \cdot 10^{-3}$	$1.41 \cdot 10^{-2}$
$-r'_{obs} \left[\frac{kmol}{kg\ cat. \cdot s} \right]$	$1.27 \cdot 10^{-6}$	$3.04 \cdot 10^{-7}$	$2.03 \cdot 10^{-7}$	$0.29 \cdot 10^{-7}$	$1.03 \cdot 10^{-6}$
n_A	1.42	1.70	1.32	1.13	0.66
$D_{i,N_2} \left[\frac{m^2}{s} \right]$	$4.75 \cdot 10^{-7}$	$3.87 \cdot 10^{-7}$	$3.06 \cdot 10^{-7}$	$2.75 \cdot 10^{-7}$	$7.56 \cdot 10^{-7}$
Re	14.14	14.14	14.14	14.14	14.14
Sc	1.28	1.57	1.99	2.22	0.81
Sh	4.45	4.62	4.84	4.94	4.10
$k_c \left[\frac{m}{s} \right]$	$1.63 \cdot 10^{-3}$	$1.38 \cdot 10^{-3}$	$1.14 \cdot 10^{-3}$	$1.04 \cdot 10^{-3}$	$2.38 \cdot 10^{-3}$
$\rho_b \left[\frac{kg}{m^3} \right]$	721	721	721	721	721
$C_{Ab} \left[\frac{kmol}{m^3} \right]$	0.97	0.97	0.97	0.97	0.97
C$_{Mears}$	$5.65 \cdot 10^{-4}$	$1.62 \cdot 10^{-4}$	$1.19 \cdot 10^{-4}$	$1.61 \cdot 10^{-5}$	$1.45 \cdot 10^{-4}$

The results in table D.5 indicate that also with the more active catalyst are external mass transport limitations of minor importance. An element of uncertainty for the results in

table D.5 is that the reaction orders obtained in the presence of H_2S are used even though the experiment is conducted with a sulfur free feed. As it is discussed in section 5.3 the kinetic parameters obtained with H_2S in the feed are not valid in a sulfur free syngas, but in lack of other data the reaction orders are still used.

It is an element of uncertainty that the Chapman-Enskog kinetic theory is used at the very high reaction pressures although the theory formally only is valid at low pressures, but despite this uncertainty the present calculations strongly suggest that external mass transport limitations are negligible in the present experiments.

Internal diffusion limitations

The evaluations in the preceding section indicated that external mass transport limitations can be neglected in the present investigations. There is however still the possibility of internal mass transport limitations. The observed experimental rates have therefore been evaluated against the Weisz-Prater criterion [383, 384], which states that internal mass transport limitations can be neglected if the following inequality is fulfilled:

$$C_{WP} = \frac{-r'_{obs} \cdot \rho_c \cdot \left(\frac{d_p}{2}\right)^2}{D_e \cdot C_{As}} \ll 1 \tag{D.22}$$

Here ρ_c is the density of the catalyst, D_e is the effective diffusion coefficient in the pores of the catalyst, and C_{As} is the concentration of reactant A at the surface of the catalyst. The origin of the Weisz-Prater criterion is that the square of the so-called Thiele modulus, ϕ, should be much smaller than 1, if mass transport limitations are to be avoided.

$$\phi^2 = \left(R_p \sqrt{\frac{k_A C_{As}^{n-1}}{D_e}}\right)^2 = \left(\frac{d_p}{2}\right)^2 \frac{k_A C_{As}^{n-1}}{D_e} = \frac{-r'_{obs} \cdot \rho_c \left(\frac{d_p}{2}\right)^2}{D_e \cdot C_{As}} \tag{D.23}$$

Here the rate constant, k_A, can be expressed in terms of the observed reaction rate, if mass transfer limitations are assumed to be absent.

$$-r'_{obs} = \frac{k_A C_{As}^n}{\rho_c} \Leftrightarrow k = \frac{-r'_{obs} \cdot \rho_c}{C_{As}^n} \tag{D.24}$$

The densities of the catalysts have been determined from mercury porosimetry and can be found in table 4.4 on page 85.

As external mass transport limitations were estimated to play an insignificant role it is assumed that the concentration of the pseudo-reactant A at the pellet surface is identical to the bulk concentration:

$$C_{As} = C_{Ab} \tag{D.25}$$

The diffusion in the catalyst pores is combined of regular diffusion and so-called Knudsen diffusion. The Knudsen diffusion coefficient, D_K, is estimated through the following expression [385]:

$$D_K\left[\tfrac{m^2}{s}\right] = 3.068 \cdot R_{pore}\left[m\right] \cdot \sqrt{\frac{T\left[K\right]}{M\left[\tfrac{kg}{mol}\right]}}$$ (D.26)

Here R_{pore} is the radius of the pores inside the catalyst. From mercury porosimetry it is observed that the pores of the catalyst KCoMo-2 predominantly are found in the 1.25-37.35 nm range. This size range is used for all of the catalysts, and the calculations are performed for both extremes of this interval. The limit at 1.25 nm may to some extent be related to the lower limit of the porosimeter, but as it will be shown, even 1.25 nm pores are relatively far from diffusional limitations, so inclusion of the smallest pores would presumably not change the conclusions significantly. The diffusion coefficient, $D_{\alpha\beta e}$, of component α diffusing through pores filled with component β is given by the following expression:

$$D_{\alpha\beta e} = \left[\frac{1}{D_K} + \frac{1}{D_{\alpha\beta}}\right]^{-1}$$ (D.27)

Inside the catalyst pellet the paths are tortuous, and the pores are of varying cross-sectional area. To account for these facts an effective diffusion coefficient, D_e, is used. The effective diffusion coefficient is given by the following expression:

$$D_e = \frac{D_{\alpha\beta e} \cdot \psi_p \cdot \sigma_c}{\tilde{\tau}}$$ (D.28)

Here ψ_p is the pellet porosity, $\tilde{\tau}$ is the tortuosity and σ_c is a constriction factor that accounts for variations in the cross sectional areas of the pores. The pellet porosity has been determined by mercury porosimetry to $\psi_p = 0.3$ for KCoMo-2 and $\psi_p = 0.25$ for KCoMo-2. For the tortuoisty and constriction factor the representative values $\tilde{\tau} = 3.0$ and $\sigma_c = 0.8$ from Scott-Fogler [501] have been used.

When the effective diffusion coefficient has been determined it is possible to test the results against the Weisz-Prater criterion. Table D.6 shows the test of the measurements from the kinetic investigations against the Weisz-Prater criterion in the case of the smallest pore radius of 1.25 nm. Table D.7 shows the same results for the largest pore radius of 37.35 nm.

Table D.6 The calculated values of the Weisz-Prater criterion for the kinetic investigations presented in section 5.3. The calculations correspond to the smallest pore radius of 1.25 nm observed in the mercury porosimetry measurements. The experiments are performed at 100 bar with 260 ppmv of H_2S in the feed.

T [°C]	y_{H_2}	y_{CO}	y_{N_2}	$C_{WP,\ 1.25\ nm}$				
				MeOH	EtOH	1-PrOH	1-BuOH	CH$_4$
277.1	0.500	0.500	0	$1.7 \cdot 10^{-3}$	$1.3 \cdot 10^{-3}$	$3.4 \cdot 10^{-4}$	$6.8 \cdot 10^{-5}$	$4.2 \cdot 10^{-4}$
300.2	0.500	0.500	0	$3.0 \cdot 10^{-3}$	$3.5 \cdot 10^{-3}$	$1.2 \cdot 10^{-3}$	$2.8 \cdot 10^{-4}$	$1.4 \cdot 10^{-3}$
326.4	0.500	0.500	0	$4.5 \cdot 10^{-3}$	$7.5 \cdot 10^{-3}$	$3.3 \cdot 10^{-3}$	$1.0 \cdot 10^{-3}$	$4.5 \cdot 10^{-3}$
340.1	0.500	0.500	0	$5.7 \cdot 10^{-3}$	$9.5 \cdot 10^{-3}$	$5.2 \cdot 10^{-3}$	$1.6 \cdot 10^{-3}$	$6.9 \cdot 10^{-3}$
324.5	0.500	0.500	0	$4.5 \cdot 10^{-3}$	$7.0 \cdot 10^{-3}$	$3.0 \cdot 10^{-3}$	$8.2 \cdot 10^{-4}$	$4.4 \cdot 10^{-3}$
324.8	0.505	0.118	0.378	$2.4 \cdot 10^{-2}$	$2.1 \cdot 10^{-2}$	$7.5 \cdot 10^{-3}$	$1.6 \cdot 10^{-3}$	$5.1 \cdot 10^{-2}$
324.5	0.187	0.510	0.303	$2.5 \cdot 10^{-3}$	$4.2 \cdot 10^{-3}$	$3.0 \cdot 10^{-3}$	$1.2 \cdot 10^{-3}$	$2.7 \cdot 10^{-3}$
324.8	0.220	0.500	0.280	$2.8 \cdot 10^{-3}$	$5.1 \cdot 10^{-3}$	$3.1 \cdot 10^{-3}$	$9.5 \cdot 10^{-4}$	$4.6 \cdot 10^{-3}$
324.8	0.500	0.190	0.310	$1.4 \cdot 10^{-2}$	$1.6 \cdot 10^{-2}$	$6.6 \cdot 10^{-3}$	$1.8 \cdot 10^{-3}$	$2.4 \cdot 10^{-2}$
325.4	0.500	0.220	0.280	$9.2 \cdot 10^{-3}$	$1.1 \cdot 10^{-2}$	$4.3 \cdot 10^{-3}$	$1.1 \cdot 10^{-3}$	$1.5 \cdot 10^{-2}$
324.5 [a]	0.500	0.500	0	$2.4 \cdot 10^{-3}$	$4.2 \cdot 10^{-3}$	$2.5 \cdot 10^{-3}$	$1.1 \cdot 10^{-3}$	$4.8 \cdot 10^{-3}$
324.5 [b]	0.500	0.500	0	$2.7 \cdot 10^{-3}$	$4.8 \cdot 10^{-3}$	$2.6 \cdot 10^{-3}$	$9.1 \cdot 10^{-4}$	$5.1 \cdot 10^{-3}$

[a] With 1600 ppmv H_2S in the feed.
[b] With 1000 ppmv H_2S in the feed.

Table D.7 The calculated values of the Weisz-Prater criterion for the kinetic investigations presented in section 5.3. The calculations correspond to the largest pore radius of 37.35 nm observed in the mercury porosimetry measurements. The experiments are performed at 100 bar with 260 ppmv of H_2S in the feed.

T [°C]	y_{H_2}	y_{CO}	y_{N_2}	$C_{WP,\ 37.35\ nm}$				
				MeOH	EtOH	1-PrOH	1-BuOH	CH$_4$
277.1	0.500	0.500	0	$9.8 \cdot 10^{-4}$	$7.7 \cdot 10^{-4}$	$2.1 \cdot 10^{-4}$	$4.2 \cdot 10^{-5}$	$2.3 \cdot 10^{-4}$
300.2	0.500	0.500	0	$1.7 \cdot 10^{-3}$	$2.0 \cdot 10^{-3}$	$0.7 \cdot 10^{-3}$	$1.7 \cdot 10^{-4}$	$7.7 \cdot 10^{-4}$
326.4	0.500	0.500	0	$2.5 \cdot 10^{-3}$	$4.3 \cdot 10^{-3}$	$2.0 \cdot 10^{-3}$	$6.0 \cdot 10^{-4}$	$2.4 \cdot 10^{-3}$
340.1	0.500	0.500	0	$3.2 \cdot 10^{-3}$	$5.3 \cdot 10^{-3}$	$3.0 \cdot 10^{-3}$	$9.1 \cdot 10^{-4}$	$3.6 \cdot 10^{-3}$
324.5	0.500	0.500	0	$2.5 \cdot 10^{-3}$	$4.0 \cdot 10^{-3}$	$1.8 \cdot 10^{-3}$	$4.9 \cdot 10^{-4}$	$2.3 \cdot 10^{-3}$
324.8	0.505	0.118	0.378	$1.3 \cdot 10^{-2}$	$1.2 \cdot 10^{-2}$	$4.4 \cdot 10^{-3}$	$9.7 \cdot 10^{-4}$	$2.7 \cdot 10^{-2}$
324.5	0.187	0.510	0.303	$1.4 \cdot 10^{-3}$	$2.4 \cdot 10^{-3}$	$1.8 \cdot 10^{-3}$	$7.0 \cdot 10^{-4}$	$1.5 \cdot 10^{-3}$
324.8	0.220	0.500	0.280	$1.6 \cdot 10^{-3}$	$2.9 \cdot 10^{-3}$	$1.8 \cdot 10^{-3}$	$5.6 \cdot 10^{-4}$	$2.4 \cdot 10^{-3}$
324.8	0.500	0.190	0.310	$8.0 \cdot 10^{-3}$	$9.0 \cdot 10^{-3}$	$3.9 \cdot 10^{-3}$	$1.1 \cdot 10^{-3}$	$1.2 \cdot 10^{-2}$
325.4	0.500	0.220	0.280	$5.1 \cdot 10^{-3}$	$6.3 \cdot 10^{-3}$	$2.6 \cdot 10^{-3}$	$6.2 \cdot 10^{-4}$	$7.7 \cdot 10^{-3}$
324.5 [a]	0.500	0.500	0	$1.4 \cdot 10^{-3}$	$2.4 \cdot 10^{-3}$	$1.5 \cdot 10^{-3}$	$6.3 \cdot 10^{-4}$	$2.5 \cdot 10^{-3}$
324.5 [b]	0.500	0.500	0	$1.5 \cdot 10^{-3}$	$2.7 \cdot 10^{-3}$	$1.5 \cdot 10^{-3}$	$5.4 \cdot 10^{-4}$	$2.7 \cdot 10^{-3}$

[a] With 1600 ppmv H_2S in the feed.
[b] With 1000 ppmv H_2S in the feed.

The results in table D.6 and table D.7 show that for the experiments conducted in the investigations of the reaction kinetics we generally have $C_{WP} \ll 1$. At most the methane production reaches $C_{WP} = 5.06 \cdot 10^{-2}$ in the case of the smallest pore radius of 1.25 nm. For the largest pore radius there values of C_{WP} are smaller, within the same order of magnetude. Although the values of C_{WP} in a few cases begins to show some significance

the conclusion is nevertheless that internal mass transport limitations are negligible in the evaluations of the reaction kinetics, since the values of C_{WP} in all cases are much smaller than 1. As described in the preceding section the experiment with the catalyst KCoMo-3 at 350 °C is the experiment that yields the highest alcohol production rate, and it is therefore also interesting to evaluate the possibility of internal mass transport limitations in this extreme case. Table D.8 summarizes the evaluations of the Weisz-Prater criterion against for the production of various products when the catalyst KCoMo-3 is operated at 350 °C. The evaluation is conducted for the two extreme pore radii.

Table D.8 The calculated Weisz-Prater criterion and intermediary values for the experiment at 350 °C with KCoMo-3 presented in table 5.5.

Component (i)	$R_{Pore} = 1.25$ nm				
	MeOH	EtOH	1-PrOH	1-BuOH	CH$_4$
$D_K \left[\frac{m^2}{s} \right]$	$5.35 \cdot 10^{-7}$	$4.46 \cdot 10^{-7}$	$3.91 \cdot 10^{-7}$	$3.52 \cdot 10^{-7}$	$7.56 \cdot 10^{-7}$
$D_e \left[\frac{m^2}{s} \right]$	$1.68 \cdot 10^{-8}$	$1.38 \cdot 10^{-8}$	$1.14 \cdot 10^{-8}$	$1.03 \cdot 10^{-8}$	$2.52 \cdot 10^{-8}$
C_{WP}	$4.73 \cdot 10^{-2}$	$1.38 \cdot 10^{-2}$	$1.11 \cdot 10^{-2}$	$1.78 \cdot 10^{-3}$	$2.56 \cdot 10^{-2}$
Component (i)	$R_{Pore} = 37.35$ nm				
	MeOH	EtOH	1-PrOH	1-BuOH	CH$_4$
$D_K \left[\frac{m^2}{s} \right]$	$1.60 \cdot 10^{-5}$	$1.33 \cdot 10^{-5}$	$1.17 \cdot 10^{-5}$	$1.05 \cdot 10^{-5}$	$2.26 \cdot 10^{-5}$
$D_e \left[\frac{m^2}{s} \right]$	$3.07 \cdot 10^{-8}$	$2.51 \cdot 10^{-8}$	$1.99 \cdot 10^{-8}$	$1.78 \cdot 10^{-8}$	$4.87 \cdot 10^{-8}$
C_{WP}	$2.58 \cdot 10^{-2}$	$7.58 \cdot 10^{-3}$	$6.37 \cdot 10^{-3}$	$1.02 \cdot 10^{-3}$	$1.32 \cdot 10^{-2}$

The results in table D.8 generally show that we also for this experiment with the highest observed alcohol production rate have $C_{WP} \ll 1$. Even for the smallest evaluated pore size the values of C_{WP} are generally about 1-2 orders of magnitude below 1. Overall the present evaluations of the Weisz-Prater criterion generally suggest that internal mass transport limitations are of very limited importance in the present experiments.

The estimated absence of diffusion limitations is consistent with the experimental results of Murchison et al. [13], who observed that the catalytic properties were unaffected by the catalyst pellet dimensions in the range from granulates of 12-20 mesh size (850 μm-1.68 mm) to 5 mm extrudates. It should however be mentioned that Surisetty et al. [405] more recently with a more active catalyst promoted by rhodium and carbon nanotubes did observed a variation in activity with the particle size.

Appendix E: Speciation of sulfur in product

Some people cause joy wherever they go, others whenever they go
- Oscar Wilde

Even when a novel does not end well, it is well that it ends
- Robert Storm Petersen

This appendix shows two examples of S-AED spectra of the condensed alcohol products. The two spectra illustrate that the thiols are dominant sulfur species in the product. It is interesting to observe a possible relationship between the dominant alcohol and the dominant thiol in the product. For the alcohol product investigated in figure E.1 methanol is the dominant alcohol (see figure 5.4 on page 97), while ethane thiol is the dominant thiol. For the product investigated in figure E.2 ethanol is the dominant alcohol, but 1-propane thiol seems to be the dominant thiol. Althoug intriguing, there is insufficient data to clarify, whether or not there is a general relationship between a C_n alcohol and the C_{n+1} thiol. Figure E.2 also illustrates that the alcohol product condensed with 450 ppmv H_2S in the feed contains a wide range of different sulfur species.
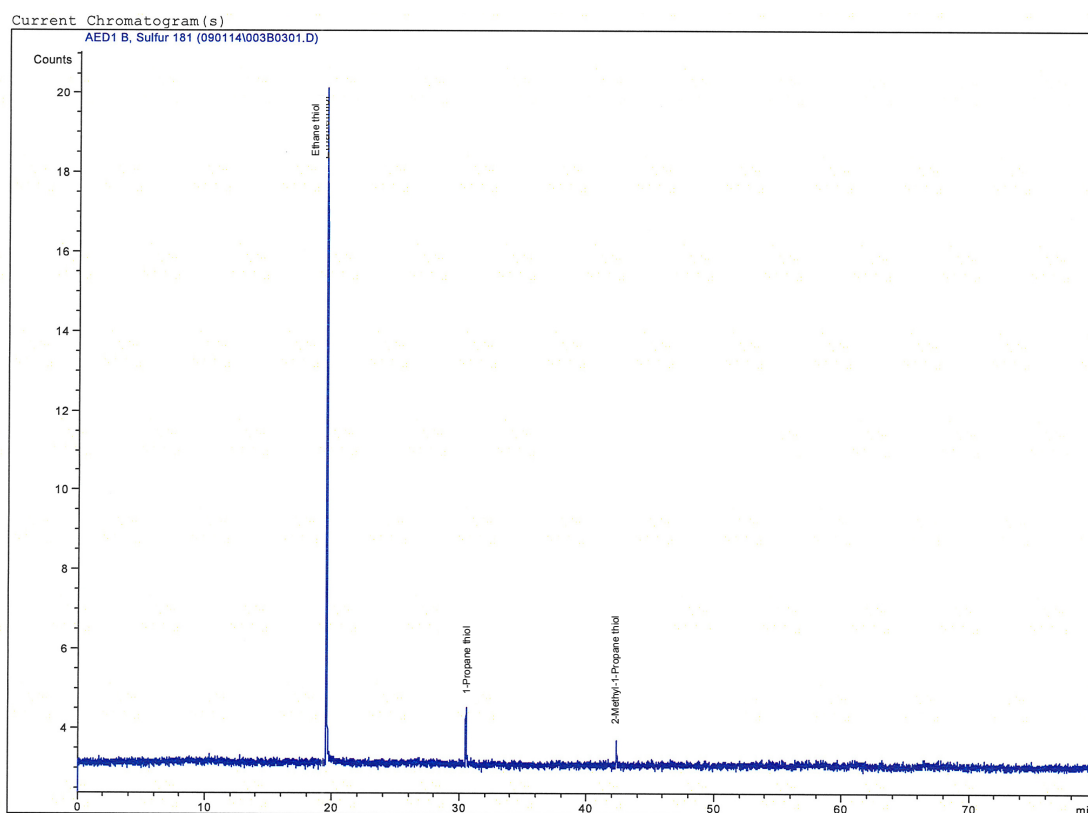

Figure E.1 The S-AED spectrum for the liquid sample in figure 5.13 on page 113 that has been on stream for 35 h in a sulfur free syngas.
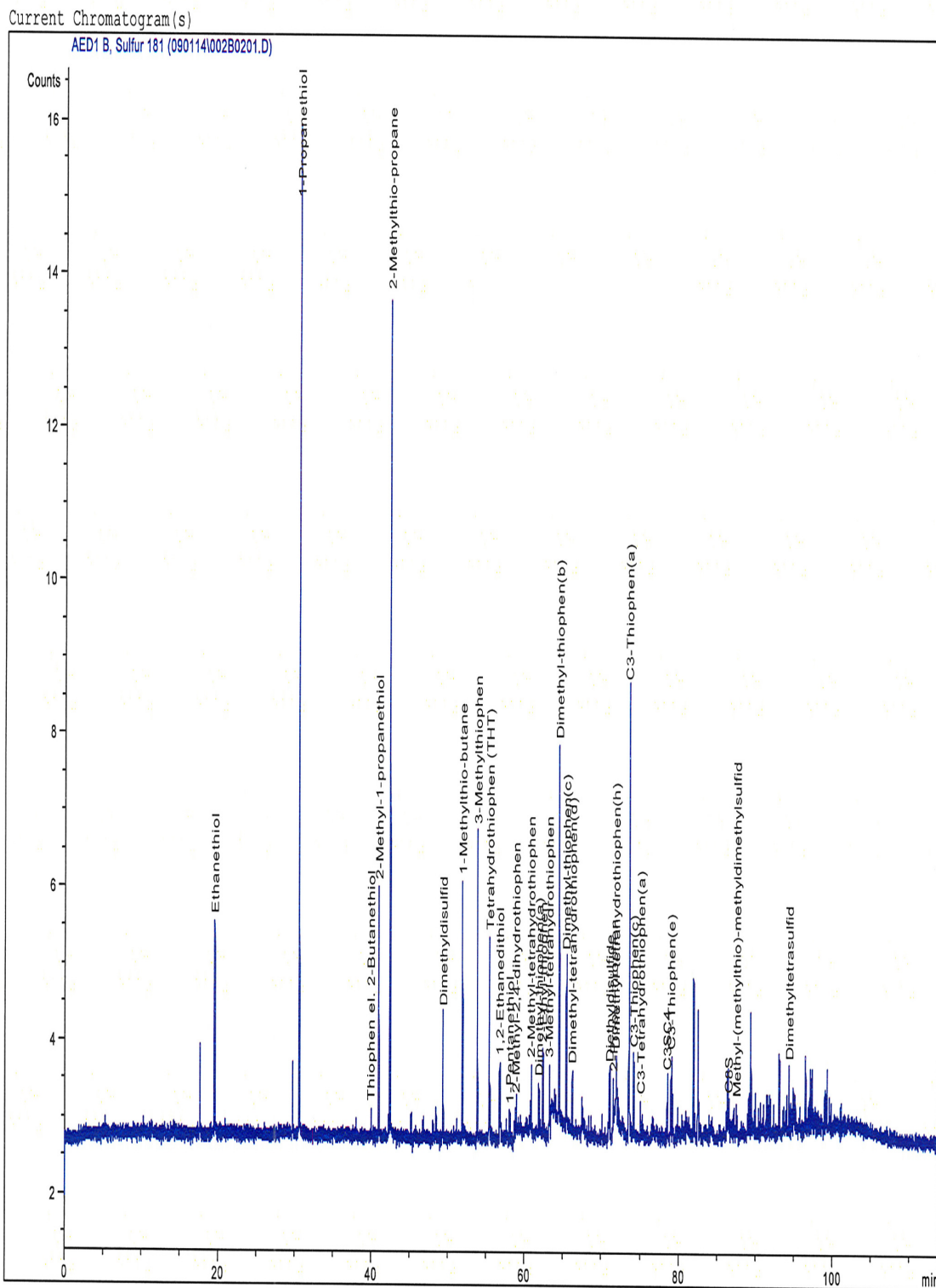
Figure E.2 The S-AED spectrum for the liquid sample that has been collected with 450 ppmv H_2S in the feed in figure 5.12 on page 112.